

SYNTHESIS AND CHARACTERIZATION OF NITRIC OXIDE-RELEASING SILICA
MATERIALS FOR SENSING APPLICATIONS

by
Jae Ho Shin

A dissertation submitted to the faculty of the University of North Carolina at Chapel Hill in partial fulfillment of the requirements for the degree of Doctor of Philosophy in the Department of Chemistry (Analytical Chemistry).

Chapel Hill
2006

Approved by

Professor Mark H. Schoenfisch

Professor Royce W. Murray

Professor Malcolm D. E. Forbes

Professor Jeffrey S. Johnson

Professor Wei You

ABSTRACT

JAE HO SHIN: Synthesis and Characterization of Nitric Oxide-Releasing Silica Materials
for Sensing Applications
(Under the direction of Professor Mark H. Schoenfisch)

Nitric oxide (NO), a free radical endogenously synthesized in the human body, regulates a range of biological processes in the cardiovascular, genitourinary, respiratory, and nervous systems. With the discovery of NO as a potent inhibitor of platelet activation and its identification as an antibacterial agent, the utility of NO has been expanded to developing more biocompatible materials that resist to biofouling. My research has focused on the development of NO-releasing glucose biosensors via xerogel/polyurethane *hybrid* membranes that release NO in a controlled fashion. This new class of glucose biosensors was characterized by both adequate analytical response to glucose and improved bacterial adhesion resistance at NO fluxes $\geq 5 \text{ pmol}\cdot\text{cm}^{-2}\cdot\text{s}^{-1}$ for 20 h.

To further elucidate the complex and wide ranging roles of NO in physiology, an amperometric xerogel-based NO microsensor was fabricated. Several silicon-based NO sensor membranes were synthesized by doping alkyl/amino-alkoxysilane-based xerogels with Nafion. The performance of xerogel-based NO sensors was then evaluated to identify the optimum xerogel composition that maximized NO permeability and provided sufficient selectivity for NO. Xerogel permeability and selectivity were further manipulated as a function of specific reaction/processing conditions. The analytical performance of the xerogel-based sensor far exceeded that of current commercial sensors.

Silica nanoparticles capable of controlled NO release were also synthesized via sol-gel chemistry. Control over both the structure and concentration of the silane precursors (i.e., tetraalkoxy- and aminoalkoxysilanes) and the synthetic conditions used to prepare the silica allowed for the preparation of NO donor-modified silica nanoparticles of widely varying size ($d = 20 - 500$ nm), NO payloads ($50 - 74000$ nmol·mg⁻¹), maximum NO release amounts ($10 - 103000$ ppb·mg⁻¹), half-lives ($0.1 - 12$ h), and NO release durations (up to 30 h). Nitric oxide-releasing silica nanoparticles may prove useful in the development of glucose sensors with extended NO release durations and as new NO-derived anti-tumor chemotherapeutics. Preliminary studies evaluating the anti-cancer efficacy of NO-releasing silica nanocomposites against human ovarian surface epithelial (HOSE) cancer cells were conducted. The viability of HOSE cancer cells was significantly reduced upon exposure to the NO-releasing silica nanoparticles. Such scaffolds may allow for future tissue/cell targeting via particle size (enhanced permeability/retention effect) and/or ligand-receptor binding chemistry.

To my parents,

who made all of this possible, with your endless loves, supports, and prayers.

Stay hungry and stay foolish

- Steve Jobs, 2005

ACKNOWLEDGEMENTS

I am grateful for the help and encouragement of numerous people throughout my graduate career. I appreciate the support of my advisor Professor Mark Schoenfish, for challenging me to incessantly dig knowledge and providing many opportunities for me. I would like to thank Professor Channing Der who helped me face and enjoy a new experience. I am grateful for the help of Professors Geun Sig Cha and Hakhyun Nam who sowed the seeds of science in my mind. I would also like to appreciate Dr. Marc Horst for many helpful discussions and directions in silicon NMR experiments.

I am thankful to my past and present colleagues in the Schoenfish lab who shared some great stories about the graduate school experience. It was a pleasure to work with Stephanie (Dr. Marxer!) who was my first collaborator in the lab and provided me invaluable insights consistently. Stephen Weinman, thank you for patiently and persistently helping me progress some important projects. Good luck in your graduate school life in Harvard! Sara Metzger, I appreciate your endless supports in our silica project that yielded great results recently. How is it going to join CIA? (Oops! I spoke out. Am I under arrest?) To my classmates, Kevin Dobmeier and Nate Stasko, thank you for your invaluable discussions in science and others. Evan Hetrick, you were so kind and nice to me, and I appreciate your tight collaboration with your capricious boys (bacteria). Carri and Susan, I cannot forget your kindness and all the chats about the graduate school life and your dogs. Furthermore, I really appreciate the former lab members, Drs. Mary Robbins, Kate Brogan, Kenyon Evans-

Nguyen, Bong Oh, and Ryan Fuierer. You tough me the hands every week and encouraged me to keep up moving ahead and on track. Anything I achieve stems from this base of support in my life.

TABLE OF CONTENTS

LIST OF TABLES	xii
LIST OF FIGURES	xiv
LIST OF ABBREVIATIONS AND SYNBOLS	xix
Chapter 1. Improving the Biocompatibility of <i>In Vivo</i> Sensors via Nitric Oxide Release	1
1.1 <i>In Vivo</i> Sensor Biocompatibility	1
1.2 Strategies for Improving the Biocompatibility of <i>In Vivo</i> Sensors	6
1.2.1 Passive Biomaterials	6
1.2.2 Active Biomaterials	8
1.3 Nitric Oxide and Prevention of Biofouling	9
1.3.1 Endogenous Pathway of Nitric Oxide Generation	10
1.3.2 Biological and Pathobiological Roles of Nitric Oxide	12
1.3.3 Implications of Nitric Oxide for Designing <i>In Vivo</i> Sensors	15
1.4 Synthetic Nitric Oxide Donors	16
1.4.1 Major Classes of Nitric Oxide Donors	17
1.4.2 Diazeniumdiolate Chemistry	17
1.4.3 Nitric Oxide-Releasing Polymers for Designing <i>In Vivo</i> Sensors	23
1.5 Sol–Gel Chemistry for Nitric Oxide-Releasing Coatings	24

1.5.1 Sol–Gel Chemistry	25
1.5.2 Nitric Oxide-Releasing Xerogels for <i>In Vivo</i> Chemical Sensing	27
1.6 <i>In Situ</i> and <i>In Vivo</i> Measurements of Nitric Oxide	31
1.6.1 Electrochemical Nitric Oxide Sensors	32
1.6.2 Optical Nitric Oxide Sensors	34
1.6.3 Protein-Based Nitric Oxide Biosensors	35
1.7 Summary of Dissertation Research	35
1.8 References	38
Chapter 2. Nitric Oxide-Releasing Xerogel Particle/Polyurethane Glucose Biosensors	49
2.1 Introduction	49
2.2 Experimental Section	51
2.2.1 Reagents and Materials	51
2.2.2 Effect of NO on Enzyme Activity in Solution	52
2.2.3 Effect of NO on MTMOS Xerogel-Based Glucose Biosensor	53
2.2.4 Sensor Performance Evaluation	53
2.2.5 Nitric Oxide-Releasing AEMP3/MTMOS Xerogel-Based Glucose Biosensor	54
2.2.6 Synthesis of <i>N</i> -Diazeniumdiolated Xerogel Particles	54
2.2.7 Preparation of <i>Hybrid</i> NO-Releasing Xerogel/Polyurethane Glucose Biosensors	55
2.2.8 Xerogel Particle Characterization	56
2.2.9 Bacterial Adhesion	56
2.3 Results and Discussion	57

2.3.1	Effect of NO on GOx	57
2.3.2	Effect of NO on GOx-Based Xerogel Films	59
2.3.3	<i>Hybrid</i> NO-Releasing Glucose Biosensors	65
2.4	Conclusions	74
2.5	References	75
Chapter 3. Sol–Gel Derived Amperometric Nitric Oxide Microsensor		80
3.1	Introduction	80
3.2	Experimental Section	83
3.2.1	Reagents and Materials	83
3.2.2	Preparation of Sol–Gel Derived Gas-Permeable Membranes	83
3.2.3	Sensor Performance Evaluation	85
3.2.4	Xerogel Material Characterization	86
3.2.5	Preparation and Evaluation of NO Microsensors	87
3.3	Results and Discussion	89
3.3.1	Optimization of Xerogel Composites as NO-Permselective Membranes	90
3.3.2	Xerogel Material Stability	102
3.3.3	Characterization of NO Microsensors	102
3.4	Conclusions	114
3.5	References	115
Chapter 4. Synthesis of Nitric Oxide-Releasing Silica Nanoparticles		121
4.1	Introduction	121
4.2	Experimental Section	125

4.2.1	Reagents and Materials	125
4.2.2	Synthesis of Nitric Oxide-Releasing Silica Nanoparticles	126
4.2.3	Characterization of Functionalized Silica	127
4.3	Results and Discussion	128
4.3.1	Synthesis and Characterization of Functionalized Silica Nanoparticles	128
4.3.2	Nitric Oxide Release Characteristics	133
4.4	Conclusions	141
4.5	References	143
Chapter 5. Nitric Oxide-Releasing Silica Nanoparticles: Synthesis, Characterization, and Efficacy Against Ovarian Cancer Cells		148
5.1	Introduction	148
5.2	Experimental Section	152
5.2.1	Reagents and Materials	152
5.2.2	Synthesis and Characterization of <i>N</i> -Diazeniumdiolate- Modified Aminoalkoxysilanes	154
5.2.3	Synthesis of Nitric Oxide Donor Silica Nanoparticles	155
5.2.4	Characterization of Functionalized Silica Nanoparticles	155
5.2.5	Cell Culture	156
5.2.6	Cell Viability Assay	156
5.2.7	Cellular Uptake	157
5.3	Results and Discussion	159
5.3.1	<i>N</i> -Diazeniumdiolate-Modified Aminoalkoxysilanes	159
5.3.2	Nitric Oxide Release Properties of Silica Nanoparticles	162

5.3.3 <i>In Vitro</i> Ovarian Cancer Cell Viability Studies	166
5.3.4 Cellular Uptake and Confocal Microscopy	171
5.4 Conclusions	176
5.5 References	178
Chapter 6. Summary and Future Research Directions	185
6.1 Summary	185
6.2 Future Research Directions	189
6.3 Conclusions	194
6.4 References	196

LIST OF TABLES

Table 1.1	Current major classes of NO donors	18
Table 2.1	Changes of solution GOx activity as a function of time	58
Table 2.2	Permeability of H ₂ O ₂ through xerogel membranes after exposure to NO and Ar for 1 h	63
Table 3.1	Electrochemical characteristics of sol–gel derived NO sensors as a function of xerogel composition and processing conditions	91
Table 3.2	Electrochemical characteristics of xerogel/Nafion composite NO sensors	101
Table 3.3	Stability of 20% AEMP3/MTMOS xerogels prepared with and without Nafion	103
Table 3.4	Performance comparison of electrochemical NO microsensors based on the direct electrooxidation of NO	109
Table 3.5	Performance comparison of electrochemical NO microsensors based on the catalytic electrooxidation of NO	111
Table 4.1	²⁹ Si chemical shifts (δ_{Si} from tetramethylsilane) and relative concentrations of T^n and Q^n structures for functionalized silica as a function of AEAP3 mol%	132
Table 4.2	NO release properties of <i>N</i> -diazoniumdiolate-modified silica nanoparticles with different tetraalkoxy- and aminoalkoxysilane precursors	136
Table 4.3	Nitrogen content (%N), amine concentration (C_{amine}), <i>N</i> -diazoniumdiolate concentration (C_{diaz}), and amine to <i>N</i> -diazoniumdiolate conversion efficiency (%Conv) of various silica nanoparticles prepared with different tetraalkoxy- and aminoalkoxysilane precursors	137
Table 5.1	Representative examples of the tumoricidal effect of previously reported small molecule NO donors against a variety of cancer cell lines <i>in vitro</i>	150
Table 5.2	Total NO concentration (t[NO]), half-life of NO release ($t_{1/2}$), and amine to <i>N</i> -diazoniumdiolate conversion efficiency (%Conv) of	

	<i>N</i> -diazoniumdiolate-modified primary/secondary and secondary amine-based alkoxysilanes	160
Table 5.3	NO release properties of <i>N</i> -diazoniumdiolate-modified silica nanoparticles with different amine ligands and contents prepared via post- and pre-charging strategies	163

LIST OF FIGURES

Figure 1.1	Illustrations of (A) pathological thrombus formation and (B) fibrous tissue encapsulation occurring at the blood- and tissue-contact interfaces, respectively	2
Figure 1.2	Schematic representation of non-specific bacterial adhesion to an implanted sensor surface	5
Figure 1.3	Biosynthesis of NO catalyzed by NOS enzyme in the body: (A) reaction scheme for the conversion of L-arginine to N^G -hydroxyl-L-arginine, followed by oxidation to L-citrulline and NO; and (B) overall catalytic reaction, cofactors, and the direction of electron flow in NOS	11
Figure 1.4	Chemical biology of NO representing its pathways for physiological and pathophysiological effects. Adapted from refs. 48 and 57	13
Figure 1.5	Reactions of NO with amine to produce (A) Zwitterionic and (B) anionic stabilized <i>N</i> -diazoniumdiolate NO donors followed by the subsequent release of NO in the presence of a proton. R_1 and R_2 represent side groups	21
Figure 1.6	Example structures of various <i>N</i> -diazoniumdiolate-modified amines and their half-lives ($t_{1/2}$) measured in phosphate-buffered saline (PBS) at pH 7.4 and 37 °C. Abbreviations: DEA, diethylamine; PIPERAZI, piperazine; EP, ethylputrescine; DETA, diethylenetriamine; DMHA, <i>N,N'</i> -dimethyl-1,6-hexanediamine; PROLI, proline; SPER, spermine; and DMAEP, 2-(dimethylamino)ethylputrescine	22
Figure 1.7	Schematic of sol-gel process illustrating (A) hydrolysis of silane precursors and (B) subsequent condensation reactions where R is typically a methyl or ethyl group and R' is an organic group for preparing functional xerogels	26
Figure 1.8	Structures of aminoalkoxysilanes: A) <i>N</i> -(2-aminoethyl)-3-aminopropyltrimethoxysilane (AEAP3); B) (aminoethylamino-methyl)phenethyltrimethoxysilane (AEMP3); C) <i>N</i> -(6-amino-hexyl)aminopropyltrimethoxysilane (AHAP3); and, D) <i>N</i> -[3-(trimethoxysilyl)propyl]diethylenetri-amine (DET3)	28
Figure 1.9	Schematic of NO generation from <i>N</i> -diazoniumdiolate-	

	modified xerogel network occurring upon exposure to aqueous conditions. <i>N</i> -[3-(Trimethoxysilyl)propyl]diethylenetriamine (DET3) was used as an example aminoalkoxysilane precursor	30
Figure 2.1	Calibration curves of glucose biosensors pre-soaked in (a) PBS (control); and (b) NO-saturated PBS for 1 h	60
Figure 2.2	Glucose response of (a) control and (b) NO exposed (5 atm NO for 1h) AEMP3/MTMOS glucose biosensors. (Inset) is the expansion of the response for the NO exposed biosensor	61
Figure 2.3	(A) Variations in permeability of H ₂ O ₂ through AEMP3/MTMOS films exposed to different pressure of NO for 1 h and controls. Electrodes were stored in PBS (pH 7.4) at ambient conditions between experiments. (B) Enlargement of graph (A)	64
Figure 2.4	Schematic of the <i>hybrid</i> xerogel/polyurethane glucose biosensor employing NO donor-modified xerogel particles in a polyurethane supporting matrix	66
Figure 2.5	NO release profiles from <i>hybrid</i> xerogel/polyurethane films cast from (●) 3, (○) 6, (▲) 12, and (□) 18 mg <i>N</i> -diazoniumdiolate-modified xerogel particles in 500 μL polyurethane solution	68
Figure 2.6	NO flux from <i>N</i> -diazoniumdiolated-modified xerogel particle/polyurethane films with (○) and without (●) a polyurethane protecting membrane (<i>n</i> = 3)	70
Figure 2.7	Dynamic glucose response and (Inset) calibration curves of biosensors (<i>n</i> =3) prepared with the following configurations: a) 2-layer (without XGP film); b) 4-layer (with unmodified XGP film); and c) 4-layer (with N ₂ O ₂ -SGP film). Initial and final concentrations are 1 and 31 mM, and the added concentration interval is 3 mM	71
Figure 2.8	Scanning electron microscopy images of surfaces of (A) polyurethane two-layer blank and (B) <i>N</i> -diazoniumdiolated-modified xerogel particle/polyurethane films	73
Figure 3.1	Schematic of the <i>hybrid</i> xerogel/Nafion-modified NO microsensor	88
Figure 3.2	(A) Solid-state ²⁹ Si NMR spectra of the AHAP3/BTMOS xerogel before (solid red line) and after (dashed blue line) NO exposure (5 atm, 1 h). (B) Cartoon representing structural changes in the porous network of xerogels after NO charging	93

Figure 3.3	NO permeability (bar graphs, for left axis) and selectivity over nitrite (scatter plots, for right axis) as a function of the concentration of AEMP3 (balance MTMOS) after exposure to 5 atm NO for 1 h. The dashed line indicates NO selectivity of the bare Pt electrode over nitrite	95
Figure 3.4	Static water contact angles as a function of AEMP3 composition (balance MTMOS) after exposure to 5 atm NO for 1 h	97
Figure 3.5	NO permeability (bar graphs, for left axis) and selectivity over nitrite (scatter plots, for right axis) as a function of the membrane thickness of 20% AEMP3/MTMOS xerogels after exposure to 5 atm NO for 1. The dashed line indicates NO selectivity of the bare Pt electrode over nitrite	98
Figure 3.6	NO permeability (bar graphs, for left axis) and selectivity over nitrite (scatter plots, for right axis) as a function of NO exposure time (5 atm) of 20% AEMP3/MTMOS. The dashed line indicates NO selectivity of the bare Pt electrode over nitrite ($n = 3$)	100
Figure 3.7	Dynamic response and calibration curves (inset) of the non-platinized (a) and platinized (b) Pt microelectrodes. The response sensitivity to NO was 19.8 ($r = 0.9919$) and 90.2 ($r = 0.9930$) pA/ μ M for the non-platinized and platinized Pt microsensors, respectively	105
Figure 3.8	Dynamic response to NO and interfering species, and calibration curve (inset) of the AEMP3/MTMOS/Nafion composite NO microsensors: (a) injection of 100 μ M each of nitrite, ascorbic acid, acetaminophen, and ammonia	106
Figure 3.9	Dynamic response and calibration curve (inset) of the MTMOS/AEMP3/Nafion composite NO microsensor in the extended NO concentrations: (a) 100 μ M of nitrite, (b) 100 μ M of ascorbic acid, and (c) 100 μ M of acetaminophen. The response sensitivity to NO was 67.7 pA/ μ M ($r = 0.9998$) from 5 to 15 μ M NO	108
Figure 3.10	Variations in response properties for NO (●, for left axis) and interfering species (○, for right axis) measured from 25 – 800 nM NO and 100 μ M each of nitrite, ascorbic acid, acetaminophen, and ammonia for the AEMP3/MTMOS/Nafion composite NO microsensor	113

Figure 4.1	Synthesis of <i>N</i> -diazoniumdiolate-modified silica nanoparticles using tetramethoxysilane (TMOS) and <i>N</i> -(6-aminohexyl)aminopropyltrimethoxysilane (AHAP3) as example tetraalkoxy- and aminoalkoxysilane precursors	124
Figure 4.2	Contact mode AFM images of (A) control silica (TEOS only); (B) silica with 10 mol% of AHAP3 (balance TEOS); and, (C) 10 mol% and (D) 17 mol% AEAP3 silica particles on a mica surface. (E) Enlargement of a single particle from (B). (F) Relationship between the AEAP3 content (balance TEOS) in the silica composite and particle size	130
Figure 4.3	(A) Solid-state ²⁹ Si CP/MAS NMR spectra of functionalized silica materials with various amounts of AEAP3: (a) 0 (control), (b) 10, (c) 13, and (d) 17 mol% (balance TEOS). (B) Schematic illustration of silicon chemical environments at the surface of AEAP3-modified silica composites. (C) Plot of % surface coverage (%SC) of functional ligands versus AEAP3 content loaded during the synthesis	131
Figure 4.4	(A) NO release profiles and (B) total NO release of 10 mol% of AHAP3 (dashed blue) and 17 mol% of AEAP3 (solid red) silica nanoparticles (balance TEOS)	135
Figure 4.5	NO release of AEAP3-based silica nanoparticles as a function of pH at 37 °C. Insert: total NO release	139
Figure 5.1	Schematic of NO delivery silica nanoparticles synthesized by two different strategies: A) post-charging; and, B) pre-charging approaches. Tetraethoxy-silane (TEOS) and <i>N</i> -(6-aminohexyl)-aminopropyltrimethoxysilane (AHAP3) were used as example tetraalkoxy- and aminoalkoxysilane precursors	153
Figure 5.2	Synthesis of fluorescein conjugated 3-aminopropyltrimethoxysilane (APTMS)	158
Figure 5.3	Example structures of secondary amine-based alkoxy-silanes studied	161
Figure 5.4	NO release profiles of 45 mol% of AHAP3 (a) and 77 mol% of MAP3 (b) silica nanoparticles. Insert: total NO concentration	164
Figure 5.5	Cytotoxicity of control and NO-releasing 45 mol% AHAP3 silica on A2780 ovarian epithelial tumor cells	168
Figure 5.6	Cytotoxicity comparison between small molecule (PYRRO/	

	N ₂ O ₂) and macromolecule (45 mol% AHAP3 silica/N ₂ O ₂) NO donors against human ovarian surface epithelial cancer cells (A2780)	169
Figure 5.7	Cytotoxicity of control and NO-releasing MAP3 silica nanoparticles on ovarian epithelial normal (T29, immortalized) and tumor (A2780) cell lines	170
Figure 5.8	Contact mode AFM images of 75 mol% S-MAP3 (A) and L-MAP3 (B)	172
Figure 5.9	Effect of the silica particle size (75 mol% MAP3, balance TEOS) on cytotoxicity against normal T29 and tumor A2780 cell lines. * <i>P</i> < 0.001 compared with control MAP3- treated group	173
Figure 5.10	Schematic of multifunctionalized silica nanoparticles synthesized via the “one-pot” co-condensation of three silane precursors including FITC-modified APTMS, <i>N</i> -diazoniumdiolated MAP3, and TEOS	174
Figure 5.11	Laser scanning microscope images of A2780 ovarian cancer cells taken at 5 min (A,C) and 60 min (B,D) after incubation with (A,B) FITC-labeled MAP3 silica nanoparticles and (C,D) 100 nm tetramethylrhodamine methyl ester (TMRM) mitochondrial stain	175
Figure 6.1	Illustration representing formation of the NO donor silica core/biodegradable polymer shell structure and its deformation/degradation	191
Figure 6.2	Folic acid activation and coupling to nanoparticle exterior: a) NHS, DCC, and DMSO; and b) primary amine terminated nanoparticle, DMSO	192
Figure 6.3	Synthesis of <i>N</i> -diazoniumdiolate-modified magnetic silica (core/shell) nanospheres	195

LIST OF ABBREVIATIONS AND SYMBOLS

$^{\circ}$	degree (of arc)
$^{\circ}\text{C}$	degree(s) Celsius
%	percentage(s)
%Conv	amine to <i>N</i> -diazoniumdiolate conversion efficiency
%N	nitrogen content percentage(s)
2N[2]-N ₂ O ₂	<i>N</i> -diazoniumdiolated <i>N</i> -(2-aminoethyl)-3-aminopropyltrimethoxy-silane ligand grafted on the silica surface
2N[6]-N ₂ O ₂	<i>N</i> -diazoniumdiolated <i>N</i> -(6-aminoethyl)aminopropyltrimethoxy-silane ligand grafted on the silica surface
±	statistical margin of error or tolerance
[N(O)NO] ⁻	diazoniumdiolate moiety
[NO] _m	maximum flux of NO release
$\alpha_{\text{NO},\text{NO}_2^-}$	permselectivity for nitric oxide over nitrite
ΔI_b	current response at the bare Pt electrode
ΔI_j	current response measured for interfering species <i>j</i>
ΔI_{NO}	current response measured for nitric oxide
ΔI_x	current response at the xerogel coated electrode
μA	microamp(s)
μg	microgram(s)
μL	microliter(s)
μm	micrometer(s)
μmol	micromole(s)
AAP3	3-(<i>N</i> -allylamino)propyltrimethoxysilane
AEAP3	<i>N</i> -(2-aminoethyl)-3-aminopropyltrimethoxysilane
AEMP3	(aminoethylaminomethyl)phenethyltrimethoxysilane
AFM	atomic force microscopy/microscope
Ag	silver
AgCl	silver chloride
AHAP3	<i>N</i> -(6-aminoethyl)aminopropyltrimethoxysilane
APTMS	aminopropyltrimethoxysilane
Ar	argon gas
atm	atmosphere(s)

BET	Brunauer-Emmett-Teller
BH ₄	(6 <i>R</i>)-5,6,7,8-tetrahydrobiopterin
BJH	Barrett-Joyner-Halenda
BTMOS	isobutyltrimethoxysilane
BuOH	buthanol
ca.	circa
Ca ²⁺	calcium ion
C _{amine}	amine concentration
C _{diaz}	<i>N</i> -diazoniumdiolate concentration
cfu	colony forming unit(s)
cGMP	cyclic guanosine monophosphate
cHAP3	cyclohexylaminopropyltrimethoxysilane
CHN	elemental (carbon hydrogen nitrogen)
<i>c_j</i>	concentration of interfering species <i>j</i>
Cl ⁻	chloride ion
cm	centimeter(s)
cm ²	square centimeter(s)
<i>c_{NO}</i>	concentration of nitric oxide
CO ₂	carbon dioxide gas
CP/MAS	cross polarization/magic angle spinning
Cr	chromium
Cu	copper
Cu ²⁺	copper ion
Cyt-P450	cytochrome P450
d	day(s)
<i>d</i>	diameter
DACA-6	<i>N</i> -(6-aminohexyl)-3-aminopropyltrimethoxysilane
DBHD/N ₂ O ₂	<i>N</i> -diazoniumdiolate-modified <i>N,N'</i> -dibutylhexanediamine
DCC	dicyclohexylcarbodiimide
DCP-OES	direct current plasma optical emission spectroscopy/spectrometer
DEA/N ₂ O ₂	<i>N</i> -diazoniumdiolate-modified diethylamine
DET3	<i>N</i> -[3-(trimethoxysilyl)propyl]diethylenetriamine
DETA/N ₂ O ₂	<i>N</i> -diazoniumdiolate-modified diethylenetriamine
DMAEP/N ₂ O ₂	<i>N</i> -diazoniumdiolate-modified 2-(dimethylamino)ethylputreanine
DMF	<i>N,N</i> -dimethylformamide
DMHA/N ₂ O ₂	<i>N</i> -diazoniumdiolate-modified <i>N,N'</i> -dimethyl-1,6-hexanediamine

DMSO	dimethyl sulfoxide
DNA	deoxyribonucleic acid
e ⁻	electron
e.g.	for example
EAI ₃	<i>N</i> -ethylaminoisobutyltrimethoxysilane
EDRF	endothelium-derived relaxing factor
<i>e</i> _{immo}	ligand immobilization efficiency
eNOS	endothelial nitric oxide synthase
EP/N ₂ O ₂	<i>N</i> -diazoniumdiolate-modified ethylputreanine
EPR	electron paramagnetic resonance
<i>et al.</i>	and others
etc.	and so forth
ETMOS	ethyltrimethoxysilane
EtOH	ethanol
FAD	flavin adenine dinucleotide
FBS	fetal bovine serum
Fe	iron
FeCl ₃	ferric chloride
Fe ₃ O ₄	magnetite
FITC	Fluorescein isothiocyanate
FK409	(+/-)-(4-ethyl-2E-(hydroxyimino)-5-nitro-3E-hexaneamide)
FMN	flavin mononucleotide
FR	folate receptor
g	gram(s)
GOx	glucose oxidase
GTN	glyceryl trinitrate
GTP	guanosine triphosphate
h	hour(s)
H ⁺	hydrogen ion
H ₂ O ₂	hydrogen peroxide
HCl	hydrochloric acid
heme	iron protoporphyrin IX
HEPES	<i>N</i> -2-hydroxyethylpiperazine- <i>N</i> '-2-ethanesulfonic acid
HNO	nitroxyl
HOSE	human ovarian surface epithelial
HPU	hydrophilic polyurethane

HRP	horseradish peroxidase
Hz	hertz(s)
i.d.	inside diameter
IAN	isoamyl nitrite
IBN	isobutyl nitrite
IC ₅₀	50% inhibitory concentration
IgG	immunoglobulin G
<i>j</i>	interfering species
i.e.	that is
iNOS	inducible nitric oxide synthase
K	kelvin(s)
K ⁺	potassium ion
K_{NO,NO_2}^{amp} , $K_{NO,j}^{amp}$	selectivity coefficient for nitric oxide over nitrite or interfering species <i>j</i> , which is determined amperometrically
KCl	potassium chloride
kDa	kilodalton(s)
kHz	kilohertz(s)
KOH	potassium hydroxide
L	liter(s)
L-MAP3	<i>N</i> -diazoniumdiolate-modified silica particle with 350 ± 50 nm in diameter
M	molar concentration
<i>m</i> -	meta position of two substituents
m ²	square meter(s)
MΩ	megohm(s)
MAHMA/N ₂ O ₂	(<i>Z</i>)-1-(<i>N</i> -methyl- <i>N</i> -[6-(<i>N</i> -methylammoniohexyl)amino]diazene)-1-ium-1,2-diolate or <i>N</i> -diazoniumdiolated <i>N,N'</i> -dimethyl-1,6-hexanediamine
MAP3	methylaminopropyltrimethoxysilane
MeO ⁻	methoxide
MeOH	methanol
mg	milligram(s)
MHz	megahertz(s)
MIC	minimum inhibitory concentration
min	minute(s)
mL	milliliter(s)

mM	millimolar concentration
mm	millimeter(s)
mmol	millimole(s)
Mn	manganese
mol	mole(s)
mol%	mole percentage(s)
MOM-PIPERAZI/N ₂ O ₂	methoxymethyl-protected <i>N</i> -diazoniumdiolated piperazine
mompipPVC/N ₂ O ₂	methoxymethyl-protected <i>N</i> -diazoniumdiolated piperazine-poly(vinyl chloride)
MTMOS	methyltrimethoxysilane
MTT	3-(4,5-dimethylthiazol-2-yl)-2,5-diphenyltetrazolium bromide
MW	molecular weight
<i>n</i>	number of samples
<i>N</i> -	nitrogen bound
<i>N</i> -diazoniumdiolate	1-amino-substituted diazen-1-ium-1,2-diolate
n/a	not applicable or not available
N ₂	nitrogen gas
N ₂ O ₂	diazoniumdiolate moiety
N ₂ O ₂ -XGP	<i>N</i> -diazoniumdiolate-modified xerogel particle
N ₂ O ₃	dinitrogen trioxide
N ₂ O ₄	dinitrogen tetroxide
nA	nanoamp(s)
Na ⁺	sodium ion
NaCl	sodium chloride
NADP ⁺	oxidized nicotinamide adenine dinucleotide phosphate
NADPH	reduced nicotinamide adenine dinucleotide phosphate
NaOMe	sodium methoxide
nBAP3	<i>n</i> -butylaminopropyltrimethoxysilane
NH ₂ OH	hydroxylamine
NH ₄ OH	ammonia solution or ammonia water
NHS	<i>N</i> -hydroxysuccinimide
Ni	nickel
Ni-TMPP	monomeric tetrakis(3-methoxy-4-hydroxyphenyl) nickel porphyrin
nM	nanomolar concentration
nm	nanometer(s)
NMR	nuclear magnetic resonance

nNOS	neuronal nitric oxide synthase
NO	nitric oxide
NO ⁺	nitrosonium ion
NO ₂	nitrogen dioxide
NO ₂ ⁻	nitrite
NO ₃ ⁻	nitrate
NOS	nitric oxide synthase
<i>o</i> -	ortho position of two substituents
o.d.	outside diameter
O ₂	oxygen gas
O ₂ ⁻	superoxide
OCH ₃	methoxy group
OD _{λ=600}	optical density at 600 nm of wavelength
OH ⁻	hydroxide ion
ONOO ⁻	peroxynitrite
$P_{NO}^e, P_{NO_2}^e$	permeability to nitric oxide (or nitrite) measured electrochemically
<i>P. aeruginosa</i>	<i>Pseudomonas aeruginosa</i>
pA	picoamp(s)
PAP3	phenylaminopropyltrimethoxysilane
PBS	phosphate-buffered saline
<i>P</i> CO ₂	partial pressure of carbon dioxide
PDMS	poly(dimethylsiloxane)
PEG	poly(ethylene glycol)
PEI/N ₂ O ₂	<i>N</i> -diazoniumdiolate-modified poly(ethyleneimine)
PEO	poly(ethylene oxide)
pH	-log of proton concentration
pHEMA	poly(hydroxyethyl methacrylates)
PIPERAZI/N ₂ O ₂	<i>N</i> -diazoniumdiolate-modified piperazine
PLGA	poly(lactic acid-co-glycolic acid)
pM	picomolar concentration
pmol	picomole(s)
<i>P</i> O ₂	partial pressure of oxygen
ppb	part(s) per billion
ppm	part(s) per million
PrOH	propanol

PROLI/N ₂ O ₂	<i>N</i> -diazoniumdiolate-modified proline
Pt	platinum
PTFE	poly(tetrafluoroethylene)
PVC	poly(vinyl chloride)
PVP	polyvinylpyrrolidone
PYRRO/N ₂ O ₂	<i>N</i> -diazoniumdiolate-modified pyrrolidin
R, R', R ₁ , R ₂	organic functional group
<i>r</i>	correlation coefficient
RNOS	reactive nitrogen oxide species
ROS	reactive oxygen species
rpm	rotation(s) per minute
RPMI	Roswell Park Memorial Institute
<i>S</i> -	sulfur bound
<i>s</i> -MAP3	<i>N</i> -diazoniumdiolate-modified silica particle with 90 ± 10 nm in diameter
S/N	signal to noise ratio
<i>s</i> , sec	second(s)
<i>S</i> _{BET}	surface areas determined by BET analysis
SC	surface coverage
<i>s</i> GC	soluble guanylate cyclase
Si	silicon
Si–O–Si	siloxane bridge
Si–OH	silanol group
Si–OR	alkoxy
SNAP	<i>S</i> -nitroso- <i>N</i> -acetyl-DL-penicillamine
SNP	sodium nitropusside
SOD	superoxide dismutase
SPER	spermine
SPER/N ₂ O ₂	<i>N</i> -diazoniumdiolate-modified spermine
SR	silicone rubber
<i>t</i>	time
<i>t</i> _{1/2}	half-life of NO release
<i>t</i> _{95%}	time to reach 95% of the steady-state response
t[NO]	total concentration of NO released
tBAP3	t-butylaminopropyltrimethoxysilane
TEOS	tetraethoxysilane

THF	tetrahydrofuran
t_m	time necessary to reach $[\text{NO}]_m$
TMOS	tetramethoxysilane
TMRM	tetramethylrhodamine methyl ester
TMS	tetramethylsilane
TPU	Tecoflex polyurethane
TSB	tryptic soy broth
UV	ultraviolet
V	volt(s)
v/v	volume/volume
v-tpy	4'-vinyl-2,2',6',2''-terpyridyl
Vis	visible
V_p	pore volume
vs.	versus
wt%	weight percentage(s)
XGP	xerogel particle
Zn	zinc

Chapter 1:
Improving the Biocompatibility of *In Vivo* Sensors via
Nitric Oxide Release

1.1 *In Vivo* Sensor Biocompatibility

The demand for implantable chemical sensors capable of monitoring the physiological status of patients on a continuous, real-time basis under physiological conditions continues to be of great importance in human health care.¹⁻⁴ *In vivo* sensors must operate reliably, rapidly, and selectively over extended periods under harsh conditions. Despite considerable efforts, designing *in vivo* sensors for clinical use remains a major challenge due to compromised sensor performance upon implantation and severe health risks to the implant recipient. These serious obstacles result primarily from undesirable interactions between the sensor surface and biological milieu.^{1,5} Indeed, the insertion of a foreign material into the body brings about immediate physiological responses that are dependent upon the location of indwelling probes (i.e., blood, tissue, etc.).

Blood-contacting sensors trigger a biofouling cascade including protein adsorption, platelet adhesion/activation, and surface-induced thrombosis (Figure 1.1A).^{1,6-9} Such biofouling often plagues intravascular sensors. The adsorption of plasma proteins (e.g., fibrinogen and von Willebrand factor) on the implant surface is the first stage of the surface fouling process. Platelets adhere to surface-bound proteins via the expression of platelet receptors (e.g., glycoprotein IIb/IIIa), and then spread on the surface to form aggregates with

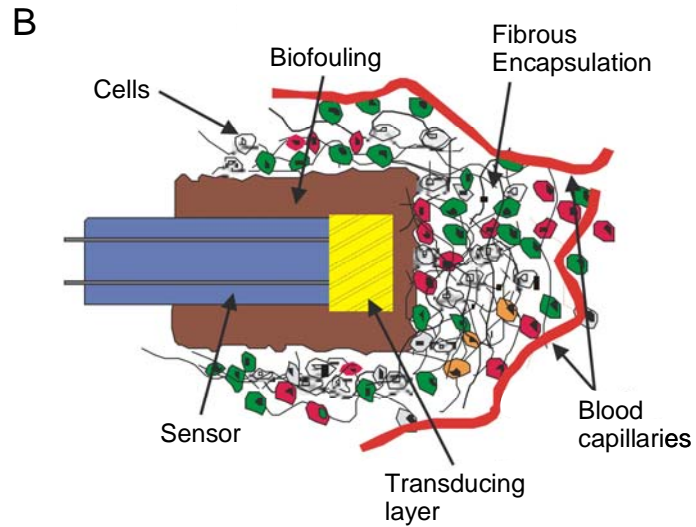
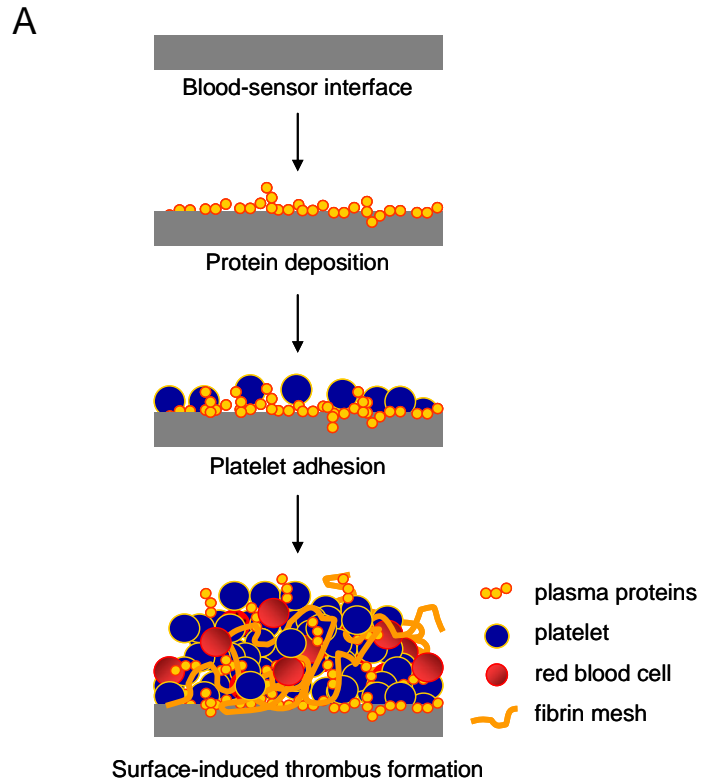


Figure 1.1. Illustrations of (A) pathological thrombus formation and (B) fibrous tissue encapsulation occurring at the blood- and tissue-contact interfaces, respectively.^{1,5}

adjacent platelets via interactions with fibrinogen and other plasma ligands. Platelet aggregation triggers structural changes in the organization of the surface membrane, leading to exposure of a highly procoagulant lipid surface to blood, which facilitates thrombin activation. Thrombin then serves to convert fibrinogen to a polymeric fibrin mesh, subsequently resulting in the accumulation of a dense network of fibrin, platelets, and entrapped blood cells, known as a thrombus (blood clot). Surface fouling leads to significant deterioration in sensor reliability and/or longevity.^{1,10,11} The adsorption of metabolically active cells (e.g., platelets) alters the chemical environment adjacent to the implant via consumption of oxygen (O₂) and production of carbon dioxide (CO₂), subsequently lowering the local or measured pH. Furthermore, normal blood flow may be inhibited by the presence of the thrombus and/or constriction of the vascular walls around the implant, increasing the risk of thrombo-embolism.

Sensors implanted in the subcutaneous tissues are more susceptible to cell adhesion and fibrous tissue encapsulation in response to the body's self-defense mechanisms.^{4,12-15} Upon implantation, tissue is disrupted and capillaries damaged, concomitantly initiating a wound healing cascade (i.e., immune response), consisting of four distinct stages that are expressed at different times ranging from seconds to weeks: 1) hemostasis, 2) inflammation, 3) repair, and 4) encapsulation (Figure 1.1B). The acute inflammatory response takes place within seconds after the sensor is implanted. During this stage, proteins and inflammatory cells adsorb to the sensor surface. Phagocytic cells (e.g., neutrophils, monocytes, and macrophages) then surround the device (minutes to hours later) and attempt to destroy it. Such membrane biofouling is detrimental to sensor function resulting in restriction of analyte diffusion to the sensor and/or degradation of the sensor membrane. Macrophages adsorbed

closely to the sensor surface also perturb local concentrations of analytes due to the consumption of glucose and O₂, and the release of reactive oxygen species (ROS; e.g., H₂O₂, O²⁻, and OH). During the repair or wound healing stage (occurring days later), the tissue surrounding the implant becomes increasingly avascular as the body attempts to encapsulate and isolate the foreign material. Encapsulation further aggravates the flux of analyte to the sensor surface.

An equally challenging problem affecting *in vivo* sensors to be implanted for extended periods is bacterial adhesion that can lead to infection with serious risks to implant recipients.¹⁶⁻²⁰ The initial adhesion of bacterial cells is preceded by the surface adsorption of a conditioning film of small organic compounds and macromolecules including proteins. Subsequently, the physicochemical forces that mediate bacterial adhesion can be divided into two time-dependent phases (Figure 1.2).^{16,18} Phase I involves reversible cellular association with the surface of the indwelling device over the first 1 – 2 h post-implantation. This non-specific association is mediated through long-range (e.g., gravitational, van der Waals, and electrostatic interactions) and short-range (e.g., hydrogen bonding, dipole-dipole, ionic, and hydrophobic interactions) forces. Phase II begins 2 – 3 h later and is characterized by stronger adhesion between the bacteria and the foreign material. Specific chemical reactions between compounds on the bacterial cells and the substrate surface result in irreversible molecular bridging. Beyond Phase II (approximately 1 d after), certain bacterial strains are capable of secreting a protective polymeric shield (biofilm) consisting of exopolysaccharides. Once formed, biofilms are formidable physiological and chemical barriers, impeding both phagocytosis by the body's immune system and the action of conventional antibiotic therapies. As a result, implant recipients often suffer from serious and persistent infections

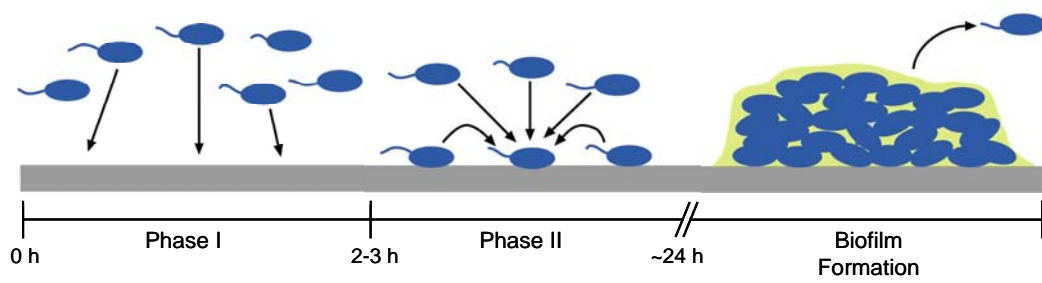


Figure 1.2. Schematic representation of non-specific bacterial adhesion to an implanted sensor surface.^{18,19}

that necessitate removal of the implanted device.

1.2 Strategies for Improving the Biocompatibility of *In Vivo* Sensors

Tremendous research has been devoted to developing coatings with improved blood and tissue compatibility and reduced bacterial adhesion/infection via either passive or active strategy.²¹ “Passive” coatings form a barrier to prevent protein and/or cell adhesion and proliferation by suppressing undesirable non-specific interactions (e.g., van der Waals, hydrophobic, and electrostatic forces). “Active” biomaterials are designed to controllably release an anticoagulant or antimicrobial agent at the implant site to reduce thrombus formation and pathogenic infection, respectively.

1.2.1 Passive Biomaterials

Biological interactions occurring at the blood- or tissue-contact interface are directly affected by a number of physicochemical properties including wettability, structural rigidity and morphology, hydrogen-bonding interactions, polarity, and surface roughness and charge.^{21,22} Passive coatings have been developed by manipulating these physicochemical properties of the materials via the use of new synthetic polymers distinctively designed as a medical-grade biomaterial and/or the surface modification of the existing polymers.

Synthetic polymers such as polyurethane, silicone rubber, poly(vinyl chloride) (PVC), polystyrene, and Nafion have been employed in biomedical applications because they are easy to manufacture and inexpensive, and can be prepared with a wide range of chemical and physical properties.²³⁻²⁹ Polyurethanes are a family of block copolymers consisting of alternating hard- and soft-segment units joined via urethane linkages.²⁵ Some medical-grade polyurethanes such as Tecoflex and Pellethane (polyether-based thermoplastic elastomers)

have been exploited not only for manufacturing implantable devices but also for formulating *in vivo* or *in vitro* ion sensors and biosensors.³⁰⁻³² Silicone rubber is an elastomeric hydrophobic polymer that has a backbone of silicon-oxygen bonds.^{23,28} This class of polymers is suitable for medical sensor applications because it is mechanically robust, chemically inert, and gas permeable, and has a high degree of biocompatibility.

Several polymeric materials including hydrogels, phospholipid-based biomimicry, Nafion, surfactant-derived membranes, diamond-like carbons, and anticoagulant-grafted films, have also been used to modify the sensor surface to passively suppress protein and cell adhesion.^{20,21,33-39} The hydrogel layer can be prepared by either incorporating or immobilizing hydrophilic polymeric chains including poly(ethylene glycol and oxide) (PEG and PEO) and poly(hydroxyethyl methacrylate) (pHEMA) to conventional polymers (e.g., polyurethane and PVC).⁴⁰ The hydrophilic nature of these hydrogels results in low interfacial energy between the sensor surface and the aqueous surrounding, thereby minimizing protein adsorption. In addition, the hydrophilicity of the polymer can be altered through gaseous (e.g., oxygen and argon) plasma exposure. Triandafillu *et al.* reported that after oxygen plasma treatment the wettability of PVC films was dramatically increased (water contact angle change from 80° to 10°), leading to significant inhibition of *Pseudomonas aeruginosa* adhesion (70% decrease).⁴¹ Nafion, a perfluorosulfonate-based anionic polymer with both hydrophilic and hydrophobic domains, has been widely used as a coating for indwelling chemical and biosensors.^{24,27,39} The polyanionic property of this material is useful to both exclude anionic interfering species from the sensor surface and prevent protein adsorption. Though successful at short periods (<10 d), the clinical use of Nafion-modified sensors still remains limited due to material degradation and long-term membrane fouling. Finally,

despite sterilization and aseptic procedures, bacterial infection remains a great impediment to the utility of all indwelling devices.¹⁷ Although helpful in minimizing bacteria, sterilization is often destructive (e.g., polymer degradation) and does not eliminate the risk of bacterial infection. Therefore, the approaches to date have not proven effective clinically (i.e., *in vivo*).

1.2.2 Active Biomaterials

Strategies based on the use of more “active” biomaterials designed to controllably release or generate an anticoagulant (e.g., heparin)^{36,38} or antimicrobial agent (e.g., antibiotics)^{42,43} at the implant site have thus been pursued. Active biomaterials interact with proteins or organisms on a molecular/cellular level, inhibiting protein activation or disrupting metabolic and replication processes to prohibit cell function.

Heparin is a highly sulfated glycosaminoglycan widely used as an anticoagulant and is used to decrease the clotting ability of the blood via the rapid complex with antithrombin III and inactivation of thrombin, thus preventing the conversion of fibrinogen to fibrin.³⁶ For example, Michanetzis *et al.* demonstrated the haemocompatibility improvement of several heparin-modified biomaterials prepared via either direct incorporation or indirect surface grafting of heparin to four polymer systems (i.e., silicone rubber, PVC, polyethylene, and polypropylene).³⁸ All heparinized polymers exhibited significantly reduced platelet adhesion and aggregation due to slow leaching of heparin under physiological conditions. In particular, heparinized PVC synthesized via the grafting method was characterized by the most effective yield of heparin immobilization. While anticoagulant treatment may be useful for preventing thrombus formation at the blood-material interface, it may also lead to undesirable systemic effects (e.g., uncontrolled bleeding), a serious problem for patients who suffer from medical conditions such as hemophilia, renal failure, or thrombocytopenia that affect blood

clotting.^{38,44}

Similar to the controlled release of anticoagulants, antibiotics have also emerged into the polymer matrix as a potential antimicrobial additive to actively resist bacterial adhesion and infection. Schierholz *et al.* reported on the synthesis of biomedical polyurethane coatings that locally delivery and release antibiotics (e.g., ciprofloxacin and gentamycin) at the implant site.⁴³ The antibacterial efficacy of these coatings is strongly dependent on the antibiotic release profile from the polymer as a function of chemical compatibility (e.g., hydrophobicity) between the drug and the polymer and drug distribution within the matrix. In addition, polyclonal antibodies (e.g., IgG) integrated into a polyurethane matrix have proven effective at reducing bacterial adhesion *in vitro*.⁴⁵ However, antibiotics in general are becoming less effective due to antibiotic resistance among pathogens and the related side effects often associated with such drugs.⁴⁶ Polymers doped with antibodies may also have *in vivo* complications associated with the host's immune system.⁴⁷ Consequently, the development of a truly biocompatible sensor has not yet been realized, despite significant advances in designing synthetic polymers for *in vivo* sensor applications.

1.3 Nitric Oxide and Prevention of Biofouling

Nitric oxide (NO), a diatomic free radical is one of the smallest and simplest biologically active molecules in mammalian species.⁴⁸ Since the first discovery of NO as a vasodilatory messenger and, in particular, after its identification as an endothelium-derived relaxing factor (EDRF) in the middle of 1980s, research efforts have been devoted to elucidating the pathways of NO generation and action *in vivo*.⁴⁹ To date, researchers have discovered that NO regulates a range of crucial biological processes in the cardiovascular, gastrointestinal, genitourinary, respiratory, and central and peripheral nervous systems.^{48,49} In

fact, these discoveries led to the designation of NO as the “Molecule of the Year” in 1992 by *Science* magazine.⁵⁰ Furthermore, three American scientists, Robert F. Furchgott, Louis J. Ignarro, and Ferid Murad, were awarded the Nobel Prize in Physiology or Medicine in 1998 for their discoveries linking “Nitric Oxide as a Signaling Molecule in the Cardiovascular System.” The relatively recent discovery of NO as a potent inhibitor of platelet adhesion and activation, and its identification as both an antimicrobial agent and angiogenic factor have extended NO research to the field of biomaterials.^{48,51-53}

1.3.1 Endogenous Pathway of Nitric Oxide Generation

Nitric oxide is endogenously synthesized in the human body via L-arginine catabolism whereby L-arginine is converted to L-citrulline by a class of enzymes known as nitric oxide synthase (NOS).^{48,54} As shown in Figure 1.3, L-arginine is first hydroxylated to *N*^G-hydroxyl-L-arginine in the presence of reduced nicotinamide adenine dinucleotide phosphate (NADPH) and oxygen (O₂).⁵⁴ This enzyme-bound intermediate is consequently oxidized to L-citrulline and NO, with additional consumption of NADPH and O₂. This biocatalytic process requires bound cofactors, including (6*R*)-5,6,7,8-tetrahydrobiopterin (BH₄), flavin adenine dinucleotide (FAD), flavin mononucleotide (FMN), calmodulin, and iron protoporphyrin IX (heme). Briefly, an electron (e⁻) is donated by NADPH to the reductase domain of the enzyme NOS and proceeds via FAD and FMN redox carriers to the oxygenase domain, where it interacts with the heme iron and BH₄ at the active site to catalyze the reaction of O₂ with L-arginine, generating L-citrulline and NO. The electron flow through the reductase domain requires the presence of bound calcium ion (Ca²⁺)/calmodulin.

Three distinct isoforms of NOS have been identified, ranging in molecular weight from about 130 - 160 kDa: neuronal, endothelial, and inducible types.^{55,56} Each isoforms is

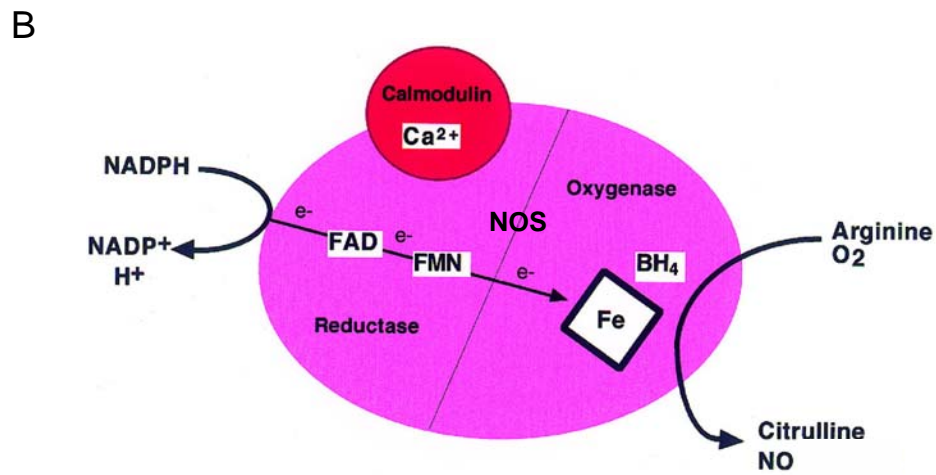
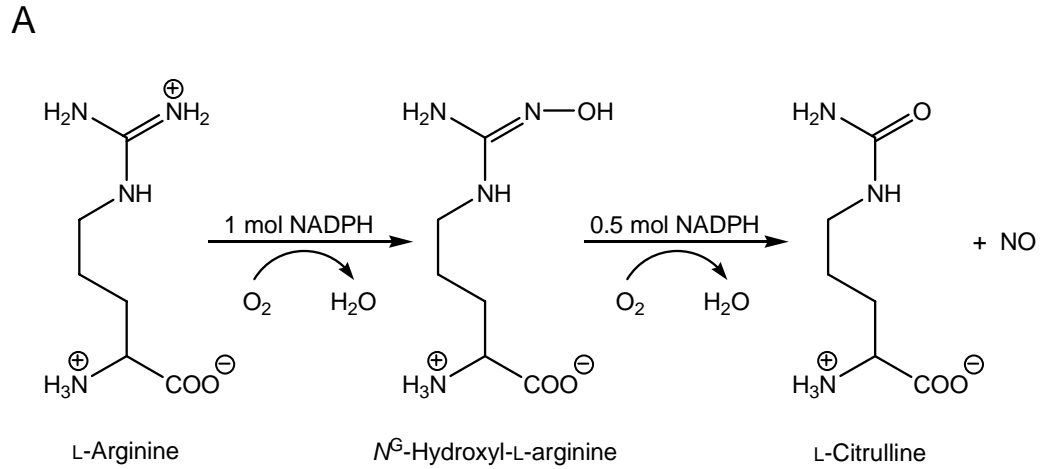


Figure 1.3. Biosynthesis of NO catalyzed by NOS enzyme in the body: (A) reaction scheme for the conversion of L-arginine to N^G -hydroxyl-L-arginine, followed by oxidation to L-citrulline and NO; and (B) overall catalytic reaction, cofactors, and the direction of electron flow in NOS.^{48,54}

associated with a particular physiological function. Neuronal NOS (nNOS) is involved in neurotransmission and long-term potentiation. Endothelial NOS (eNOS) regulates vasodilation, smooth muscle relaxation, and blood pressure. These two isoforms (i.e., nNOS and eNOS) represent constitutive enzymes, modulated by Ca^{2+} influxes (Ca^{2+} -dependent), and generate a relatively small amount ($\sim\text{nM}$) of NO. Conversely, inducible NOS (iNOS) is found in many cell types (e.g., macrophages) and is mediated by inflammatory cytokines and host defense stimuli. The iNOS produces high levels ($\sim\mu\text{M}$) of NO for extended periods of time. At micromolar concentrations, NO participates in a response to pathogens and tumor cells. This iNOS has tightly bound calmodulin with Ca^{2+} , and therefore functions via a Ca^{2+} -independent mechanism.

1.3.2 Biological and Pathobiological Roles of Nitric Oxide

The complex and wide ranging roles of NO in biology are primarily determined by its chemical properties.^{48,57} Most of the actions of NO are ascribed to either its free radical nature or its participation in a number of redox reactions. In an attempt to ascertain the pertinence of these diverse reactions to biological systems, Wink and coworkers introduced the concept of “the chemical biology of NO.”⁵⁷ This scheme divides the NO’s chemical reactions into two categories: direct and indirect effects (Figure 1.4).^{48,57}

Direct effects of NO are attributed to reactions that are fast enough to occur between specific biological targets and NO at nanomolar concentrations (generated by nNOS or eNOS).⁵⁵ Of several types of reactions of NO with metals and radicals, nitrosyl formation with a metal (usually iron)-centered heme is particularly facile and should be of primary consideration in any mechanism involving NO. Many basic regulatory actions of NO engage in interactions preferentially with heme complexes including guanylate cyclase and

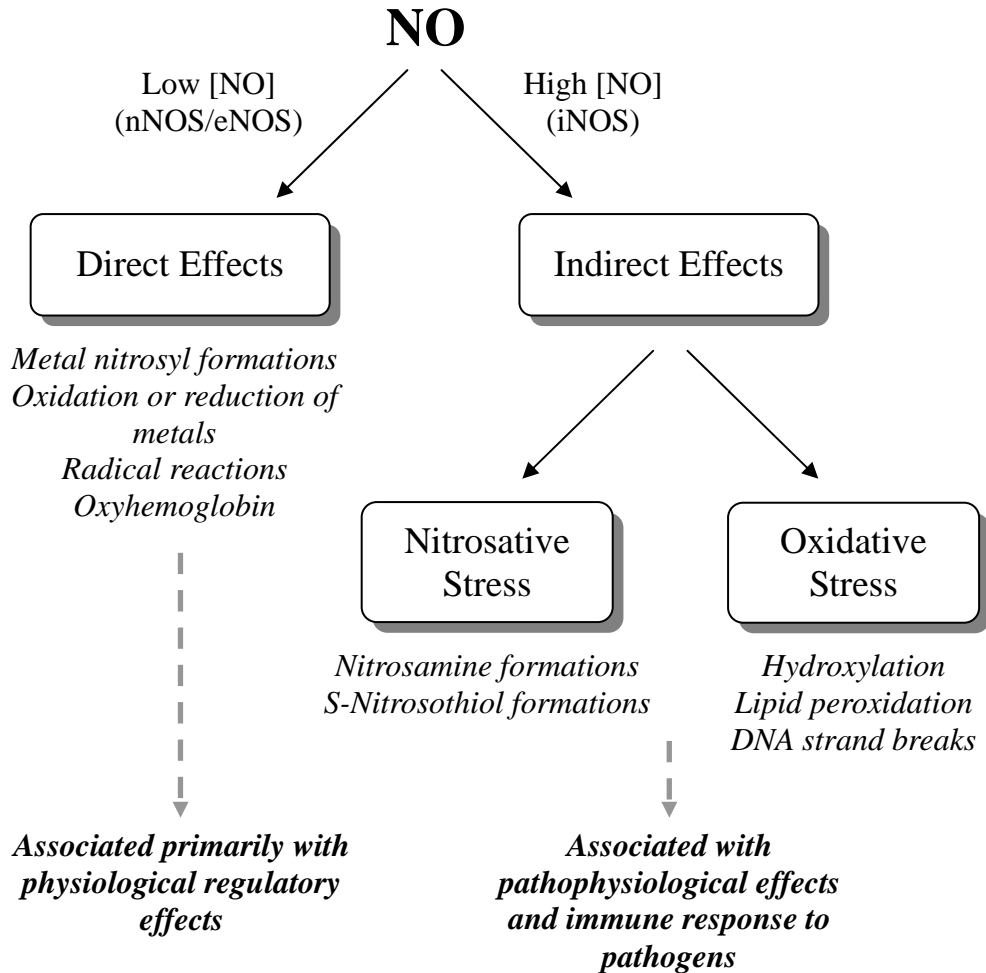


Figure 1.4. Chemical biology of NO representing its pathways for physiological and pathophysiological effects. Adapted from refs. 48 and 57.

cytochrome P-450.⁵⁸ *In vivo*, the most notable heme protein that forms an iron–NO adduct is soluble guanylate cyclase (sGC), an enzyme involved in vasodilation and neurotransmission.⁵⁹ In the presence of NO, the iron heme of sGC is highly susceptible to formation of the five-coordinate nitrosyl complex by decoupling the distal histidine. This configurational change in the protein activates the enzyme, leading to conversion of guanosine triphosphate (GTP) to cyclic guanosine monophosphate (cGMP). Ultimately, the increased production of cGMP results in the relaxation of smooth muscle, thereby mediating vasodilation. This mechanism (i.e., the NO-induced activation of sGC) is also responsible for both regulating blood flow and pressure and modulating platelet activity. Furthermore, subsequent studies have revealed that NO binds directly to other heme-containing proteins including hemoglobin, peroxidase, NOS, and myoglobin.^{55,60}

Indirect effects of NO arise via intermediate formation of reactive nitrogen oxide species (RNOS; e.g., NO₂, NO₂⁻, ONOO⁻, and N₂O₃) derived from the reactions of NO with either O₂ or superoxide (O₂⁻). Such indirect effects require much higher concentrations (~μM) of NO (generated by iNOS). These RNOS are generally more reactive than NO itself and associated with the immune system and pathological mechanisms of NO. Indirect effects can be further divided into two categories of nitrosative and oxidative stress.⁶¹

In nitrosative stress, two equivalents of NO react with O₂ to form dinitrogen tetraoxide (N₂O₄), which can quickly decompose into nitrogen dioxide (NO₂) under physiological conditions.⁶¹ Subsequently, dinitrogen trioxide (N₂O₃) is generated through the coupling of NO and NO₂. Thiols and amines are the biological targets for nitrosation reactions involving N₂O₃ and N₂O₄. The nitrosative NO-derived species (e.g., N₂O₃) are trapped by thiols to yield S-nitroso compounds, species believed to play a role in NO transport and storage.⁶² S-

Nitrosation of free thiols in proteins also disrupts DNA repair and enzyme function by displacing metallothionein pairs or creating disulfide bridges. Nitrosative reactions with primary and secondary amines have been linked to the creation of DNA mutations through the deamination of nucleic acids and DNA damage and carcinogenesis via nitrosamine formation, respectively.^{63,64}

Oxidative stress involves NO's reacts with O_2^- at diffusion-controlled rates yielding the potent oxidizing species, peroxynitrite ($ONOO^-$), which is theorized as a primary pathway of macrophage-mediated cell death.^{65,66} The oxidative reactions from $ONOO^-$ also lead to the oxidation of thiols, lipid peroxidation, and the cleavage of DNA strands.^{67,68} Nitrite (NO_2^-), the end-product of NO autoxidation and ubiquitous degradation product of NO under aqueous conditions, and nitrate (NO_3^-), the stable end-product of NO's reaction with oxygenated heme proteins, both participate in NO elimination reactions.

1.3.3 Implications of Nitric Oxide for Designing *In Vivo* Sensors

The four biological roles of NO including thromboresistivity, phagocytosis, wound healing, and angiogenesis may effectively help reduce biofouling and increase blood flow, thus minimizing the body's response that tend to diminish the performance of *in vivo* sensors (for monitoring K^+ , Na^+ , Ca^{2+} , Cl^- , pH, PCO_2 , PO_2 , glucose, and lactate, for example). The non-thrombogenic properties of the vascular endothelium are primarily attributed to NO.^{69,70} Both basal and stimulated endothelial cells continuously release NO into the lumen of blood vessels at an estimated flux of $0.5 - 1.0 \times 10^{-10} \text{ mol}\cdot\text{cm}^{-2}\cdot\text{min}^{-1}$.⁷¹ The NO release regulates blood flow and pressure, and prevents platelet aggregation under normal conditions. The generation of NO by macrophages has been implicated in fighting invading microorganisms (e.g., bacteria).⁴⁸ Monocytes and macrophages stimulated by foreign cells produce NO to

destroy such pathogens via pathways mediated by NO and its RNOS (e.g., ONOO⁻ and N₂O₃). Nitric oxide plays a role in wound healing. Although NO's action in this process is not fully understood, NO may mediate immune and inflammatory responses. Finally, NO's action is involved in angiogenesis or the formation and growth of new blood vessels.⁴⁸ With respect to subcutaneous sensor applications, NO may allow for increased blood flow to or near the sensor surface, thus enhancing mass transfer of analyte, while reducing bacterial adhesion and associated infection risks.

In addition to NO's numerous biological and pathobiological functions, its effects are localized due to its short half-life (ranging from 1 s to a few minutes depending on the concentration of oxygen and the presence of NO scavengers such as oxyhemoglobin) in biological milieu.^{48,72} For example, NO released from the surface of a sensor is rapidly consumed via reactions with oxygen and other scavengers (e.g., hemoglobin and thiols). Thus, certain health risks associated with systemic administration of anticoagulants and antibiotics may be avoided by employing NO-release coatings.

1.4 Synthetic Nitric Oxide Donors

Elucidating the complex and multifaceted roles of NO in physiology demands methods for stable storage and specific delivery of NO to biological targets. Because of the limited utility of NO gas in experimental systems and its instability in the presence of oxidants (e.g., oxygen, oxyhemoglobin, and thiols), synthetic compounds that chemically store and release NO in a controlled fashion have been developed. Such "NO donors" facilitate the improved understanding of the pivotal function of NO in biological systems and may potentially serve as therapeutic agents for a number of disease states.

1.4.1 Major Classes of Nitric Oxide Donors

Although little had been known about their physiological mechanism of action, nitroglycerin and nitroprusside NO donors have been used for medicinal purposes since the mid-1800s.^{73,74} The growing interest of NO in biology since the middle of 1980s has led to the development of new NO donors that offer several advantages over nitroglycerin and nitroprusside, including spontaneous release of NO, donation of NO under controlled rates, and even the targeting of NO to certain tissues.

Due to the structural diversity of NO donors, the pathways for NO generation by each class of compounds may differ significantly.^{73,74} As each class of compound offers distinct biochemical properties, it allows one to choose a compound that best meets the demands of specific investigations. Classification of all NO donors can be confusing, since all nitrogen- or oxygen-bound compounds have the potential to decompose, be oxidized, or be reduced to reactive nitrogen species. However, similar chemical structures usually have a similar NO-releasing mechanism, so all current major classes of NO donors and their pathways of NO generation are summarized in Table 1.1 according to their chemical classification.⁷⁵⁻⁹⁰

1.4.2 Diazeniumdiolate Chemistry

A number of synthetic NO donors including nitrosothiols, NO-metal complexes, nitrosamines, diazeniumdiolates, and organic nitrates/nitrites have been used to design polymer coatings capable of slowly releasing therapeutic levels of NO that are effective in reducing biofouling.⁷⁴ Of these NO donor species, 1-amino-substituted diazen-1-ium-1,2-diolates (or simply “*N*-diazeniumdiolates”) have emerged as attractive candidates for designing more biocompatible coatings due to their ability to generate NO spontaneously under physiological conditions.⁷⁵⁻⁷⁷ Since the first report on the synthesis of *N*-

Table 1.1. Current major classes of NO donors^{a,b}

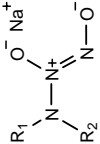
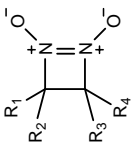
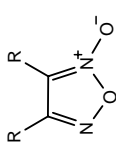
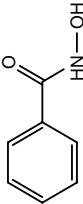
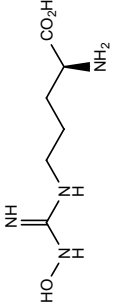
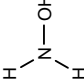
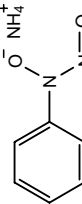
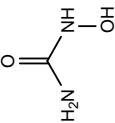
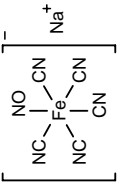
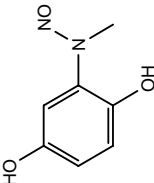
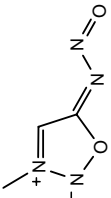
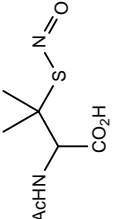
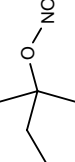
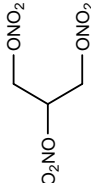
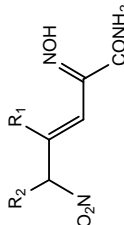
Class	Representative compound		Pathway of NO generation		Ref.
	Structure	Example	Non-enzymatic	Enzymatic	
Diazeniumdiolate		PROLI/NO, DETA/NO	H ⁺ , heat		75-77
Diazetidine dioxide		3,3,4,4,- Tetramethyl-1,2,- diazetidine 1,2,- dioxide	Spontaneous, thiols	Unknown	78,79
Furoxan and benzofuroxan		4-Aryl-3- methylfuroxan	Thiols	Unknown enzyme	80
Hydroxamic acid			Unknown	Guanylate cyclase	81
<i>N</i> -Hydroxyguanidine and guanidine			Oxidants	NOS, Cyt-P450	82
Hydroxylamine				Catalase/H ₂ O ₂	83,84
<i>N</i> -Hydroxyl nitrosamine		Cupferron, alansoine	Light, heat	Peroxidases	85
Hydroxyurea			H ₂ O ₂ /CuZn-SOD or ceruloplasmin, H ₂ O ₂ /Cu ²⁺ , heme- containing proteins	Peroxidases	86,87

Table 1.1. (continued)

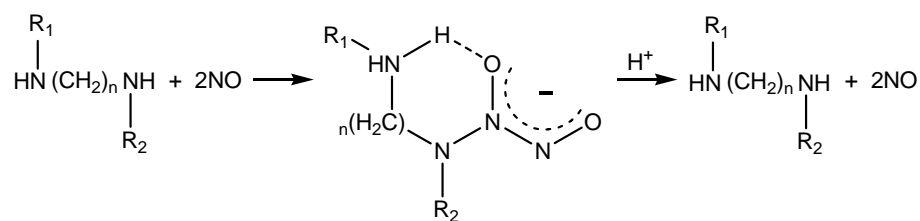
Class	Representative compound		Pathway of NO generation		Ref.
	Structure	Example	Non-enzymatic	Enzymatic	
Metal-NO complex		SNP, dinitrosyl-iron complex	Light, thiols, reductants, nucleophiles	A membrane bound enzyme	74
<i>N</i> -Nitrosamine		Dephostain, <i>N</i> -nitrosourea	Light, OH ⁻	Cyt-P450 related enzymes	88
Nitrosimine		1,3,4-thiadiazole-2-nitrosimine	Thiols, light		74
Nitrosothiols		SNAP, <i>S</i> -nitrosoglutathione	Light, metal ions, thiols, spontaneous	Unknown enzymes	89,90
Organic nitrite		IAN, IBN	Hydrolysis, light, heat	Xanthine oxidase	74
Organic nitrate		GTN	Thiols	Cyt-P450, glutathione transferase	74
Oxime		FK409	Spontaneous, O ₂ /F ^{III} -porphyrin	Cyt-P450	74

^aRepresented from Ref. 74. ^bAbbreviations: PROLI/NO, *N*-diazoniumdiolated proline; DETA/NO, *N*-diazoniumdiolated diethylenetriam NOS, nitric oxide synthase; cyt-P450, cytochrome P450; SOD, superoxide dismutase; SNP, sodium nitroprusside; SNAP, *S*-nitroso-*N*-acetylpenicillamine; IAN, isoamyl nitrite; IBN, isobutyl nitrite; GTN, glyceryl trinitrate; and, FK409, (+/-)-(4-ethyl-2E-(hydroxyimino)-5-nitrohexenamide).

diazeniumdiolates by Drago and Paulik in 1960,⁹¹ several diazeniumdiolate species have been synthesized using a range of nucleophilic residues that encompass simple primary/secondary amines, polyamines, and secondary amino acids.⁷⁵⁻⁷⁷ Keefer and coworkers have reviewed the synthesis of these nucleophilic NO adducts via the reaction of polyamines with NO at elevated pressure.⁷⁵ *N*-Diazeniumdiolates can be classified within two broad categories: 1) zwitterionic, and 2) anionic stabilized species (Figure 1.5).⁷⁵⁻⁷⁷ Initially, one equivalent of amine (*N*) reacts with two equivalents of NO for both types of *N*-diazeniumdiolates. A second equivalent of base (i.e., another amine) is then protonated to sustain the newly formed [N(O)NO]⁺ group, yielding zwitterionic stabilized structures (Figure 1.5A). In the presence of a stronger base such as methoxide (MeO⁻), a second equivalent of MeO⁻ removes a proton from a secondary amine nitrogen to create the anionic structure. (Figure 1.5B). While stable under ambient conditions, *N*-diazeniumdiolates decompose spontaneously in aqueous media to generate NO at rates dependent upon pH, temperature, and/or the structure of the amine moiety.

The majority of *N*-diazeniumdiolates are relatively stable in solid form at low temperatures. However, such NO donors spontaneously decompose and release up to two molecules of NO in solution.⁷⁵ Figure 1.6 shows example structures of *N*-diazeniumdiolates and their half-lives ranging from 2 s to 20 h at pH 7.4 and 37 °C.⁹² Decomposition and dissociation follow first-order kinetics at constant hydrogen activity. One interesting characteristic of *N*-diazeniumdiolates is that decomposition is greatly slowed at elevated pH. This provides significant convenience for the preparation of the *N*-diazeniumdiolate stock solutions.

A



B

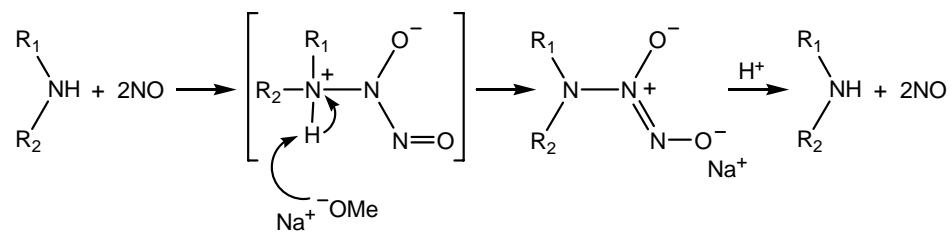


Figure 1.5. Reactions of NO with amine to produce (A) Zwitterionic and (B) anionic stabilized *N*-diazoniumdiolate NO donors followed by the subsequent release of NO in the presence of a proton. R₁ and R₂ represent side groups.⁷⁵

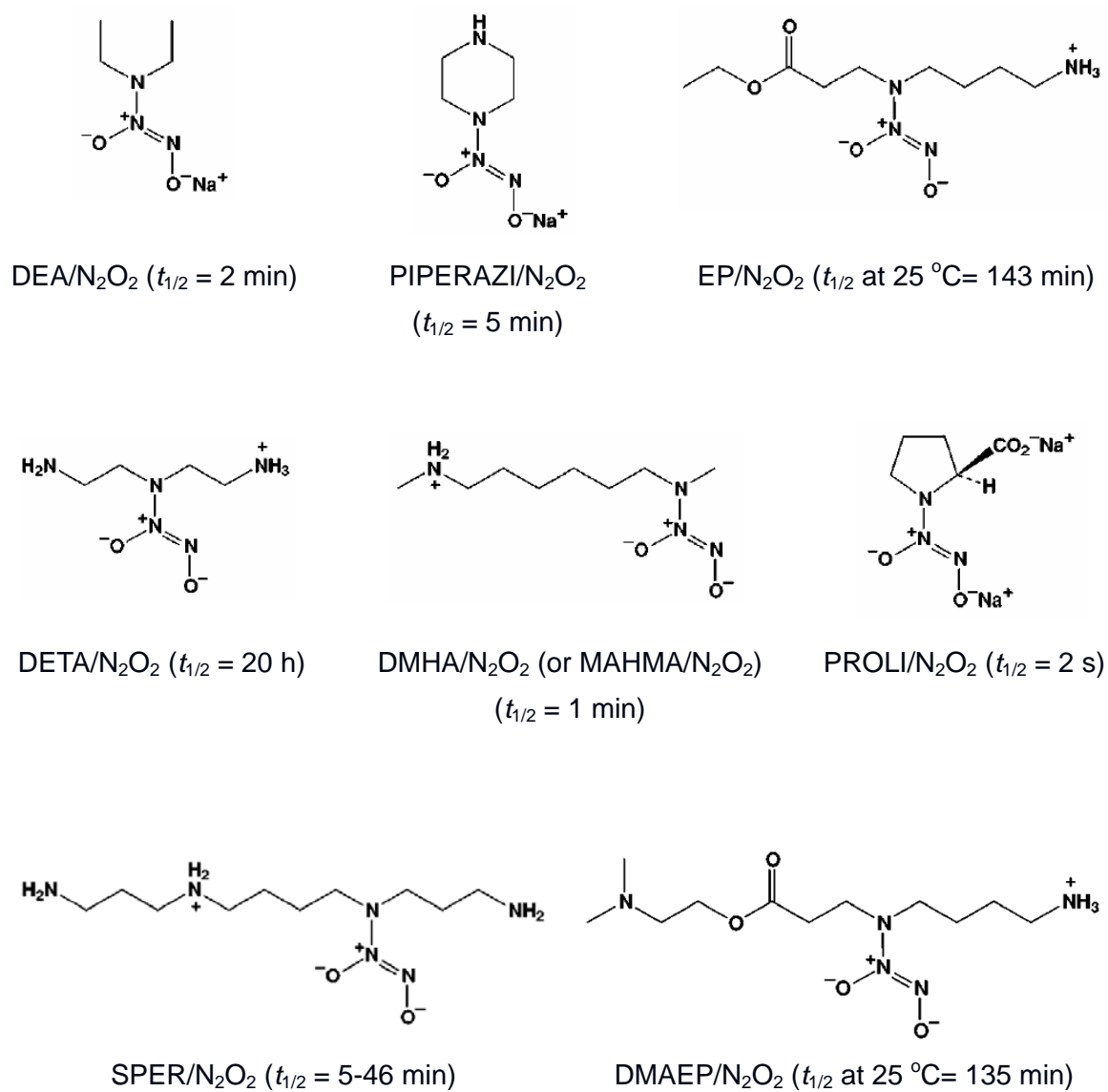


Figure 1.6. Example structures of various *N*-diazeniumdiolate-modified amines and their half-lives ($t_{1/2}$) measured in phosphate-buffered saline (PBS) at pH 7.4 and 37 °C. Abbreviations: DEA, diethylamine; PIPERAZI, piperazine; EP, ethylputrescine; DETA, diethylenetriamine; DMHA, *N,N'*-dimethyl-1,6-hexanediamine; PROLI, proline; SPER, spermine; and DMAEP, 2-(dimethylamino)ethylputrescine.⁹²

1.4.3 Nitric Oxide-Releasing Polymers for Designing *In Vivo* Sensors

The original approach for preparing NO-releasing polymers was to incorporate or disperse small molecule *N*-diazoniumdiolate NO donors into a polymer during synthesis of the polymer. Espadas-Torre *et al.* demonstrated the utility of such NO-releasing polymers to prepare potentiometric ion sensors for the measurements of potassium (K^+) and hydrogen (H^+).⁹³ Plasticized PVC and polyurethane membranes were doped with an appropriate ionophore (i.e., valinomycin for K^+ and tridodecylamine for H^+ , respectively) and (*Z*)-1-(*N*-methyl-*N*-[6-(*N*-methylammoniohexyl)amino]diazene)-1-ium-1,2-diolate or diazeniumdiolate-modified *N,N'*-dimethyl-1,6-hexanediamine (MAHMA/ N_2O_2). Schoenfisch *et al.* subsequently reported the fabrication of a Clark-style amperometric oxygen-sensing catheter using a MAHMA/ N_2O_2 -doped silicone rubber (SR) polymer film as a gas-permeable outer membrane.⁹⁴ These intravascular sensors generated NO upon exposure to aqueous solutions (e.g., blood) and exhibited significantly improved *in vitro* and *in vivo* hemocompatibility without impaired analytical performance. Unfortunately, the non-covalently entrapped NO donors (e.g., MAHMA/ N_2O_2) and their carcinogenic decomposition byproducts (e.g., diamines and corresponding nitrosamines) were found to leach from the polymer matrix into the surrounding media.⁹⁵

To address leaching concerns, efforts were devoted to (1) utilize more lipophilic NO donors that would preferentially remain in the organic polymer phase; and, (2) covalently tether the NO donor agents to the polymer backbone. Batchelor *et al.* increased the lipophilicity of the original NO donor MAHMA/ N_2O_2 by using longer alkyl chains (i.e., diazeniumdiolated *N,N'*-dibutylhexanediamine; DBHD/ N_2O_2).⁹⁶ A catheter-type amperometric oxygen sensor coated with a hydrophobic SR membrane containing such lipophilic

NO donors (i.e., DBHD/N₂O₂) was then fabricated and its analytical performance evaluated *in vivo*.¹⁰ The NO-release properties of the sensor were controllable by varying the amount of NO donors blended into the polymer casting solution. Both leaching of the NO donor and platelet aggregation were significantly reduced. In an alternative approach, the *N*-diazoniumdiolate moiety has been covalently attached to the backbone of the polymer. For example, the synthesis of diazeniumdiolated polymethacrylate, piperazine-modified PVC, poly(ethyleneimine), diamine-modified silicone rubber, and polyurethane has been reported.^{95,97,98} Mowery *et al.* demonstrated the fabrication of K⁺- and H⁺-selective membrane electrodes using diazeniumdiolated poly(ethyleneimine) (PEI/N₂O₂) and methoxymethyl-protected diazeniumdiolated piperazine-PVC (mompipPVC/N₂O₂).⁹⁹ Hydrophobic silicone materials were similarly synthesized by cross-linking *N*-(6-aminohexyl)-3-aminopropyltrimethoxysilane (DACA-6) with poly(dimethylsiloxane) (PDMS), followed by forming *N*-diazoniumdiolates *in situ* (DACA-6/N₂O₂-SR).¹⁰⁰ DACA-6/N₂O₂-SR films was also successfully employed as NO-releasing outer coatings for the fabrication of amperometric¹⁰⁰ and fluorescence-based oxygen sensors,¹⁰¹ and a potentiometric carbon dioxide-sensing catheter.¹⁰

1.5 Sol–Gel Chemistry for Nitric Oxide-Releasing Coatings

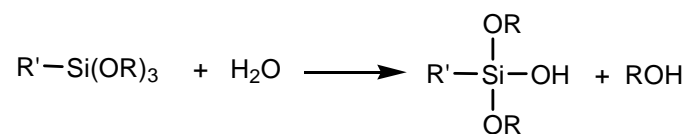
Schoenfisch and coworkers have focused on the synthesis and characterization of silicon-based sol–gel materials (e.g., silica xerogels) whereby the *N*-diazoniumdiolate NO donors are covalently bound to the xerogel backbone.¹⁰²⁻¹⁰⁹ Similar to the above diazeniumdiolated polymers, undesirable leaching of residual amines is avoided because the NO donor remains covalently linked to the silane.

1.5.1 Sol–Gel Chemistry

Sol–gel chemistry allows for the synthesis of inorganic and inorganic-organic *hybrid* ceramic materials for a range of applications.^{110,111} Although various metal alkoxides (based on titanium, zirconium, vanadium, tungsten, aluminum, and borate) exist for preparing sol–gel derived materials, the most common precursors are silicon alkoxides. Materials of many forms can be prepared including powders (particles), fibers, monoliths, films, and coatings.¹¹²⁻¹¹⁴ The exact form of the silica ceramic can be prepared via control over the composition of silane precursors and reaction/processing conditions (i.e., sol–gel chemistry).

The sol–gel process can be divided into the following four categories: mixing (to form a sol), gelation, aging, and drying.¹¹²⁻¹¹⁴ In a typical procedure, alkyl- and organoalkoxysilane precursors are mixed with appropriate amounts of water, methanol or ethanol, and a catalyst (e.g., acid or base), to form a solution (the sol). The silane precursors are hydrolyzed, resulting in the formation of silanol groups (Si–OH) (Figure 1.7A). The reactive silanols subsequently cross-react (i.e., condense) with either alkoxy (Si–OR) or other silanol groups to yield siloxane bridges (Si–O–Si) where R is typically a methyl or ethyl group, and R' is an organic functional group (Figure 1.7B). Eventually, polycondensation reactions lead to the formation of a polymeric gel network. Several organically modified silane precursors with different functional groups have been reported in the literature, including those with alkyl chains, amines, thiols, epoxides, and methacrylates. In the following aging and drying processes, polycondensation reactions continue and residual solvent is removed from the interconnected pore network, thereby increasing the strength and density of the gel. Control over the silane precursors and reaction/processing conditions (e.g., pH, solvent, silane/water ratio, catalyst, and drying time and temperature) allows for tremendous physical and

A



B

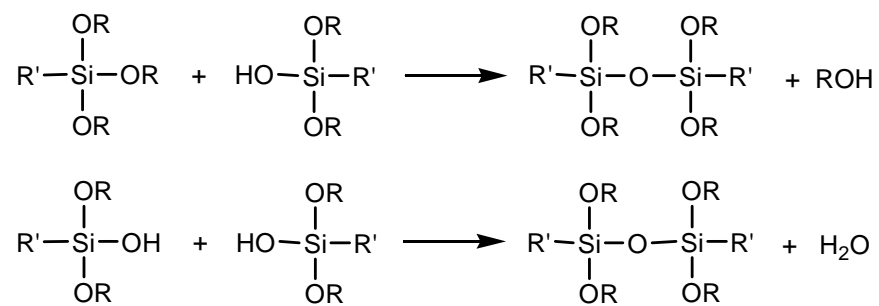


Figure 1.7. Schematic of sol-gel process illustrating (A) hydrolysis of silane precursors and (B) subsequent condensation reactions where R is typically a methyl or ethyl group and R' is an organic group for preparing functional xerogels.¹¹²

chemical flexibility in creating xerogels with tunable porosity, rigidity, and wettability.

A range of inorganic-organic *hybrid* xerogels functionalized for sensor applications have been synthesized using sol-gel chemistry.^{110,111} Indeed, xerogels have emerged as a class of materials suitable for a wide range of biosensor applications since they are: (1) synthesized under mild conditions; (2) enable tremendous chemical flexibility; and, (3) generally porous ($700 - 900 \text{ m}^2 \cdot \text{g}^{-1}$), thus facilitating the diffusion of analyte to the transducer (usually electrochemical and optical). Sol-gel derived films also exhibit strong adhesion to a variety of sensor substrates (e.g., metal/metal oxides and silica substances). The chemical flexibility allowed via sol-gel chemistry can be further manipulated by doping other molecules (e.g., biomolecules, polymers, and electrochemical or optical sensing elements) within the xerogel network.

1.5.2 Nitric Oxide-Releasing Xerogels for *In Vivo* Chemical Sensing

The Schoenfish group has focused on synthesizing sol-gel derived materials capable of generating NO at variable rates and amounts (without concomitant leaching) that can be subsequently used for implantable devices, including *in vivo* sensors.^{102,109} A range of *N*-diazoniumdiolate-modified xerogels have been synthesized and their properties tailored by varying the type and amount of alkyl- and aminoalkoxysilane precursors and specific reaction/processing conditions. Several alkyl- and aminoalkoxysilane precursors have been employed for this purpose, including methyl-, ethyl-, and butyltrimethoxysilanes (MTMOS, ETMOS, and BTMOS, respectively), (aminoethylaminomethyl)phenethyltrimethoxysilane (AEMP3), *N*-(2-aminoethyl)-3-aminopropyltrimethoxysilane (AEAP3), *N*-(6-aminoethyl)-aminopropyltrimethoxysilane (AHAP3), and *N*-[3-(trimethoxysilyl)propyl]diethylenetriamine (DET3) (Figure 1.8). The amine functional groups in the cured xerogel structure are

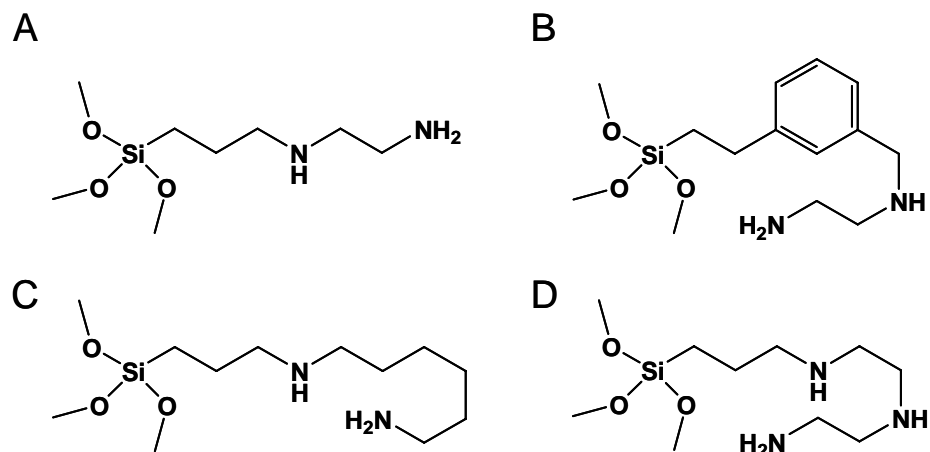


Figure 1.8. Structures of aminoalkoxysilanes: A) *N*-(2-aminoethyl)-3-aminopropyltrimethoxysilane (AEAP3); B) (aminoethylaminomethyl)phenethyltrimethoxysilane (AEMP3); C) *N*-(6-aminoethyl)aminopropyltrimethoxysilane (AHAP3); and, D) *N*-[3-(trimethoxysilyl)propyl]diethylenetriamine (DET3).

converted to *N*-diazoniumdiolate NO donors via exposure to high pressures (5 atm) of NO. As described earlier, the generation of NO from diazoniumdiolated xerogels is triggered by the presence of a proton donor such as water (Figure 1.9).

Xerogel coatings with average NO surface flux ranging from <1 to 60 pmol·cm⁻²·s⁻¹ have been synthesized by simply altering the identity and relative ratios of the aminoalkoxysilane precursor in the sol. The flux of NO from these xerogels is sufficient to reduce platelet and bacterial (*P. aeruginosa*) adhesion by 90% and 70 – 80%, respectively.^{109,115} More recently, *in vitro* cell adhesion experiments were expanded to include other clinically relevant bacterial species including *Proteus mirabilis*, *Staphylococcus aureus*, and *Staphylococcus epidermidis*.^{106,108} Similar to *P. aeruginosa*, NO-releasing xerogel coatings inhibited cell adhesion to these pathogens (50 – 90% reduction) as well. Such coatings may thus prove useful for reducing biofouling and the occurrence of implant-related infection for *in vivo* sensor applications.

Marxer *et al.* reported on an amperometric sol–gel derived sensor that released NO and was capable of measuring physiologically relevant concentrations of oxygen.¹¹⁶ The sensor consisted of a platinum electrode coated with 20% AHAP3 (balance ETMOS) *hybrid* xerogel film. Hydrophilic polyurethane (HPU) was doped into the xerogel membrane to increase oxygen permeability and reduce the time required to hydrate the membrane. *N*-Diazoniumdiolate NO donors were formed within the polymer matrix by exposing the cured film to high pressures of NO. The coating released up to 4.3 × 10⁻¹⁰ mol·cm⁻²·min⁻¹ of NO over the first 12 h and maintained measurable levels of NO release through 48 h. Oxygen sensors modified with HPU-doped, NO-releasing xerogels effectively inhibited platelet adhesion without serious deterioration in sensor performance. In addition, the HPU-doped

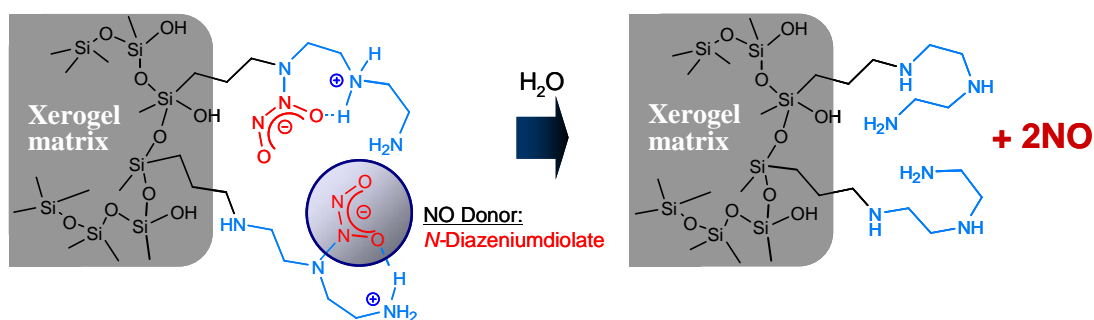


Figure 1.9. Schematic of NO generation from *N*-diazeniumdiolate-modified xerogel network occurring upon exposure to aqueous conditions. *N*-[3-(Trimethoxysilyl)propyl]diethylenetriamine (DET3) was used as an example aminoalkoxysilane precursor.

xerogel coating was stable in buffer solution for over 48 h. While advances in the synthesis of NO-releasing polymers have led to significant progress in the development of intravascular sensors for blood gas and electrolyte measurements,^{1,10,116} the application of such coatings to subcutaneous glucose sensors may also prove beneficial, and represents a portion of this dissertation research.

1.6 *In Situ* and *In Vivo* Measurements of Nitric Oxide

Despite the above discoveries, much is still not understood about NO's many biological roles and metabolic pathways in the body. Furthermore, the demand for *in situ*, real-time measurement of NO at or near the surface of materials that controllably release NO to elucidate the relationship between local NO concentrations and surface fouling would aid in the design more effective biomaterials. The importance of NO determination has resulted in an increasing interest in the development of methods for detecting and monitoring this molecule. Designing appropriate sensors, however, has not been trivial due to difficulties associated with measuring NO in physiological media due to its low concentration (nM – μ M), high reactivity with various endogenous components (e.g., free radicals, transition metal ions, and oxygen) and short half-life (usually < 10 s).^{48,117} Moreover, the complexity and limited dimensions of biological samples ranging from tissue to cells, for example, significantly hinder the detection of NO. Most techniques for measuring NO are indirect, relying on the determination of a secondary species such as L-citrulline (a coproduct of NO synthesis), nitrite or nitrate (oxidation products of NO).^{118,119} Indirect methods have often fail to accurately reflect the spatial and temporal distribution of NO in biological environments. Of the feasible approaches to overcome such drawbacks, electrochemical (e.g., amperometric redox)¹²⁰⁻¹²³ and optical (e.g., chemiluminescence¹²⁴ and fluorescence¹²⁵) sensors represent

the most promising strategies for detecting NO. Such sensors provide direct, real-time measurement of NO both *in vitro* and *in vivo*, and their microfabrication is inexpensive.^{126,127}

1.6.1 Electrochemical Nitric Oxide Sensors

Electrochemical detection of NO in biological media can be accomplished via either direct or electrocatalytic reduction or oxidation of NO.¹²⁸ Although a number of reactions have been identified for the direct reduction of NO, the kinetics are typically slow and give rise to large overpotentials ranging from ca. -0.9 to -1.2 V (versus Ag/AgCl).¹²⁸ This reaction can be summarized as follows (Equation 1.1):



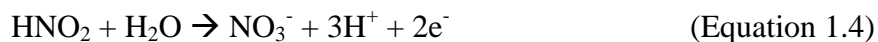
Intermediates for this reaction include NO^- and/or HNO : these species are also reduced to NH_2OH . The direct electroreductive methods for detecting NO usually provide better specificity since most potential interfering species are not reduced at these potentials. However, molecular oxygen is reduced at these working potentials, rendering this detection system inadequate for *in vivo* applications. Recently, electrodes modified with electropolymerized films of transition metal complexes (e.g., $[\text{Cr}(\text{v-tpy})_2]^{3+}$) have been reported, where v-tpy is the ligand 4'-vinyl-2,2',6',2''-terpyridyl.¹²⁹ This chemistry has resulted in the design of sensors that reduce NO at less negative potentials.

Alternatively, the electrochemical oxidation of NO proceeds via the following reactions:^{120,121,128}



In the first step (Equation 1.2) an electron is transferred from NO to the electrode,

generating an oxidation current. Since nitrosonium ion (NO^+) is a relatively strong Lewis acid, it is converted to nitrite (NO_2^-) in the presence of OH^- (Equation 1.3). Ultimately NO_2^- is further oxidized to nitrate (NO_3^-) the final product of electrochemical oxidation of NO, and results in the additional transfer of two electrons:



Because the direct electrooxidation of NO requires a relatively high working potential (ca. +0.7 to +1.0 V vs. Ag/AgCl), its amperometric detection is often hindered by the presence of readily oxidizable species including nitrite, ascorbic acid, uric acid, acetaminophen, and dopamine.^{120,121} Current electrooxidative techniques for *in situ* and *in vivo* detection of NO are based on either Clark-style electrodes or surface-modified electrodes.¹²⁰⁻¹²³

Clark-style electrodes are fabricated by placing the working (platinum) and pseudo-reference (silver) electrodes into a micropipette filled with an internal electrolyte solution and sealed/covered with a gas-permeable membrane.¹³⁰ In this configuration, platinum and silver wires are placed in close proximity coaxially (tip diameter of 10 μm). The microelectrode can thus be used to measure NO in tissue and isolated cells with relatively high spatial resolution. Several gas-permeable membranes have been used to achieve high selectivity for NO over the aforementioned interfering species, including chloroprene, collodion/polystyrene, Nafion/cellulose acetate, and nitrocellulose/silicone. Unfortunately, Clark-style sensors are limited by both low sensitivity and comparatively slow response times relative to the rate of physiological changes in NO levels.^{121,130}

Surface-modified electrodes are fabricated by coating various electrodes (e.g., platinum,

glassy carbon and carbon fiber) with catalytically active materials such as metalloporphyrins (e.g., Ni-, Fe-, and Mn-porphyrins), *o*-phenylenediamine, or metal phthalocyanine to lower the working potential by ca. 0.3 V relative to an unmodified electrode.^{122,131} Bare electrodes are typically modified via electrochemical polymerization by either entrapping the catalytic compounds during the polymerization of a given monomer or using monomers that have covalently linked electrocatalysts. Control of the polymer thickness can be achieved by measuring the charge transferred during the polymer-formation process. Such composite electrodes may be further modified with a permselective barrier membrane (e.g., cellulose acetate and Nafion) to reduce interferences by size exclusion and/or electrostatic repulsion. For this particular design, a carbon fiber is coated sequentially with monomeric tetrakis(3-methoxy-4-hydroxyphenyl) nickel porphyrin (Ni-TMPP), Nafion, and finally *o*-phenylenediamine.¹³¹

1.6.2 Optical Nitric Oxide Sensors

The reaction of NO with ozone or luminol-H₂O₂ is the basis of chemiluminescence-based optical NO sensors, and represents a promising alternative to electrochemical methods.^{124,132,133} Indeed, optical sensors exhibit excellent detection limits (ca. 10⁻¹³ mol·L⁻¹), but consequently require a large sample size.¹³² Recently, however, fiber-optic based sensors have been introduced, significantly reducing the sample size requirement (~300 μm to 3 mm).¹³³ Nitric oxide from a sample diffuses through a gas-permeable silicone rubber membrane and enters an internal solution composed of H₂O₂ and luminol. The NO immediately reacts with H₂O₂ to form peroxynitrite (ONOO⁻), a strong oxidant that quickly reacts with luminol to generate light. A fiber-optic probe collects a fraction of the produced light and directs it to a photomultiplier tube for detection. Detection limits of ca. 1.3 × 10⁻⁶

mol·L⁻¹ can be achieved using fiber optics.¹³³

1.6.3 Protein-Based Nitric Oxide Biosensors

To achieve optimum selectivity for NO in complex biological conditions, a number of enzyme- and metalloprotein-based biosensors have been developed in which the interaction of the protein with NO leads to an appropriate electrochemical or fluorescent signal.^{126,127}

Nitric oxide is known to inactivate biologically important enzymes including glucose oxidase, horseradish peroxidase, and polyphenol oxidase via reaction with the metal center, *S*-nitrosylation or sulfhydryl oxidation. However, the exact inhibition mechanism is not clearly defined, and most likely differs depending on the protein system employed. Because immobilizing enzymes onto electrodes and detecting changes in enzyme product are both reasonably straightforward, several electrochemically-based biosensor systems have been developed. However, fiber optic-based fluorescent sensors using metalloproteins such as cytochrome *c'* and sGC are equally capable of detecting and monitoring NO.^{134,135} Briefly, cytochrome *c'* is labeled with a fluorescent spectator dye. The quantum yield (e.g., ability to fluoresce) of the dye molecule decreases in the presence of NO.

1.7 Summary of Dissertation Research

The goal of my dissertation research was to explore the feasibility of coupling sol-gel derived NO release with the chemistry of electrochemical glucose sensing to improve lingering biofouling problems. A *hybrid* xerogel/polyurethane glucose biosensor was developed via the use of NO-releasing xerogel particles that were prepared by grinding xerogel films. Although such NO-releasing *hybrid* coatings represent useful materials for reducing bacterial adhesion, their *in vivo* applications remained limited due to the relatively

short NO release duration (<15 – 20 h at higher than therapeutic concentration of NO). To improve the longevity of NO release, *N*-diazeniumdiolate-modified silica nanoparticles with more tunable NO release properties were prepared via a one-pot synthesis. In addition, an amperometric sol–gel derived NO microsensor having superior analytical performance compared to existing sensors was developed.

The specific aims of my research included:

- 1) the evaluation of xerogel permeability before and after exposure to high pressures of NO necessary to form *N*-diazeniumdiolate NO donors;
- 2) the preparation and characterization of NO-releasing xerogel/polyurethane *hybrid* coatings for use as glucose sensor membranes;
- 3) the investigation of the *in vitro* glucose sensor performance with respect to sensitivity, response time, and long-term stability;
- 4) the synthesis of *N*-diazeniumdiolated silica nanoparticles using various primary/secondary and secondary amine-based alkoxy silane precursors;
- 5) the comparison and optimization of synthetic strategies for preparing silica nanoparticles with enhanced NO release properties;
- 6) exploring the feasibility of using xerogel films as permselective membranes for sensing NO amperometrically; and,
- 7) determining the optimum xerogel composition for maximizing NO permeability while providing sufficient selectivity for NO in the presence of common interfering species.

The goal of this introduction chapter was to provide both a brief overview of the current

advances and the potential implication of NO in the development of biomaterials for *in vivo* sensor applications. The research discussed in Chapter 2 describes the preparation of a NO-releasing xerogel/polyurethane *hybrid* coating and its application to *in vivo* glucose sensing. The utility of xerogel films for fabricating amperometric NO microsensors is discussed in Chapter 3. Chapter 4 focuses on the synthesis and characterization of NO-releasing silica nanoparticles with tunable physical and chemical properties (e.g., size, porous structures, functionality, and NO release). Finally, Chapter 5 discusses the synthesis of a NO delivery scaffold based on inorganic-organic *hybrid* silica nanocomposites and its tumoricidal efficacy against human ovarian surface epithelial cancer cells.

1.8 References

- (1) Frost, M. C.; Meyerhoff, M. E. "Implantable chemical sensors for real-time clinical monitoring: Progress and challenges," *Curr. Opin. Chem. Biol.* **2002**, *6*, 633-641.
- (2) Shin, J. H.; Schoenfisch, M. H. "Improving the biocompatibility of in vivo sensors via nitric oxide release," *Analyst* **2006**, *131*, 609-615.
- (3) Wilson, G. S.; Hu, Y. "Enzyme-based biosensors for in vivo measurements," *Chem. Rev.* **2000**, *100*, 2693-2704.
- (4) Wilson, G. S.; Gifford, R. "Biosensors for real-time in vivo measurements," *Biosens. Bioelectron.* **2005**, *20*, 2388-2403.
- (5) Wisniewski, N.; Moussy, F.; Reichert, W. M. "Characterization of implantable biosensor membrane biofouling," *Fresenius J. Anal. Chem.* **2000**, *366*, 611-621.
- (6) Anderson, J. M. "Biological responses to materials," *Annu. Rev. Mater. Res.* **2001**, *31*, 81-110.
- (7) Cazenave, J.-P.; Mulvihill, J. In *The role of platelets in blood-biomaterial interactions*; Missirlis, Y. F.; Wautier, J.-L., Eds.; Kluwer: Dordrecht, 1993, pp 69-80.
- (8) Ordinas, A.; Escolar, G.; White, J. G. *Ultrastructure of platelets and platelet-surface interactions*. In *The role of platelets in blood-biomaterial interactions*; Missirlis, Y. F.; Wautier, J.-L., Eds.; Kluwer Academic Publishers: Dordrecht, 1993, pp 3-13.
- (9) van Mourik, J. A.; van Aken, W. G. *Initiation of blood coagulation and fibrinolysis*. In *Blood-surface interactions: Biological principles underlying haemocompatibility with artificial materials*; Cazenave, J.-P.; Davies, J. A.; Kazatchkine, M. D.; van Aken, W. G., Eds.; Elsevier: New York, 1986.
- (10) Frost, M. C.; Batchelor, M. M.; Lee, Y.; Zhang, H.; Kang, Y.; Oh, B. K.; Wilson, G. S.; Gifford, R.; Rudich, S. M.; Meyerhoff, M. E. "Preparation and characterization of implantable sensors with nitric oxide release coatings," *Microchem. J.* **2003**, *74*, 277-288.
- (11) Meyerhoff, M. E. "In vivo blood-gas and electrolyte sensors: Progress and challenges," *Trends Anal. Chem.* **1993**, *12*, 257-266.
- (12) Sharkaway, A. A.; Klitzman, B.; Truskey, G. A.; Reichert, W. M. "Engineering the tissue which encapsulates subcutaneous implants. II. Plasma-tissue exchange properties," *J. Biomed. Mater. Res.* **1998**, *40*, 586-597.
- (13) Sharkaway, A. A.; Klitzman, B.; Truskey, G. A.; Reichert, W. M. "Engineering the tissue which encapsulates subcutaneous implants. III. Effective tissue response times," *J. Biomed. Mater. Res.* **1998**, *1998*, 598-605.

- (14) Sharkaway, A. A.; Klitzman, B.; Truskey, G. A.; Reichet, W. M. "Engineering the tissue which encapsulates subcutaneous implants. I. Diffusion properties," *J. Biomed. Mater. Res.* **1997**, *37*, 401-412.
- (15) von Recum, A. F. *Handbook of biomaterials evaluation: Scientific, technical, and clinical testing of implant materials*, 2nd ed.; Taylor & Francis: Philadelphia, 1999.
- (16) An, Y. H.; Friedman, R. J. *Handbook of bacterial adhesion: Principles, methods, and applications*; Humana Press: Totowa, NJ, 2000.
- (17) Dankert, J.; Hogt, A. H.; Feijen, J. "Biomedical polymers: Bacterial adhesion, colonization, and infection," *Crit. Rev. Biocompat.* **1986**, *2*, 219-301.
- (18) Hetrick, E. M.; Schoenfisch, M. H. "Reducing implant-related infections: Active release strategies," *Chem. Soc. Rev.* **2006**, *35*, 780-789.
- (19) Sawan, S. P.; Manivannan, G. *Antimicrobial/anti-infective materials: Principles, applications and device*; Technomic Publishing Co.: Lancaster, 2000.
- (20) Wisniewski, N.; Reichert, M. "Methods for reducing biosensor membrane biofouling," *Colloids Surf., B* **2000**, *18*, 197-219.
- (21) Ishihara, K. *Biocompatible polymers*. In *Biomedical applications of polymeric materials*; Tsuruta, T.; Hayashi, T.; Ishihara, K.; Kataoka, K.; Kimura, Y., Eds.; CRC Press: Ann Arbor, 1993, pp 89-162.
- (22) Pusineri, C. *Artificial materials*. In *Blood-surface interactions: Biological principles underlying haemocompatibility with artificial materials*; Cazanave, J.-P.; Davies, J. A.; Kazatchkine, M. D.; van Aken, W. G., Eds.; Elsevier: New York, 1986, pp 29-44.
- (23) El-Zaim, H. S.; Hegggers, J. P. *Silicones for pharmaceutical and biomedical applications*. In *Polymeric biomaterials*, 2nd ed.; Dumitriu, S., Ed.; Marcel Dekker: New York, 2002.
- (24) Harrison, D. J.; Turner, R., F.; Baltes, H. P. "Characterization of perfluorosulfonic acid polymer coated enzyme electrodes and a miniaturized integrated potentiostat for glucose analysis in whole blood," *Anal. Chem.* **1988**, *60*, 2002-2007.
- (25) Lamba, N. M. K.; Woodhouse, K. A.; Cooper, S. L. *Polyurethanes in biomedical applications*; CRC Press: Boca Ration, 1997.
- (26) Malinowska, E.; Oklejas, V.; Hower, R.; Brown, R. B.; Meyerhoff, M. E. "Enhanced electrochemical performance of solid-state ion sensors based on silicone rubber membranes," *Sens. Actuators B* **1996**, *33*, 161-167.
- (27) Moussy, F.; Harrison, D. J.; O'Brien, D. W.; Rajotte, R. V. "Performance of subcutaneously implanted needle-type glucose sensors employing a novel trilayer coating," *Anal. Chem.* **1993**, *65*, 2072-2077.

- (28) Shin, J. H.; Sakong, D. S.; Nam, H.; Cha, G. S. "Enhanced serum carbon dioxide measurements with a silicone rubber-based carbonate ion-selective electrode and a high-pH dilution buffer," *Anal. Chem.* **1996**, *68*, 221-225.
- (29) Yoda, R. "Elastomers for biomedical applications," *J. Biomater. Sci. Polym. Ed.* **1998**, *9*, 561-626.
- (30) Cosofret, V. V.; Erdosy, M.; Raleigh, J. S.; Johnson, T. A.; Neuman, M. R.; Buck, R. P. "Aliphatic polyurethane as a matrix for pH sensors: effects of native sites and added proton carrier on electrical and potentiometric properties," *Talanta* **1996**, *43*.
- (31) Shin, J. H.; Yoon, S. Y.; Yoon, I. J.; Choi, S. H.; Lee, S. D.; Nam, H.; Cha, G. S. "Potentiometric biosensors using immobilized enzyme layers mixed with hydrophilic polyurethane," *Sens. Actuators B* **1998**, *50*, 19-26.
- (32) Yun, S. Y.; Hong, Y. K.; Oh, B. K.; Cha, G. S.; Nam, H.; Lee, S. B.; Jin, J.-I. "Potentiometric properties of ion-selective electrode membranes based on segmented polyether urethane matrices," *Anal. Chem.* **1997**, *69*, 868-873.
- (33) Alexander, H.; Brunski, J.; Cooper, S. L.; Hench, L. L.; Hergenrother, R. W.; Hoffman, A. S.; Kohn, J.; Langer, R.; Peppas, N.; Ratner, B. D.; Shalaby, W.; Visser, S. A.; Yannas, I. *Classes of materials used in medicine*. In *Biomaterials science: An introduction to materials in medicine*; Ratner, B. D.; Hoffman, A. S.; Schoen, F. J.; Lemons, J. E., Eds.; Academic Press: New York, 1996.
- (34) Espadas-Torre, C.; Meyerhoff, M. E. "Thrombogenic properties of untreated and poly(ethylene oxide)-modified polymeric matrixes useful for preparing intraarterial ion-selective electrodes," *Anal. Chem.* **1995**, *67*, 3108-3114.
- (35) Gavalas, V. G.; Berrocal, M. J.; Bachas, L. G. "Enhancing the blood compatibility of ion-selective electrodes," *Anal. Bioanal. Chem.* **2006**, *384*, 65-72.
- (36) Huang, J.-C.; Jennings, E. M. "The effect of temperature on controlled release of heparin from polyurethane and ethylene vinyl acetate copolymer," *Int. J. Polym. Mater.* **2004**, *53*, 69-78.
- (37) Ishihara, K. "Novel polymeric materials for obtaining blood-compatible surfaces," *Trends Polym. Sci.* **1997**, *5*, 401-407.
- (38) Michanetzis, G. P. A.; Katsala, N.; Missirlis, Y. F. "Comparison of haemocompatibility improvement of four polymeric biomaterials by two heparinization techniques," *Biomaterials* **2003**, *24*, 677-688.
- (39) Valdes, T. I.; Moussy, F. "A ferric chloride pre-treatment to prevent calcification of Nafion membrane used for implantable biosensors," *Biosens. Bioelectron.* **1999**, *14*, 579-585.
- (40) Kishida, A.; Ikada, Y. *Hydrogels for biomedical and pharmaceutical applications*. In

- Polymeric Biomaterials*, Second ed.; Dumitriu, S., Ed.; Marcel Dekker, Inc.: New York, 2002, pp 133-146.
- (41) Triandafillu, K.; Balazs, D. J.; Aronsson, B.-O.; Descouts, P.; Tu Quoc, P.; van Delden, C.; Mathieu, H. J.; Harms, H. "Adhesion of *Pseudomonas aeruginosa* strains to untreated and oxygen-plasma treated poly(vinyl chloride) (PVC) from endotracheal intubation devices," *Biomaterials* **2003**, *24*, 1507-1518.
- (42) Hendricks, S. K.; Kwok, C.; Shen, M.; Horbett, T. A.; Ratner, B. D.; Bryers, J. D. "Plasma-deposited membranes for controlled release of antibiotic to prevent bacterial adhesion and biofilm formation," *J. Biomed. Mater. Res.* **2000**, *50*, 160-170.
- (43) Schierholz, J. M.; Steinhauser, H.; Rump, A. F. E.; Berkels, R.; Pulverer, G. "Controlled release of antibiotics from biomedical polyurethanes: Morphological and structural features," *Biomaterials* **1997**, *18*, 839-844.
- (44) Walpoth, B. H.; Rogulenko, R.; Tikhvinskaia, E.; Gogolewski, S.; Schaffner, T.; Hess, O. M.; Althaus, U. "Improvement of patency rate in heparin-coated small synthetic vascular grafts," *Circulation* **1998**, *98*, II319-323; discussion II324.
- (45) Rojas, I. A.; Slunt, J. B.; Grainger, D. W. "Polyurethane coatings release bioactive antibodies to reduce bacterial adhesion," *J. Control. Release* **2000**, *63*, 175-189.
- (46) Ruszczak, Z.; Friess, W. "Collagen as a carrier for on-site delivery of antibacterial drugs," *Adv. Drug Deliv. Rev.* **2003**, *55*, 1679-1698.
- (47) Poelstra, K. A.; Berekzi, N. A.; Rediske, A. M.; Felts, A. G.; Slunt, J. B.; Grainger, D. W. "Prophylactic treatment of gram-positive and gram-negative abdominal implant infections using locally delivered polyclonal antibodies," *JOURNAL OF BIOMEDICAL MATERIALS RESEARCH* **2002**, *60*, 206-215.
- (48) Ignarro, L. J. *Nitric Oxide: Biology and Pathobiology*; Academic Press: San Diego, 2000.
- (49) Radomski, M. W.; Palmer, R. M. J.; Moncada, S. "The anti-aggregating properties of vascular endothelium: Interactions between prostacyclin and nitric oxide," *Br. J. Pharmacol.* **1987**, *92*, 639-646.
- (50) Koshland, D. E., Jr. "The molecule of the year," *Science* **1992**, *258*, 1861.
- (51) Annich, G. M.; Meinhardt, J. P.; Mowery, K. A.; Ashton, B. A.; Merz, S. I.; Hirschl, R. B.; Meyerhoff, M. E.; Bartlett, R. H. "Reduced platelet activation and thrombosis in extracorporeal circuits coated with nitric oxide release polymers," *Crit. Care Med.* **2000**, *28*, 915-920.
- (52) Bohl, K. S.; West, J. L. "Nitric oxide-generating polymers reduce platelet adhesion and smooth muscle cell proliferation," *Biomaterials* **2000**, *21*, 2273-2278.

- (53) Ziche, M.; Morbidelli, E.; Masini, E.; Amerini, S.; Granger, H. J.; Maggi, C.; Geppetti, P.; Ledda, F. "Nitric oxide mediates angiogenesis in vivo and endothelial cell growth and migration in vitro," *J. Clin. Invest.* **1994**, *94*, 2036-2044.
- (54) Alderton, W. K.; Cooper, C. E.; Knowles, R. G. "Nitric oxide synthases: structure, function and inhibition," *Biochem. J.* **2001**, *357*, 593-615.
- (55) Moncada, S.; Higgs, A. "The L-arginine-nitric oxide pathway," *N. Engl. J. Med.* **1993**, *329*, 2002-2012.
- (56) Rosen, G. M.; Tsai, P.; Puro, S. "Mechanism of free-radical generation by nitric oxide synthase," *Chem. Rev.* **2002**, *102*, 1191-1199.
- (57) Wink, D. A.; Hanbauer, I.; Grisham, M. B.; Laval, F.; Nims, R. W.; Laval, J.; Cook, J.; Pacelli, R.; Liebmann, J.; Krishna, M.; Ford, P. C.; Mitchell, J. B. "Chemical biology of nitric oxide: Regulation and protective and toxic mechanisms," *Curr. Top. Cell. Regul.* **1996**, *34*, 159-187.
- (58) Moncada, S.; Higgs, A. "The L-arginine-nitric oxide pathway," *N. Engl. J. Med.* **1993**, *30*, 2002-2011.
- (59) Yu, A. E.; Hu, S. Z.; Spiro, T. G.; Burstyn, J. N. "Resonance raman-spectroscopy of soluble guanylyl cyclase reveals displacement of distal and proximal heme ligands by NO," *J. Am. Chem. Soc.* **1994**, *116*, 4117-4118.
- (60) Radomski, M. W.; Palmer, R. M. J.; Moncada, S. "An L-arginine/nitric oxide pathway present in human platelets regulates aggregation," *Proc. Natl. Acad. Sci. USA* **1990**, *87*, 5193-5197.
- (61) Wink, D. A.; Mitchell, J. B. "Chemical biology of nitric oxide: Insights into regulatory, cytotoxic, and cytoprotective mechanisms of nitric oxide," *Free Radic. Biol. Med.* **1998**, *25*, 434-456.
- (62) Lemaire, G.; Alvarez-Pachon, F. J.; Beuneu, C.; Lepoivre, M.; Petit, J. F. "Differential cytostatic effects of NO donors and NO producing cells," *Free Radic. Biol. Med.* **1999**, *26*, 1274-1283.
- (63) Proksch, E. "Toxicological evaluation of nitrosamines in condoms," *Int. J. Hygiene Environ. Health* **2001**, *204*, 103-110.
- (64) Schuller, H. M. "Nasal cavity carcinogenesis by N-nitrosamines: A critical appraisal," *Mut. Res. Fund. Mol. Mech. Mut.* **1997**, *1997*, 13-18.
- (65) Pryor, W. A.; Church, D. F.; Govindan, C. K.; Crank, G. "Oxidation of thiols by nitric oxide and nitrogen dioxide: synthetic utility and toxicological implications," *J. Org. Chem.* **1982**, *47*, 156-159.
- (66) Pryor, W. A.; Lightsey, J. W.; Church, D. F. "Reaction of nitrogen-dioxide with

- alkenes and poly-unsaturated fatty-acids - addition and hydrogen abstraction mechanisms," *J. Am. Chem. Soc.* **1982**, *104*, 6685-6692.
- (67) Murphy, M. E.; Sies, H. "Reversible conversion of nitroxyl anion to nitric-oxide by superoxide-dismutase," *Proc. Natl. Acad. Sci. USA* **1991**, *88*, 10860-10864.
- (68) Wink, D. A.; Feelisch, M.; Fukuto, J.; Chistodoulou, D.; Jourd'heuil, D.; Grisham, M. B.; Vodovotz, Y.; Cook, J. A.; Krishna, M.; Degraff, W. G.; Kim, S.; Gamson, J.; Mitchell, J. B. "The cytotoxicity of nitroxyl: Possible implications for the pathophysiological role of NO," *Arch. Biochem. Biophys.* **1998**, *35*, 66-74.
- (69) Lopez-Farre, A.; Rodriguez-Feo, J. A.; Sanchez de Miguel, L.; Rico, L. "Role of nitric oxide in the control of apoptosis in the microvasculature," *The International Journal of Biochemistry & Cell Biology* **1998**, *30*, 1095-1106.
- (70) Marletta, M. A.; Yoon, P. S.; Iyengar, R.; Leaf, C. D.; Wishnok, J. S. "Macrophage oxidation of L-arginine to nitrite and nitrate: nitric oxide is an intermediate," *Biochemistry* **1988**, *27*, 8706-8711.
- (71) Vaughn, M. W.; Kuo, L.; Liao, J. C. "Estimation of nitric oxide production and reaction rates in tissue by use of a mathematical model," *Am. J. Physiol.* **1998**, *274* (*Heart Circ. Physiol.* *43*), H2163-H2176.
- (72) Kelm, M. "Nitric oxide metabolism and breakdown," *Biochim. Biophys. Acta* **1999**, *1411*, 273-289.
- (73) Wang, P. G.; Cai, T. B.; Taniguchi, N. *Nitric oxide donors: For pharmaceutical and biological applications*; Wiley-VCH: Weinheim, German, 2005.
- (74) Wang, P. G.; Xian, M.; Tang, X.; Wu, X.; Wen, Z.; Cai, T.; Janczuk, A. J. "Nitric Oxide Donors: Chemical Activities and Biological Applications," *Chem. Rev.* **2002**, *102*, 1091-1134.
- (75) Hrabie, J. A.; Keefer, L. K. "Chemistry of the nitric oxide-releasing diazeniumdiolate ("nitrosohydroxylamine") functional group and its oxygen-substituted derivatives," *Chem. Rev.* **2002**, *102*, 1135-1154.
- (76) Hrabie, J. A.; Klose, J. R.; Wink, D. A.; Keefer, L. K. "New nitric oxide-releasing zwitterions derived from polyamines," *J. Org. Chem.* **1993**, *58*, 1472-1476.
- (77) Keefer, L. K.; Nims, R.; Davies, K. M.; Wink, D. A. *NONOates (1-substituted diazenium-1,2-diulates) as nitric oxide donors: Convenient nitric oxide dosage forms*. In *Methods in Enzymology*; Academic Press, 1996; Vol. 268, pp 281-293.
- (78) Singh, P.; Boocock, D. G. B.; Ullman, E. F. "Attempted formation of the unknown tetramethylaziridinyl-1-oxyl by photolysis and thermolysis of diazetidine 1,2-dioxide," *Tetrahedron Lett.* **1971**, *42*, 3935-3938.

- (79) Khlestkin, V. K.; Mazhukin, D. G.; Tikhonov, A. Y.; Rybalova, T. V.; Bagryanskaya, I. Y.; Gatilov, Y. V. "Intramolecular cyclization of 1,2-bis(*N*-alkoxy-*N*-nitrosoamino)-alkanes: A unique route to 4,5-dihydro-1,2,3-triazole 2-oxides.," *Synthesis* **2000**, 5, 681-690.
- (80) Sheremetev, A. B.; Makhova, N. N.; Friedrichsen, W. "Monocyclic furazans and furoxans," *Adv. Heterocycl. Chem.* **2001**, 78, 65-188.
- (81) Corrie, J. E. T.; Kirby, G. W.; Mackinnon, J. W. M. "Reactions of transient C-nitrosocarbonyl compounds with dienes, monoolefins, and nucleophiles," *J. Chem. Soc. Perkin Trans.* **1985**, 1, 883-886.
- (82) Fukuto, J. M. "Chemistry of *N*-hydroxy-L-arginine," *Methods Enzymol.* **1996**, 268, 365-375.
- (83) Klink, M.; Swierzko, A.; Sulowska, Z. "Nitric oxide generation from hydroxylamine in the presence of neutrophils and in the cell-free system," *APMIS* **2001**, 109, 493-499.
- (84) Taira, J.; Misik, V.; Riesz, P. "Nitric oxide formation from hydroxylamine by myoglobin and hydrogen peroxide," *Biochim. Biophys. Acta* **1997**, 1336, 502-508.
- (85) Tyagi, A. K.; Cooney, D. A. "Biochemical pharmacology, metabolism, and mechanism of action of L-alanosine, a novel, natural antitumor agent," *Adv. Pharmacol. Chemother.* **1984**, 20, 69-121.
- (86) King, S. B. "Nitric oxide production from hydroxyurea," *Free Radic. Biol. Med.* **2004**, 37, 737-744.
- (87) King, S. B. "*N*-hydroxyurea and acyl nitroso compounds as nitroxyl (HNO) and nitric oxide (NO) donors," *Curr. Top. Med. Chem.* **2005**, 5, 665-673.
- (88) Gnewuch, C. T.; Sosnovsky, G. "A critical appraisal of the evolution of *N*-nitrosoureas as anticancer drugs," *Chem. Rev.* **1997**, 97, 829-1041.
- (89) Al-Sa'doni, H. H.; Ferro, A. "*S*-Nitrosothiols as nitric oxide-donors: Chemistry, biology and possible future therapeutic applications," *Curr. Med. Chem.* **2004**, 11, 2679-2690.
- (90) Gaston, B.; Singel, D.; Doctor, A.; Stamler, J. S. "*S*-Nitrosothiol signaling in respiratory biology," *Am. J. Respir. Crit. Care Med.* **2006**, 173, 1186-1193.
- (91) Drago, R. S.; Paulik, F. E. "The Reaction of Nitrogen(II) Oxide with Diethylamine," *J. Am. Chem. Soc.* **1960**, 82, 96-98.
- (92) Keefer, L. K. "Progress toward clinical application of the nitric oxide-releasing diazeniumdiolates," *Ann. Rev. Pharmacol. Toxicol.* **2003**, 43, 585-607.

- (93) Espadas-Torre, C.; Oklejas, V.; Mowery, K.; Meyerhoff, M. E. "Thromboresistant chemical sensors using combined nitric oxide release/ion sensing polymeric films," *J. Am. Chem. Soc.* **1997**, *119*, 2321-2322.
- (94) Schoenfisch, M. H.; Mowery, K. A.; Rader, M. V.; Baliga, N.; Wahr, J. A.; Meyerhoff, M., E. "Improving the thromboresistivity of chemical sensors via nitric oxide release: Fabrication and *in vivo* evaluation of NO-releasing oxygen-sensing catheters," *Anal. Chem.* **2000**, *72*, 1119-1126.
- (95) Mowery, K. A.; Schoenfisch, M. H.; Saavedra, J. E.; Keefer, L. K.; Meyerhoff, M. E. "Preparation and characterization of hydrophobic polymeric films that are thromboresistant via nitric oxide release," *Biomaterials* **2000**, *21*, 9-21.
- (96) Batchelor, M. M.; Reoma, S. L.; Fleiser, P. S.; Nuthakki, V. K.; Callahan, R. E.; Shanley, C. J.; Politis, J. K.; Elmore, J.; Merz, S. I.; Meyerhoff, M. E. "More lipophilic dialkyldiamine-based diazeniumdiolates: Synthesis, characterization, and application in preparing thromboresistant nitric oxide release polymeric coatings," *J. Med. Chem.* **2003**, *46*, 5153-5161.
- (97) Parzuchowski, P. G.; Frost, M. C.; Meyerhoff, M. E. "Synthesis and characterization of polymethacrylate-based nitric oxide donors," *J. Am. Chem. Soc.* **2002**, *124*, 12182-12191.
- (98) Zhang, H.; Annich, G. M.; Miskulin, J.; Osterholzer, K.; Merz, S. I.; Bartlett, R. H.; Meyerhoff, M. E. "Nitric oxide releasing silicone rubbers with improved blood compatibility: preparation, characterization, and *in vivo* evaluation," *Biomaterials* **2002**, *23*, 1485-1494.
- (99) Mowery, K. A.; Schoenfisch, M. H.; Baliga, N.; Wahr, J. A.; Meyerhoff, M. E. "More biocompatible electrochemical sensors using nitric oxide release polymers," *Electroanalysis* **1999**, *11*, 681-686.
- (100) Frost, M. C.; Rudich, S. M.; Zhang, H.; Maraschio, M. A.; Meyerhoff, M. E. "In vivo biocompatibility and analytical performance of intravascular amperometric oxygen sensors prepared with improved nitric oxide-releasing silicone rubber coating," *Anal. Chem.* **2002**, *74*, 5942-5947.
- (101) Schoenfisch, M. H.; Zhang, H.; Frost, M. C.; Meyerhoff, M. E. "Nitric oxide-releasing fluorescence-based oxygen sensing polymeric films," *Anal. Chem.* **2002**, *74*, 5937-5941.
- (102) Marxer, S. M.; Rothrock, A. R.; Nablo, B. J.; Robbins, M. E.; Schoenfisch, M. H. "Preparation of nitric oxide (NO)-releasing sol-gels for biomaterial applications," *Chem. Mater.* **2003**, *15*, 4193-4199.
- (103) Nablo, B. J.; Chen, T.-Y.; Schoenfisch, M. H. "Sol-gel derived nitric oxide-releasing materials that reduce bacterial adhesion," *J. Am. Chem. Soc.* **2001**, *123*, 9712-9713.

- (104) Nablo, B. J.; Prichard, H. L.; Butler, R. D.; Klitzman, B.; Schoenfisch, M. H. "Inhibition of implant-associated infections via nitric oxide release," *Biomaterials* **2005**, *26*, 6984-6990.
- (105) Nablo, B. J.; Schoenfisch, M. H. "Antibacterial properties of nitric oxide-releasing sol-gels," *J. Biomed. Mater. Res.* **2003**, *67A*, 1276-1283.
- (106) Nablo, B. J.; Schoenfisch, M. H. "Poly(vinyl chloride)-coated sol-gels for studying the effects of nitric oxide release on bacterial adhesion," *Biomacromolecules* **2004**, *5*, 2034-2041.
- (107) Nablo, B. J.; Schoenfisch, M. H. "In vitro cytotoxicity of nitric oxide-releasing sol-gel derived materials," *Biomaterials* **2005**, *26*, 4405-4415.
- (108) Nablo, B. J. B. J.; Rothrock, A. R. A. R.; Schoenfisch, M. H. M. H. "Nitric oxide-releasing sol-gels as antibacterial coatings for orthopedic implants," *Biomaterials* **2005**, *26*, 917-924.
- (109) Robbins, M. E.; Oh, B. K.; Hopper, E. D.; Schoenfisch, M. H. "Nitric oxide-releasing xerogel microarrays prepared with surface-tailored poly(dimethylsiloxane) templates," *Chem. Mater.* **2005**, *17*, 3288-3296.
- (110) Schottner, G. "Hybrid sol-gel derived polymers: Applications of multifunctional materials," *Chem. Mater.* **2001**, *13*, 3422-3435.
- (111) Schubert, U.; Husing, N.; Lorenz, A. "Hybrid inorganic-organic materials by sol-gel processing of organofunctional metal alkoxides," *Chem. Mater.* **1995**, *7*, 2010-2027.
- (112) Brinker, C. J.; Scherer, G. W. *Sol-gel science: The physics and chemistry of sol-gel processing*; Academic Press: New York, 1990.
- (113) Hench, L. L.; West, J. K. "The sol-gel process," *Chem. Rev.* **1990**, *90*, 33-72.
- (114) Pierre, A. C. *Introduction to sol-gel processing*; Kluwer Academic Publishers: Boston, MA, 1998.
- (115) Oh, B. K.; Robbins, M. E.; Nablo, B. J.; Schoenfisch, M. H. "Miniaturized glucose biosensor modified with a nitric oxide-releasing xerogel microarray," *Biosens. Bioelectron.* **2005**, *21*, 749-757.
- (116) Marxer, S. M.; Robbins, M. E.; Schoenfisch, M. H. "Sol-gel derived nitric oxide-releasing oxygen sensors," *Analyst* **2005**, *130*, 206-212.
- (117) Beckman, J. S.; Wink, D. A.; Crow, J. P. *Nitric Oxide and Peroxynitrite*. In *Methods in Nitric Oxide Research*; Feelisch, M.; Stamler, J. S., Eds.; John Wiley: Chichester, U.K., 1996, pp Chapter 6.
- (118) Archer, S. "Measurement of nitric oxide in biological models," *FASEB J.* **1993**, *7*,

349-360.

- (119) Taha, Z. H. "Nitric oxide measurements in biological samples," *Talanta* **2003**, *61*, 3-10.
- (120) Bedioui, F.; Trevin, S.; Devynck, J. "Chemically modified microelectrodes designed for the electrochemical determination of nitric oxide in biological systems," *Electroanalysis* **1996**, *8*, 1085-1091.
- (121) Bedioui, F.; Villeneuve, N. "Electrochemical nitric oxide sensors for biological samples - Principles, selected examples and applications," *Electroanalysis* **2003**, *15*, 5-18.
- (122) Ciszewski, A.; Milczarek, G. "Electrochemical detection of nitric oxide using polymer modified electrodes," *Talanta* **2003**, *61*, 11-26.
- (123) Zhang, X. "Real time and In vivo monitoring of nitric oxide by electrochemical sensors - From dream to reality," *Front. Biosci.* **2004**, *9*, 3434-3446.
- (124) Beckman, J. S.; Conger, K. A. "Direct measurement of dilute nitric oxide in solution with an ozone chemiluminescent detector," *Methods* **1995**, *7*, 35-39.
- (125) Gabe, Y.; Urano, Y.; Kikuchi, K.; Kojima, H.; Nagano, T. "Highly sensitive fluorescence probes for nitric oxide based on boron dipyrromethene chromophore-rational design of potentially useful bioimaging fluorescence probe," *J. Am. Chem. Soc.* **2004**, *126*, 3357-3367.
- (126) Casero, E.; Darder, M.; Pariente, F.; Lorenzo, E. "Peroxidase enzyme electrodes as nitric oxide biosensors," *Anal. Chim. Acta* **2000**, *403*, 1-9.
- (127) Kilinc, E.; Ozsoz, M.; Sadik, O. A. "Electrochemical detection of NO by inhibition on oxidase activity," *Electroanalysis* **2000**, *12*, 1467-1471.
- (128) de Vooy, A. C. A.; Beltramo, G. L.; van Riet, B.; van Veen, J. A. R.; Koper, M. T. M. "Mechanisms of electrochemical reduction and oxidation of nitric oxide," *Electrochim. Acta* **2004**, *49*, 1307-1314.
- (129) Maskus, M.; Pariente, F.; Wu, Q.; Toffanin, A.; Shapleigh, J. P.; Abruna, H. D. "Electrocatalytic reduction of nitric oxide at electrodes modified with electropolymerized films of $[\text{Cr}(\text{v-tpy})_2]^{3+}$ and their application to cellular NO determinations," *Anal. Chem.* **1996**, *68*, 3128-3134.
- (130) Kitamura, Y.; Uzawa, T.; Oka, K.; Komai, Y.; Takizawa, N.; Kobayashi, H.; Tanishita, K. "Microcoaxial electrode for in vivo nitric oxide measurement," *Anal. Chem.* **2000**, *72*, 2957-2962.
- (131) Kumar, S. M.; Porterfield, D. M.; Muller, K. J.; Smith, P. J. S.; Sahley, C. L. "Nerve injury induces a rapid efflux of nitric oxide (NO) detected with a novel NO

- microsensor," *J. Neurosci. Methods* **2001**, *21*, 215-220.
- (132) Robinson, J. K.; Bollinger, M. J.; Birks, J. W. "Luminol/H₂O₂ chemiluminescence detector for the analysis of nitric oxide in exhaled breath," *Anal. Chem.* **1999**, *71*, 5131-5136.
- (133) Zhou, X.; Arnold, M. A. "Response characteristics and mathematical modeling for a nitric oxide fiber-optic chemical sensor," *Anal. Chem.* **1996**, *68*, 1748-1754.
- (134) Barker, S. L. R.; Zhao, Y.; Marletta, M. A.; Kopelman, R. "Cellular applications of a sensitive and selective fiber-optic nitric oxide biosensor based on a dye-labeled heme domain of soluble guanylate cyclase," *Anal. Chem.* **1999**, *71*, 2071-2075.
- (135) Blyth, D. J.; Aylott, J. W.; Moir, J. W. B.; Richardson, D. J.; Russell, D. A. "Optical biosensing of nitric oxide using the metalloprotein cytochrome *c*'," *Analyst* **1999**, *124*, 129-134.

Chapter 2:

Nitric Oxide-Releasing Xerogel Particle/Polyurethane Glucose Biosensors

2.1 Introduction

Mild synthesis conditions and tremendous chemical flexibility have made sol–gel chemistry the focus of much biosensor research. The porous nature of most sol–gel derived materials (i.e., xerogels) makes them ideal for sensor coatings since analyte diffusion is minimally obstructed. In addition, ambient and aqueous processing conditions favor the entrapment of enzymes for biosensor fabrication.¹⁻³ For example, glucose oxidase (GOx) retains its activity and exhibits increased stability when immobilized within a xerogel. The above attributes have led to the development of several classes of xerogels based glucose biosensors.⁴⁻¹⁵

Designing *in vivo* glucose biosensors for clinical use, however, remains a significant challenge due to poor biocompatibility resulting largely from bacterial adhesion and scar tissue formation around the sensor.¹⁶ Indeed, surface fouling negatively impacts the long-term utility of such devices by reducing glucose diffusion to the sensor and increasing the risk of infection.¹⁷ To address surface fouling, a number of strategies have been explored including modifying the outer surfaces of biosensors with a range of polymeric membranes that resist biofouling *in vitro* including silicone rubber and polyurethane,¹⁸⁻²⁰ hydrogels,²¹ and Nafion,²² for example. Antimicrobial agents including antibiotics²³ and polyclonal antibodies²⁴ have also been doped into polymers such that their slow leaching with time

decreases bacterial adhesion and biofilm formation at the material-tissue interface. Unfortunately, none of the above strategies has dramatically improved the long-term performance of *in vivo* glucose sensors. Infection and scar tissue formation still dictate sensor durability.

With the discovery of nitric oxide (NO) as a potent inhibitor of platelet adhesion and activation,²⁵ and its identification as both an angiogenic factor²⁶ and antibacterial agent,²⁷ the study of NO has been extended to the field of biomaterials.²⁷⁻³⁵ Due to its short half-life in biological milieu (<1 s),³⁶ NO represents an attractive species for improving the biocompatibility of *in vivo* sensors because its effect will be local, not systemic. Furthermore, the potential to both reduce bacterial adhesion and enhance wound healing at the sensor site may prove effective in improving the biocompatibility of subcutaneous tissue-based glucose biosensors. The most promising NO-releasing coatings developed to date are based on the incorporation of *N*-diazoniumdiolate NO donors into hydrophobic polymers.³³ *N*-Diazoniumdiolates are synthesized by the reaction of di- and triamines with NO at elevated pressure (Figure 1.5, where R₁ and R₂ represent side groups), and capable of generating NO spontaneously in aqueous environments at rates dependent upon pH, temperature, and the identity of the amine precursor.^{29,37-39}

Recently the synthesis of sol-gel derived NO-releasing materials whereby amine-functionalized silicon alkoxides (aminoalkoxysilanes) were bound to a xerogel backbone was reported.^{27,40} Through exposure to high pressures of NO, the covalently linked amine groups were converted to *N*-diazoniumdiolates. These materials represent ideal sensor coatings because they combine the utility of NO release with the versatility of sol-gel chemistry. A range of *N*-diazoniumdiolate-modified xerogels can be synthesized and their properties

tailored by varying the type and content of alkyl- and aminoalkoxysilane precursors and processing conditions.⁴⁰ Furthermore, the flux of NO from these xerogels was sufficient to reduce bacterial adhesion,^{27,35,41,42} indicating that such coatings may prove useful for reducing the occurrence of implant-related infection.

While advances in the synthesis of NO-releasing materials have led to significant progress in the development of intravascular (i.e., blood contacting) gas sensors,⁴³⁻⁴⁵ the application of these materials to enzymatic-based biosensors has not yet been explored. Although NO has proven to be beneficial at low concentrations, it is a highly reactive radical and may effect enzymatic activity. Indeed, NO has been shown participate in the inactivation of several enzymes.⁴⁶⁻⁴⁸ Herein, we explore the feasibility of coupling NO release with the chemistry of enzymatic biosensing. We report on the fabrication and *in vitro* performance of a glucose biosensor using a new type of NO-releasing coating, a *hybrid* polyurethane/xerogel film that contains anchored *N*-diazoniumdiolate functional groups on xerogel particles. These *hybrid* polymers inhibit undesirable leaching of the potentially toxic *N*-diazoniumdiolate precursors while providing steady, tunable NO release.⁴⁰ The optimal design of the NO-releasing glucose biosensor, its NO generation profiles, and the stability of the xerogel particles in the supporting polymer matrix are discussed.

2.2 Experimental Section

2.2.1 Reagents and Materials

Glucose oxidase (GOx; type VII-S from *Aspergillus niger*; 245,900 units/g), horseradish peroxidase (HRP; type I, 148 units/mg), *o*-dianisidine, hydrogen peroxide (H₂O₂; 3 wt% solution in water), and β-D-glucose anhydrous were purchased from Sigma (St. Louis, MO). Methyltrimethoxysilane (MTMOS) and isobutyltrimethoxysilane (BTMOS) were

purchased from Aldrich (Milwaukee, WI). (Aminoethylaminomethyl)phenethyltrimethoxysilane (AEMP3) and *N*-(6-aminohexyl)aminopropyltrimethoxysilane (AHAP3) were purchased from Gelest (Tullytown, PA); Tecoflex polyurethane (TPU; SG-80A) was purchased from Thermedics (Woburn, MA). Nitric oxide (NO) and argon (Ar) gases were purchased from National Welders Supply (Durham, NC). Hydrophilic polyurethane (HPU; MW 5.74×10^5 g/mol; 40 wt% water uptake) was a gift from Professor Geun Sig Cha of the Department of Chemistry at Kwangwoon University (Seoul, Republic of Korea). Other solvents and chemicals were analytical-reagent grade, and used as received. Water was purified with a Milli-Q UV Gradient A10 System (Millipore Corp.) Final resistivity of the ultrapure water was 18.2 M Ω ·cm, and the total organic content was ≤ 6 ppb.

2.2.2 *Effect of NO on Enzyme Activity in Solution*

In the homogeneous solution-based assay, GOx was introduced to both control and NO-saturated (approximately 2 mM NO) phosphate buffered saline (PBS) solutions (0.1 M, pH 7.4) to assess the effect of NO on enzyme activity. PBS was purged with Ar for 20 min to remove oxygen and then saturated with NO for 20 min to produce a ca. 2 mM NO PBS solution.⁴⁹ Control and NO-saturated buffers were used to prepare dilute solutions of GOx (0.1 μ g GOx/mL). The activity of the GOx was measured via an absorbance assay using *o*-dianisidine, a H₂O₂ sensitive dye, and a PerkinElmer Lambda 40 UV/Vis Spectrometer (Norwalk, CT).⁵⁰ Exactly 200 μ L of 400 mM glucose, 200 μ L HRP (5.4 units/mL), and 100 μ L of GOx solution (i.e., control or NO-saturated) were added to a cuvette containing 500 μ L of 0.3 mM *o*-dianisidine (in phosphate buffer). The absorbance change due to oxidized *o*-dianisidine was measured at 436 nm. The activity of the NO-exposed GOx was normalized to

control GOx solutions not exposed to NO.

2.2.3 Effect of NO on MTMOS Xeroge-Based Glucose Biosensor

Functional glucose biosensors were prepared as follows to determine the effect of NO on xerogel immobilized GOx. Cylindrical polycrystalline platinum (Pt) working electrodes (0.031 cm^2) were mechanically polished with successively finer grades of alumina slurries down to $0.05 \text{ }\mu\text{m}$. An ultrasonic cleaner was used to remove residual alumina loosely bound to the surface. A GOx-containing sol was prepared by mixing $50 \text{ }\mu\text{L}$ of water containing 6 mg GOx, $100 \text{ }\mu\text{L}$ of ethanol, and $25 \text{ }\mu\text{L}$ of MTMOS. A $5\text{-}\mu\text{L}$ aliquot of this solution was cast onto the Pt working electrode. A TPU/HPU polyurethane polymer solution was prepared by mixing 5 mg TPU, 5 mg HPU, $250 \text{ }\mu\text{L}$ THF, and $250 \text{ }\mu\text{L}$ ethanol. A $25 \text{ }\mu\text{L}$ aliquot of this solution was applied to the sensor surface as a barrier membrane to limit glucose diffusion to the electrode and enhance analyte response over a wide range of glucose concentrations. The sensors were dried for 1 d under ambient conditions and soaked in either PBS (control) or NO-saturated PBS for 1 h. The sensor response to glucose was then evaluated as described below.

2.2.4 Sensor Performance Evaluation

To evaluate the analytical performance of the glucose biosensors, amperometric measurements were performed using a CH Instruments 660A potentiostat (Austin, TX). The electrode assembly (3-electrode configuration) consisted of a xerogel modified Pt working electrode, Pt wire counter electrode, and a Ag/AgCl (3.0 M KCl) reference electrode. Response and calibration curves were obtained by adding aliquots of a 1.0 M glucose solution to 50 mL of 0.01 M PBS (pH 7.4) at room temperature with constant stirring.

Current was recorded at an applied potential of +0.7 V vs. Ag/AgCl. The permeability of H₂O₂ through the xerogel film was evaluated by measuring the ratio of peak currents at the xerogel coated and bare (control) Pt electrodes ($\Delta I_x/\Delta I_b$) in the presence of 0.1 mM H₂O₂.⁵¹ Current was recorded at an applied potential of +0.7 V vs. Ag/AgCl. Biosensors were stored in PBS at room temperature between measurements.

2.2.5 Nitric Oxide-Releasing AEMP3/MTMOS Xerogel-Based Glucose Biosensor

The effect of exposing GOx to the conditions necessary for *N*-diazoniumdiolate formation was evaluated by entrapping the enzyme in xerogels containing aminoalkoxysilanes and directly exposing them to high pressures of NO. The biosensor coating was prepared by mixing 25 μ L of total silane consisting of 0 to 5 μ L of AEMP3 (balance MTMOS), 100 μ L of ethanol, and 50 μ L of water with and without 6 mg of GOx for 10 min. A 5- μ L aliquot of the silane mixture was deposited onto a platinum (Pt) working electrode and dried under ambient conditions for 1 d. The xerogel coated Pt electrodes were placed in an in-house NO reaction vessel,²⁷ flushed with Ar to remove air and water, and then exposed to 1, 3, and 5 atm of NO or Ar (control) for 1 h. The response of the biosensors to glucose was then evaluated as described above.

2.2.6 Synthesis of *N*-Diazoniumdiolated Xerogel Particles

Aminoalkoxysilane-based xerogel particles (XGPs) were prepared by mixing the aminoalkoxysilane AHAP3 with either MTMOS or BTMOS. Xerogel monoliths were initially synthesized by mixing 80 μ L of AHAP3, 120 μ L of the alkylalkoxysilane (MTMOS or BTMOS), 200 μ L of ethanol, and 600 μ L of water. To make BTMOS-based xerogels, 10

μL of 0.5 M HCl was added as a catalyst. All solutions were mixed for 10 min, poured into Teflon plates, and allowed to dry and age at 70 °C for 3 d. The monoliths were then ground into powders (roughly 10 – 200 μm in diameter) using a mortar and pestle. The ensuing XGPs were placed in an in-house NO reactor as described above, and exposed to 5 atm NO for 3 d to convert accessible amine groups to NO donors (*N*-diazoniumdiolates). Prior to removing the *N*-diazoniumdiolate-modified particles, the reactor was purged with Ar to eliminate residual NO not chemically bound to the XGPs. The *N*-diazoniumdiolated-modified xerogel particles (N_2O_2 -XGPs) were stored in a sealed container at -20 °C until used.

2.2.7 Preparation of Hybrid NO-Releasing Xerogel/Polyurethane Glucose Biosensors

Hybrid XGP-based glucose biosensors were fabricated by applying enzyme-immobilized MTMOS (layer 1), inner polyurethane (layer 2), NO-donor XGP (N_2O_2 -XGP) (layer 3), and outer polyurethane membranes (layer 4), in that order, onto a polished cylindrical Pt working electrode (0.3 cm^2). Layer 1 was formed by casting 3 μL of a MTMOS sol consisting of 6 mg of GOx, 25 μL MTMOS, 100 μL ethanol, and 50 μL of water, onto the Pt electrode. Layer 2 was formed by casting 10 μL of TPU/HPU solution prepared by mixing 5 mg TPU, 5 mg HPU, 250 μL THF, and 250 μL ethanol. Layer 3 was prepared by casting 5 μL of the above polyurethane solution containing either 6 mg N_2O_2 -XGPs or XGPs (controls). Finally, a barrier polyurethane membrane (layer 4) was added by applying 20 μL of polyurethane solution (the same composition as layer 2) on top of the XGP-containing polyurethane layer. Each layer on the sensor was dried under ambient condition for 30 min before casting the subsequent layer. All biosensors (i.e., control and NO-releasing) were stored in air at 4°C until use to preserve both GOx and *N*-

diazoniumdiolate stability. Following initial evaluation, sensors were stored in PBS at room temperature.

2.2.8 Xerogel Particle Characterization

NO release from the N₂O₂-XGPs modified sensors was measured in PBS at room temperature using a chemiluminescence-based Sievers Nitric Oxide Analyzer 280 (Boulder, CO). NO release profiles were obtained for the different N₂O₂-XGPs and their *hybrid* films containing 3, 6, 12, and 18 mg N₂O₂-XGPs in 500 μ L polyurethane (solution).

The stability of the XGPs in the multilayer membrane was evaluated by incubating the *hybrid* films in PBS for 24 and 48 h at room temperature. The Si content from the soak solutions, an indicator of XGP leaching from the PU matrix, was measured using an ARL-Fisons Spectraspan 7 direct current plasma optical emission spectrometer (DCP-OES; Beverly, MA).

2.2.9 Bacterial Adhesion

Pseudomonas aeruginosa cultures were grown from -80 °C stock in tryptic soy broth (TSB) for 12 h at 37 °C. A 1 mL aliquot of the cell culture was incubated in 150 mL of TSB for ~6 h at 37 °C until a $\sim 10^8$ cfu/mL culture ($OD_{\lambda=600} = 0.2$) was obtained. Cultures were centrifuged and resuspended in PBS. To fluorescently label *P. aeruginosa*, BacLight fluorescent probe (Molecular Probes; Eugene, OR) was incubated with the bacterial suspension for 30 min. The labeled cells were pelleted, rinsed, and resuspended in PBS. Cell counts on tryptic soy agar were performed to obtain the cell concentration. Control and NO-releasing XGP-modified polyurethane films cast on glass slides were immersed into 5 mL of the labeled cell suspension for 30 min at 37 °C. Fluorescent optical micrographs were

obtained using a Zeiss Axiovert 200 inverted microscope (Chester, VA) equipped with a Syto 9 filter set from Chroma (Brattleboro, VT).

2.3 Results and Discussion

The biochemical interactions of NO with mammalian proteins are among the most important biological reactions in which NO participates.⁵²⁻⁵⁴ Metal centers, including heme, non-heme, and metal-sulfur clusters of proteins, all form nitrosyl complexes with NO. Furthermore, NO and its derivatives are highly reactive with non-metallic coordination sites such as thiol and sulfhydryl groups. For enzymes, reaction with NO often has both reversible and irreversible effects on biological activity. While the influence of NO on enzyme activity has been evaluated for a number of enzymes including xanthine oxidase, glutathione peroxidase, and NADPH-oxidase,^{47,52} the influence of NO on GOx, a flavoprotein consisting of two identical polypeptide chain subunits linked covalently by a disulfide bond,⁵⁵ remains unknown. Thus, the influence of NO on GOx in solution was studied to determine the feasibility of developing a NO-releasing glucose biosensor.

2.3.1 Effect of NO on GOx

The effect of NO on GOx was assessed using a solution-based spectrophotometric GOx activity assay. As shown in Table 2.1, the activity of GOx decreased considerably (approximately 40% at $t = 0$) upon exposure to a saturated buffer solution of NO (~2 mM). The activity of the GOx recovers to 100% after 24 h, indicating that the inhibitory effect of NO is reversible. Of note, bubbling the buffer solution with NO decreased the pH of the solution from 7.4 to 6.7. Since the activity of the enzyme is maximized between pH 5 – 6,⁵⁶ a corresponding increase in GOx activity was observed. To account for this, the pH of the

Table 2.1. Changes of solution GOx activity as a function of time

Time (days)	Normalized GOx activity ^a	
	Control	2 mM NO
0	1.00 ± 0.02	0.62 ± 0.21
1	1.20 ± 0.11	1.18 ± 0.03
4	1.01 ± 0.12	1.05 ± 0.04

^aActivities are normalized to the control at $t = 0$.

control solution was also adjusted to pH 6.7. These results indicate that while enzyme activity in solution is reduced in the presence of NO, the influence of NO on the enzyme is neither devastating nor irreversible, and thus should not preclude the development of a NO-releasing glucose biosensor.

To further evaluate the feasibility of coupling NO release with GOx-based glucose sensing, the effect of NO on the activity of GOx immobilized within a xerogel was assessed. A functional sol-gel derived glucose biosensor was prepared and exposed to a NO-saturated buffer (~2 mM) for 1 h. As shown in Figure 2.1, the sensitivity of the biosensor decreased from -6.3×10^{-2} to -1.9×10^{-2} $\mu\text{A}/\text{mM}$ (roughly 70%) upon NO exposure. Remarkably, the response of the biosensor remained linear ($r = 0.9997$) suggesting that although high concentrations of NO may decrease GOx activity, such high NO concentrations do not completely compromise the sensor's analytical utility. In contrast to GOx in solution, the effect of NO on the biosensor was permanent (i.e., the response of the biosensor did not return to its original value) indicating that immobilized GOx is more harshly influenced by NO than GOx in solution. Although xerogels are known to promote enzyme stability, once denatured, proteins are unlikely to return to their native state due to interaction with the xerogel matrix.⁵⁷

2.3.2 Effect of NO on GOx-Based Xerogel Films

To introduce NO release capability, aminoalkoxysilane-based xerogel glucose sensors were doped with GOx and exposed to 5 atm NO for 1 h. The response of the GOx-aminoalkoxysilane-based xerogel sensor to glucose before and after NO exposure is shown in Figure 2.2. As expected based on the above data, the response of the biosensor after NO exposure is reduced by 99.8% (Figure 2.2b). This decreased sensitivity is significantly

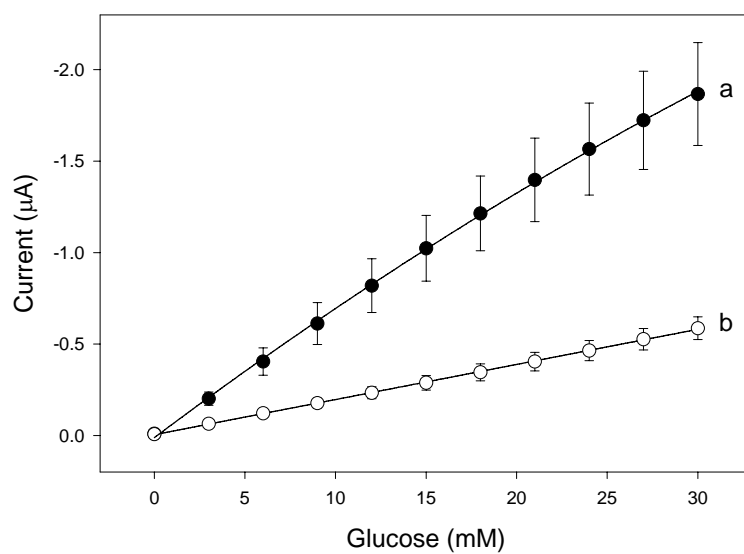


Figure 2.1. Calibration curves of glucose biosensors pre-soaked in (a) PBS (control); and (b) NO-saturated PBS for 1 h.

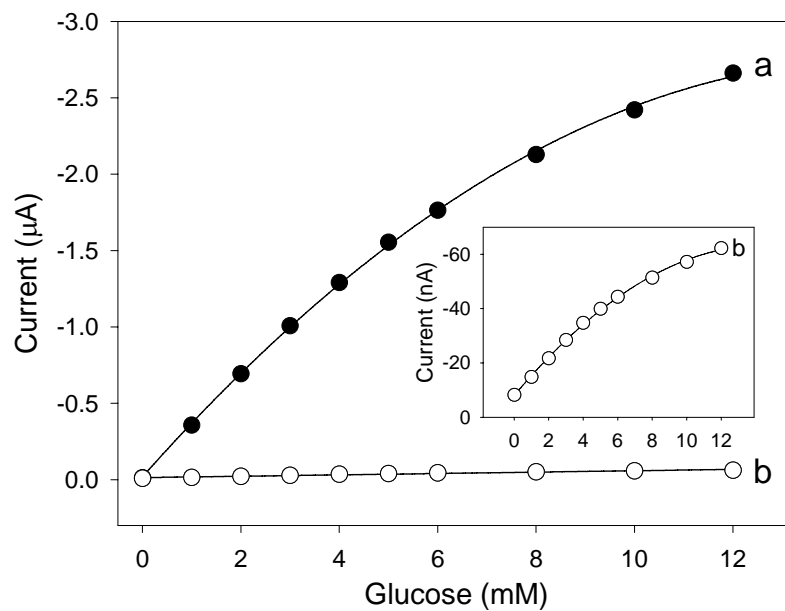


Figure 2.2. Glucose response of (a) control and (b) NO exposed (5 atm NO for 1h) AEMP3/MTMOS glucose biosensors. (Inset) is the expansion of the response for the NO exposed biosensor.

greater than for the biosensor that had been exposed to 2 mM NO, indicating that more than reduced GOx activity is altering the sensor's analytical sensitivity. Indeed, this behavior is attributed to both enzyme inactivation and reduced xerogel permeability upon exposure to high pressures of NO.

To assess the effect of NO on the permeability of the xerogel film, the diffusion of H₂O₂ through MTMOS and AEMP3/MTMOS xerogel films (without enzyme) exposed to either 5 atm NO or Ar was evaluated. (The ambient laboratory air served as the blank.) As shown in Table 2.2, the aminoalkoxysilane-based xerogel is less permeable than typical xerogel without aminoalkoxysilanes (e.g., MTMOS alone). These permeability differences likely account for part of the reduced sensor response to glucose (see Figure 2.2). Notably, the permeability of xerogels exposed to Ar decreased only slightly, indicating that exposure to high pressures alone does not significantly affect the physical structure of the xerogel. The permeability of aminoalkoxysilane-based coatings after NO exposure was remarkably diminished. To further evaluate the effect of NO on the xerogel matrix, the permeability of AEMP3/MTMOS membranes exposed to 1 – 5 atm NO was measured as a function of time the electrode was soaked in PBS solution. Irrespective of the pressure, exposure to NO significantly reduced the permeability of AEMP3/MTMOS xerogel films. Furthermore, the reduced permeability was irreversible (see Figure 2.3).

The basis of sol–gel chemistry is the formation of a polymeric gel through the hydrolysis and polycondensation of silicon alkoxides.⁵⁸ The degree of polycondensation, determined by the type and concentration of the silicon alkoxide precursors, the reaction conditions (e.g., pH, catalyst, and water content), and the drying/aging time and temperature, influences both the physical porosity and rigidity of the resulting xerogel.^{58,59} In general, high

Table 2.2. Permeability of H₂O₂ through xerogel membranes after exposure to NO and Ar for 1 h

Conditions	Permeability (i_s/i_b)	
	MTMOS	AEMP3/MTMOS
Ambient	0.059 ± 0.005	0.034 ± 0.003
5 atm NO	0.031 ± 0.008	< 0.0001
5 atm Ar	n/a	0.026 ± 0.006

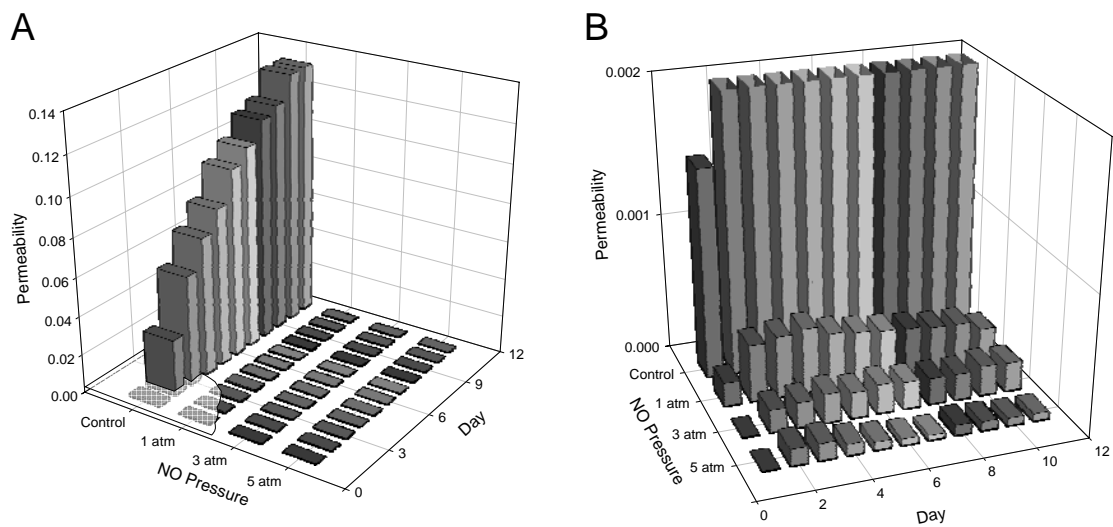


Figure 2.3. (A) Variations in permeability of H₂O₂ through AEMP3/MTMOS films exposed to different pressure of NO for 1 h and controls. Electrodes were stored in PBS (pH 7.4) at ambient conditions between experiments. (B) Enlargement of graph (A).

concentrations of residual silanol groups lead to highly porous xerogel materials. We hypothesize that the markedly lower permeability of xerogel films following NO exposure is the result of enhanced poly-condensation catalyzed by NO.

2.3.3 Hybrid NO-Releasing Glucose Biosensors

Since the analytical response characteristics of aminoalkoxysilane-derived xerogel glucose biosensors are compromised due to inadequate permeability and reduced GOx activity, *hybrid* polyurethane/xerogel coatings capable of NO release were synthesized using *N*-diazoniumdiolate-modified xerogel “particles” and polyurethane membranes. Xerogel particles were prepared by grinding xerogel films or monoliths to a fine powder resulting in particles with diameters ranging from 10 – 200 μm . To facilitate NO release, the diamine groups in the xerogel were converted to *N*-diazoniumdiolates by exposing the powder to 5 atm NO for 3 d. A multi-membrane NO-releasing glucose biosensor was then prepared as depicted in Figure 2.4. To start, a glucose oxidase-containing xerogel film (<25 μm) was cast onto a polished Pt electrode. Microencapsulation of the enzyme within a xerogel was chosen over simple physisorption to minimize enzyme leaching.⁷ An “enzyme protecting” polyurethane layer was cast on the GOx-based xerogel to minimize the effect of NO on GOx activity by separating the xerogel encapsulated GOx and the NO releasing layer. The third layer consisted of the *N*-diazoniumdiolate-modified xerogel particles (or unmodified xerogel particle controls) dispersed in polyurethane. Additional polyurethane was cast on top of this layer as a barrier membrane to reduce the potential of xerogel particle leaching. The polyurethane layers also serve to limit the diffusion of glucose relative to oxygen, maximizing the sensor’s dynamic response to glucose.

As previously reported, the amount and duration of NO-release are easily controlled

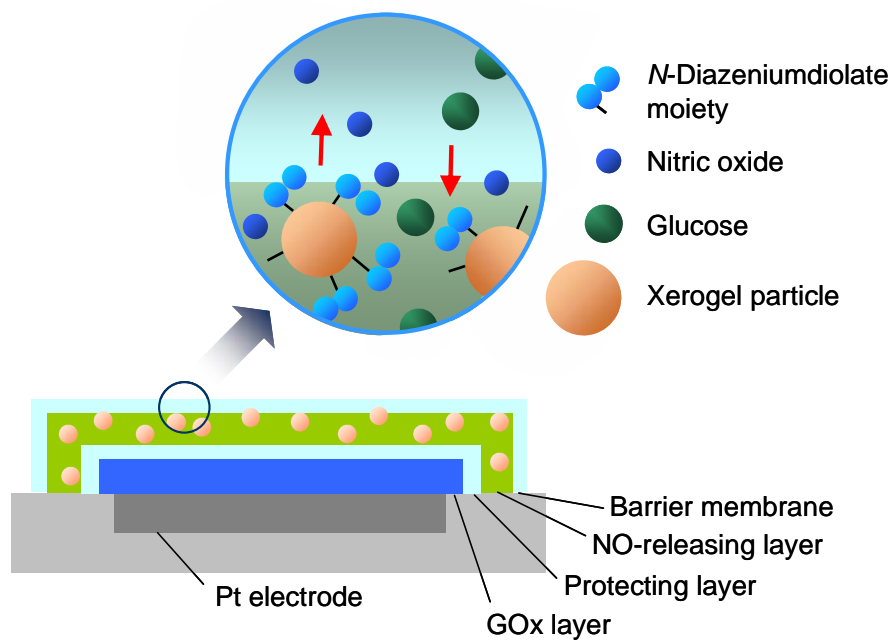


Figure 2.4. Schematic of the *hybrid* xerogel/polyurethane glucose biosensor employing NO donor-modified xerogel particles in a polyurethane supporting matrix.

using xerogel chemistry by varying the type and amount of the aminoalkoxysilane precursor in the sol.⁴⁰ Of the xerogel precursors studied to date, AHAP3/BTMOS xerogels release both the highest levels of NO and for the longest periods (up to 20 d with average fluxes up to 10^{-11} mol·s⁻¹·cm⁻² (for 50 μm thin films)).⁴⁰ Thus, AHAP3-based xerogels were evaluated for their utility as NO-releasing xerogel particles. The combination of AHAP3/MTMOS proved to be superior over other mixtures including AHAP3/BTMOS for xerogel particle synthesis because of the ability to form a fine powder. Indeed, other aminoalkoxysilane/BTMOS combinations often resulted in less glass-like (i.e., more flexible) materials that were difficult to crush and grind. The NO-release kinetics of AHAP3/MTMOS xerogels was similar to AHAP3/BTMOS xerogels with NO release increasing as a function of the concentration of AHAP3 in the xerogel (data not shown).

Upon dispersing the xerogel particles in polyurethane films, a slight decrease in the flux of NO release was observed. This result is not surprising since water must presumably be absorbed by the polymer for NO release to commence. Mowery *et al.* previously noted the influence of water uptake on the NO release kinetics of *N*-diazoniumdiolate-doped hydrophobic polyurethane and poly(vinyl chloride) polymers.⁴³ Both the amount and duration of NO release from the xerogel/polyurethane *hybrid* films was varied by doping different amounts of the AHAP3/MTMOS xerogel particles in the polyurethane. As shown in Figure 2.5, the flux and duration of NO release was amplified proportionately by increasing the mass of xerogel particles in the polyurethane. Of note, previous studies have revealed that only approximately 1 – 20% of the amines in a xerogel matrix are converted to NO donors.⁴⁰ Efforts to lengthen the duration of NO release by employing different aminoalkoxysilane precursors and/or increasing the efficiency of how amines are converted to *N*-

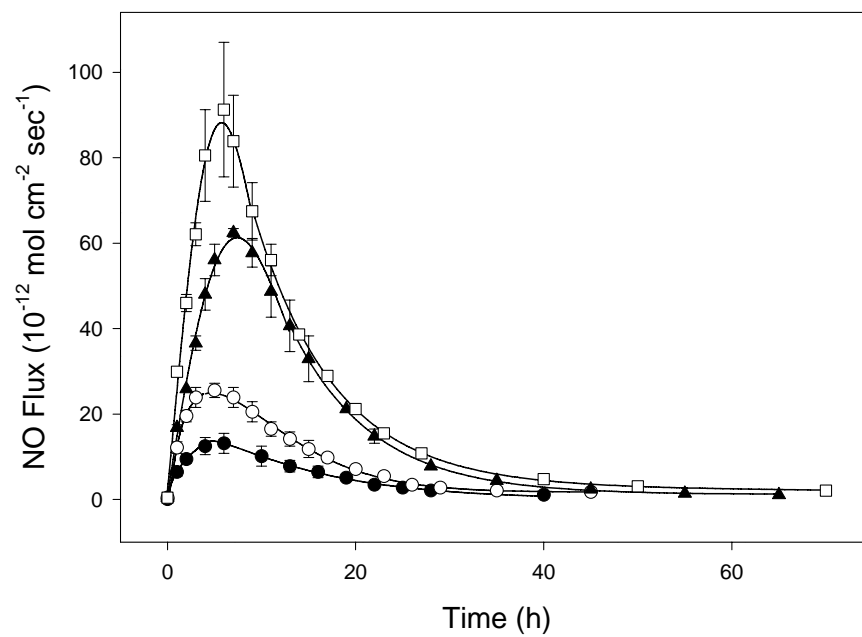


Figure 2.5. NO release profiles from *hybrid* xerogel/polyurethane films cast from (●) 3, (○) 6, (▲) 12, and (□) 18 mg *N*-diazoniumdiolate-modified xerogel particles in 500 μ L polyurethane solution.

diazoniumdiolates by incorporating proton sponges (e.g., sodium methoxide) in the sol cocktail to better stabilize the *N*-diazoniumdiolate structure³⁴ are currently underway. Improvements in the NO release longevity will certainly impact the development of more biocompatible *in vivo* NO-releasing glucose biosensors, particularly with respect to reducing bacterial adhesion at extended periods. However, how much NO and for how long NO release are necessary to improve *in vivo* biocompatibility remains to be studied.

The stability of the xerogel particle-doped polyurethane membrane in buffer solution is an equally important consideration for sensor development. Direct current plasma-optical emission spectroscopy (DCP-OES) analysis was used to assess whether the xerogel particle leached from the polyurethane into solution when immersed in PBS. The percent fragmentation of silicon by mass relative to the mass of the xerogel for *hybrid* xerogel particle/polyurethane films prepared without the barrier membrane was 6.0 ± 0.7 and $12.5 \pm 0.9\%$, after 24 and 48 h, respectively, indicating slight leaching of the xerogel particles from the polyurethane. The xerogel particle leaching decreased significantly to 1.1 ± 0.4 and $3.0 \pm 0.2\%$, after 24 and 48 h, respectively with the addition of the outer polyurethane “barrier” layer (layer 4). Notably, a difference in the NO release kinetics was not observed with the addition of this thin outer barrier layer (see Figure 2.6).

The calibration and response curves of glucose sensors prepared using a) two-layer blank; b) four-layer control (with unmodified XGPs); and, c) four-layer NO-releasing (N_2O_2 -XGPs) polymer membrane configurations are shown in Figure 2.7. The sensitivity for the NO-releasing xerogel/polyurethane glucose biosensors was $-3.8 \times 10^{-2} \mu A/mM$ ($r = 0.9968$), and only slightly lower than the control ($-5.7 \times 10^{-2} \mu A/mM$; $r = 0.9971$) and blank ($-4.8 \times 10^{-2} \mu A/mM$; $r = 0.9973$) sensors. Surprisingly, the sensitivity of the control biosensor was

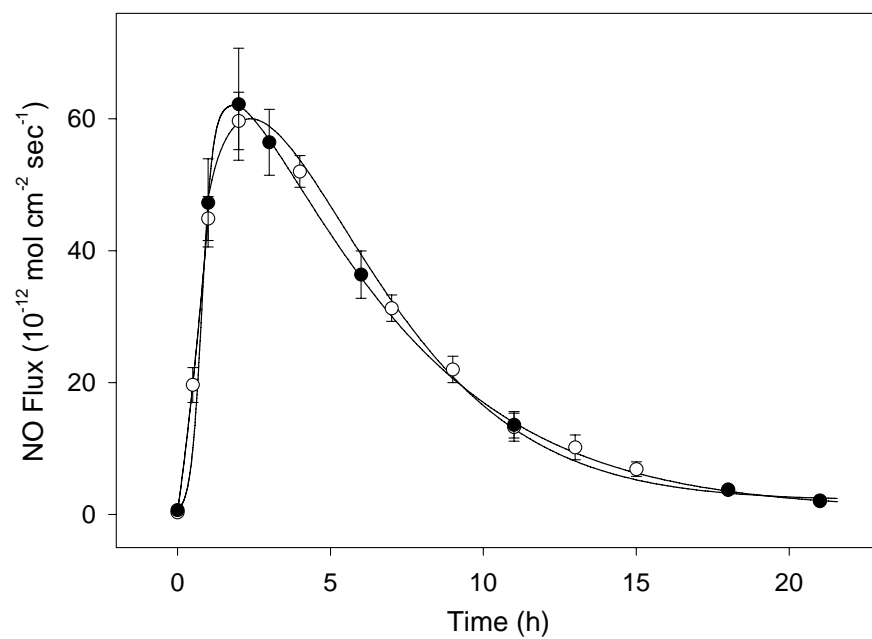


Figure 2.6. NO flux from *N*-diazoniumdiolated-modified xerogel particle/polyurethane films with (○) and without (●) a polyurethane protecting membrane ($n = 3$).

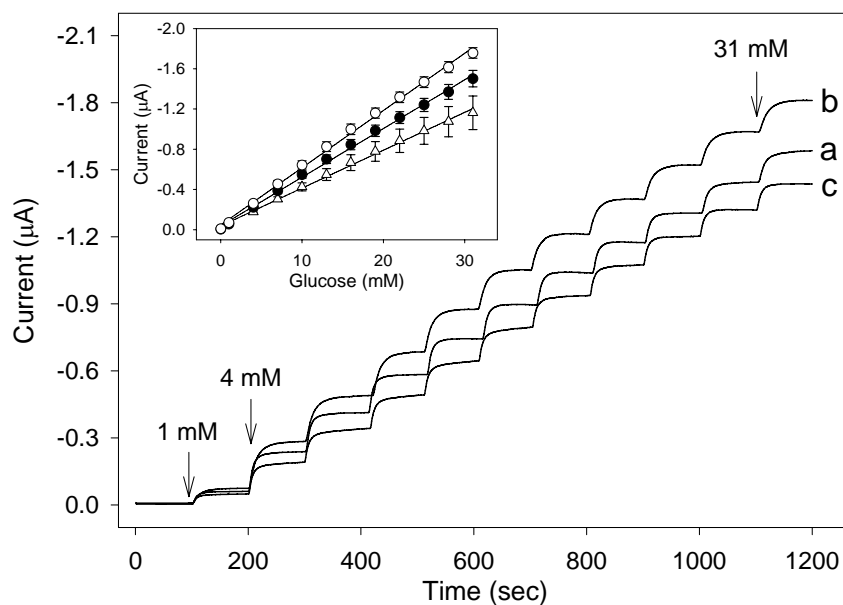


Figure 2.7. Dynamic glucose response and (Inset) calibration curves of biosensors ($n = 3$) prepared with the following configurations: a) 2-layer (without XGP film); b) 4-layer (with unmodified XGP film); and c) 4-layer (with N₂O₂-XGP film). Initial and final concentrations are 1 and 31 mM, and the added concentration interval is 3 mM.

increased slightly relative to the blank (-5.7×10^{-2} vs. -4.8×10^{-2} $\mu\text{A}/\text{mM}$). We attribute this to greater glucose diffusion through the XGP-doped polymer via gaps or channels created by the particles. An elevated surface roughness was noted in the scanning electron microscopy images of NO-releasing and control XGP-containing polyurethane membranes relative to blanks (see Figure 2.8). The analytical sensitivity of the NO-releasing xerogel particle/polyurethane *hybrid* glucose biosensor is dramatically improved over the AEMP3/MTMOS xerogel film-based biosensors that were subsequently exposed to NO to establish NO release (Figure 2.2b). The slight decrease in sensor response is attributed to enzyme inactivation by the NO that diffuses back through the protecting polyurethane membrane (layer 2). Although slight enzyme deactivation occurred in the short-term, the response of the NO releasing biosensor increased slightly after 24 h indicating that the degradation does not continue with NO release. In fact, the response characteristics of the *hybrid* NO-releasing glucose biosensor remained stable through 18 d, after which the linear range decreased from 0 – 60 mM to 0 – 20 mM glucose, and the response time ($t_{95\%}$) increased from less than 20 s to over 65 s. Of note, the sensors were tested on days 1, 2, 3, and 5, and then every 3 – 4 d until day 22, at which point sensor performance was compromised.

To evaluate the potential biocompatibility of N_2O_2 -XGP modified glucose biosensors, *P. aeruginosa* adhesion to control and NO-releasing membranes was assessed using fluorescence microscopy.^{36,38,56} While cell adhesion was observed in the scanning electron microscopy analysis of control and NO-releasing xerogel/polyurethane membranes, the relative amounts of bacterial adhesion were difficult to quantify due to fluorescence from the XGPs (data not shown). In a separate study, NO fluxes as low as $5 \text{ pmol}\cdot\text{cm}^{-2}\cdot\text{s}^{-1}$ were determined sufficient to reduce *P. aeruginosa* adhesion to poly(vinyl chloride)-coated NO-

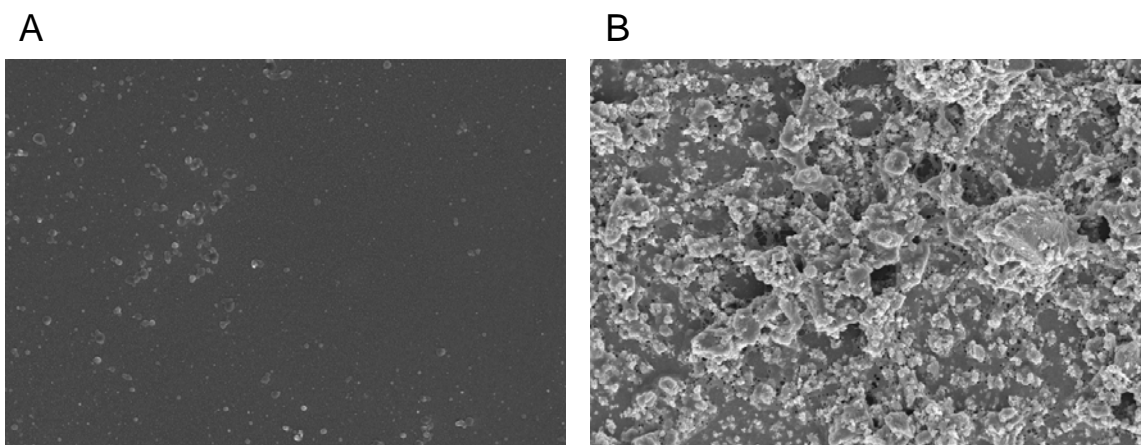


Figure 2.8. Scanning electron microscopy images of surfaces of (A) polyurethane two-layer blank and (B) *N*-diazeniumdiolated-modified xerogel particle/polyurethane films.

releasing xerogels.⁴²

2.4 Conclusions

Sol-gel chemistry represents a flexible approach for combining the chemistries of NO release and enzyme-based glucose sensing. Despite a major compromise in the sensitivity of xerogel film-based glucose biosensors after exposure to NO, functional NO-releasing glucose biosensors can be prepared by doping *N*-diazoniumdiolate-modified xerogel particles in a polyurethane membrane. This NO-releasing layer is sandwiched by additional polyurethane membranes to reduce both enzyme inactivation by NO (by minimizing NO exposure) and xerogel particle leaching. The NO release is easily controlled by varying the amount of *N*-diazoniumdiolate-modified xerogel particles in the polyurethane. The NO-releasing xerogel particle/polyurethane glucose biosensors demonstrate good sensitivity and reproducibility, and fast response times. Studies in progress include identifying methods to improve the duration of NO release and comprehensive *in vivo* biocompatibility testing of NO-releasing xerogels.

2.5 References

- (1) Avnir, D.; Braun, S.; Lev, O.; Ottolenghi, M. "Enzymes and other proteins entrapped in sol-gel materials," *Chem. Mater.* **1994**, *6*, 1605-1614.
- (2) Bhatia, R. B.; Brinker, C. J.; Gupta, A. K.; Singh, A. K. "Aqueous sol-gel process for protein encapsulation," *Chem. Mater.* **2000**, *12*, 2434-2441.
- (3) Gill, I. "Bio-doped nanocomposite polymers: Sol-gel bioencapsulates," *Chem. Mater.* **2001**, *13*, 3404-3421.
- (4) Yamanaka, S. A.; Nishida, F.; Ellerby, L. M.; Nishida, C. R.; Dunn, B.; Valentine, J. S.; Zink, J. I. "Enzymatic activity of glucose oxidase encapsulated in transparent glass by the sol-gel method," *Chem. Mater.* **1992**, *4*, 495-497.
- (5) Chen, Q.; Kenausis, G. L.; Heller, A. "Stability of oxidases immobilized in silica gels," *J. Am. Chem. Soc.* **1998**, *120*, 4582-4585.
- (6) Heller, J.; Heller, A. "Loss of activity or gain in stability of oxidases upon their immobilization in hydrated silica: Significance of the electrostatic interactions of surface arginine residues at the entrances of the reaction channels," *J. Am. Chem. Soc.* **1998**, *120*, 4586-4590.
- (7) Narang, U.; Prasad, P. N.; Bright, F. V.; Ramanathan, K.; Kumar, N. D.; Malhotra, B. D.; Kamalasanan, M. N.; Chandra, S. "Glucose biosensor based on a sol-gel-derived platform," *Anal. Chem.* **1994**, *66*, 3139-3144.
- (8) Shtelzer, S.; Braun, S. "An optical biosensor based upon glucose oxidase immobilized in sol-gel silicate matrix," *Biotechnol. Appl. Biochem.* **1994**, *19*, 293-305.
- (9) Bharathi, S.; Lev, O. "Sol-gel-derived nanocrystalline gold-silicate composite biosensor," *Anal. Commun.* **1998**, *35*, 29-31.
- (10) Wang, B.; Li, B.; Deng, Q.; Dong, S. "Amperometric glucose biosensor based on sol-gel organic-inorganic hybrid material," *Anal. Chem.* **1998**, *70*, 3170-3174.
- (11) Marcos, S. d.; Galindo, J.; Sierra, J. F.; Galban, J.; Castillo, J. R. "An optical glucose biosensor based on derived glucose oxidase immobilized onto a sol-gel matrix," *Sens. Actuators B* **1999**, *57*, 227-232.
- (12) Pandey, P. C.; Upadhyay, S.; Pathak, H. C. "A new glucose sensor based on encapsulated glucose oxidase within organically modified sol-gel glass," *Sens. Actuators B* **1999**, *60*, 83-89.
- (13) Chen, X.; Hu, Y.; Wilson, G. S. "Glucose microbiosensor based on alumina sol-gel matrix/electropolymerized composite membrane," *Biosens. Bioelectron.* **2002**, *17*,

1005-1013.

- (14) Pandey, P. C.; Upadhyay, S.; Shukla, N. K.; Sharma, S. "Studies on the electrochemical performance of glucose biosensor based on ferrocene encapsulated ORMOSIL and glucose oxidase modified graphite paste electrode," *Biosens. Bioelectron.* **2003**, *18*, 1257-1268.
- (15) Wang, J.; Pamidi, P. V. A.; Park, D. S. "Screen-printable sol-gel enzyme-containing carbon inks," *Anal. Chem.* **1996**, *68*, 2705-2708.
- (16) Frost, M. C.; Meyerhoff, M. E. "Implantable chemical sensors for real-time clinical monitoring: Progress and challenges," *Curr. Opin. Chem. Biol.* **2002**, *6*, 633-641.
- (17) Wisniewski, N.; Moussy, F.; Reichert, W. M. "Characterization of implantable biosensor membrane biofouling," *Fresenius J. Anal. Chem.* **2000**, *366*, 611-621.
- (18) Lamba, N. M. K.; Woodhouse, K. A.; Cooper, S. L. *Polyurethanes in biomedical applications*; CRC Press: Boca Ration, 1997.
- (19) Lindner, E.; Cosofret, V. V.; Ufer, S.; Buck, R. P.; Kao, W. J.; Neuman, M. R.; Anderson, J. M. "Ion-selective membranes with low plasticizer content: Electroanalytical characterization and biocompatibility studies," *J. Biomed. Mater. Res.* **1994**, *28*, 591-601.
- (20) Yoda, R. "Elastomers for biomedical applications," *J. Biomater. Sci. Polymer Edn* **1998**, *9*, 561-626.
- (21) Moussy, F.; Harrison, D. J.; Rajotte, R. V. "A miniaturized Nafion-based glucose sensor: In vitro and in vivo evaluation in dogs," *Int. J. Artif. Organs* **1994**, *17*, 88-94.
- (22) Valdes, T. I.; Moussy, F. "A ferric chloride pre-treatment to prevent calcification of Nafion membrane used for implantable biosensors," *Biosens. Bioelectron.* **1999**, *14*, 579-585.
- (23) Hendricks, S. K.; Kwok, C.; Shen, M.; Horbett, T. A.; Ratner, B. D.; Bryers, J. D. "Plasma-deposited membranes for controlled release of antibiotic to prevent bacterial adhesion and biofilm formation," *J. Biomed. Mater. Res.* **2000**, *50*, 160-170.
- (24) Rojas, I. A.; Slunt, J. B.; Grainger, D. W. "Polyurethane coatings release bioactive antibodies to reduce bacterial adhesion," *J. Control. Release* **2000**, *63*, 175-189.
- (25) Radomski, M. W.; Palmer, R. M. J.; Moncada, S. "The anti-aggregating properties of vascular endothelium: Interactions between prostacyclin and nitric oxide," *Br. J. Pharmacol.* **1987**, *92*, 639-646.
- (26) Ziche, M.; Morbidelli, E.; Masini, E.; Amerini, S.; Granger, H. J.; Maggi, C. A.;

- Geppetti, P.; Ledda, F. "Nitric oxide mediates angiogenesis in vivo and endothelial cell growth and migration in vitro," *J. Clin. Invest.* **1994**, *94*, 2036-2044.
- (27) Nablo, B. J.; Chen, T.-Y.; Schoenfisch, M. H. "Sol-gel derived nitric oxide-releasing materials that reduce bacterial adhesion," *J. Am. Chem. Soc.* **2001**, *123*, 9712-9713.
- (28) Hanson, S. R.; Hutsell, T. C.; Keefer, L. K.; Mooradian, D. L.; Smith, D. J. "Nitric oxide donors: A continuing opportunity in drug design," *Adv. Pharmacol.* **1995**, *34*, 383-398.
- (29) Smith, D. J.; Chakravarthy, D.; Pulfer, S.; Simmons, M. L.; Hrabie, J. A.; Citro, M. L.; Saavedra, J. E.; Davies, K. M.; Hutsell, T. C.; Mooradian, D.; Hanson, S. R.; Keefer, L. K. "Nitric oxide-releasing polymers containing the [N(O)NO]- group," *J. Med. Chem.* **1996**, *39*, 1148-1156.
- (30) Espadas-Torre, C.; Oklejas, V.; Mowery, K. A.; Meyerhoff, M., E. "Thromboresistant chemical sensors using combined nitric oxide release/ion sensing polymeric films," *J. Am. Chem. Soc.* **1997**, *119*, 2321-2322.
- (31) Annich, G. M.; Meinhardt, J. P.; Mowery, K. A.; Ashton, B. A.; Merz, S. I.; Hirschl, R. B.; Meyerhoff, M. E.; Bartlett, R. H. "Reduced platelet activation and thrombosis in extracorporeal circuits coated with nitric oxide release polymers," *Crit. Care Med.* **2000**, *28*, 915-920.
- (32) Bohl, K. S.; West, J. L. "Nitric oxide-generating polymers reduce platelet adhesion and smooth muscle cell proliferation," *Biomaterials* **2000**, *21*, 2273-2278.
- (33) Mowery, K. A.; Schoenfisch, M. H.; Saavedra, J. E.; Keefer, L. K.; Meyerhoff, M., E. "Preparation and characterization of hydrophobic polymeric films that are thromboresistant via nitric oxide release," *Biomaterials* **2000**, *21*, 9-21.
- (34) Zhang, H.; Annich, G. M.; Miskulin, J.; Osterholzer, K.; Merz, S. I.; Bartlett, R. H.; Meyerhoff, M., E. "Optical chloride sensor based on dimer-monomer equilibrium of indium(III) octaethylporphyrin in polymeric film," *Biomaterials* **2002**, *23*, 1485-1494.
- (35) Nablo, B. J.; Schoenfisch, M. H. "Antibacterial properties of nitric oxide-releasing sol-gels," *J. Biomed. Mater. Res.* **2003**, *67*, 1276-1283.
- (36) Kelm, M.; Yoshida, K. *Metabolic fate of nitric oxide and related N-oxides*. In *Methods in nitric oxide research*; Feelisch, M., Stamler, J. S., Eds.; John Wiley & Sons: New York, NY, 1996, pp 47-58.
- (37) Hrabie, J. A.; Klose, J. R.; Wink, D. A.; Keefer, L. K. "New nitric oxide-releasing zwitterions derived from polyamines," *J. Org. Chem.* **1993**, *58*, 1472-1476.
- (38) Keefer, L. K.; Nims, R.; Davies, K. M.; Wink, D. A. *NONOates (1-substituted diazen-*

- l-ium-1,2-diolates) as nitric oxide donors: Convenient nitric oxide dosage forms. In Methods in enzymology; Academic Press, 1996; Vol. 268, pp 281-293.*
- (39) Davies, K. M.; Wink, D. A.; Saavedra, J. E.; Keefer, L. K. "Chemistry of the diazeniumdiolates. 2. Kinetics and mechanism of dissociation to nitric oxide in aqueous solution," *J. Am. Chem. Soc.* **2001**, *123*, 5473-5481.
- (40) Marxer, S. M.; Rothrock, A. R.; Nablo, B. J.; Robbins, M. E.; Schoenfisch, M. H. "Preparation of nitric oxide (NO)-releasing sol-gels for biomaterial applications," *Chem. Mater.* **2003**, *15*, 4193-4199.
- (41) Nablo, B. J.; Rothrock, A. R.; Schoenfisch, M. H. "Nitric oxide-releasing sol-gels as antibacterial coatings for orthopedic implants," *Biomaterials* **2005**, *26*, 917-924.
- (42) Nablo, B. J.; Schoenfisch, M. H. "Poly(vinyl chloride)-coated sol-gels for studying the effects of nitric oxide release on bacterial adhesion," *Biomacromolecules* **2005**, *5*, 2034-2041.
- (43) Mowery, K. A.; Meyerhoff, M., E. "More biocompatible electrochemical sensors using nitric oxide release polymers," *Electroanalysis* **1999**, *11*, 681-686.
- (44) Schoenfisch, M. H.; Zhang, H.; Frost, M. C.; Meyerhoff, M. E. "Nitric oxide-releasing fluorescence-based oxygen sensing polymeric films," *Anal. Chem.* **2002**, *74*, 5937-5941.
- (45) Frost, M. C.; Rudich, S. M.; Zhang, H.; Maraschio, M. A.; Meyerhoff, M., E. "In vivo biocompatibility and analytical performance of intravascular amperometric oxygen sensors prepared with improved nitric oxide-releasing silicone rubber coating," *Anal. Chem.* **2002**, *74*, 5942-5947.
- (46) Fujii, H.; Ichimori, K.; Hoshiai, K.; Nakazawa, H. "Nitric oxide inactivates NADPH oxidase in pig neutrophils by inhibiting its assembling process," *J. Biol. Chem.* **1997**, *272*, 32773-32778.
- (47) Ichimori, K.; Fukahori, M.; Nakazawa, H.; Okamoto, K.; Nishino, T. "Inhibition of xanthine oxidase and xanthine dehydrogenase by nitric oxide. Nitric oxide converts reduced xanthine-oxidizing enzymes into the desulfo-type inactive form," *J. Biol. Chem.* **1999**, *274*, 7763-7768.
- (48) Gopalakrishna, R.; Chen, Z. H.; Gundimeda, U. "Nitric oxide and nitric oxide-generating agents induce a reversible inactivation of protein kinase C activity and phorbol ester binding," *J. Biol. Chem.* **1993**, *268*, 27180-27185.
- (49) Shaw, A. W.; Vosper, A. J. "Solubility of nitric oxide in aqueous and nonaqueous solvents," *J. Chem. Soc. Faraday Trans. I* **1977**, *8*, 1239-1244.

- (50) Bergmeyer, H. U. *Methods of enzymatic analysis*, 3rd ed.; Verlag Chemie: Deerfield Beach, 1983.
- (51) Collinson, M. M. "Sol-gel strategies for the preparation of selective materials for chemical analysis," *Crit. Rev. Anal. Chem* **1999**, *29*, 289-311.
- (52) Ignarro, L. J. *Nitric oxide: Biology and pathobiology*; Academic Press: New York, NY, 2000.
- (53) Cooper, C. E. "Nitric oxide and iron proteins," *Biochim. Biophys. Acta* **1999**, *1411*, 290-309.
- (54) Torres, J.; Wilson, M. T. "The reactions of copper proteins with nitric oxide," *Biochim. Biophys. Acta* **1999**, *1411*, 310-322.
- (55) O'Malley, J. J.; Weaver, J. L. "Subunit structure of glucose oxidase from *Aspergillus niger*," *Biochemistry* **1972**, *11*, 3527-3532.
- (56) Kalisz, H. M.; Hecht, H.; Schomburg, D.; Schmid, R. D. "Crystallization and preliminary x-ray diffraction studies of a deglycosylated glucose oxidase from *Aspergillus niger*," *J. Mol. Biol.* **1990**, *213*, 207-209.
- (57) Jin, W.; Brennan, J. D. "Properties and applications of proteins encapsulated within sol-gel derived materials," *Anal. Chim. Acta* **2002**, *461*, 1-36.
- (58) Brinker, C. J.; Scherer, G. W. *Sol-gel science: The physics and chemistry of sol-gel processing*; Academic Press, Inc.: New York, NY, 1990.
- (59) Harreld, J. H.; Su, K.; Katsoulis, D. E.; Suto, M.; Stucky, G. D. "Surfactant and pH-mediated control over the molecular structure of poly(phenylsilsesquioxane) resins," *Chem. Mater.* **2002**, *14*, 1174-1182.

Chapter 3:

Sol–Gel Derived Amperometric Nitric Oxide Microsensor

3.1 Introduction

Endogenously produced nitric oxide (NO) has been studied extensively in recent years due to its roles in numerous physiological processes including neurotransmission, vasodilatation, blood pressure regulation, platelet adhesion and activation, angiogenesis, wound healing, and phagocytosis.¹⁻³ *In vivo* measurements of NO have proven challenging because NO is both present in low concentrations in the body (sub-micromolar levels) and highly reactive with numerous endogenous species including free radicals, transition metals, metalloproteins, peroxides, and oxygen.^{2,4} Indeed, the half-life of NO in biological milieu is <10 s.⁴ Consequently, indirect detection methods (e.g., spectroscopically determining a secondary species such as L-citrulline⁵ or nitrite/nitrate⁶) often fail to accurately reflect the spatial and temporal distributions of NO in biological environments. Direct measurement strategies are therefore necessary for investigating the physiological origin and action of endogenously produced NO.

Several methods exist for directly measuring NO including electron paramagnetic resonance (EPR) spectroscopy,⁷ chemiluminescence,^{8,9} fluorescence,^{10,11} and electrochemical sensing.¹²⁻¹⁴ Of these approaches, miniaturized electrochemical (e.g., amperometric and voltammetric) sensors represent the most promising means for determining the spatial and temporal distributions of NO near its physiological source.¹⁴ In addition to providing real-

time measurements of NO, electrochemical sensors are readily miniaturized thereby allowing for the fabrication of relatively inexpensive microelectrode devices. The most straightforward detection scheme to date involves the electrochemical oxidation of NO at a metal (e.g., platinum and gold) or carbon electrode.¹³ The direct electrooxidation of NO, however, requires a relatively high working potential (+0.7 to +0.9 V vs Ag/AgCl), thus interference from other readily oxidizable biological species including nitrite, ascorbic acid, uric acid, and acetaminophen often precludes selective detection of NO.¹⁴

Attempts to enhance selectivity for NO in the presence of such interfering species have included modifying the electrode surface with either an electrocatalytic metal complex or a thin polymeric film.^{12,14} Metalloporphyrins,^{15,16} metal phthalocyanines,^{17,18} and other organometallic compounds¹⁹⁻²² containing nickel, cobalt, iron, and copper centers have been employed to lower the oxidation potential of NO at both carbon and metal (e.g., platinum) electrodes. However, further surface modification with permselective membranes (e.g., cellulose acetate and Nafion) is required to achieve the desired selectivity for NO via size exclusion and/or electrostatic repulsion.^{16,18,20}

Alternatively, Shibuki reported on a Clark-style NO microsensor in which the working (platinum) and reference (Ag/AgCl) electrodes were placed in a glass micropipette filled with an internal electrolyte solution, and subsequently sealed with a chloroprene gas-permeable membrane.²³ While effective at improving the selectivity for NO, the use of such sensors for *in vivo* measurements remains limited due to inherent difficulties in sensor miniaturization and slow response times with respect to the rate of physiological changes in NO concentrations.¹⁴ To improve NO permeation properties and facilitate the fabrication of NO microsensors, significant efforts have been devoted to developing more efficient

permselective coatings.^{12,14} Indeed, several polymeric materials have been evaluated as gas-permeable or permselective membranes including polycarbazole,²⁴ *o*- and *m*-phenylenediamine,²⁵ collodion,²⁶ Nafion,²⁷ poly(tetrafluoroethylene) (PTFE),²⁸ polydimethylsiloxane (silicone rubber),²⁹⁻³¹ cellulose acetate,^{19,32} and multilayer *hybrids* of these polymers. Notably, the utility of these polymeric membranes for improving *in vivo* sensor performance also remains limited.

Sol-gel derived materials (i.e., xerogels) have emerged as a class of materials suitable for a wide range of sensing applications since they are synthesized under mild conditions, enable tremendous chemical flexibility, and strongly adhere to a variety of substrates (e.g., metal/metal oxides and silica substrates).^{33,34} The physical and chemical properties of sol-gel derived sensors are readily tailored by varying the silicon alkoxide precursors and/or coupling specific functional compounds (e.g., ion-exchange or redox polymers, biomolecules, and electrochemical or optical sensing elements) to the polymer backbone.^{34,35} Organically-modified xerogel films are particularly advantageous for gas sensing applications. The porous inorganic network provides an open, rigid structure that allows for rapid diffusion of gaseous molecules while the organic groups impart hydrophobicity to the membrane thereby preventing leaching of the internal electrolyte.^{36,37}

Herein, we explore the feasibility of using sol-gel derived materials as gas-permeable membranes for amperometric NO sensing. A systematic evaluation of silicon-based xerogel films is performed to identify the optimum formulation for maximizing NO permeability while providing sufficient selectivity for NO in the presence of common interfering species. Electrochemistry and surface wettability measurements are used to monitor changes in the chemical structure of the xerogel as a function of sol-gel composition and reaction/processing

conditions. The effect of incorporating Nafion (a perfluorinated cation-exchange polymer) into the xerogel matrix and the stability of the ensuing xerogel/Nafion *hybrid* film are also discussed. Finally, we report on the fabrication and in situ performance of a NO-selective microsensor prepared with the optimized xerogel composite membrane.

3.2 Experimental Section

3.2.1 Reagents and Materials

Methyltrimethoxysilane (MTMOS), isobutyltrimethoxysilane (BTMOS), *N*-[3-(trimethoxysilyl)propyl]diethylenetriamine (DET3), Nafion (5 wt% solution in a mixture of lower aliphatic alcohols and water), glutaraldehyde (25% in water), and uric acid were purchased from Aldrich (Milwaukee, WI). (Aminoethylaminomethyl)phenethyltrimethoxysilane (AEMP3), *N*-(6-aminoethyl)aminopropyltrimethoxysilane (AHAP3), and aminopropyltrimethoxysilane (APTMS) were purchased from Gelest (Tullytown, PA). Polyvinylpyrrolidone (PVP; MW 10000) was purchased from Fluka (Buchs, Switzerland). Ascorbic acid, acetaminophen, and sodium nitrite were purchased from Sigma (St. Louis, MO). Platinizing solution (3% chloroplatinic acid in water) was purchased from LabChem (Pittsburgh, PA). Nitric oxide (NO), argon (Ar), and nitrogen (N₂) gases were obtained from National Welders Supply (Raleigh, NC). Other solvents and chemicals were analytical-reagent grade, and used as received. A Millipore Milli-Q UV Gradient A10 System (Bedford, MA) was used to purify distilled water to a final resistivity of 18.2 MΩ·cm and a total organic content of ≤6 ppb.

3.2.2 Preparation of Sol–Gel Derived Gas-Permeable Membranes

Glass slides were cleaned in 10% nitric acid (v/v in water) for 20 min at 80 °C, and then modified by sequential immersion in 10% APTMS (v/v in water, pH 6.5) for 1 h at 80 °C and

10% glutaraldehyde (v/v in water) for 1 h at room temperature.³⁸ The surfaces were rinsed thoroughly with water and dried with a stream of N₂ prior to modification with xerogel films. Cylindrical polycrystalline platinum (Pt) working electrodes (2 mm diameter; 6 mm diameter including the surrounding insulator) were mechanically polished with successively finer grades of agglomerated alumina slurries down to 0.05 μm. An ultrasonic cleaner was used to remove residual alumina loosely bound to the surface. Xerogel casting solutions were prepared by mixing 25 – 50 μL MTMOS or BTMOS with 200 μL of ethanol and 100 μL of water for 10 min. The synthesis of BTMOS-based xerogels was catalyzed by the addition of 10 μL of 0.5 M HCl. The aminoalkoxysilane content was varied from 0 to 50% (v/v, balance MTMOS or BTMOS) by the addition of 0 – 25 μL of AEMP3, AHAP3, or DET3 (for a total silane volume of 50 μL). To formulate the xerogel/Nafion *hybrid* composites, 5, 10, or 15 μL aliquots of Nafion (corresponding to 9, 17, and 23%, v/v in 50 μL of total silane, respectively) were added to the sol and mixed for an additional 5 min. The ensuing solution was then deposited onto either the modified glass substrates (for material characterization) or the Pt working electrodes (0.02, 0.04, 0.08 and 0.12 μL·mm⁻²) and allowed to cure for 24 h under ambient conditions. The porous structure of the cured sol–gel derived films was varied via one of the following processing conditions: (1) aging under ambient conditions for 7 d; (2) heat-annealing at 80 °C for 24 h; or, (3) NO-induced catalytic polycondensation by exposure to 1 – 5 atm of NO, hereafter referred to as “charging”.^{39,40} Xerogel-coated electrodes were charged with NO in an in-house reactor that was first flushed with Ar to remove oxygen and any residual moisture, and then pressured to 1, 3, or 5 atm NO or Ar (control) for 10 min to 5 h. Prior to removing the modified xerogel electrodes, unreacted, physically adsorbed NO was purged from the chamber with Ar. Xerogel film

thickness was measured using a Tencor Alpha Step-100 profilometer (Brumley South; Mooresville, NC).⁴¹

3.2.3 Sensor Performance Evaluation

To evaluate the analytical performance of the NO sensors, amperometric measurements were performed using a CH Instruments 660A potentiostat (Austin, TX). The electrode assembly (3-electrode configuration) consisted of a xerogel-modified Pt working electrode (2 mm diameter), Pt coiled counter electrode (0.6 mm diameter), and a Ag/AgCl (3.0 M KCl) reference electrode. The permeability of the sol-gel derived films to NO (P_{NO}^e) and nitrite ($P_{NO_2^-}^e$) was evaluated electrochemically by measuring the ratio of peak currents at the xerogel coated and bare Pt electrodes ($\Delta I_x/\Delta I_b$) in 10 μ M NO and 100 μ M nitrite solutions, respectively.⁴² The selectivity of the xerogel-modified sensors for NO in the presence of interfering species was determined using the separation solution method.⁴³ The amperometric selectivity coefficients ($\log K_{NO,j}^{amp}$) were calculated using the following equation (3.1):

$$\log K_{NO,j}^{amp} = \log \left(\frac{\frac{\Delta I_j}{c_j}}{\frac{\Delta I_{NO}}{c_{NO}}} \right) \quad (\text{Equation 3.1})$$

where ΔI_{NO} and ΔI_j are the measured current values for the target analyte (NO) and interfering species ($j =$ nitrite, ascorbic acid, uric acid, and acetaminophen), respectively. The concentration of each interfering substance (c_j) was selected to be 100 μ M, roughly 10 times greater than the concentration of NO (c_{NO}). To further evaluate the ability of xerogel films to

differentiate NO over nitrite, the ratio of NO and nitrite permeability was used to determine permselectivity (α_{NO,NO_2^-}):⁴⁴

$$\alpha_{NO,NO_2^-} = \frac{P_{NO}^e}{P_{NO_2^-}^e} \quad (\text{Equation 3.2})$$

A standard NO solution (1.9 mM) was prepared by purging phosphate-buffered saline (PBS; 0.01 M, pH 7.4) with Ar for 20 min to remove oxygen, followed by NO (99.5%) for 20 min.²⁸ The solutions of NO and interfering species were freshly prepared every 2 d, and stored at 4 °C. All sensors were pre-polarized for at least 0.5 h and tested in deoxygenated PBS at room temperature with constant stirring, and currents were recorded at an applied potential of +0.8 V (vs. Ag/AgCl). Sensors were stored in PBS at room temperature between measurements.

3.2.4 Xerogel Material Characterization

Xerogel surface wettability was evaluated with a KSV Instruments Cam 200 optical contact angle meter (Helsinki, Finland). Static water contact angles were obtained before and after NO charging.

Solid-state cross polarization/magic angle spinning (CP/MAS) ²⁹Si nuclear magnetic resonance (NMR) spectra were obtained at 293 K on a Bruker 360 MHz DMX spectrometer (Billerica, MA) equipped with wide-bore magnets (triple axis pulsed field gradient double resonance probes). Xerogel samples (before and after exposure to 5 atm NO for 1 h) were packed into 7 mm rotors (double resonance frequency of 71.548 MHz) and spun at a speed of 8.0 kHz. The chemical shifts were determined in ppm relative to a tetramethylsilane (TMS) external standard.

Film stability was evaluated by soaking xerogel-coated glass slides in PBS (pH 7.4) under ambient conditions for 1 to 10 d. Xerogel fragmentation was determined by measuring the Si concentration in the soak solutions using an ARL-Fisons Spectrascan 7 direct current plasma optical emission spectrometer (DCP-OES; Beverly, MA). After converting the measured silicon concentration (ppm) to moles, the extent of fragmentation was calculated as a function of exposed xerogel surface area ($\mu\text{mol}\cdot\text{cm}^{-2}$).

3.2.5 Preparation and Evaluation of NO Microsensors

The NO microsensor (2-electrode configuration) consisted of a Pt wire working electrode and a Ag/AgCl reference electrode (see Figure 3.1). A septum theta borosilicate glass capillary (1.5/1.02 mm o.d./i.d.; World Precision Instruments; Sarasota, FL) was used as a sensor sleeve to prevent direct electrical contact between the working and reference electrodes. Platinum (127 μm diameter) and silver (250 μm diameter) wires were inserted into separate barrels of the capillary. The end of the sleeve was shielded using a flame torch and mechanically polished with successive alumina slurries down to 0.05 μm to expose the Pt and Ag disks. The Ag/AgCl reference electrode was formed by immersing the sensing tip in an aqueous 0.1 M FeCl₃ solution for 2 min. The Pt working electrode was platinized in 3% chloroplatinic acid (v/v in water) by cycling the potential from +0.6 to -0.35 V at a scan rate of 20 mV/sec using a CH Instruments 660A potentiostat.²⁸ The internal electrolyte layer (thickness \sim 1.5 μm) was deposited by dipping the capillary electrode into a solution of 30 mM NaCl, 0.3 mM HCl, and 1% PVP (w/w in water), and drying for 10 min under ambient conditions. The electrode was then modified with the optimized xerogel/Nafion-derived gas-permeable membrane by dip-coating the sensor tip into a solution consisting of 40 μL of

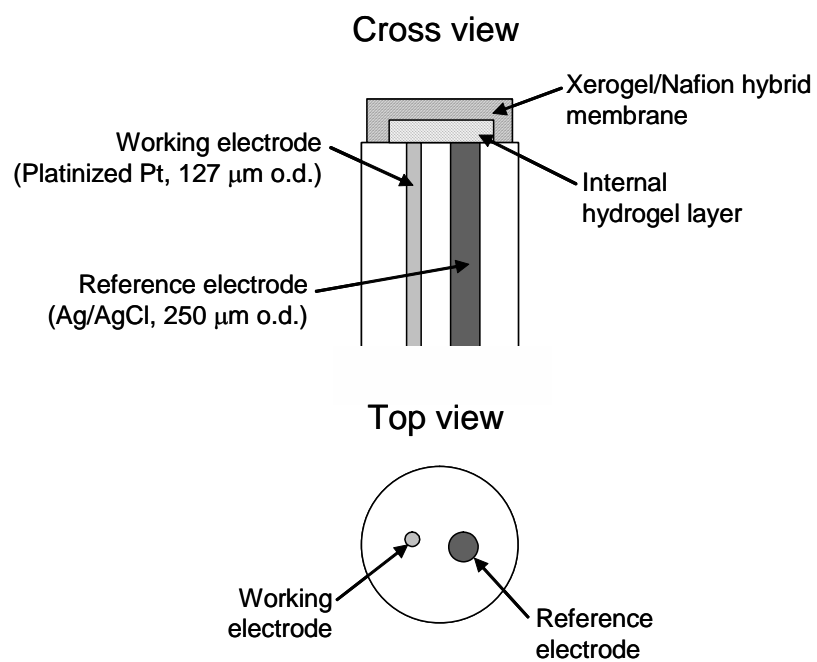


Figure 3.1. Schematic of the *hybrid* xerogel/Nafion-modified NO microsensor.

MTMOS, 10 μL of AEMP3, 10 μL of Nafion, 200 μL of ethanol, and 100 μL of water. After allowing the xerogel layer to cure for 5 min, the process was repeated to yield a membrane with a thickness of ~ 2.5 μm . The modified electrode was then allowed to dry for 24 h under ambient conditions. Finally, the resulting xerogel-coated microsensor was exposed to 5 atm NO for 10 min to catalyze further polymer condensation.

Response and calibration curves were obtained by injecting aliquots of the standard NO solution (1.9 mM) into 100 mL of PBS (pH 7.4; not deoxygenated) at room temperature under constant stirring. All microelectrodes were pre-polarized for 3 to 5 h. Currents were recorded every second at an applied potential of +0.7 and +0.8 V (vs. Ag/AgCl) for the platinized and non-platinized working electrodes, respectively.

3.3 Results and Discussion

Despite the versatility of sol–gel chemistry for preparing a variety of useful sensors, xerogels have yet to be employed as permselective membranes for NO sensors due to difficulties in discriminating NO from biologically important interfering species based on size. Although both the physical porosity and hydrophobicity of a xerogel are readily controlled by the extent of polycondensation and the type and concentration of alkylalkoxysilane precursors, most xerogels are quite porous (e.g., 100 – 1000 m^2/g).⁴⁵ Recently, we reported that the porosity of aminoalkoxysilane/alkylalkoxysilane *hybrid* xerogels was significantly reduced compared to their alkylalkoxysilane counterparts due to enhanced polycondensation catalyzed by the aminoalkoxysilane.^{40,42,46} The permeability of the cured aminoalkoxysilane-based xerogels was further reduced upon exposure to high pressures of NO.⁴²

In the present study, the effects of the xerogel composition, sol-gel reaction/processing

conditions, and NO exposure on permselectivity are evaluated to determine the feasibility of developing a xerogel derived membrane for selective amperometric detection of NO.

3.3.1 Optimization of Xerogel Composites as NO-Permselective Membranes

Several xerogel films prepared by combining an alkylalkoxysilane (i.e., MTMOS or BTMOS) with an aminoalkoxysilane (i.e., AEMP3, AHAP3, or DET3) were evaluated as potential gas-permeable membranes for NO sensing (Table 3.1). Of note, AHAP3/MTMOS and DET3/ MTMOS xerogels were not pursued due to their instability in aqueous solution.⁴⁰ The concentration of the aminoalkoxysilane used to prepare each xerogel was 20% (v/v, balance MTMOS or BTMOS). The influence of the reaction/processing conditions (i.e., drying/aging time and temperature, and exposure of the cured film to high pressures of NO) on membrane NO permeability (P_{NO}^e) and selectivity over nitrite (α_{NO,NO_2^-} and K_{NO,NO_2}^{amp}) was investigated. With respect to measuring NO electrochemically, nitrite is the most problematic interfering species present in biological milieu due to its similarity in size to NO. To identify the optimum xerogel composition and processing conditions, the performance of xerogel-modified NO sensors using macroelectrodes (Pt, 2 mm diameter) was evaluated.

Both the permeability and selectivity of xerogel-based NO sensors were significantly affected by the type of alkyl/aminoalkoxysilanes used to prepare the membrane and specific reaction/processing conditions (Table 3.1). Films with high NO permeability (P_{NO}^e) were characterized by poor selectivity (K_{NO,NO_2}^{amp}). Such behavior was expected since glassy and rubbery polymers previously employed as permselective membranes for sensor and separation applications exhibit poor selectivity due to high overall permeability regardless of the analyte's size.⁴⁷ Of the xerogel combinations studied, AEMP3 (balance MTMOS,

Table 3.1. Electrochemical characteristics of sol-gel derived NO sensors as a function of xerogel composition and processing conditions^a

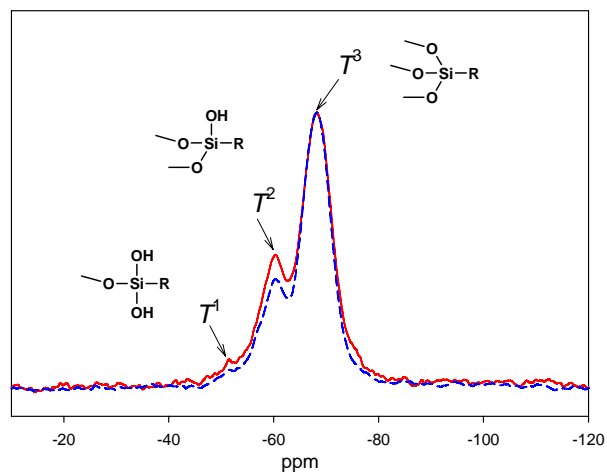
Composition ^{b,c/} processing conditions ^d	Permeability, ^e P_i^e		Permselectivity, α_{NO,NO_2^-}	Selectivity, ^{e,f} $\log K_{NO,NO_2^-}^{amp}$
	$i = NO$	$i = NO_2^-$		
Bare Pt (control)				-1.51 ± 0.09
MTMOS	0.52 ± 0.05	0.32 ± 0.09	1.6 ± 0.5	-1.74 ± 0.16
MTMOS (NO)	0.65 ± 0.04	0.40 ± 0.05	1.6 ± 0.2	-1.66 ± 0.06
BTMOS	0.83 ± 0.08	0.83 ± 0.12	1.0 ± 0.2	-1.60 ± 0.03
BTMOS (NO)	0.95 ± 0.08	0.89 ± 0.17	1.1 ± 0.2	-1.64 ± 0.03
AEMP3/MTMOS	0.11 ± 0.01	0.008 ± 0.001	14 ± 2	-2.49 ± 0.41
AEMP3/MTMOS (aging)	0.09 ± 0.009	0.006 ± 0.002	15 ± 5	-3.28 ± 0.11
AEMP3/MTMOS (heat)	0.16 ± 0.02	0.004 ± 0.001	40 ± 11	-2.90 ± 0.10
AEMP3/MTMOS (Ar)	0.09 ± 0.02	0.010 ± 0.003	9 ± 3	-2.55 ± 0.32
AEMP3/MTMOS (NO)	0.03 ± 0.006	<0.0001	300	-4.38 ± 0.49
AEMP3/BTMOS	0.15 ± 0.07	0.007 ± 0.002	21 ± 12	-2.87 ± 0.33
AEMP3/BTMOS (NO)	0.02 ± 0.002	0.002 ± 0.001	10 ± 5	-3.62 ± 0.11
AHAP3/BTMOS	0.27 ± 0.04	0.21 ± 0.04	1.3 ± 0.3	-1.77 ± 0.11
AHAP3/BTMOS (NO)	0.28 ± 0.05	0.02 ± 0.002	14 ± 3	-2.75 ± 0.04
DET3/BTMOS	0.20 ± 0.05	0.11 ± 0.01	1.8 ± 0.5	-1.85 ± 0.09
DET3/BTMOS (NO)	0.17 ± 0.02	0.05 ± 0.03	3.4 ± 2.1	-2.16 ± 0.24

^aNumber of samples: $n = 3$ or 5 . ^bMTMOS, methyltrimethoxysilane; BTMOS, isobutyltrimethoxysilane; AEMP3, (aminoethylaminomethyl)phenethyltrimethoxysilane; AHAP3, *N*-(6-aminohexyl)aminopropyltrimethoxysilane; and DET3, *N*-[3-(trimethoxysilyl)propyl]diethyl-enetriamine. ^cAll aminosilane-based xerogels contain 20% of aminosilane (balance MTMOS or BTMOS). ^dAll xerogel coatings were dried under ambient conditions for 24 h. The term aging refers to drying under ambient conditions for 7 d; heat = annealing at 80 °C for 24 h; and NO and Ar = exposing to 5 atm of NO and Ar for 1 h, respectively. ^eMeasured in deoxygenated PBS (0.01 M, pH 7.4). Values were determined at 10 μ M of NO and 100 μ M of NO_2^- , respectively. ^fTo determine selectivity, the separate solution method was employed.

hereafter AEMP3/MTMOS) membranes exhibited the most ideal compromise between permeability and selectivity. Indeed, AEMP3/MTMOS xerogels were characterized by approximately an order of magnitude greater NO selectivity over nitrite (14 of α_{NO,NO_2^-} and -2.49 of $K_{NO,NO_2^-}^{amp}$) compared to other aminoalkoxysilane/alkylalkoxysilane combinations (Table 3.1). The sensor performance of AEMP3/MTMOS xerogels was thus further manipulated by varying the following reaction/ processing conditions: 1) aging under ambient conditions for 7 d; 2) heat-annealing at 80 °C for 24 h; and, 3) NO or Ar charging at 5 atm for 1 h. As shown in Table 3.1, exposing the AEMP3/MTMOS xerogel sensor to high pressures of NO was more effective than aging or annealing. In fact, sensors fabricated with 20% AEMP3/MTMOS xerogels charged with 5 atm NO for only 1 h demonstrated a dramatically improved selectivity (-4.38 of $K_{NO,NO_2^-}^{amp}$) compared to controls. Neither the permeability nor the selectivity of analogous sensors charged with 5 atm Ar were changed, indicating that exposure to high pressures alone does not significantly affect the physical structure of the xerogel.

To better understand the influence of NO exposure on xerogel structure, solid-state ^{29}Si NMR spectra were collected for AEMP3/MTMOS and AHAP3/BTMOS xerogel samples (Figure 3.2). Three peaks were observed in the ^{29}Si NMR spectra of the aminoalkoxysilane-modified xerogels, indicating three distinct silicon chemical environments. Indeed, the peaks at chemical shifts of -51 , -60 , and -68 ppm are representative of silicon connected to two hydroxyl groups ($-\text{OSi}(\text{OH})_2\text{R}$; designated T^1), one hydroxyl group ($-\text{O}_2\text{Si}(\text{OH})\text{R}$; T^2), and zero hydroxyl groups ($-\text{O}_3\text{SiR}$; T^3), respectively.⁴⁸ After NO charging, the relative intensities of the T^1 and T^2 peaks were reduced, while the intensity of the T^3 peak remained constant. Quantitative analysis of these structures is complicated because the intensity of each peak

A



B

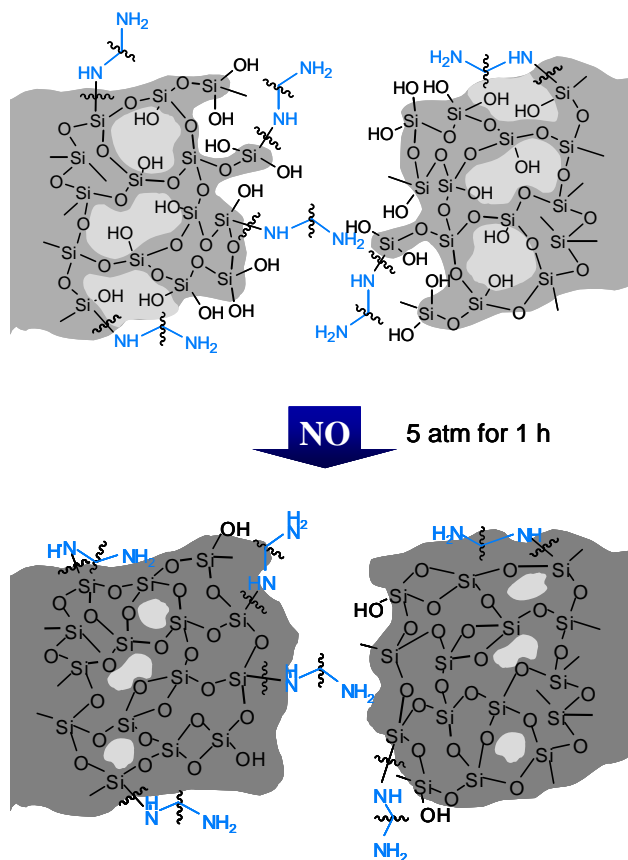


Figure 3.2. (A) Solid-state ^{29}Si NMR spectra of the AHAP3/BTMOs xerogel before (solid red line) and after (dashed blue line) NO exposure (5 atm, 1 h). (B) Cartoon representing structural changes in the porous network of xerogels after NO charging.

depends on the efficiency of cross polarization and the proton relaxation time.⁴⁹ Nonetheless, the reduced intensity of the T^1 and T^2 peaks upon NO exposure suggests slightly enhanced polycondensation, as expected based on the permeability data.

In addition to changing certain physical properties of the xerogel (e.g., permeability), the NO charging process may trigger the formation of diazeniumdiolate NO donor molecules. We have reported previously on the synthesis of NO-releasing xerogels via exposure of aminoalkoxysilane-derived xerogels to high pressures of NO.^{39,40} Such materials slowly release NO upon immersion in aqueous solutions as the diazeniumdiolate NO donor decomposes to NO and the precursor aminoalkoxysilane. Although perhaps not surprising based on the inability to measure NO (via chemiluminescence; detection limit <1 ppb) from AEMP3-derived xerogels charged for short periods (5 atm, 1 h), changes in the magnitude of the background current of the NO sensor due to NO generation within the xerogel membrane were not observed. This result suggests that NO charging for short periods (less than 1 h) does not effectively convert amines within the xerogel to NO donors, even though such conditions are enough to alter the overall permeability and selectivity of the membrane.

To evaluate the effect of varying the xerogel aminoalkoxysilane concentration on membrane permeability and sensor performance, the relative percent AEMP3 used to prepare the membrane was varied from 10 to 50% (balance MTMOS). Based on the above results, xerogel films were cured under ambient conditions for 24 h and charged with NO (5 atm, 1 h) to enhance the polycondensation of the xerogel network. As shown in Figure 3.3, electrodes modified with a 20% AEMP3 xerogel membrane were characterized by the highest NO permeability. Although membranes prepared with 40% AEMP3 were most effective at discriminating NO over nitrite, their permeability to NO was significantly

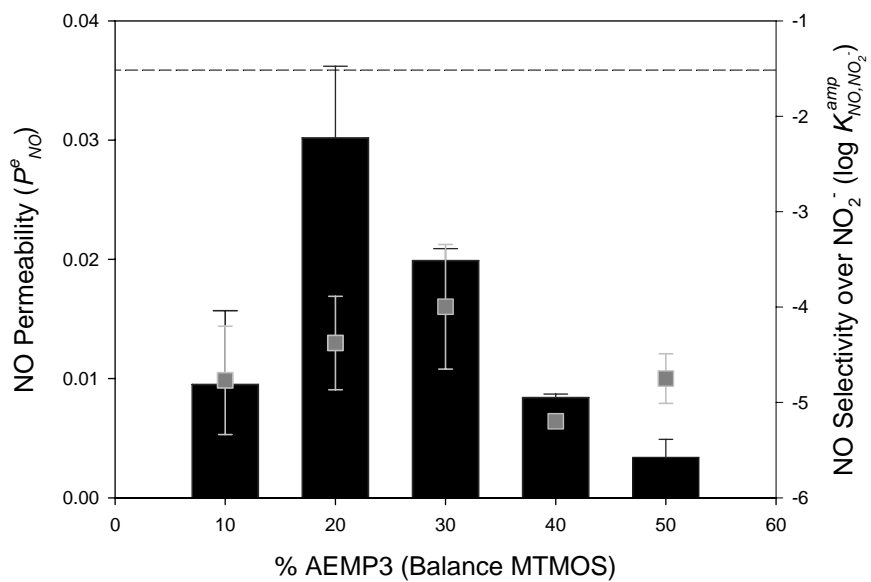


Figure 3.3. NO permeability (bar graphs, for left axis) and selectivity over nitrite (scatter plots, for right axis) as a function of the concentration of AEMP3 (balance MTMOS) after exposure to 5 atm NO for 1 h. The dashed line indicates NO selectivity of the bare Pt electrode over nitrite.

reduced. Coatings prepared with 20% AEMP3 exhibited the most ideal characteristics for maximizing NO permeability while imparting selectivity for NO over nitrite (<-4 of K_{NO,NO_2}^{amp}).

The observed trends in permeability and selectivity may be the result of subtle changes in the hydrophobicity of the xerogel matrix. Static water contact angle measurements confirmed variations in surface wettability for xerogels prepared with 0 – 50% AEMP3 (Figure 3.4). In fact, 20% AEMP3-derived membranes were the most hydrophobic of all the xerogel coatings investigated. As such, an enhanced partitioning of NO into the 20% AEMP3 membranes would be expected since NO is a hydrophobic molecule.² Pontie *et al.* reported a similar correlation between NO sensitivity and surface wettability for NO microsensors fabricated using carbon/o-phenylenediamine/Nafion and carbon/nickel tetrasulfonated phthalocyanine/Nafion composite membranes.¹⁸

The thickness of 20% AEMP3 xerogels was also varied to identify the optimum membrane thickness for maximizing NO permeability without compromising sensor selectivity. Sensors coated with 0.02, 0.04, 0.08, and 0.12 $\mu\text{L}\cdot\text{mm}^{-2}$ of sol resulted in membrane thicknesses of 0.2, 0.7, 2.5, and 5.9 μm , respectively. As shown in Figure 3.5, the 0.2 and 0.7 μm thick membranes exhibited greater NO permeability than the 2.5 and 5.9 μm membranes. Unfortunately, the thinner membranes were characterized by poorer selectivity over nitrite. The optimum xerogel membrane thickness was thus determined to be 2.5 μm since this film demonstrated the best compromise between permeability and selectivity.

The influence of treating the xerogels with NO gas was further evaluated as a function of NO pressure and exposure time. Significant changes in xerogel permeability or selectivity were not observed upon varying the pressure of NO from 1 to 5 atm (data not shown). Increasing the NO exposure time from 10 min to 5 h at 5 atm reduced the xerogel's

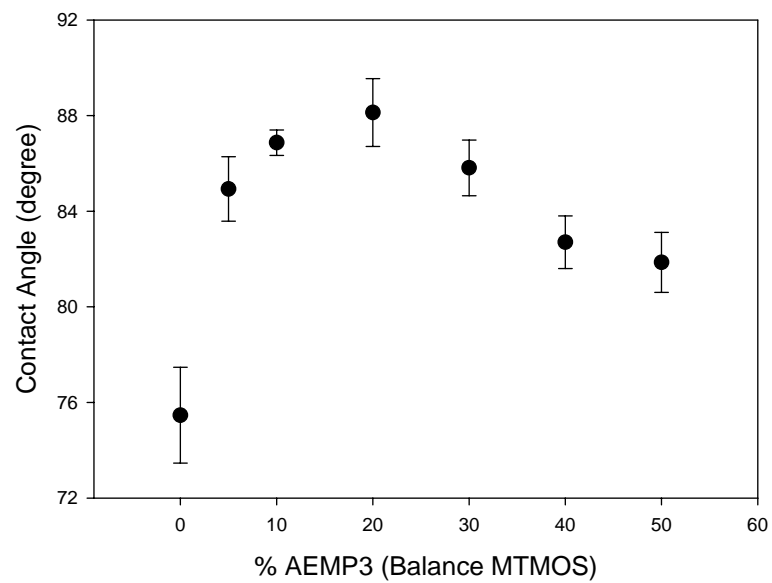


Figure 3.4. Static water contact angles as a function of AEMP3 composition (balance MTMOS) after exposure to 5 atm NO for 1 h.

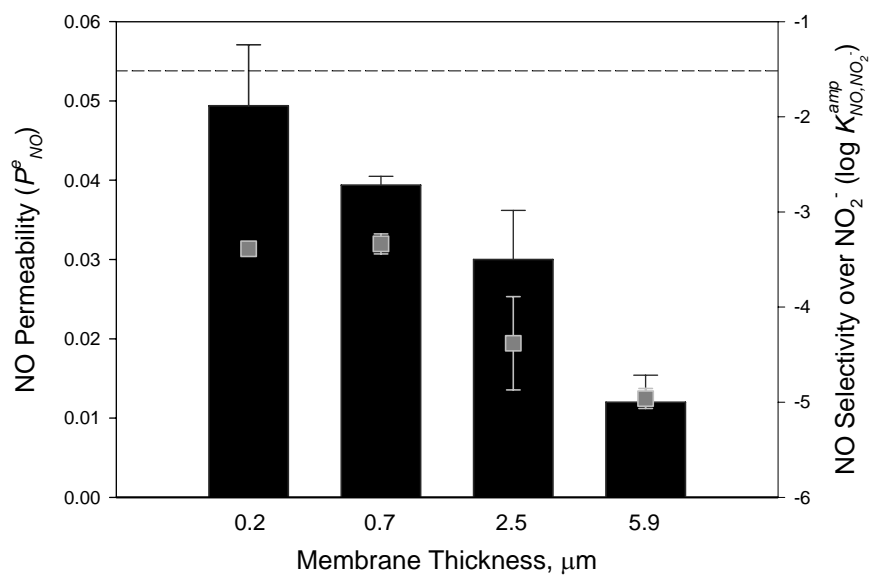


Figure 3.5. NO permeability (bar graphs, for left axis) and selectivity over nitrite (scatter plots, for right axis) as a function of the membrane thickness of 20% AEMP3/MTMOS xerogels after exposure to 5 atm NO for 1. The dashed line indicates NO selectivity of the bare Pt electrode over nitrite.

permeability to NO and slightly improved its selectivity over nitrite (Figure 3.6). Even only a minimal exposure to 5 atm of NO (~10 min) significantly altered the xerogel's permeability and selectivity relative to controls. For the sake of preparation time, 5 atm of NO at 10 min was chosen as the optimum NO exposure condition for subsequent experiments.

Nafion, a commercially available perfluorosulphonate cation exchange polymer, was doped into the xerogel matrix to determine whether the selectivity over nitrite and other negatively charged species could be further improved. The amount of Nafion was systematically varied from 9 to 23% (v/v in 50 μ L of total silane). The Nafion-doped xerogels (20% AEMP3/MTMOS) were cured under ambient conditions for 24 h and charged with 5 atm NO for 10 min. As shown in Table 3.2, increasing the Nafion concentration led to corresponding enhancements in both permeability and selectivity. The change in NO permeability may be the result of slight changes in the hydrophobicity of the xerogel/Nafion composite films. Indeed, as the amount of Nafion was increased from 0 to 17% (v/v), the surface water contact angles increased from 88 ± 1.4 to $95 \pm 2.3^\circ$, respectively. Although membranes doped with greater amounts of Nafion (23%) might be expected to have even more enhanced permeability and selectivity, such composite were not pursued due to the inhomogeneity of the starting sols. Based on the above results, a 2.5 μ m thick 20% AEMP3/MTMOS xerogel containing 17% Nafion (v/v, total silane) exposed to 5 atm NO for 10 min was determined to be the optimum membrane for fabricating a xerogel-based NO sensor. The resulting xerogel/Nafion *hybrid* composite was characterized by a NO permeability of 0.1 and selectivity ($\log K_{NO,j}^{amp}$) of -5.8 , <-6 , <-6 , and <-6 for j = nitrite, ascorbic acid, uric acid, and acetaminophen, respectively.

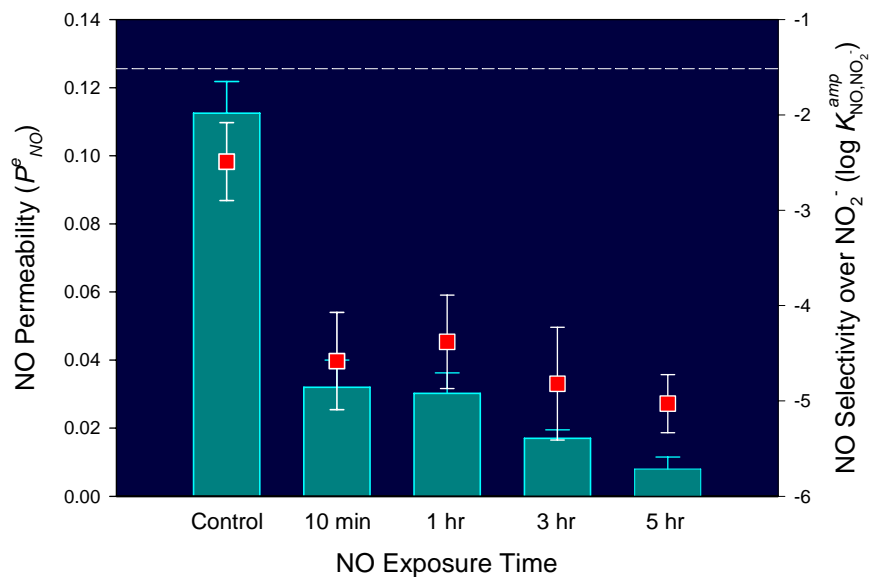


Figure 3.6. NO permeability (bar graphs, for left axis) and selectivity over nitrite (scatter plots, for right axis) as a function of NO exposure time (5 atm) of 20% AEMP3/MTMOS. The dashed line indicates NO selectivity of the bare Pt electrode over nitrite ($n = 3$).

Table 3.2. Electrochemical characteristics of xerogel/Nafion composite NO sensors^{a,b}

	Permeability, ^c P_i^e		Permselectivity, α_{NO,NO_2^-}	Selectivity, ^{c,d} $\log K_{NO,NO_2^-}^{amp}$
	$i = NO$	$i = NO_2^-$		
Control ^e	0.03 ± 0.006	<0.0001	300	-4.58 ± 0.51
9% (v/v) Nafion ^f	0.06 ± 0.02	<0.0001	600	-4.91 ± 0.13
17% (v/v) Nafion ^f	0.10 ± 0.03	<0.0001	1000	-5.79 ± 0.08

^aNumber of samples: $n = 3$. ^bXerogel composition used: 20% AEMP3/MTMOS. All composite coatings were dried under ambient conditions for 24 h and charged with NO (5 atm, 10 min). ^cMeasured in deoxygenated PBS (0.01 M, pH 7.4). Values were determined at 10 μ M of NO and 100 μ M of NO_2^- , respectively. ^dTo determine selectivity, the separate solution method was employed. ^eComposition without Nafion. ^fThe addition of 5 or 10 μ L of Nafion in 50 μ L of total silane (20% AEMP3/MTMOS), respectively.

3.3.2 Xerogel Material Stability

The stability of the sol–gel derived coatings under biological conditions is a critical consideration for the development of *in vivo* NO sensors. Fragmentation of the xerogel film may present toxicity concerns and lead to loss of sensor function. Furthermore, the addition of Nafion to the xerogel could compromise the stability of the film by disrupting the cross-linking (polycondensation) of silane precursors. Thus, DCP-OES analysis was performed to monitor the stability of xerogels prepared with and without Nafion.

Xerogels prepared with the aforementioned optimized composition (20% AEMP3, balance MTMOS and doped with Nafion of 17% (v/v, total silane) were cured, charged with NO (5 atm, 10 min), and then immersed in PBS for 1 to 10 d. While a slight increase in silicon (Si) fragmentation was observed at longer immersion times, both control and composite films were relatively stable with a maximum Si fragmentation of only $0.61 \pm 0.08 \mu\text{mol}\cdot\text{cm}^{-2}$ (Table 3.3) at 10 d. These results indicate that Nafion doping does not compromise xerogel stability. Although the addition of Nafion did not influence xerogel fragmentation, previous studies have indicated that film stability is significantly affected by both the type and amount of alkyl- and aminoalkoxysilanes used to prepare the sol.⁴⁰ Of the xerogel precursors and combinations studied herein, 20% AEMP3 (balance MTMOS) is the most stable xerogel formulation with negligible fragmentation for immersion times up to 2 weeks.⁴⁰

3.3.3 Characterization of NO Microsensors

An integrated NO microsensor was fabricated by placing both a Pt wire working electrode and a Ag/AgCl wire reference electrode into a borosilicate glass capillary. Before modifying the end of the glass capillary that exposed the wire electrodes with an internal

Table 3.3. Stability of 20% AEMP3/MTMOS xerogels prepared with and without Nafion^{a,b}

	Xerogel fragmentation, Si ($\mu\text{mol}\cdot\text{cm}^{-2}$)			
	1 d	4 d	6 d	10 d
Control ^c	< 0.04 ^d	0.06 \pm 0.02	0.22 \pm 0.06	0.61 \pm 0.08
17% (v/v) Nafion ^e	< 0.04	0.05 \pm 0.03	0.20 \pm 0.04	0.52 \pm 0.10

^aNumber of samples: $n = 15$. ^bDetermined using DCP-OES analysis. ^cComposition without Nafion. ^dThe detection limit of the instrument. ^eThe addition of 10 μL of Nafion (17%) in 50 μL of total silane (20% AEMP3/MTMOS).

hydrogel layer and the xerogel permselective membrane, the surface of the bare Pt wire electrode was platinized. Platinization has been shown to improve sensitivity by increasing the effective surface area of the electrode and slightly lowering the working potential for NO oxidation.²⁸ To assess the influence of the platinization process on the electrode response properties, calibration plots for NO were obtained at an applied potential of +0.7 and +0.8 V vs. Ag/AgCl for the platinized and non-platinized Pt electrodes, respectively (Figure 3.7). Notably, the sensitivity of the platinized electrodes was roughly 5 times greater than that of the non-platinized electrodes. Therefore, all subsequent experiments were conducted with platinized Pt microelectrodes.

Prior to xerogel coating, the platinized Pt microelectrode was modified with an internal hydrogel layer (30 mM NaCl, 0.3 mM HCl, and 1% PVP; pH 3.5). The sensor was then coated with the optimized xerogel/Nafion-derived NO-permselective membrane by immersing the tip of the sensor into a solution consisting of 40 μ L of MTMOS, 10 μ L of AEMP3, 10 μ L of Nafion, 200 μ L of ethanol, and 100 μ L of water. (A final membrane thickness of \sim 2.5 μ m was achieved by repeating this procedure.) After curing for 24 h under ambient conditions, the xerogel was charged (5 atm NO for 10 min) to increase polycondensation of the network. The analytical performance of the resulting NO microsensor was then investigated. The calibration and dynamic response curves for NO and various interfering species (e.g., nitrite, ascorbic acid, acetaminophen, and ammonia) are shown in Figure 3.8. The concentration of each interfering substance was chosen to be greater than the highest level that would be present in a physiological sample (i.e., 100 μ M each of nitrite, ascorbic acid, acetaminophen, and ammonia). The performance of the NO microsensor prepared using the MTMOS/AEMP3/Nafion *hybrid* permselective membrane

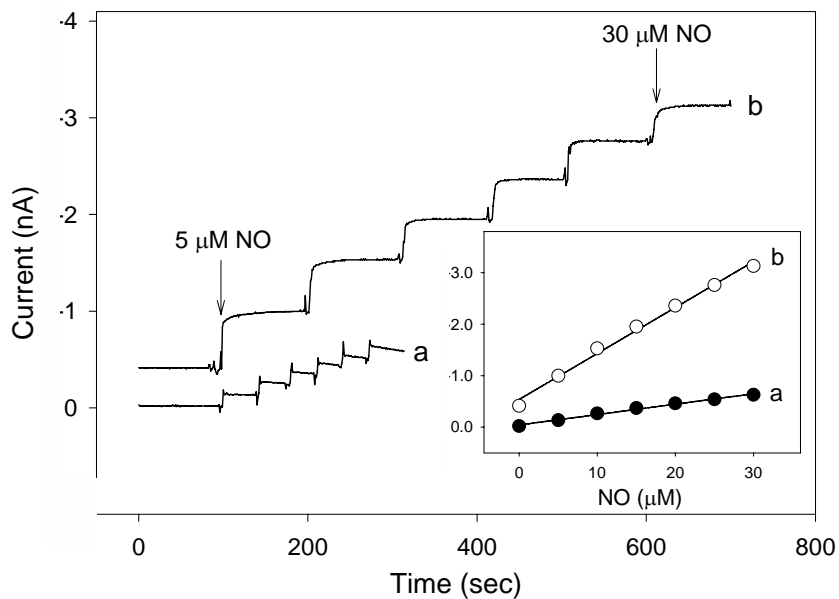


Figure 3.7. Dynamic response and calibration curves (inset) of the non-platinized (a) and platinized (b) Pt microelectrodes. The response sensitivity to NO was 19.8 ($r = 0.9919$) and 90.2 ($r = 0.9930$) pA/ μ M for the non-platinized and platinized Pt microsensors, respectively.

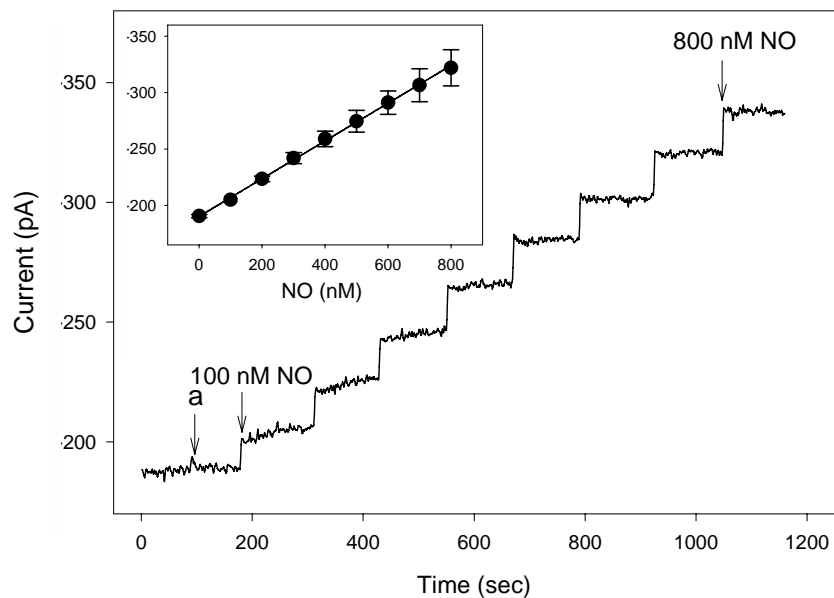


Figure 3.8. Dynamic response to NO and interfering species, and calibration curve (inset) of the AEMP3/MTMOS/Nafion composite NO microsensors: (a) injection of 100 μ M each of nitrite, ascorbic acid, acetaminophen, and ammonia.

was comparable to that of previously reported NO sensors with respect to sensitivity (0.17 ± 0.02 pA/nM), linearity ($r = 0.9991$, 25 – 800 nM NO range), detection limit (25 nM, based on $S/N = 3$), and response time ($t_{95\%} = 9$ sec for an increase in NO concentration from 400 to 500 nM). Remarkably, the xerogel-derived sensor responded linearly to NO up to 15 μM (67.7 pA/ μM , $r = 0.9998$; Figure 3.9). In total, the analytical performance of the xerogel-derived NO microsensor was comparable to other recently reported NO microsensors (Tables 3.4 and 3.5).⁵⁰⁻⁷⁴ In contrast to other sensor configurations, however, the fabrication of NO microsensors via sol-gel chemistry is significantly more straightforward.

The response variation of the microsensor to NO (0 – 800 nM) and multiple interfering species (100 μM each of nitrite, ascorbic acid, acetaminophen, and ammonia) for the xerogel/Nafion composite NO microsensor is shown in Figure 3.10. The sensor retained 93% of its initial sensitivity at 4 d. Even after 8 d, 82% of the sensor's initial response (sensitivity) was maintained when soaked in PBS under ambient conditions. Furthermore, the selectivity of the sensor did not change as a function of soak time. The gradual decrease in analytical sensitivity over 8 d is likely due to the accumulation of nitrate produced by the electrochemical oxidation of NO within the internal hydrogel layer,³² as opposed to destabilization of the xerogel/Nafion composite film. Fragmentation of the *hybrid* membrane would significantly impact sensor performance by increasing analyte permeability and reducing sensor selectivity. The microsensor's ability to maintain excellent selectivity indicates that neither significant structural changes (i.e., pore size and membrane thickness) nor Nafion leaching occurred during the initial 8 d.

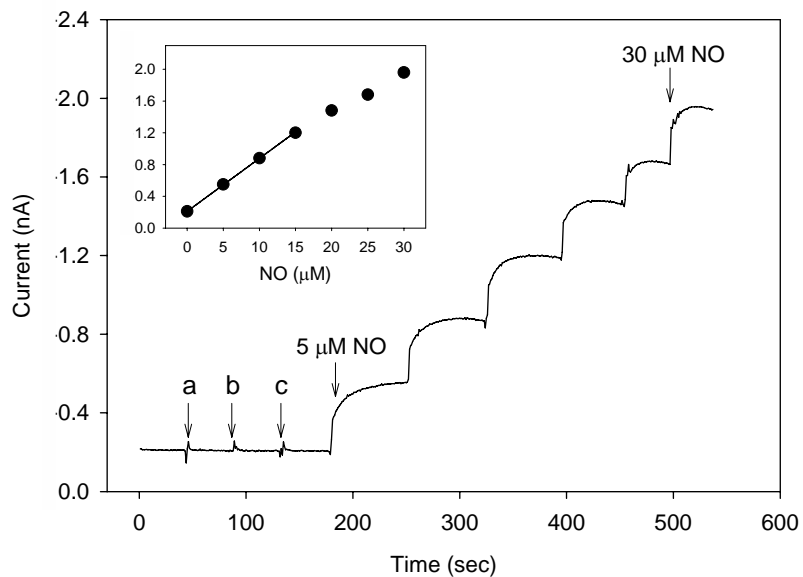


Figure 3.9. Dynamic response and calibration curve (inset) of the MTMOS/AEMP3/Nafion composite NO microsensor in the extended NO concentrations: (a) 100 μM of nitrite, (b) 100 μM of ascorbic acid, and (c) 100 μM of acetaminophen. The response sensitivity to NO was 67.7 $\text{pA}/\mu\text{M}$ ($r = 0.9998$) from 5 to 15 μM NO.

Table 3.4. Performance comparison of electrochemical NO microsensors based on the direct electrooxidation of NO^{a,b}

Sensor assembly			NO response characteristics				Ref.	
Electrode Material	Membrane	Modif. method	Oxidation potential	Operational mode	Sensitivity (LOD)	Linear response range		Selectivity
CFE ($\phi=30-35 \mu\text{m}$, $l=100-150 \mu\text{m}$)	Nafion <i>o</i> -PD	DC/ED	0.77 V vs SCE	A	31 pC/ μM (35 nM)	0.1 – 1 μM	NRI: 935, AA: 756, DA: 175	25
CFE ($\phi=30-35 \mu\text{m}$, $l=500 \mu\text{m}$)	Nafion (<i>m</i> -PD + resorcinol)	DC/ED	0.7 V vs Ag/AgCl	DPA	0.5 nA/ μM (60 – 80 nM)	0.2 – 1 μM	NRI: 600, AA: 2000, DA: 200	50
GCDE ($\phi=2 \text{ mm}$)	CA	DD	0.9 V vs Ag/AgCl	A	n.r. (20 nM)	0.1 – 4.5 μM		19
PtDE ($\phi=2 \text{ mm}$)	PolyDHB	ED	0.75 V vs Ag/AgCl	A	n.r. (40 nM)	0.1 – 4.5 μM		19
CFE ($\phi=8 \mu\text{m}$, $l=0.8 \text{ mm}$)	Nafion (<i>m</i> -PD + resorcinol)	DC/ED	0.73 V vs SCE	DPA	4.9 nA/ μM (72 nM)	40 – 200 nM	NRI: 1000, AA: 1300	51
PtFE ($\phi=15 \mu\text{m}$, $l=\text{n.r.}$)	Nafion PVP (Pd/IrO ₂)	DD/ED/ED	0.66 V vs SCE	DPA	n.r. (15 – 50 nM)	0.058 – 6.4 μM		52
CFE ($\phi=8 \mu\text{m}$, $l=1 \text{ mm}$)	Nafion <i>o</i> -PD	DC/ED	0.76 V vs SCE	DNPA	9.6 nA/ μM (n.r.)	100 – 500 nM		18
CFE ($\phi=7 \mu\text{m}$, $l=15 \text{ mm}$)	Nafion WPI	n.r./n.r.	0.86 V vs Ag/AgCl	A	1.03 pA/nM (5 nM)	0.01 – 5 μM	NRI: 10 ⁴ , AA: 10 ⁴ , DA: 10 ³	27
PtFE ($\phi=10 \mu\text{m}$, $l=\text{n.r.}$)	Collodion PS	DC/DC	0.6 V vs Ag/AgCl	A	0.8 pA/ μM (75 nM)	0.1 – 1 μM		26
PtDE ($\phi=1.6 \text{ mm}$)	PDMS	DC	0.82 V vs Ag/AgCl	A	n.r. (20 nM)	10 – 50 μM		30
CDE ($\phi=0.5 \text{ mm}$)	PDDA α -CD Nafion	DC/DC/DC	0.6-0.7 V vs Ag/AgCl	DPA	420 pA/nM (n.r.)	– 1.9 μM		53
PtDE ($A=0.0078 \text{ cm}^2$)	Polycarbazole	ED	0.65 V vs Ag/AgCl	DPV	n.r. (50 nM)	10 nM – 1 mM		24
PtDE ($A=4.4 \times 10^{-5} \text{ cm}^2$)	CA	DC	0.7 V vs Ag/AgCl	DNPA	175 pA/ μM (50 nM)	1 – 10 μM	NRI: 168, AA: 2300, UA: 3460, DA: 6910	32
CFE ($\phi=0.1 \mu\text{m}$, $l=150 \mu\text{m}$)	WPI	n.r.	0.86 V vs Ag/AgCl	A	0.5 pA/nM (2 nM)	0.01 – 1 μM		54
CFE ($\phi=6 \mu\text{m}$, $l=2-4 \text{ mm}$)	CA Nafion	DD/DD	0.87 V vs SCE	A	0.44 nA/ μM (n.r.)	1 – 120 μM		55

Table 3.4. (cont.)

Sensor assembly			NO response characteristics				Ref.
Electrode material	Membrane	Modif. method	Oxidation potential	Operational mode	Sensitivity (LOD)	Linear response range	
Pt/IrFE ($\phi=130$ μm , $l=3$ mm)	Nafion <i>o</i> -PD	DC/ED	0.9 V vs Ag/AgCl	DPA	0.07 nA/nM (15 nM)	0.001 – 1 μM	56
CDE (2500 disks with $\phi=2$ μm)	Nafion PDMS WPI	n.r./n.r./n.r.	0.86 V vs Ag/AgCl	A	17 pA/nM (0.3 nM)	50 – 400 nM	57
GCDE CNT ($\phi=n.r.$)	Nafion	DD	0.72 V vs SCE	DPA	n.r. (80 nM)	0.2 – 150 μM	58
AuDE ($\phi=1.6$ mm)	Poly-L-lysine + PSS	DC	0.7-0.75 V vs Ag/AgCl	DPSCA	n.r. (8.4 nM)	0.01 – 4 μM	59
PPtDE ($\phi=76$ μm)	PTFE	MF	0.75 V vs Ag/AgCl	A	0.8-1.3 pA/nM (1 nM)	1 – 350 nM	28
PPtDE ($\phi=127$ μm)	Xerogel + Nafion	DC	0.7 V vs Ag/AgCl	A	0.17 pA/nM (25 nM)	25 – 800 nM (15 μM)	NRI: 1000, AA: 1000, UA: 1000

^aElectrochemical NO sensors compared to this work were selected from examples published since 1995. ^bAbbreviations: CFE, carbon fiber electrode; GCDE, glassy carbon disk electrode; PtDE, platinum disk electrode; PtFE, platinum fiber electrode; CDE, carbon disk electrode; Pt/IrFE, platinum/iridium (10%) fiber electrode; CNT, carbon nanotube; AuDE, gold disk electrode; PPtDE, platinumized platinum disk electrode; *o*- or *m*-PD, *ortho*- or *meta*-phenylenediamine; CA, cellulose acetate; PolyDHB, poly[4,4'-dihydroxybenzophenone]; PVP, poly(vinyl pyridine); WPI, company (World Precision Inc.) confidential product; PS, polystyrene; PDMS, polydimethylsiloxane; PDDA, poly(diallyldimethylammonium chloride); α -CD, α -cyclodextrin; PSS, poly(4-styrenesulfonate); PTFE, poly(tetrafluoroethylene); DC, dip-coating; ED, electrochemical deposition; DD, droplet deposition; MF, mounting and fixing; SCE, saturated calomel reference electrode; A, amperometry; DPA, differential pulse amperometry; DPNA, differential normal pulse amperometry; DPV, differential pulse voltammetry; DPSCA, double potential step chronoamperometry; NRI, nitrite; AA, ascorbic acid; DA, dopamine; UA, uric acid; n.r., not reported; LOD, limit of detection.

Table 3.5. Performance comparison of electrochemical NO microsensors based on the catalytic electrooxidation of NO^{a,b}

Electrode material	Sensor assembly			NO response characteristics				Ref.
	Catalyst membrane	Modif. method	Oxidation potential	Operational mode	Sensitivity (LOD)	Linear response range	Selectivity	
CFE ($\phi=8 \mu\text{m}$, $l=2 \text{ mm}$)	NiTHMPP Nafion	ED/DC	0.75 V vs SCE	DPA	6.28 nA/ μM (1.5 nM)	1.5 nM – 3.4 μM		60
CFE ($\phi=8 \mu\text{m}$, $l=2 \text{ mm}$)	Poly[NiP] Nafion	ED/DC	0.75 V vs SCE	DPA	3.12 nA/ μM (1.5 nM)	15 – 300 nM		61
CFE ($\phi=8 \mu\text{m}$, $l=0.8 \text{ mm}$)	NiTSPc Nafion	ED/DC	0.7 V vs SCE	DPA	11.3 nA/ μM (20 nM)	20 – 200 nM		62
CFE ($\phi=30 \mu\text{m}$, $l=500 \mu\text{m}$)	(PMePy + FePW ₁₁) Nafion	ED/ED	0.72 V vs Ag/AgCl	DPA	2.65 nA/ μM (100 nM)	0.1 μM – 1 mM		63
CFE ($\phi=30\text{-}40 \mu\text{m}$, $l=200\text{-}250 \mu\text{m}$)	NiTHMPP Nafion AAO Polylysine	ED/DC/ DD/DD	0.65 V vs Ag/AgCl	DPV	1.34 pC/ μM (0.5 nM)	1 nM – 100 μM	NRI: 292, AA: 5830, DA: 80	64
GCDE ($\phi=n.r.$)	NiTHMPP Poly-Eugenol	ED/ED	0.75-0.8 V vs Ag/AgCl	A	10.5 nA/ μM (85 nM)	0.5 – 20 μM	NRI: 1010, AA: 5830, DA: 80	65
PtDE ($\phi=1.6 \text{ mm}$)	CytC–PITO Nafion	DD/DD	0.75 V vs Ag/AgCl	A	0.25 $\mu\text{A}/\mu\text{Mcm}^2$ (n.r.)	0.05 – 100 μM		66
PtDE ($\phi=15 \mu\text{m}$)	PolyCoTAPc Nafion	ED/DD	0.7 V vs SCE	DPV	n.r. (100 nM)	0.2 – 4.1 μM		67
CDE ($\phi=10 \mu\text{m}$)	CuPtC ₆ Nafion	ED/DD	0.7 V vs Ag/AgCl	DPV/DPA	19.7 $\mu\text{A}/\mu\text{Mcm}^2$ (5 nM)	0.01 – 200 μM		68
PtDE ($\phi=200 \mu\text{m}$)	Ni(ABED) Nafion	DD/DC	0.7 V vs SCE	DPA	6.5 nA/ μM (5 nM)	0.01 – 1 μM		20
PtDE ($\phi=15 \mu\text{m}$)	Ni(chitin) ₂ Nafion	DD/DD	0.74 V vs SCE	DPA	n.r. (50 nM)	0.085 – 15 μM		69
GCDE ($\phi=3 \text{ mm}$)	CuPtBr ₆	ED	0.79 V vs SCE	DPA	n.r. (20 nM)	0.05 – 100 μM		70
PtDE ($\phi=15 \mu\text{m}$)	M(salen) Nafion	ED/DD	0.68-0.71 V vs Ag/AgCl	DPA	n.r. (5 – 20 nM)	19.6 nM – 40 μM		21
PtDE ($\phi=100 \mu\text{m}$)	Nafion Co(phen)	DD/DC	0.7 V vs Ag/AgCl	CV	13.3 nA/ μM (37 nM)	0.14 – 5 μM		71
GCDE (A=7.1 mm ²)	CoTPPCl + Nafion	DD	0.8 V vs Ag/AgCl	A	0.029 nA/nM (1.2 nM)	5 – 150 nM		72

Table 3.5. (cont.)

Electrode material	Sensor assembly		NO response characteristics				Ref.
	Catalyst membrane	Modif. method	Oxidation potential	Operational mode	Sensitivity (LOD)	Linear response range	
GCDE ($A=0.07 \text{ cm}^2$)	Fc-tetraazaNi	ED	0.75 V vs SCE	CV	0.27 $\mu\text{A}/\mu\text{M}$ (1 μM)	10 – 100 μM	22
PtDE ($\phi=50 \mu\text{m}$)	Poly(pyrrrole-MnTCPP) Nafion	ED/DD	0.72 V vs Ag/AgCl	A	17.6 nA/ μM (0.1 μM)	0.3 – 2.4 μM	16
PtDE ($\phi=50 \mu\text{m}$)	NiTSPc	ED	0.78 V vs SCE	DNPA	84 nA/ μMmm^{-2} (1 μM)	n.r.	73
AuDE ($\phi=1.5 \text{ mm}$)	MoO ₃ <i>trans</i> -[Ru(NH ₃) ₄ (SO ₄) ₄ pic] ⁺	ED/ED	0.7 V vs Ag/AgCl	SWV	3.1 nA/ μM (n.r.)	1 – 10 μM	74

^aExamples of NO microsensors based on the catalytic electrooxidation of NO were selected from publications since 1995. ^bAbbreviations as in Table 3.4 and NiTHMPP, tetrakis(3-methoxy-4-hydroxyphenylporphyrin)nickel(II); Poly[NiP], polymerized tetrakis(3-methoxy-4-hydroxyphenyl)nickel(II) porphyrin; NiTSPc, tetrasulfonatophthalocyanine(nickel(II)); PMePy, poly(*N*-methylpyrrole); FePW₁₁, iron substituted Keggin-type heteropolyanion or [H₂OFe(III)PW₁₁O₃₉]; AAO, ascorbic acid oxidase; CytC-PiTO, cytochrome C associated to 2-(4-carboxyphenyl)-4,4,5,5-tetramethyl imidazole-1-oxyl-3-oxide; PolyCoTAPc, cobalt(II)tetraaminophthalocyanine; Ni(ABED), *ortho*-aminobenzaldehydeethylenediamine; Ni(chitin)₂, nickel(II)chitin; M(salen), metal ethylenebis(salicylideneiminato); Co(phen), Cobalt phenantroline; CoTPPCl, tetraphenylporphyrin cobalt(III) chloride; Fc-tetraazaNi, 6,17-diferrocenyl-dibenzo[*b*,*j*]5,9,14,18-tetraaza[14]annulen-nickel(II); pyrrole-MnTCPP, pyrrole substituted tetracarboxyphenylporphyrin manganese (II); 4pic, 4picoline; CV, cyclic voltammetry; SWV, square wave voltammetry.

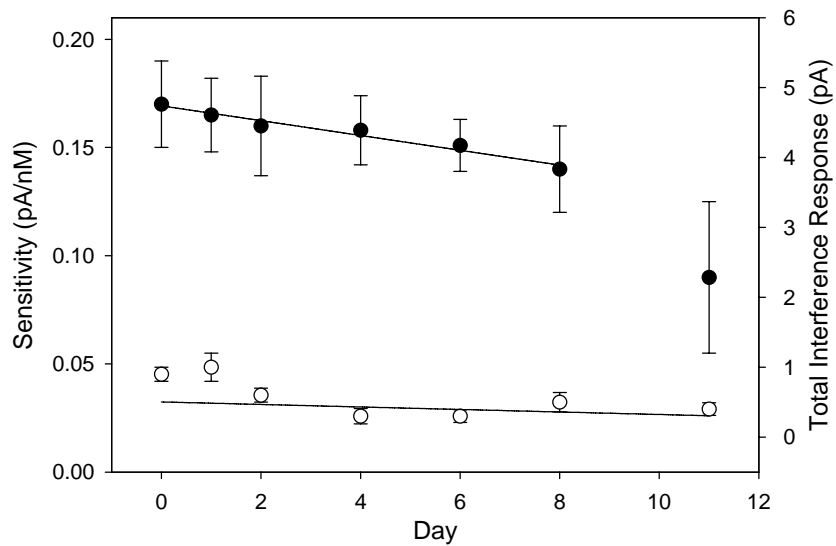


Figure 3.10. Variations in response properties for NO (●, for left axis) and interfering species (○, for right axis) measured from 25 – 800 nM NO and 100 μ M each of nitrite, ascorbic acid, acetaminophen, and ammonia for the AEMP3/MTMOS/Nafion composite NO microsensor.

3.4 Conclusions

Sol-gel chemistry represents a novel approach for preparing permselective membranes for NO gas sensors. Several xerogel films were fabricated by varying the type and concentration of alkyl- and aminoalkoxysilane precursors as well as the reaction/processing conditions to identify the optimum membrane composition. The addition of Nafion to the xerogel matrix enhanced both the sensitivity and selectivity of the xerogel-derived NO sensors, and did not adversely affect the stability of the xerogel matrix under aqueous conditions. In contrast to other electrochemical NO sensor designs, xerogel-based NO microsensors are fabricated using a simple dip-coating procedure, characterized by high sensitivity, selectivity, and reproducibility. Studies are currently underway to alter the porous structures of the xerogel by incorporating silane precursors with increased hydrophobicity to further improve microsensor sensitivity and allow for the measurement of nanomolar concentrations of NO.

3.5 References

- (1) Ignarro, L. J.; Bugga, G. M.; Wood, K. S.; Byrns, R. E.; Chaudhuri, G. "Endothelium-derived relaxing factor produced and released from artery and vein is nitric oxide," *Proc. Natl. Acad. Sci. USA* **1987**, *84*, 9265-9269.
- (2) Ignarro, L. J. *Nitric oxide: Biology and pathobiology*; Academic Press: New York, 2000.
- (3) Lincoln, J.; Hoyle, C. H.; Burnstock, G. *Nitric oxide in health and disease*; Cambridge University Press: Cambridge, 1997.
- (4) Beckman, J. S.; Wink, D. A.; Crow, J. P. In *Methods in nitric oxide research*; Feelisch, M.; Stamler, J. S., Eds.; John Wiley: Chichester, U.K., 1996, pp Chapter 6.
- (5) Guthohrlein, G.; Knappe, J. "Modified determination of citrulline," *Anal. Biochem.* **1968**, *26*, 188-191.
- (6) Granger, D. L.; Taintor, R. R.; Boockvar, K. S.; Hibbs, J. B., Jr. "Measurement of nitrate and nitrite in biological samples using nitrate reductase and Griess reaction," *Methods Enzymol.* **1996**, *268*, 142-151.
- (7) Fujii, S.; Yoshimura, T. "A new trend in iron-dithiocarbamate complexes: As an endogenous NO trapping agent," *Coord. Chem. Rev.* **2000**, *198*, 89-99.
- (8) Robinson, J. K.; Bollinger, M. J.; Birks, J. W. "Luminol/H₂O₂ chemiluminescence detector for the analysis of nitric oxide in exhaled breath," *Anal. Chem.* **1999**, *71*, 5131-5136.
- (9) Zhou, X.; Arnold, M. A. "Response characteristics and mathematical modeling for a nitric oxide fiber-optic chemical sensor," *Anal. Chem.* **1996**, *68*, 1748-1754.
- (10) Gabe, Y.; Urano, Y.; Kikuchi, K.; Kojima, H.; Nagano, T. "Highly sensitive fluorescence probes for nitric oxide based on boron dipyrromethene chromophore-rational design of potentially useful bioimaging fluorescence probe," *J. Am. Chem. Soc.* **2004**, *126*, 3357-3367.
- (11) Hilderbrand, S. A.; Lim, M. H.; Lippard, S. J. "Dirhodium tetracarboxylate scaffolds as reversible fluorescence-based nitric oxide sensors," *J. Am. Chem. Soc.* **2004**, *126*, 4972-4978.
- (12) Bedioui, F.; Trevin, S.; Devynck, J. "Chemically modified microelectrodes designed for the electrochemical determination of nitric oxide in biological systems," *Electroanalysis* **1996**, *8*, 1085-1091.
- (13) de Vooy, A. C. A.; Beltramo, G. L.; van Riet, B.; van Veen, J. A. R.; Koper, M. T. M.

- "Mechanisms of electrochemical reduction and oxidation of nitric oxide," *Electrochim. Acta* **2004**, *49*, 1307-1314.
- (14) Bedioui, F.; Villeneuve, N. "Electrochemical nitric oxide sensors for biological samples - Principles, selected examples and applications," *Electroanalysis* **2003**, *15*, 5-18.
- (15) Malinski, T.; Taha, Z. "Nitric oxide release from a single cell measured *in situ* by a porphyrinic-based microsensor," *Nature* **1992**, *358*, 676-678.
- (16) Diab, N.; Schuhmann, W. "Electropolymerized manganese porphyrin/polypyrrole films as catalytic surfaces for the oxidation of nitric oxide," *Electrochim. Acta* **2001**, *47*, 265-273.
- (17) Pontie, M.; Lecture, H.; Bedioui, F. "Improvement in the performance of a nickel complex-based electrochemical sensor for the detection of nitric oxide in solution," *Sens. Actuators B* **1999**, *56*, 1-5.
- (18) Pontie, M.; Gobin, C.; Pauporte, T.; Bedioui, F.; Devynck, J. "Electrochemical nitric oxide microsensors: Sensitivity and selectivity characterisation," *Anal. Chim. Acta* **2000**, *411*, 175-185.
- (19) Pallini, M.; Curulli, A.; Amine, A.; Palleschi, G. "Amperometric nitric oxide sensors: A comparative study," *Electroanalysis* **1998**, *10*, 1010-1016.
- (20) Tu, H.; Mao, L.; Cao, X.; Jin, L. "A novel electrochemical microsensor for nitric oxide based on electropolymerized film of *o*-aminobenzaldehyde-ethylene-diamine nickel," *Electroanalysis* **1999**, *11*, 70-74.
- (21) Mao, L.; Yamamoto, K.; Zhou, W.; Jin, L. "Electrochemical nitric oxide sensors based on electropolymerized film of M(salen) with central ions of Fe, Co, Cu, and Mn," *Electroanalysis* **2000**, *12*, 72-77.
- (22) Casero, E.; Pariente, F.; Lorenzo, E.; Beyer, L.; Losada, J. "Electrocatalytic oxidation of nitric oxide at 6,17-diferrocenyl-dibenzo[b,i]5,9,14,18-tetraaza[14]annulen-nickel(II) modified electrodes," *Electroanalysis* **2001**, *13*, 1411-1416.
- (23) Shibuki, K. "An electrochemical microprobe for detecting nitric oxide release in brain tissue," *Neurosci. Res.* **1990**, *9*, 69-76.
- (24) Prakash, R.; Srivastava, R. C.; Seth, P. K. "Polycarbazole modified electrode: Nitric oxide sensor," *Polym. Bull.* **2001**, *46*, 487-490.
- (25) Friedemann, M. N.; Robinson, S. W.; Gerhardt, G. A. "*o*-Phenylenediamine-modified carbon fiber electrodes for the detection of nitric oxide," *Anal. Chem.* **1996**, *68*, 2621-2628.

- (26) Kitamura, Y.; Uzawa, T.; Oka, K.; Komai, Y.; Takizawa, N.; Kobayashi, H.; Tanishita, K. "Microcoaxial electrode for in vivo nitric oxide measurement," *Anal. Chem.* **2000**, *72*, 2957-2962.
- (27) Zhang, X.; Cardosa, L.; Broderick, M.; Fein, H.; Lin, J. "An integrated nitric oxide sensor based on carbon fiber coated with selective membranes," *Electroanalysis* **2000**, *12*, 1113-1117.
- (28) Lee, Y.; Oh, B. K.; Meyerhoff, M. E. "Improved planar amperometric nitric oxide sensor based on platinized platinum anode. 1. Experimental results and theory when applied for monitoring NO release from diazeniumdiolate-doped polymeric films," *Anal. Chem.* **2004**, *76*, 536-544.
- (29) Kato, D.; Sakata, M.; Hirayama, C.; Hirata, Y.; Mizutani, F.; Kunitake, M. "Selective permeation of nitric oxide through two dimensional cross-linked polysiloxane LB films," *Chem. Lett.* **2002**, 1190-1191.
- (30) Mizutani, F.; Hirata, Y.; Yabuki, S.; Iijima, S. "Amperometric measurement of nitric oxide (NO) using an electrode coated with polydimethylsiloxane," *Chem. Lett.* **2000**, 802-803.
- (31) Mizutani, F.; Yabuki, S.; Sawaguchi, T.; Hirata, Y.; Sato, Y.; Iijima, S. "Use of siloxane polymer for the preparation of amperometric sensors: O₂ and NO sensors and enzyme sensors," *Sens. Actuators B* **2001**, *76*, 489-493.
- (32) Cserey, A.; Gratzl, M. "Stationary-state oxidizing platinum microsensor for selective and on-line monitoring of nitric oxide in biological preparations," *Anal. Chem.* **2001**, *73*, 3965-3974.
- (33) Hench, L. L.; West, J. K. "The sol-gel process," *Chem. Rev.* **1990**, *90*, 33-72.
- (34) Walcarius, A. "Electrochemical applications of silica-based organic-inorganic hybrid materials," *Chem. Mater.* **2001**, *13*, 3351-3372.
- (35) Walcarius, A. "Analytical applications of silica-modified electrodes. A comprehensive review," *Electroanalysis* **1998**, *10*, 1217-1235.
- (36) Tsionsky, M.; Lev, O. "Electrochemical composite carbon-ceramic gas sensors: Introduction and oxygen sensing," *Anal. Chem.* **1995**, *67*, 2409-2414.
- (37) Rabinovich, L.; Lev, O.; Tsirlina, G. A. "Electrochemical characterisation of Pd modified ceramic|carbon electrodes: Partially flooded versus wetted channel hydrophobic gas electrodes," *J. Electroanal. Chem.* **1999**, *466*, 45-59.
- (38) Chowdhury, P. B.; Luckham, P. F. "Probing recognition process between an antibody and an antigen using atomic force microscopy," *Colloids Surf. A* **1998**, *143*, 53-57.

- (39) Nablo, B. J.; Chen, T.-Y.; Schoenfisch, M. H. "Sol-gel derived nitric-oxide releasing materials that reduce bacterial adhesion," *J. Am. Chem. Soc.* **2001**, *123*, 9712-9713.
- (40) Marxer, S. M.; Rothrock, A. R.; Nablo, B. J.; Robbins, M. E.; Schoenfisch, M. H. "Preparation of nitric oxide (NO)-releasing sol-gels for biomaterial applications," *Chem. Mater.* **2003**, *15*, 4193-4199.
- (41) Porat, Z.; Crooker, J. C.; Zhang, Y.; Mest, Y. L.; Murray, R. W. "*iR_{UNC}* advantages and real geometrical dimensions of microband electrodes," *Anal. Chem.* **1997**, *69*, 5073-5081.
- (42) Shin, J. H.; Marxer, S. M.; Schoenfisch, M. H. "Nitric oxide-releasing sol-gel particle/polyurethane glucose biosensors," *Anal. Chem.* **2004**, *76*, 4543-4549.
- (43) Stefan, R.-I.; van Staden, J. F.; Aboul-Enein, H. Y. In *Electrochemical Sensors in Bioanalysis*; Marcel Dekker: New York, 2001.
- (44) Cruz, J.; Kawasaki, M.; Gorski, W. "Electrode coatings based on chitosan scaffolds," *Anal. Chem.* **2000**, *72*, 680-686.
- (45) Brinker, C. J.; Scherer, G. W. *Sol-gel science: The physics and chemistry of sol-gel processing*; Academic Press: New York, 1990.
- (46) Robbins, M. E.; Hopper, E. D.; Schoenfisch, M. H. "Synthesis and characterization of nitric oxide-releasing sol-gel microarrays," *Langmuir* **2004**, *20*, 10296-10302.
- (47) Dai, Y.; Guiver, M. D.; Robertson, G. P.; Kang, Y. S.; Lee, K. J. "Enhancement in the gas permeabilities of novel polysulfones with pendant 4-trimethylsilyl- α -hydroxybenzyl substituents," *Macromolecules* **2003**, *36*, 6807-6816.
- (48) Albert, K.; Bayer, E. "Characterization of bonded phases by solid-state NMR spectroscopy," *J. Chromatogr.* **1991**, *544*, 345-370.
- (49) Bruch, M. D.; Fatunmbi, H. O. "Nuclear magnetic resonance analysis of silica gel surfaces modified with mixed, amine-containing ligands," *J. Chromatogr. A* **2003**, *1021*, 61-70.
- (50) Park, J.-K.; Tran, P. H.; Chao, J. K. T.; Ghodadra, R.; Rangarajan, R.; Thakor, N. V. "In vivo nitric oxide sensor using non-conducting polymer-modified carbon fiber," *Biosens. Bioelectron.* **1998**, *13*, 1187-1195.
- (51) Pontie, M.; Bedioui, F.; Devynck, J. "New composite modified carbon microfibers for sensitive and selective determination of physiologically relevant concentrations of nitric oxide in solution," *Electroanalysis* **1999**, *11*, 845-850.
- (52) Xian, Y.; Sun, W.; Xue, J.; Luo, M.; Jin, L. "Iridium oxide and palladium modified

- nitric oxide microsensor," *Anal. Chim. Acta* **1999**, *381*, 191-196.
- (53) Kitajima, A.; Teranishi, T.; Miyake, M. "Detection of nitric oxide on carbon electrode modified with ionic polymers and α -cyclodextrin," *Electrochemistry* **2001**, *69*, 16-20.
- (54) Zhang, X.; Kislyak, Y.; Lin, J.; Dickson, A.; Cardoso, L.; Broderick, M.; Fein, H. "Nanometer size electrode for nitric oxide and S-nitrosothiols measurement," *Electrochem. Commun.* **2002**, *4*, 11-16.
- (55) Katrlík, J.; Zalesakova, P. "Nitric oxide determination by amperometric carbon fiber microelectrode," *Bioelectrochemistry* **2002**, *56*, 73-76.
- (56) Kilinc, E.; Yetik, G.; Dalbasti, T.; Ozsoz, M. "Comparison of electrochemical detection of acetylcholine-induced nitric oxide (NO) release and contractile force measurement of rabbit isolated carotid artery endothelium," *J. Pharmacol. Biomed. Anal.* **2002**, *28*, 345-354.
- (57) Zhang, X.; Lin, J.; Cardoso, L.; Broderick, M.; Darley-Usmar, V. "A novel microchip nitric oxide sensor with sub-nM detection limit," *Electroanalysis* **2002**, *14*, 697-703.
- (58) Wu, F.-H.; Zhao, G.-C.; Wei, X.-W. "Electrochemical oxidation of nitric oxide at multi-walled carbon nanotubes modified electrode," *Electrochem. Commun.* **2002**, *4*, 690-694.
- (59) Kamei, K.-i.; Mie, M.; Yanagida, Y.; Aizawa, M.; Kobatake, E. "Construction and use of an electrochemical NO sensor in a cell-based assessing system," *Sens. Actuators B* **2004**, *99*, 106-112.
- (60) Lantoine, F.; Trevin, S.; Bedioui, F.; Devynck, J. "Selective and sensitive electrochemical measurement of nitric oxide in aqueous solution: Discussion and new results," *J. Electroanal. Chem.* **1995**, *392*, 85-89.
- (61) Trevin, S.; Bedioui, F.; Devynck, J. "Electrochemical and spectrophotometric study of the behavior of electropolymerized nickel porphyrin films in the determination of nitric oxide in solution," *Talanta* **1996**, *43*, 303-311.
- (62) Bedioui, F.; Trevin, S.; Devynck, J.; Lantoine, F.; Brunet, A.; Devynck, M.-A. "Elaboration and use of nickel planar macrocyclic complex-based sensors for the direct electrochemical measurement of nitric oxide in biological media," *Biosens. Bioelectron.* **1997**, *12*, 205-212.
- (63) Fabre, B.; Bulet, S.; Cespuglio, R.; Bidan, G. "Voltammetric detection of NO in the rat brain with an electronic conducting polymer and nafion bilayer-coated carbon fibre electrode," *J. Electroanal. Chem.* **1997**, *426*, 75-83.
- (64) Mitchell, K.; Michaelis, E. K. "Multimembrane carbon fiber electrodes for

- physiological measurements of nitric oxide," *Electroanalysis* **1998**, *10*, 81-88.
- (65) Ciszewski, A.; Milczarek, G. "A new Nafion-free bipolymeric sensor for selective and sensitive detection of nitric oxide," *Electroanalysis* **1998**, *10*, 791-793.
- (66) Haruyama, T.; Shiino, S.; Yanagida, Y.; Kobatake, E.; Aizawa, M. "Two types of electrochemical nitric oxide (NO) sensing systems with heat-denatured Cyt C and radical scavenger PTIO," *Biosens. Bioelectron.* **1998**, *13*, 763-769.
- (67) Mao, L.; Shi, G.; Tian, Y.; Liu, H.; Jin, L.; Yamamoto, K.; Tao, S.; Jin, J. "A novel thin-layer amperometric detection based on chemically modified ring-disc electrode and its application for simultaneous measurements of nitric oxide and nitrite in rat brain combined with in vivo microdialysis," *Talanta* **1998**, *46*, 1547-1556.
- (68) Pei, J.; Yu, N.-T.; Li, X.-Y. "Electrocatalytic detection of biological nitric oxide at an ultramicroelectrode modified with an electrodeposited CuPtCl₆ film," *Anal. Chim. Acta* **1999**, *402*, 145-155.
- (69) Xian, Y.; Xue, J.; Zhang, S.; Ying, X.; Jin, L. "An Ni(chitin)₂ modified nitric oxide microsensor," *Fresenius J. Anal. Chem.* **1999**, *365*, 587-591.
- (70) Pei, J.; Li, X.-y.; Buffle, J. "Preparation, characterization and application of an electrode modified with electropolymerized CuPtBr₆ film," *Electrochim. Acta* **2000**, *45*, 1581-1593.
- (71) He, X. C.; Mo, J. Y. "Electrocatalytic oxidation of NO at electrode modified with Nafion-Co^{II}-1,10-phenanthroline film and its application to NO detection," *Analyst* **2000**, *125*, 793-795.
- (72) Kashevskii, A. V.; Safronov, A. Y.; Ikeda, O. "Behaviors of H₂TPP and CoTPPCL in Nafion film and the catalytic activity for nitric oxide oxidation," *J. Electroanal. Chem.* **2001**, *510*, 86-95.
- (73) Pereira-Rodrigues, N.; Albin, V.; Koudelka-Hep, M.; Auger, V.; Pailleret, A.; Bedioui, F. "Nickel tetrasulfonated phthalocyanine based platinum microelectrode array for nitric oxide oxidation," *Electrochem. Commun.* **2002**, *4*, 922-927.
- (74) Mori, V.; Toledo, J. C.; Silva, H. A. S.; Franco, D. W.; Bertotti, M. " Anodic oxidation of free nitric oxide at gold electrodes modified by a film of trans-[Ru(III)(NH₃)₄(SO₄)₄pic]⁺ and molybdenum oxide," *J. Electroanal. Chem.* **2003**, *547*, 9-15.

Chapter 4:

Synthesis of Nitric Oxide-Releasing Silica Nanoparticles

4.1 Introduction

Nitric oxide (NO) is a diatomic free radical endogenously synthesized in the human body when L-arginine is converted to L-citrulline by a class of enzymes known as nitric oxide synthase (NOS).^{1,2} Since the first reports describing NO's action as an endothelium-derived relaxation factor (EDRF) in the mid-1980s, much research has been devoted to elucidating the pathways of NO generation and action *in vivo*.³ To date, researchers have discovered that NO regulates a range of biological processes in the cardiovascular, gastrointestinal, genitourinary, respiratory, and central and peripheral nervous systems.^{2,4} Furthermore, the discoveries of NO as a vasodilator,⁵ antibacterial agent,^{6,7} and tumoricidal factor⁸⁻¹⁰ has made NO a promising pharmaceutical agent. To further comprehend the complex and wide ranging roles of NO and facilitate its therapeutic use, a number of synthetic compounds that chemically store and release NO in a controlled fashion have been developed.

Several classes of NO donors exist including nitrosothiols, nitrosamines, diazeniumdiolates, NO-metal complexes, and organic nitrites and nitrates.^{11,12} Of these, 1-amino-substituted diazen-1-ium-1,2-diolates (or simply *N*-diazeniumdiolates) are particularly attractive due to their ability to generate NO spontaneously under biological conditions.^{13,14} Since the first report on the synthesis of *N*-diazeniumdiolates via the reaction of amines with NO at elevated pressure in the 1960s,^{15,16} several *N*-diazeniumdiolate compounds have been

synthesized using a range of nucleophilic residues that encompass primary and secondary amines, polyamines, and secondary amino acids.¹³ While stable under ambient conditions, *N*-diazoniumdiolates decompose spontaneously in aqueous media to generate NO at rates dependent upon pH, temperature, and the structure of the amine moiety.¹³ For example, *N*-diazoniumdiolate-modified proline (PROLI/N₂O₂), 2-(dimethylamino)ethylputreanine (DMAEP/N₂O₂), *N,N'*-dimethylhexanediamine (DMHA/N₂O₂), and diethylenetriamine (DETA/N₂O₂) have been developed as effective small molecule NO donors with diverse NO release half-lives ranging from 2 s to 20 h at pH 7.4 and 37 °C.^{13,17}

Considerable effort has been devoted to developing NO storage/delivery systems whereby such NO donors are attached to macromolecular frameworks.¹⁸⁻²² Such scaffolds possess large quantities of NO with readily modifiable NO release kinetics. For example, Pulfer *et al.* reported the synthesis of *N*-diazoniumdiolate-modified polyethyleneimine microspheres ($d = 10 - 50 \mu\text{m}$) that were embedded into vascular grafts to prevent thrombosis and restenosis.²⁰ Likewise, Hrabie *et al.* synthesized water-soluble NO donor–protein conjugates via covalent attachment of methoxymethyl-protected *N*-diazoniumdiolated piperazine (MOM-PIPERAZI/N₂O₂) ligands to the lysine residues of both bovine and human serum albumin.¹⁸ Jeh *et al.* demonstrated the delivery of NO to the alveolar region of the lungs via inhalable, biodegradable microparticles ($d = 10 - 35 \mu\text{m}$) prepared using poly-lactic-co-glycolic acid or polyethylene oxide-co-lactic acid copolymer that encapsulated small molecule NO donors (e.g., PROLI/N₂O₂).¹⁹ More recently, our laboratory has focused on the synthesis and characterization of NO-releasing monolayer protected gold clusters²¹ and dendrimer conjugates.²² Despite their small size, unprecedented NO release properties,

and potential for targeting the delivery of NO, the complex synthesis and potential toxicity of the gold cluster and dendrimer constructs remain notable concerns.

Inorganic-organic *hybrid* silica nanoparticles, functionalized ceramic materials prepared from silicon dioxide, have been employed as carrier systems for the controlled delivery of drugs, genes, and proteins.²³⁻²⁷ The drug delivery potential of silica has received much attention because of its physical and chemical versatility (e.g., ability to tune the mesoporous structure and control specific surface properties) and non-toxic nature.²⁸⁻³¹ The synthesis of inorganic-organic *hybrid* silica modified with reactive organic groups (e.g., amines, carboxylates, thiols, olefins, halides, and epoxides) capable of further functionalization with deliverable molecules has been reported.^{30,31} Indeed, silane-coupling agents with the aforementioned functional moieties are available for surface grafting (via free silanol groups) of drugs and other therapeutics.³² Meyerhoff and coworkers previously reported the synthesis of NO-releasing fumed silica (amorphous particles of $d = 0.2 - 0.3 \mu\text{m}$) via grafting amine-functionalized silylation reagents onto the silica surface, and then converting the amines to *N*-diazoniumdiolates.³³ Despite the unique advantages of combining the *N*-diazoniumdiolate chemistry with the versatility of micro- and nanocomposite materials, the usefulness of such scaffolds as therapeutic NO delivery systems remains hindered by the complicated synthesis and purification, and limited size control.

Herein, we report a new synthetic approach to preparing NO-releasing silica nanoparticles via a one-pot^{31,34,35} sol-gel process (Figure 4.1) followed by exposure to 5 atm of NO under basic conditions. Amine-functionalized *hybrid* silica composites were prepared via co-condensation of tetraethoxy- or tetramethoxysilane (TEOS or TMOS) and aminoalkoxysilane with appropriate amounts of ethanol (or methanol), water, and ammonia.

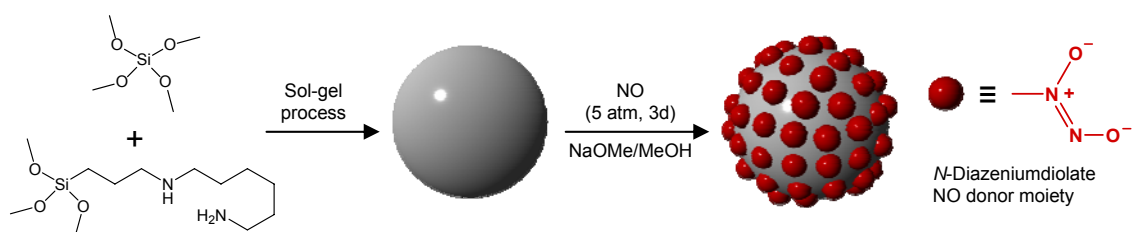


Figure 4.1. Synthesis of *N*-diazeniumdiolate-modified silica nanoparticles using tetramethoxysilane (TMOS) and *N*-(6-aminohexyl)aminopropyltrimethoxysilane (AHAP3) as example tetraalkoxy- and aminoalkoxysilane precursors.

The amine functional groups within the silica particles were subsequently converted to *N*-diazoniumdiolate NO donors via exposure to high pressures of NO (5 atm) in the presence of sodium methoxide (NaOMe) base.¹³ The advantage of a one-pot approach for preparing the silica is that the *N*-diazoniumdiolate NO donor precursors are distributed uniformly throughout the particle as opposed to only at the surface (as is the case for amine-modified silica³³ or gold particles²¹ formed via surface grafting methods). The selection of the silane precursors (e.g., type and concentration) and specific reaction/processing conditions (e.g., solvent, catalyst, pH, and temperature) allows for tremendous chemical flexibility in creating nanoparticles of diverse size^{31,36} and NO release properties (e.g., NO payload and delivery kinetics).

4.2 Experimental Section

4.2.1 Reagents and Materials

Tetraethoxysilane (TEOS), tetramethylsilane (TMS), and sodium methoxide (NaOMe) were purchased from Fluka (Buchs, Switzerland). (Aminoethylaminomethyl)phenethyltrimethoxysilane (AEMP3), *N*-(6-aminohexyl)aminopropyltrimethoxysilane (AHAP3), and *N*-(2-aminoethyl)-3-aminopropyltrimethoxysilane (AEAP3) were purchased from Gelest (Tullytown, PA). Tetramethoxysilane (TMOS) and *N,N*-dimethylformamide (DMF) were purchased from Sigma (St. Louis, MO). Methanol (MeOH), ethanol (EtOH), toluene, and ammonia solution (NH₄OH, 30 wt% in water) were purchased from Fisher Scientific (Fair Lawn, NJ). Nitric oxide (NO, 99.5%), argon (Ar), and nitrogen (N₂) gases were obtained from AGA Gas (Maumee, OH) or National Welders Supply (Raleigh, NC). Other solvents and chemicals were analytical-reagent grade and used as received. A Millipore Milli-Q UV Gradient A10 System (Bedford, MA) was used to purify distilled water to a final resistivity

of 18.2 M Ω ·cm and a total organic content of ≤ 6 ppb.

4.2.2 Synthesis of Nitric Oxide-Releasing Silica Nanoparticles

Amine-functionalized silica composite particles were synthesized via a co-condensation process (Figure 4.1).^{31,34,35} First, the silane solutions were prepared by mixing 2.78 mmol (620 μ L) of TEOS or TMOS with different concentrations of AEAP3, AHAP3, or AEMP3 (0 – 18.6 mmol corresponding to 0 – 87 mol%, balance TEOS or TMOS) for 5 min. The silane solution was then combined with 22 mL of EtOH or MeOH and 6 mL of ammonia (30 wt% in water), and vigorously stirred for 30 min under ambient conditions. The white precipitate was collected by centrifugation (5000 rpm, 5 min), washed with EtOH copiously, and dried under vacuum overnight.

The resulting amine-functionalized silica was resuspended in 18 mL of DMF and 2 mL of MeOH in the presence of NaOMe (0.32 – 18.6 mmol; adding an equimolar amount of NaOMe corresponding to the secondary amine content of silica composites)^{13,33} and placed in 10 mL-vials equipped with a stir bar. The vials were placed in a Parr bottle (200 mL), connected to an in-house NO reactor, and flushed with Ar for 10 min six times to remove oxygen in the suspension. The reaction bottle was then charged with NO to 5 atm and sealed for 3 d while stirring. The NO gas was purified over KOH pellets for 2 h to remove trace NO degradation products. Prior to removing the silica particles, unreacted NO was purged from the chamber with Ar. The *N*-diazoniumdiolate-modified silica particles were recollected by centrifugation at 5000 rpm for 5 min, washed copiously with ethanol, dried under ambient conditions for 1 h, and stored in a sealed container at -20 °C until used.

4.2.3 Characterization of Functionalized Silica

Prior to analysis via atomic force microscopy (AFM), the silica particles were suspended in toluene, deposited on a freshly cleaved mica surface (SPI; West Chester, PA), and dried under ambient conditions for 3 h. Contact mode AFM images were obtained in air using a Molecular Force Probe 3D Atomic Force Microscope (Asylum Research; Santa Barbara, CA) controlled with a MFP-3D software running under Igor Pro (Wavemetrics; Lake Oswego, OR). Triangular silicon nitride cantilevers with a nominal spring constant of $0.12 \text{ N}\cdot\text{m}^{-1}$ and resonance frequency of 20 kHz (Veeco; Santa Barbara, CA) were used to acquire height/topography images at a scan rate of 0.5 Hz.

Solid-state cross polarization/magic angle spinning (CP/MAS) ^{29}Si nuclear magnetic resonance (NMR) spectra^{37,38} were obtained at 293 K on a Bruker 360 MHz DMX spectrometer (Billerica, MA) equipped with wide-bore magnets (triple axis pulsed field gradient double resonance probes). Silica composite particles were packed into 4 mm rotors (double resonance frequency of 71.548 MHz) and spun at a speed of 8.0 kHz. The chemical shifts were determined in ppm relative to a TMS external standard.

Nitric oxide release profiles of the *N*-diazoniumdiolate-modified silica nanoparticles were measured in deoxygenated phosphate-buffered saline (PBS, 0.01 M; 37 °C) at a pH 3.3, 4.3, 5.3, 6.0, 7.4, and 9.5 using a Sievers NOA 280i chemiluminescence nitric oxide analyzer (Boulder, CO).^{22,39} Nitric oxide released from the silica was transported to the analyzer by a stream of N_2 ($70 \text{ mL}\cdot\text{min}^{-1}$) passed through the reaction cell. The instrument was calibrated with air passed through a zero filter (0 ppm NO) and 24.1 ppm of NO standard gas (balance N_2 , purchased from AGA Gas).

The surface area and pore volume of the silica were determined via nitrogen

adsorption/desorption isotherms³⁸ collected with a Beckman Coulter SA3100 Surface Area and Pore Size Analyzer (Fullerton, CA). The surface area and pore volume were calculated using the Brunauer-Emmett-Teller (BET) and Barrett-Joyner-Halenda (BJH) methods. Prior to the measurements, all silica samples were degassed at 200 °C for 3 h.

Elemental (CHN) analyses were performed by Midwest Microlab, LLC (Indianapolis, IN) to determine the concentration of amines incorporated in the functionalized silica nanoparticles.

4.3 Results and Discussion

4.3.1 Synthesis and Characterization of Functionalized Silica Nanoparticles

To synthesize organically-modified *hybrid* silica via a one-pot strategy, two silicon alkoxide precursors, tetramethoxy- and tetraethoxysilanes (TMOS and TEOS), were used as backbone silanes (Figure 1.7).⁴⁰ The choice of the tetraalkoxysilane is crucial for the formation of silica composites with homogeneous distributions of active functionalities.⁴¹⁻⁴³ For example, differences in the hydrolysis and condensation rates of tetraalkoxy- and organoalkoxysilanes often result in disordered, inhomogeneous silica.^{36,41,42,44} As such, matching the hydrolysis and condensation rates of bi- and multicomponent silane systems plays an important role in synthesizing well-ordered, mesoporous materials.^{36,41,42,44} In general, the following factors can be used to predict hydrolysis and condensation propensities of the silanes: 1) a methoxy ligand is more readily hydrolyzed than an ethoxy one; 2) the hydrolysis of organoalkoxysilanes is slower than fully hydrolysable tetraalkoxysilane with the same alkoxy identity; and, 3) the long alkyl chain, steric hindrance, and hydrophobic nature of the organic group often impede the overall hydrolytic polycondensation reactions.^{36,41,42,44} With these factors in mind, TEOS was selected as the initial silicon

alkoxide backbone for study because of its similar hydrolysis rate to the aminoalkoxysilanes (i.e., AHAP3, AEAP3, and AEMP3) used in this study.

Control over both the structure and concentration of the aminoalkoxysilane precursors and specific synthetic conditions allowed for the preparation of NO donor silica nanoparticles of widely varying size and NO release properties. As shown in Figure 4.2, the size of the silica nanoparticles was tunable by varying the type and concentration of aminoalkoxysilane used. The diameter of control (TEOS only) silica particles was 250 ± 20 nm. Adding 10 mol% AHAP3 to the TEOS solution decreased the diameter of the particles to 20 ± 2 nm. In contrast, silica particles prepared from 10 mol% AEAP3 (balance TEOS) were roughly twice as large ($d = 500 \pm 45$ nm) as TEOS controls. As the mol% of AEAP3 was increased from 10 to 17 mol%, the diameter of the particle decreased to 92 ± 16 nm, revealing a pseudo-linear relationship between particle size and aminoalkoxysilane concentration (Figure 4.2F). Particle size was not altered upon conversion of the amines to *N*-diazoniumdiolates, indicating that the structural integrity of the silica particles is not compromised by the conditions necessary to form the NO donor (data not shown).

Solid-state ^{29}Si NMR was used to (1) confirm the incorporation of aminoalkyl functionalities within the silica network (Figure 4.3), and (2) determine the surface coverage of such ligands (Table 4.1).³⁸ Cross polarization and magic angle spinning (CP/MAS) techniques were employed to increase the signal resolution and sensitivity. The spectra for control and amine-functionalized silica particles prepared from 0 and 10 – 17 mol% AEAP3 (balance TEOS) are shown in Figure 4.3. For TEOS control silica, three distinct peaks in the ^{29}Si NMR spectrum were observed at -90, -101, and -109 ppm, respectively, representative of Q^2 (geminal silanol; $-\text{O}_2\text{Si}(\text{OH})_2$), Q^3 (single silanol; $-\text{O}_3\text{Si}(\text{OH})$), and Q^4 (siloxane;

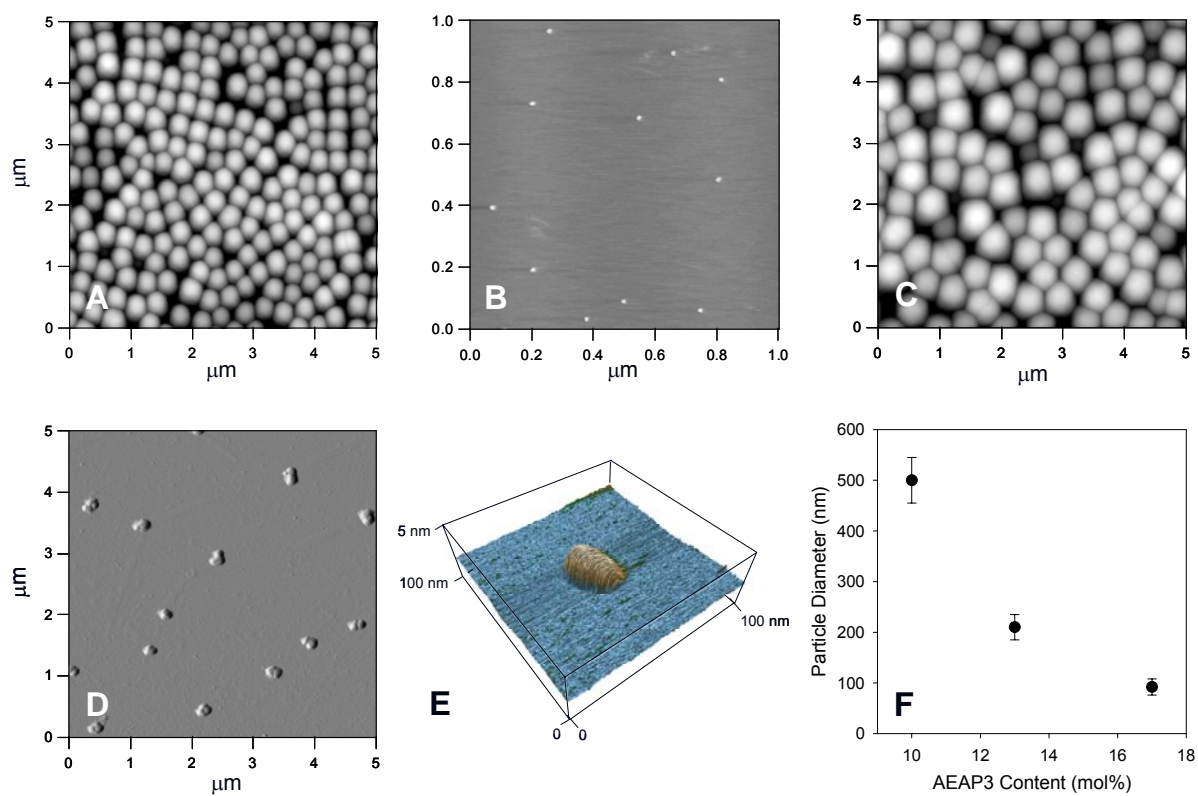


Figure 4.2. Contact mode AFM images of (A) control silica (TEOS only); (B) silica with 10 mol% of AHAP3 (balance TEOS); and, (C) 10 mol% and (D) 17 mol% AEAP3 silica particles on a mica surface. (E) Enlargement of a single particle from (B). (F) Relationship between the AEAP3 content (balance TEOS) in the silica composite and particle size.

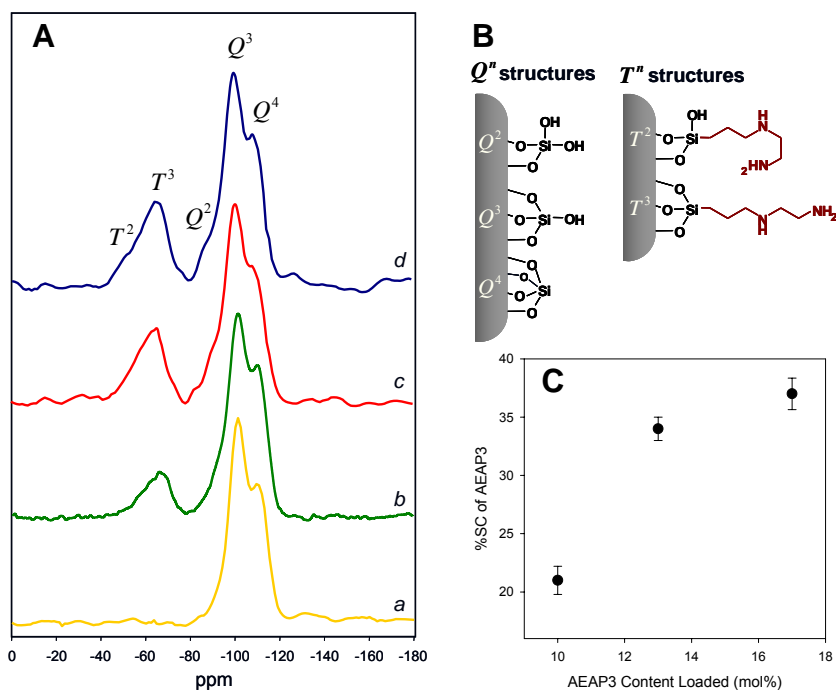


Figure 4.3. (A) Solid-state ^{29}Si CP/MAS NMR spectra of functionalized silica materials with various amounts of AEAP3: (a) 0 (control), (b) 10, (c) 13, and (d) 17 mol% (balance TEOS). (B) Schematic illustration of silicon chemical environments at the surface of AEAP3-modified silica composites. (C) Plot of % surface coverage (%SC) of functional ligands versus AEAP3 content loaded during the synthesis.

Table 4.1. ^{29}Si chemical shifts (δ_{Si} from tetramethylsilane) and relative concentrations of T^n and Q^n structures for functionalized silica as a function of AEAP3 mol%^a

tetraalkoxy- silane ^b	aminoalkoxysilane		Si structure (%)					%SC ^d	e_{immo} ^e
	type	mol% ^c	T^2 (-52 ppm)	T^3 (-65 ppm)	Q^2 (-90 ppm)	Q^3 (-101 ppm)	Q^4 (-109 ppm)		
TEOS	AEAP3 ^f	10	5	9	16	38	32	21	2.1
		13	9	14	17	27	33	34	2.6
		17	7	19	11	34	29	37	2.2
TMOS	AEAP3	10	3	4	37	39	17	8	0.8
		30	3	19	22	36	20	28	0.9
		70	7	20	23	26	24	36	0.5

^aData obtained via deconvolution of ^{29}Si CP/MAS NMR spectra. ^bTEOS, tetraethoxysilane; and TMOS, tetramethoxysilane. ^cBalance TEOS or TMOS. ^dSurface coverage was calculated with the equation of $\text{SC} = (T^2 + T^3)/(T^2 + T^3 + Q^2 + Q^3)$. ^eImmobilization efficiency (e_{immo}) was determined as the ratio of %SC and mol% of AEAP3 loaded during the synthesis. ^fAEAP3, *N*-(2-aminoethyl)-3-aminopropyltrimethoxy-silane.

$-\text{O}_4\text{Si}$) silicons.^{37,38} For the aminoalkoxysilane-modified silica particles, five peaks were observed in the spectra, indicating two additional silicon chemical environments (graphs b-d in Figure 4.3A). Indeed, the peaks at chemical shifts of approximately -52 and -65 ppm are representative of silicon connected to T^2 ($-\text{O}_2\text{Si}(\text{OH})\text{R}$) and T^3 ($-\text{O}_3\text{SiR}$) structures, respectively (where R is an aminoethylaminopropyl group).^{37,38} The presence of T^n bands suggests the existence of covalent linkages between aminoalkyl groups and the silica backbone. The Q^2 , Q^3 , and Q^4 resonance lines also appeared at the expected positions. As the AEAP3 content was increased from 10 to 17 mol%, the surface coverage of aminoalkyl ligands [$\text{SC} = (T^2 + T^3)/(T^2 + T^3 + Q^2 + Q^3)$]^{38,45} increased from 21 to 37% (Figure 4.3C), respectively. The ligand immobilization efficiency (e_{immo}), defined as the ratio of %SC and AEAP3 content (mol%) incorporated in the starting sol, was between 2.1 and 2.6, indicating effective immobilization of aminoalkyl groups. Of note, the integration and quantitative analysis of these structures is complicated because the intensity of each peak depends on the efficiency of cross polarization and the proton relaxation time.⁴⁶

The surface area and pore volume of the silica nanoparticles were evaluated via nitrogen adsorption-desorption isotherms.³⁸ As expected, the amine-functionalized silica proved to be nonporous with surface areas (S_{BET}) of $10 - 20 \text{ m}^2 \cdot \text{g}^{-1}$ and pore volumes (V_p) of $0.02 - 0.06 \text{ mL} \cdot \text{g}^{-1}$ (at $p/p_0 = 0.98$). Indeed, previous reports of organically-modified *hybrid* silica synthesized by the co-condensation method indicated highly dense, nonporous, and amorphous structures.^{30,31}

4.3.2 Nitric Oxide Release Characteristics

Nitric oxide release was evaluated as a function of tetraalkoxy- and aminoalkoxysilane

structure and concentration. The NO release profiles of two representative silica nanoparticles (10 mol% AHAP3 and 17 mol% AEAP3, balance TEOS) are shown in Figure 4.4. These representative compositions illustrate the drastic effects of amine-derivatization on several NO release properties including the total amount of NO ($t[\text{NO}]$), half-life of NO release ($t_{1/2}$), maximum flux of NO release ($[\text{NO}]_m$), and time necessary to reach $[\text{NO}]_m$ (t_m). Both the NO payload and release rates were significantly affected by the concentration and chemical identity of the amine ligands (e.g., AEAP3, AHAP3, and AEMP3) used to prepare the silica nanoparticles (Table 4.2). At a fixed aminoalkoxysilane concentration of 10 mol% (balance TEOS), the trend in $t[\text{NO}]$ was AHAP3>AEAP3>AEMP3 (380, 145, and 53 nmol·mg⁻¹, respectively). For AEAP3 and AEMP3 silica, increasing the concentration of aminoalkoxysilanes from 10 to 20 mol% led to notable increases in both $t[\text{NO}]$ and $[\text{NO}]_m$. For the AEAP3 system, both the $t_{1/2}$ and t_m decreased with increasing aminoalkoxysilane concentration (12 to 3.4 h and 8.0 to 2.1 h for 10 to 17 mol% AEAP3 silica, respectively).

The decrease in NO release kinetics corresponded directly with nanoparticle size and predicted water uptake. A shorter water diffusion distance to interior NO donor ligands would be expected for smaller diameter particles, resulting in more rapid *N*-diazoniumdiolate breakdown and NO release. For AEMP3 silica nanoparticles, the $t_{1/2}$ and t_m were constant regardless of the aminoalkoxysilane concentration. Such fixed NO release kinetics for AEMP3 was expected due to the similar size of the particles (~30 – 50 nm) over the range of aminoalkoxysilane concentrations studied (i.e., 10 – 20 mol%, balance TEOS). As shown in Table 4.3, the amine to *N*-diazoniumdiolate conversion efficiencies for the TEOS-derived silica nanoparticles ranged from ~6 to 19%, depending on the size and composition of the nanoparticle. Larger silica nanoparticles were characterized by lower conversion efficiencies

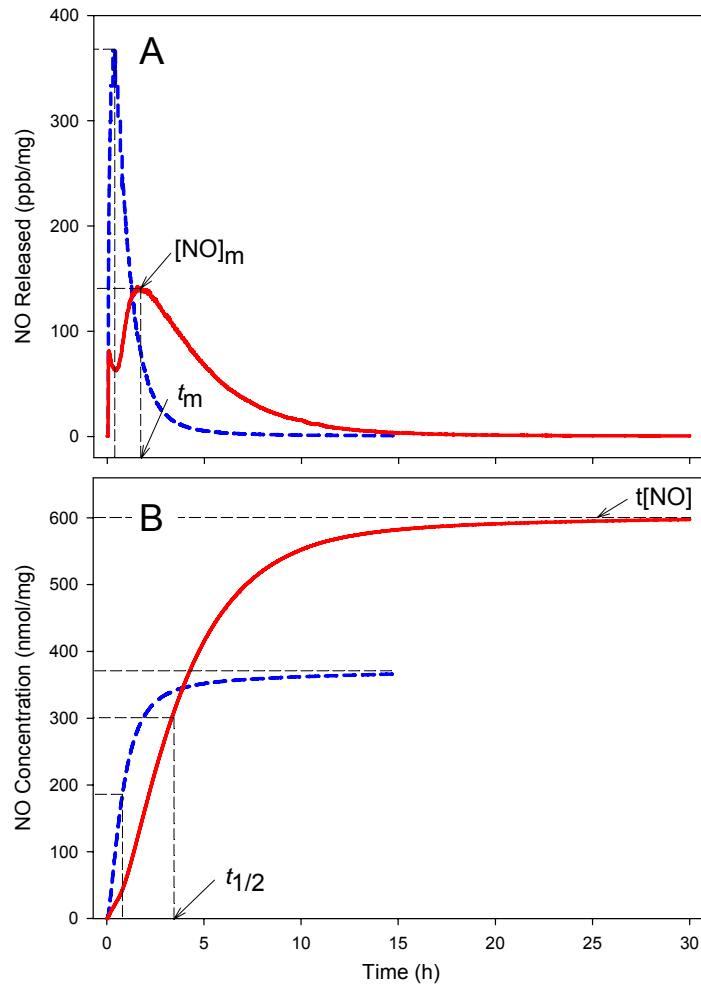


Figure 4.4. (A) NO release profiles and (B) total NO release of 10 mol% of AHAP3 (dashed blue) and 17 mol% of AEAP3 (solid red) silica nanoparticles (balance TEOS).

Table 4.2. NO release properties of *N*-diazoniumdiolate-modified silica nanoparticles with different tetraalkoxy- and aminoalkoxysilane precursors^{a,b}

tetraalkoxy-silane ^c	aminoalkoxysilane		particle size ^f (nm)	t[NO] (nmol·mg ⁻¹)	<i>t</i> _{1/2} (h)	[NO] _m (ppb·mg ⁻¹)	<i>t</i> _m (h)	
	type ^d	mol% ^e						
TEOS	AEMP3	10	50 ± 5	53 ± 3	6.0 ± 0.2	10 ± 2	0.12 ± 0.01	
		13	43 ± 4	81 ± 3	6.5 ± 0.3	22 ± 2	0.10 ± 0.01	
		17	40 ± 5	118 ± 5	5.7 ± 0.5	32 ± 2	0.11 ± 0.02	
		20	30 ± 4	170 ± 10	5.4 ± 0.3	40 ± 3	0.11 ± 0.01	
	AEAP3	10	500 ± 45	145 ± 10	12 ± 4	14 ± 3	8 ± 1	
		13	210 ± 25	392 ± 15	6 ± 1.5	92 ± 5	4 ± 1	
		17	92 ± 16	600 ± 25	3.4 ± 0.4	140 ± 10	2.1 ± 0.3	
	AHAP3	10	20 ± 2	380 ± 20	0.9 ± 0.1	370 ± 10	0.35 ± 0.05	
	TMOS	AEAP3	10	270 ± 25	46 ± 4	1.9 ± 0.3	40 ± 7	0.18 ± 0.04
30			130 ± 10	156 ± 10	1.7 ± 0.1	146 ± 20	0.08 ± 0.01	
50			98 ± 8	308 ± 35	1.9 ± 0.4	308 ± 100	0.25 ± 0.04	
70			74 ± 8	414 ± 20	1.6 ± 0.1	1100 ± 240	0.14 ± 0.01	
87			58 ± 10	330 ± 10	0.1 ± 0.02	5500 ± 300	0.06 ± 0.01	
AHAP3		10	64 ± 4	101 ± 5	0.2 ± 0.04	560 ± 40	0.07 ± 0.02	
		30	55 ± 5	230 ± 40	0.3 ± 0.09	730 ± 290	0.10 ± 0.03	
		50	51 ± 6	440 ± 30	0.7 ± 0.2	510 ± 30	0.11 ± 0.04	
		60	58 ± 5	680 ± 40	0.5 ± 0.01	1900 ± 190	0.07 ± 0.01	
		70	48 ± 7	1700 ± 20	0.9 ± 0.1	2660 ± 190	0.12 ± 0.07	
		77	65 ± 5	1780 ± 50	0.9 ± 0.2	2810 ± 210	0.11 ± 0.3	
			2N[2] ^g	200 – 300	580	2.4		
			2N[6] ^g	200 – 300	560 ± 60	0.7		

^a*n* is at least 3. ^bValues were measured in phosphate-buffered saline (PBS) at pH 7.4 and 37 °C. ^cTEOS, tetraethoxysilane; and TMOS, tetramethoxysilane. ^dAEMP3, (aminoethylaminomethyl)-phenethyltrimethoxysilane; AEAP3, *N*-(2-aminoethyl)-3-aminopropyltrimethoxysilane; and AHAP3, *N*-(6-amino-hexyl)aminopropyltrimethoxysilane. ^eBalance TEOS or TMOS. ^fDiameter. ^gRef. 33. Amine-modified silica particles were prepared via the surface-grafting method.

Table 4.3. Nitrogen content (%N), amine concentration (C_{amine}), *N*-diazoniumdiolate concentration (C_{diaz}), and amine to *N*-diazoniumdiolate conversion efficiency (%Conv) of various silica nanoparticles prepared with different tetraalkoxy- and aminoalkoxysilane precursors

tetraalkoxy-silane ^a	aminoalkoxysilane		%N ^d	C_{amine} ^e ($\mu\text{mol}\cdot\text{mg}^{-1}$)	C_{diaz} ^f ($\mu\text{mol}\cdot\text{mg}^{-1}$)	%Conv
	type ^b	mol% ^c				
TEOS	AEAP3	10	3.39	1.21	0.07	5.8
		13	3.90	1.39	0.20	14.4
		17	5.45	1.95	0.30	15.4
	AHAP3	10	2.74	0.98	0.19	19.4
TMOS	AEAP3	30	1.94	0.69	0.08	11.6
		50	2.91	1.04	0.15	14.4
		70	3.69	1.32	0.21	15.9
		87	3.22	1.15	0.17	14.8
	AHAP3	10	1.45	0.52	0.05	9.6
		30	2.84	1.01	0.11	10.9
		50	3.12	1.11	0.22	19.8
		60	4.19	1.50	0.34	22.7
		70	4.74	1.69	0.85	50.3
		77	4.81	1.72	0.89	51.7
	2N[2] ^g			1.23	0.29	24
	2N[6] ^g			0.86	0.28	33

^aTEOS, tetraethoxysilane; and TMOS, tetramethoxysilane. ^bAEAP3, *N*-(2-aminoethyl)-3-aminopropyltrimethoxysilane; and AHAP3, *N*-(6-aminoethyl)aminopropyltrimethoxysilane. ^cBalance TEOS or TMOS. ^dObtained by elemental analyses within 0.3% error. ^eAmine concentration is the concentration of diamine. ^fDetermined by measuring the total NO concentration (t[NO]) released from the particles using a chemiluminescence nitric oxide analyzer. ^gRef. 33. Amine-modified silica particles were prepared via the surface-grafting method.

than smaller sized particles (e.g., 6 vs. 15% for 10 and 17 mol% AEAP3 silica, respectively).

Similar to other *N*-diazoniumdiolate NO donor scaffolds, the mechanism of NO release was proton initiated as evidenced by pH-dependent NO release behavior. The effect of pH on the NO release kinetics from the silica scaffolds was also evaluated (Figure 4.5). Consistent with the behavior of small molecule *N*-diazoniumdiolates, NO release was accelerated under acidic conditions (pH 3.3). Conversely, NO release was slowed considerably at elevated pH (9.5), consequently demonstrating a simple method for storing and transporting NO donor nanoparticles without significant deterioration of the *N*-diazoniumdiolate. The $t[\text{NO}]$ was similar at all pH values, but the NO release kinetics were dramatically increased at lower pH. A nine-fold increase in the maximum flux of NO released ($[\text{NO}]_m$) was observed at pH 3.3 compared to that at pH 7.4. Such behavior, combined with the pH dependent dissociation of *N*-diazoniumdiolates confirms that the dominate mechanism of NO release for the silica scaffolds is proton initiated.

Although a diverse range of NO release properties were obtained from the silica prepared via combination of TEOS and AHAP3, AEAP3, or AEMP3, the aminoalkoxysilane content was limited to <20 mol% due to aggregation resulting from hydrogen bonding interactions between amines and adjacent silanols and/or other amines.⁴⁷ The synthesis of particles using TMOS as the backbone precursor was thus evaluated as a strategy for increasing the aminoalkoxysilane concentration and bolstering NO storage capacity since the rate of TMOS hydrolysis is faster than TEOS.^{36,42} Accelerated hydrolytic polycondensation reactions (i.e., quick production and consumption of silanols) would be expected to reduce potential amine-silanol and/or amine-amine interactions during particle formation. As shown in Table 4.2, the concentration of aminoalkoxy ligand that could be used to prepare non-

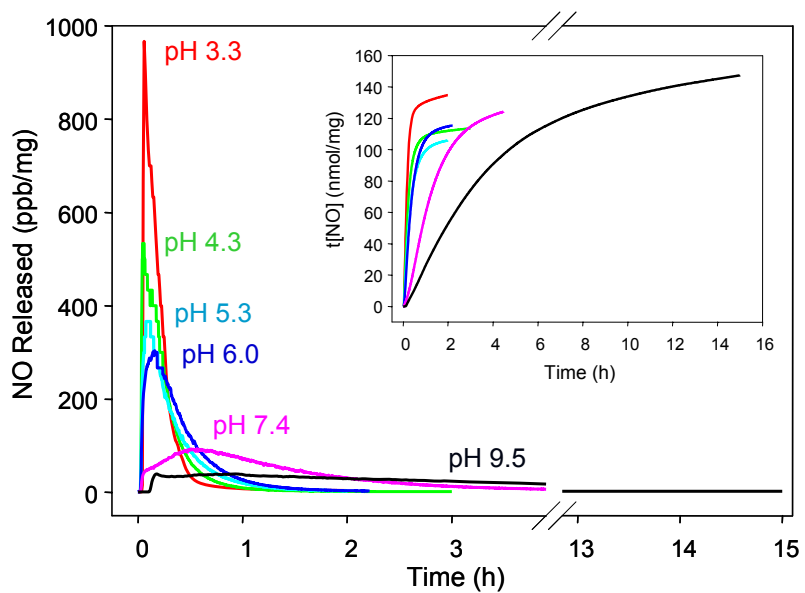


Figure 4.5. NO release of AEAP3-based silica nanoparticles as a function of pH at 37 °C. Insert: total NO release.

aggregated particles approached 77 and 87 mol% for AHAP3- and AEAP3-based TMOS particles, respectively. Similar to TEOS, the diameter of TMOS-derived particles decreased with increasing aminoalkoxysilane concentration (270 to 58 nm for 10 to 87 mol% AEAP3 and 64 to 48 nm for 10 to 70 mol% AHAP3, respectively).

Surprisingly, the NO payload of aminoalkoxysilane/TMOS particles prepared using 10 mol% aminoalkoxysilane was slightly lower than that for similarly prepared TEOS silica (145 versus 46 nmol·mg⁻¹ and 380 versus 101 nmol·mg⁻¹ for 10 mol% AEAP3 and AHAP3, respectively) (Table 4.2), indicating that the immobilization efficiency of the aminoalkoxy ligand depends on the tetraalkoxysilane backbone. Both ²⁹Si NMR (Table 4.1) and elemental analyses (Table 4.3) indicate that the levels of aminoalkoxy ligands in the silica particles are not directly proportional to the aminoalkoxysilane concentration in the sol. Indeed, the e_{immo} of AEAP3/TMOS silica ranged from 0.5 – 0.9, three to five times less than AEAP3/TEOS ($e_{\text{immo}} = 2.1 - 2.6$). Nevertheless, the $t[\text{NO}]$ and $[\text{NO}]_{\text{m}}$ of AHAP3/TMOS silica was significantly enhanced (up to 1780 nmol·mg⁻¹ and 2810 ppb·mg⁻¹, respectively) relative to the TEOS silica systems. Both the $t_{1/2}$ and t_{m} also increased with increasing aminoalkoxysilane concentration (0.2 to 0.9 h and 0.07 to 0.12 h for 10 to 70 mol% AHAP3, respectively).

The NO release characteristics of *N*-diazoniumdiolate-modified silica nanoparticles prepared via a one-pot strategy are significantly expanded than that of both small molecule *N*-diazoniumdiolates and the 200–300 nm NO-releasing fumed silica prepared by surface grafting. The greatest $t[\text{NO}]$, 1780 nmol·mg⁻¹, was achieved with 77 mol% AHAP3/TMOS silica, a concentration roughly three times greater than 2N[6]-N₂O₂ surface-grafted silica ($t[\text{NO}] = 560 \text{ nmol}\cdot\text{mg}^{-1}$) prepared using the equivalent amine precursor structure (i.e., aminohexylaminopropyl ligand).³³ The greatest $t_{1/2}$ for AHAP3/TMOS silica was 0.9 h (54

min), significantly longer than the analogous small molecule DMHA/N₂O₂ ($t_{1/2}$ = 3 min) and 2N[6]-N₂O₂ surface-grafted silica ($t_{1/2}$ = 0.7 h or 42 min) systems. Likewise, $t_{1/2}$ of AEAP3 silica was 3.4 – 12 h (204 – 720 min) (depending on the aminoalkoxysilane concentration), while $t_{1/2}$ of the surface-grafted AEAP3 silica (i.e., 2N[2]-N₂O₂) was only 2.4 h (144 min).³³

4.4 Conclusions

The synthesis of NO-releasing nanoparticles represents an important step toward the development of NO storage/delivery systems that bridge the gap between small molecule *N*-diazoniumdiolates and *N*-diazoniumdiolate-modified macromolecules. Control over both the structure and concentration of tetraalkoxy- and aminoalkoxysilane precursors allows for the preparation of NO donor-modified silica nanoparticles of widely varying sizes (d = 20 – 500 nm) and NO release properties (e.g., NO payload of 50 – 1780 nmol·mg⁻¹, maximum NO fluxes (10 – 5500 ppb·mg⁻¹), half-lives (0.1 – 12 h), and NO release durations (15 – 30 h). Silica nanoparticles prepared via a one-pot approach exhibit an increased NO payload of up to three times greater than that attainable via surface-grafted silica.³³ In addition, the diversity of NO release kinetics and scaffold size, and favorable toxicity represent distinct advantages for silica over previously reported nanoparticles. Indeed, the ability to tune both the NO storage/release characteristics and size of the silica nanoparticles may facilitate the development of new pharmaceuticals for medical conditions and/or diseases requiring NO-based therapy. Recent work suggests that the size of the delivery vehicle is particularly important in determining cellular/tissue uptake and accumulation, with particles having a diameter between 20 and 100 nm as most optimal.⁴⁸⁻⁵⁰ The NO-releasing silica nanoparticles synthesized herein fit this range. The silica particles also avoid some practical limitations of previously reported nanoconstructs (e.g., dendrimers) in that their synthesis and purification

is simple, and their precursors inexpensive. Since concentration dictates NO's biological action, a scaffold with wide-ranging NO payloads and NO release kinetics may prove useful for a range of applications (e.g., pM to nM for regulating vasodilation and angiogenesis, and sub- μ M to μ M for killing bacteria or tumor cells).

4.5 References

- (1) Butler, A. R.; Nicholson, R. *Life, death and nitric oxide*; Royal Society of Chemistry: Cambridge, 2003.
- (2) Ignarro, L. J. *Nitric oxide: Biology and pathobiology*; Academic Press: San Diego, 2000.
- (3) Ignarro, L. J.; Buga, G. M.; Wood, K. S.; Byrns, R. E.; Chaudhuri, G. "Endothelium-derived relaxing factor produced and released from artery and vein is nitric oxide," *Proc. Natl. Acad. Sci. U.S.A* **1987**, *84*, 9265-9269.
- (4) Moncada, S.; Higgs, A. "The L-arginine-nitric oxide pathway," *N. Engl. J. Med.* **1993**, *30*, 2002-2011.
- (5) Radomski, M. W.; Palmer, R. M. J.; Moncada, S. "The anti-aggregating properties of vascular endothelium: Interactions between prostacyclin and nitric oxide," *Br. J. Pharmacol.* **1987**, *92*, 639-646.
- (6) Albina, J. E.; Reichner, J. S. "Role of nitric oxide in mediation of macrophage cytotoxicity and apoptosis," *Canc. Metas. Rev.* **1998**, *17*, 19-53.
- (7) Nablo, B. J.; Chen, T.-Y.; Schoenfisch, M. H. "Sol-gel derived nitric oxide-releasing materials that reduce bacterial adhesion," *J. Am. Chem. Soc.* **2001**, *123*, 9712-9713.
- (8) Cobbs, C. S.; Brenman, J. E.; Aldape, K. D.; Bredt, D. S.; Israel, M. A. "Expression of nitric oxide synthase in human central nervous system tumors," *Cancer Res.* **1995**, *55*, 727-730.
- (9) Jenkins, D. C.; Charles, I. G.; Thomsen, L. L.; Moss, D. W.; Holmes, L. S.; Baylis, S. A.; Rhodes, P.; Westmore, K.; Emson, P. C.; Moncada, S. "Roles of nitric oxide in tumor growth," *Proc. Natl. Acad. Sci. U.S.A.* **1995**, *92*, 4392-4396.
- (10) Thomsen, L. L.; Miles, D. W.; Happerfield, L.; Bobrow, L. G.; Knowles, R. G.; Moncada, S. "Nitric oxide synthase activity in human breast cancer," *Br. J. Cancer* **1995**, *72*, 41-44.
- (11) Wang, P. G.; Cai, T. B.; Taniguchi, N. *Nitric oxide donors: For pharmaceutical and*

biological applications; Wiley-VCH: Weinheim, German, 2005.

- (12) Wang, P. G.; Xian, M.; Tang, X.; Wu, X.; Wen, Z.; Cai, T.; Janczuk, A. J. "Nitric oxide donors: Chemical activities and biological applications," *Chem. Rev.* **2002**, *102*, 1091-1134.
- (13) Hrabie, J. A.; Keefer, L. K. "Chemistry of the nitric oxide-releasing diazeniumdiolate functional group and its oxygen-substituted derivatives," *Chem. Rev.* **2002**, *102*, 1135-1154.
- (14) Napoli, C.; Ignarro, L. J. "Nitric oxide-releasing drugs," *Annu. Rev. Pharmacol. Toxicol.* **2003**, *43*, 97-123.
- (15) Drago, R. S.; Karstetter, B. R. "The reaction of nitrogen(II) oxide with various primary and secondary amines," *J. Am. Chem. Soc.* **1961**, *83*, 1819-1822.
- (16) Drago, R. S.; Paulik, F. E. "The reaction of nitrogen(II) oxide with diethylamine," *J. Am. Chem. Soc.* **1960**, *82*, 96-98.
- (17) Keefer, L. K. "Progress toward clinical application of the nitric oxide-releasing diazeniumdiolates," *Annu. Rev. Pharmacol. Toxicol.* **2003**, *43*, 585-607.
- (18) Hrabie, J. A.; Saavedra, J. E.; Roller, P. P.; Southan, G. J.; Keefer, L. K. "Conversion of proteins to diazeniumdiolate-based nitric oxide donors," *Bioconjugate Chem.* **1999**, *10*, 838-842.
- (19) Jeh, H. S.; Lu, S.; George, S. C. "Encapsulation of PROLI/NO in biodegradable microparticles," *J. Microencapsulation* **2004**, *21*, 3-13.
- (20) Pulfer, S. K.; Ott, D.; Smith, D. J. "Incorporation of nitric oxide-releasing crosslinked polyethylenimine microspheres into vascular grafts," *J. Biomed. Mater. Res.* **1997**, *37*, 182-189.
- (21) Rothrock, A. R.; Donkers, R. L.; Schoenfisch, M. H. "Synthesis of nitric oxide-releasing gold nanoparticles," *J. Am. Chem. Soc.* **2005**, *127*, 9362-9363.
- (22) Stasko, N. A.; Schoenfisch, M. H. "Dendrimers as a scaffold for nitric oxide release," *J. Am. Chem. Soc.* **2006**, *128*, 8265-8271.

- (23) Lai, C.-Y.; Trewyn, B. G.; Jeftinija, D. M.; Jeftinija, K.; Xu, S.; Jeftinija, S.; Lin, V. S.-Y. "A mesoporous silica nanosphere-based carrier system with chemically removable CdS nanoparticle caps for stimuli-responsive controlled release of neurotransmitters and drug molecules," *J. Am. Chem. Soc.* **2003**, *125*, 4451-4459.
- (24) Munoz, B.; Ramila, A.; Perez-Pariente, J.; Diaz, I.; Vallet-Regi, M. "MCM-41 organic modification as drug delivery rate regulator," *Chem. Mater.* **2003**, *15*, 500-503.
- (25) Roy, I.; Ohulchanskyy, T. Y.; Bharali, D. J.; Pudavar, H. E.; Mistretta, R. A.; Kaur, N.; Prasad, P. N. "Optical tracking of organically modified silica nanoparticles as DNA carriers: a nonviral, nanomedicine approach for gene delivery," *Proc. Natl. Acad. Sci. U.S.A* **2005**, *102*, 279-284.
- (26) Trewyn, B. G.; Whitman, C. M.; Lin, V. S.-Y. "Morphological control of room-temperature ionic liquid templated mesoporous silica nanoparticles for controlled release of antibacterial agents," *Nano Lett.* **2004**, *4*, 2139-2143.
- (27) Yoshitake, H. "Highly-controlled synthesis of organic layers on mesoporous silica: their structure and application to toxic ion adsorptions," *New J. Chem.* **2005**, *29*, 1107-1117.
- (28) Kim, J. S.; Yoon, T. J.; Yu, K. N.; Kim, B. G.; Park, S. J.; Kim, H. W.; Lee, K. H.; Park, S. B.; Lee, J. K.; Cho, M. H. "Toxicity and tissue distribution of magnetic nanoparticles in mice," *Toxicol. Sci.* **2006**, *89*, 338-347.
- (29) Kneuer, C.; Sameti, M.; Haltner, E. G.; Schiestel, T.; Schirra, H.; Schmidt, H.; Lehr, C. M. "Silica nanoparticles modified with aminosilanes as carriers for plasmid DNA," *Int. J. Pharm.* **2000**, *196*, 257-261.
- (30) Sayari, A.; Hamoudi, S. "Periodic mesoporous silica-based organic-inorganic nanocomposite materials," *Chem. Mater.* **2001**, *13*, 3151-3168.
- (31) Stein, A.; Melde, B. J.; Schrodin, R. C. "Hybrid inorganic-organic mesoporous silicates-nanoscope reactors coming of age," *Adv. Mater.* **2000**, *12*, 1403-1419.
- (32) Anwender, R.; Palm, C.; Stelzer, J.; Groeger, O.; Engelhardt, G. "Silazane-silylation of mesoporous silicates: Towards tailor-made support materials," *Stud. Surf. Sci.*

- Catal.* **1998**, *117*, 135-142.
- (33) Zhang, H.; Annich, G. M.; Miskulin, J.; Stankiewicz, K.; Osterholzer, K.; Merz, S. I.; Bartlett, R. H.; Meyerhoff, M. E. "Nitric oxide-releasing fumed silica particles: Synthesis, characterization, and biomedical application," *J. Am. Chem. Soc.* **2003**, *125*, 5015-5024.
- (34) Hatton, B.; Landskron, K.; Whitnall, W.; Perovic, D.; Ozin, G. "Past, present, and future of periodic mesoporous organosilicates - The PMOs," *Acc. Chem. Res.* **2005**, *38*, 305-312.
- (35) Lin, H.-P.; Mou, C.-Y. "Structural and morphological control of cationic surfactant-templated mesoporous silica," *Acc. Chem. Res.* **2002**, *35*, 927-935.
- (36) Lim, M. H.; Stein, A. "Comparative studies of grafting and direct syntheses of inorganic-organic hybrid mesoporous materials," *Chem. Mater.* **1999**, *11*, 3285-3295.
- (37) Albert, K.; Bayer, E. "Characterization of bonded phases by solid-state NMR spectroscopy," *J. Chromatogr.* **1991**, *544*, 345-370.
- (38) Huh, S.; Wiench, J. W.; Yoo, J.-C.; Pruski, M.; Lin, V. S.-Y. "Organic functionalization and morphology control of mesoporous silicas via a co-condensation synthesis method," *Chem. Mater.* **2003**, *15*, 4247-4256.
- (39) Beckman, J. S.; Conger, K. A. "Direct measurement of dilute nitric oxide in solution with an ozone chemiluminescent detector," *Methods Companion Methods Enzymol.* **1995**, *7*, 35-39.
- (40) Brinker, C. J.; Scherer, G. *Sol-gel science: The physics and chemistry of sol-gel processing*; Academic Press: Boston, 1989.
- (41) Pagliaro, M.; Ciriminna, R.; Man, M. W. C.; Camestrini, S. "Better chemistry through ceramics: The physical bases of the outstanding chemistry of ORMOSIL," *J. Phys. Chem. B* **2006**, *110*, 1976-1988.
- (42) Wight, A. P.; Davis, M. E. "Design and preparation of organic-inorganic hybrid catalysts," *Chem. Rev.* **2002**, *102*, 3589-3614.

- (43) Melero, J. A.; van Grieken, R.; Morales, G. "Advances in the synthesis and catalytic applications of organosulfonic-functionalized mesostructured materials," *Chem. Rev.* **2006**, *106*, 3790-3812.
- (44) Liu, J.; Yang, Q.; Kapoor, M. P.; Setoyama, N.; Inagaki, S.; Yang, J.; Zhang, L. "Structural relation properties of hydrothermally stable functionalized mesoporous organosilicas and catalysis," *J. Phys. Chem. B* **2005**, *109*, 12250-12256.
- (45) Radu, D. R.; Lai, C.-Y.; Wiench, J. W.; Pruski, M.; Lin, V. S.-Y. "Gatekeeping layer effect: A poly(lactic acid)-coated mesoporous silica nanosphere-based fluorescence probe for detection of amino-containing neurotransmitters," *J. Am. Chem. Soc.* **2004**, *126*, 1640-1641.
- (46) Bruch, M. D.; Fatunmbi, H. O. "Nuclear magnetic resonance analysis of silica gel surfaces modified with mixed, amine-containing ligands," *J. Chromatogr. A* **2003**, *1021*, 61-70.
- (47) McKittrick, M. W.; Jones, C. W. "Toward single-site functional materials-preparation of amine-functionalized surfaces exhibiting site-isolated behavior," *Chem. Mater.* **2003**, *15*, 1132-1139.
- (48) Kumar, C. S. S. R.; Hormes, J.; Leuschner, C. *Nanofabrication towards biomedical applications: Techniques, tools, applications, and impact*; Wiley-VCH: Weinheim, German, 2005.
- (49) Chithrani, B. D.; Ghazani, A. A.; Chen, W. C. W. "Determining the size and shape dependence of gold nanoparticle uptake into mammalian cells," *Nano Lett.* **2006**, *6*, 662-668.
- (50) Schwartzberg, A. M.; Olson, T. Y.; Talley, C. E.; Zhang, J. Z. "Synthesis, characterization, and tunable optical properties of hollow gold nanospheres," *J. Phys. Chem. B* **2006**, *110*, 19935-19944.

Chapter 5:

Nitric Oxide-Releasing Silica Nanoparticles: Synthesis, Characterization, and Efficacy Against Ovarian Cancer Cells

5.1 Introduction

Nitric oxide (NO), a free radical bioregulator endogenously synthesized in the body, impacts multiple stages of tumor development, spanning cytostatic processes, cellular transformation, formation of neoplastic lesions, and regulation of various aspects of tumor biology.¹⁻⁴ Some consequences of NO production demonstrate that NO has tumoricidal effects, including inhibition of several classes of enzymes and iron metabolism proteins, cell apoptosis, and alternation of metastasis.⁴⁻⁷ Studies have shown that reactive nitrogen oxide species (RNOS; e.g., NO₂, NO₂⁻, ONOO⁻, and N₂O₃) derived from NO affect the expression and activity of proteins critical to the cell cycle and apoptosis.^{4,8,9} Additional properties of NO that may be beneficial in the treatment of cancer include its roles in the anti-pathogenic and tumoricidal response of the immune system.^{4,10} In seminal experiments involving co-cultures of macrophages and lymphoma cells, Hibbs *et al.*¹¹ and Stuehr *et al.*¹² reported that NO generated from macrophages inhibited cellular respiration in cancer cells. Subsequent reports demonstrated that NO derived from macrophages, natural killer cells, and endothelial cells is tumoricidal against many types of tumors.¹³⁻¹⁵

To harness the tumoricidal potency of NO, a variety of small molecule NO donors (e.g., NO-metal complexes, nitrosothiols, organic nitrites/nitrates, and diazeniumdiolates) have

been developed and evaluated with respect to NO storage capacity and efficacy against tumor cells (Table 5.1).¹⁶⁻²⁷ Of these, 1-amino-substituted diazen-1-ium-1,2-diolates (or simply *N*-diazoniumdiolates) are particularly attractive due to their ability to generate NO spontaneously under biological conditions.^{19-21,28} Several small molecule *N*-diazoniumdiolate species have been synthesized using a range of nucleophilic residues that encompass simple primary/secondary amines, polyamines, and secondary amino acids.^{29,30} While stable under ambient conditions, *N*-diazoniumdiolates decompose spontaneously in aqueous media to generate NO at rates dependent on pH, temperature, and/or their structures.²⁹ Although small molecule NO donors have shown some efficacy against tumor cells, their usefulness as anti-cancer agents remains hindered by difficulties in controlling their NO release properties (e.g., quantities and delivery rates) and imparting cell- or tissue-specific targeting ability.

Based on the unique size-dependent physical and chemical properties, nanoparticles have the potential to revolutionize the field of medicine.^{31,32} Nanotechnology has already been employed for a number of biomedical applications including drug and gene delivery,³³ fluorescent biological labels,³⁴ pathogen and protein detectors,³⁵ DNA structure probes,³⁶ and MRI contrast agents.³⁷ Considerable effort has been expended towards developing NO storage/delivery systems via macromolecular frameworks that can store large quantities of NO, impart cell- or tissue-specific targeting, and modulate NO release kinetics.³⁸⁻⁴² Several NO donor micro- and nanocomposite materials have been developed using polyethyleneimine microspheres,³⁸ albumin conjugates,³⁹ poly-lactic-co-glycolic acid copolymers,⁴⁰ gold clusters,⁴¹ and dendrimers.⁴²

Mesoporous silica nanoparticles, ceramic materials prepared from silicon dioxide, have been explored as carrier systems for controlled delivery of drugs, biocides, genes, and

Table 5.1. Representative examples of the tumoricidal effect of previously reported small molecule NO donors against a variety of cancer cell lines *in vitro*

Class of NO donor	Name of NO donor	Cancer type	Effect	Ref.
NO-metal complex	SNP ^a	Prostate (PC-3)	anti-proliferative and apoptotic effects through arrest of G1 phase of cell cycle	18
Diazeniumdiolate	DETA/N ₂ O ₂ ^b	Breast (MDA-MB-231)	induced cytostasis, arrested in the G ₁ phase of cell cycle	19
	PABA/N ₂ O ₂ ^c	Ovarian (A2780, OVCAR-3) Melanoma (LOXIMVI) Colon (HCT-15)	<i>in vitro/in vivo</i> anticancer activity	20
	MAHMA/N ₂ O ₂ ^d	Colon (HT-29)	anti-proliferative through inhibition of ornithine decarboxylase activity	21
Nitrosothiol	S-Nitrosocaptopril (CapNO)	Prostate (PC-3, CaP)	enhanced the effect of Taxol induced cytotoxicity	22
	SNAP ^e	Oral (CAL27, HSC-2)	cytotoxicity against oral cancer cells <i>in vitro</i>	23
	Glyconitrosothiol (fructose-1-SNAP)	Prostate (DU-145)	cytotoxicity against prostate cancer cells <i>in vitro</i>	24
NO-NSAID ^f	NO-donor aspirin (NO-ASA)	Lung, Colon, Breast, Skin	inhibition of cell proliferation and induced apoptosis	25
	NCX-4016 ^g	Ovarian (CS, CR)	enhanced cytotoxic effect of cisplatin against cisplatin-resistant cells <i>in vitro</i>	26
Organic nitrate	Glyceryl trinitrate (GTN)	Breast (MCF-7)	cytotoxicity against cancer cells <i>in vitro</i>	27

^aSodium nitroprusside. ^b(Z)-1-[N-(2-aminoethyl)-N-(2-ammonioethyl)amino]diazen-1-ium-1,2-diolate.

^cO²-[2,4-dinitro-5-(4-carboxylatophenyl)amino]phenyl 1-(N,N-dimethylamino)diazen-1-ium-1,2-diolate.

^d(Z)-1-{N-methyl-N-[6-(N-methylammoniohexyl)amino]}diazen-1-ium-1,2-diolate. ^eS-Nitroso-N-acetylpenicillamine.

^fConjugates of NO donor and non-steroidal anti-inflammatory drug. ^g2-(Acetyloxy)-benzoic acid 3-(nitrooxymethyl)phenyl ester.

proteins.⁴³⁻⁴⁷ The drug delivery potential of silica has received a great deal of attention because of its non-toxic nature,⁴⁸ and tunable physical and chemical properties (e.g., ability to tune the size and mesoporous structure).^{49,50} The synthesis of *hybrid* inorganic-organic silica nanospheres modified with reactive functional groups (e.g., amines, thiols, carboxylates, and halides) has been widely reported.^{49,50} Such chemistry allows for further functionalization with drug molecules, for example. Zhang *et al.* previously reported the synthesis of NO-releasing fumed silica (amorphous particles of $d = 0.2 - 0.3 \mu\text{m}$) by grafting the silica surface with amine-functionalized silylation reagents, followed by *N*-diazoniumdiolate formation.⁵¹ The silica particles prepared via this surface-grafting method released NO up to $0.56 \mu\text{mol}\cdot\text{mg}^{-1}$. More recently, Shin *et al.* demonstrated a new synthetic strategy for preparing NO-releasing silica prepared via a “one-pot” co-condensation of tetraalkoxysilane and aminoalkoxysilane. The amine functional groups in the silica were converted to *N*-diazoniumdiolate NO donors via exposure to high pressures of NO (5 atm). As described in Chapter 4, control over both the structure and concentration of the silane precursors allowed for the preparation of NO donor silica particles of widely varying sizes ($d = 20 - 500 \text{ nm}$) and higher NO payloads (up to $1.8 \mu\text{mol}\cdot\text{mg}^{-1}$).

Although the total NO release levels of the silica nanoparticles prepared via a “one-pot” approach were significantly greater than small molecule and surface-grafted silica NO donor counterparts,^{30,51} the aminoalkoxysilane content used to prepare the nanoparticles was limited to <20 mol% due to particle aggregation at higher aminoalkoxysilane concentrations, attributed to interactions between the amines and adjacent silanols and/or other amines via hydrogen bonding.^{52,53}

To increase the concentration of aminoalkoxysilanes and bolster NO storage capability, I investigated an alternative strategy for synthesizing the silica nanoparticles. In contrast to synthesizing the silica nanoparticles prior to “charging” with NO (necessary to form *N*-diazoniumdiolate NO donors, hereafter referred to as post-synthesis charging or simply “post-charging”), the *N*-diazoniumdiolate moieties were synthesized prior to preparing the silica nanocomposites (“pre-charging”) (Figure 5.1). Briefly, an appropriate amount of aminoalkoxysilane was dissolved in a mixture of EtOH, MeOH, and NaOMe. The stirring solution was pressured with NO (5 atm, 3 d) to allow the formation of *N*-diazoniumdiolate-modified amino-alkoxysilanes. The nanoparticles were then synthesized by mixing TEOS with different ratios of the *N*-diazoniumdiolate-modified aminoalkoxysilane in the presence of an ammonia catalyst. The pre-charging strategy should facilitate greater access of NaOMe and NO to the amine precursors without aggregation as the hydrogen-bonding interactions of amine sites during particle formation are avoided. The cytotoxicity of such NO donor vehicles against human ovarian surface epithelial immortalized and cancer cell lines is also presented.

5.2 Experimental Section

5.2.1 Reagents and Materials

Tetraethoxysilane (TEOS), methylaminopropyltrimethoxysilane (MAP3), pyrrole, and sodium methoxide (NaOMe) were purchased from Fluka (Buchs, Switzerland). (Aminoethylaminomethyl)phenethyltrimethoxysilane (AEMP3), *N*-(6-aminoethyl)aminopropyltrimethoxysilane (AHAP3), *N*-(2-aminoethyl)-3-aminopropyltrimethoxysilane (AEAP3), aminopropyltrimethoxysilane (APTMS), *N*-[3-(trimethoxysilyl)propyl]diethylenetriamine (DET3), *N*-

phenylaminopropyltrimethoxysilane (PAP3), n-butylaminopropyltrimethoxysilane (nBAP3), cyclohexylaminopropyltrimethoxysilane (cHAP3), 3-(*N*-allylamino)propyltrimethoxysilane (AAP3), *N*-ethylaminoisobutyltrimethoxysilane (EAI3), and t-butylaminopropyltrimethoxysilane (tBAP3) were purchased from Gelest (Tullytown, PA). Fluorescein isothiocyanate (FITC), tetramethylrhodamine methyl ester (TMRM), dimethyl sulfoxide (DMSO), 3-(4,5-dimethylthiazol-2-yl)-2,5-diphenyltetrazolium bromide (MTT), *N*-2-hydroxyethylpiperazine-*N'*-2-ethanesulfonic acid (HEPES), *N,N*-dimethylformamide (DMF), Roswell Park Memorial Institute (RPMI) 1640 medium, and insulin were purchased from Sigma (St. Louis, MO). Fetal bovine serum (FBS) was purchased from Hyclone (Logan, UT). Methanol (MeOH), ethanol (EtOH), 2-propanol (PrOH), 1-butanol (BuOH), toluene, and ammonia solution (NH₄OH, 30 wt% in water) were purchased from Fisher Scientific (Fair Lawn, NJ). Nitric oxide (NO), carbon dioxide (CO₂, 5%), argon (Ar), and nitrogen (N₂) gases were obtained from AGA Gas (Maumee, OH) or National Welders Supply (Raleigh, NC). Other solvents and chemicals were analytical-reagent grade and used as received. A Millipore Milli-Q UV Gradient A10 System (Bedford, MA) was used to purify distilled water to a final resistivity of 18.2 MΩ·cm and a total organic content of ≤6 ppb.

5.2.2 Synthesis and Characterization of *N*-Diazeniumdiolate-Modified Aminoalkoxysilanes

An aminoalkoxysilane solution was prepared by dissolving 10.3 mmol of an aminoalkoxysilane precursor (e.g., AHAP3, MAP3, nBAP3, etc.) in 24 mL of EtOH and 6 mL of MeOH in the presence of NaOMe (10.3 mmol, an equimolar amount corresponding to the secondary amine content of silane structures). The solution was then placed into 10-mL vials equipped with a stir bar. The vials were placed in a Parr bottle, connected to an in-house NO reactor, and flushed with Ar six times to remove oxygen in the solution. The reaction bottle

was charged with NO to 5 atm for 3 d under stirring. Prior to removing the modified silane sample, unreacted, physically adsorbed NO was purged from the chamber with Ar.

Nitric oxide release profiles of the *N*-diazoniumdiolate-modified aminoalkoxysilane were measured in deoxygenated phosphate-buffered saline (PBS, 0.01 M) at pH 7.4 and 37 °C using a Sievers NOA 280i chemiluminescence nitric oxide analyzer (Boulder, CO).^{ref} Nitric oxide released from the silane precursor was transported to the analyzer by a stream of N₂ (70 mL·min⁻¹) passed through the reaction cell. The instrument was calibrated with air passed through a zero filter (0 ppm NO) and 24.1 ppm of NO standard gas (balance N₂, purchased from AGA Gas).

5.2.3 Synthesis of Nitric Oxide Donor Silica Nanoparticles

The silane solutions were prepared by mixing 1.4 mmol (310 μL) of TEOS with different contents (0.16 – 4.17 mmol corresponding to 10 – 75 mol%, balance TEOS) of *N*-diazoniumdiolated AEAP3, AHAP3 or MAP3 for 5 min. The silane solution was then added into 22 mL of solvent [i.e., 100% EtOH, 50/50% (v/v) EtOH/PrOH, or 50/50% (v/v) EtOH/BuOH] and 6 mL of ammonia (30 wt% in water), and vigorously stirred for 30 min at 4 °C. (The reaction was performed at low temperatures of 4 °C to minimize the thermal decomposition of *N*-diazoniumdiolates.) The white precipitate was collected by centrifugation (5000 rpm, 5 min), washed with EtOH copiously, dried under ambient conditions for 1 h, and stored in a sealed container at –20 °C until used.

5.2.4 Characterization of Functionalized Silica Nanoparticles

For atomic force microscopy (AFM) analysis, the silica particles were suspended in toluene, deposited on a freshly cleaved mica surface (SPI; West Chester, PA), and dried

under ambient conditions for 3 h. Contact mode AFM images were obtained in air using a Molecular Force Probe 3D Atomic Force Microscope (Asylum Research; Santa Barbara, CA) controlled with MFP-3D software running under Igor Pro (Wavemetrics; Lake Oswego, OR). Triangular silicon nitride cantilevers with a nominal spring constant of $0.12 \text{ N}\cdot\text{m}^{-1}$ and resonance frequency of 20 kHz (Veeco; Santa Barbara, CA) were used to acquire height/topography images at a scan rate of 0.5 Hz.

Chemiluminescence data for the NO-releasing silica particles were represented in two graphical forms or plots: (1) chemiluminescence response in ppb NO/mg silica vs. time; and, (2) the total amount of NO release ($t[\text{NO}]$) vs. time. The maximum flux of NO release ($[\text{NO}]_m$) and the time required to reach that maximum (t_m) were obtained from plot 1. The half-life ($t_{1/2}$) of NO release as well as the $t[\text{NO}]$ ($\mu\text{mol NO/mg}$) were determined from plot 2.

5.2.5 Cell Culture

Immortalized human ovarian surface epithelial cells (T29) and carcinoma cells (A2780 and OVCAR-3) were obtained from Dr. Gordon Mills (M. D. Anderson Cancer Center; Houston, TX) and American Type Culture Collection (ATCC; Manassas, VA), respectively. Cells were cultured in RPMI 1640 medium supplemented with 10% FBS and $10 \mu\text{g}\cdot\text{mL}^{-1}$ insulin at $37 \text{ }^\circ\text{C}$ in a humidified atmosphere containing 5% CO_2 .

5.2.6 Cell Viability Assay

The MTT cell viability assay was employed to determine the relative sensitivities of T29, A2780, and OVCAR-3 cell lines to NO donor small molecule (i.e., PYRRO/ N_2O_2) and silica nanoparticles (i.e., 45 mol% AHAP3 and 75 mol% MAP3). Viable cells were seeded in 6 replicates at $1 - 5 \times 10^3$ cells per well in 96-well microtiter plates (polystyrene; BD

Biosciences, Franklin Lakes, NJ), incubated overnight, and exposed to different concentrations (from 0.013 to 1 mg·mL⁻¹) of NO-releasing and control nanoparticle solutions at 37 °C and 5% CO₂ for 48 h. The NO-releasing medium was then removed and replaced by MTT solution (1 mg·mL⁻¹ in PBS, pH 7.4), upon which the cells were subsequently incubated for an additional 4 h at 37°C. Following removal of the MTT, 100 µL of DMSO was added, and the absorption of the solution was measured at 560 nm using a SpectraMaxPlus 2.01 microplate reader (Molecular Devices; Sunnyvale, CA). The absorption of the MTT/DMSO solution was used as a zero reference.

5.2.7 Cellular Uptake

The NO-releasing silica nanoparticles were fluorescently labeled via the “one-pot” co-condensation of three silane precursors including FITC-modified APTMS, *N*-diazoniumdiolated MAP3, and TEOS. First, FITC-APTMS conjugates were synthesized by dissolving 16 µmol of FITC and 0.64 mmol of APTMS in 500 µL of DMF, and stirring in the dark for 24 h (Figure 5.2). A silane solution was then prepared by mixing 1.4 mmol of TEOS with 4.17 mmol of *N*-diazoniumdiolated MAP3 (75 mol%, balance TEOS), and 0.32 mmol of FITC-APTMS conjugate for 5 min. The silane solution was combined with 22 mL of EtOH and 6 mL of ammonia (30 wt% in water), and vigorously stirred for 30 min at 4 °C. The yellow precipitate was collected by aforementioned procedures including centrifugation, washing, and drying. The resulting multifunctionalized silica nanoparticles (FITC-labeled and NO donor-modified 75 mol% MAP3) were stored in a sealed container at -20 °C in the dark until used.

Human ovarian epithelial cancer cells (A2780) were plated to ~20% confluency on glass bottom microscopy plates and incubated overnight at 37 °C and 5% CO₂. Prior to

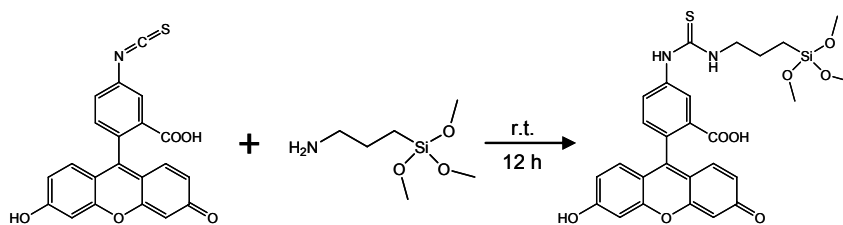


Figure 5.2. Synthesis of fluorescein conjugated 3-aminopropyltrimethoxysilane (APTMS).

imaging, the incubation medium was discarded and replaced with Krebs-Henseleit imaging buffer (10 mM HEPES, pH 7.4) containing 100 nM of TMRM dye to selectively stain the mitochondria of the A2780 cancer cells (30 min incubation). A 100- μ L aliquot of FITC-labeled NO-releasing MAP3 silica nanoparticles dissolved in the imaging buffer was added directly to the cells on the stage of the microscope, yielding a nanoparticle concentration of 100 μ g·mL⁻¹. A Zeiss Laser Scanning Microscope (LSM 510; Germany) was used to perform the fluorescence measurements. The red fluorescence of TMRM (helium-neon laser excitation at 543 nm) and the green fluorescence of the FITC-labeled silica nanoparticles (argon laser excitation at 488 nm) were monitored at 650 and 520 nm, respectively. Confocal images were collected for 1 h at 5 min intervals to monitor the cellular uptake of the green fluorescent nanoparticles.

5.3 Results and Discussion

5.3.1 *N*-Diazeniumdiolate-Modified Aminoalkoxysilanes

Prior to preparing silica nanoparticles, several primary/secondary and secondary amine-based alkoxy silanes were converted to *N*-diazeniumdiolate NO donors via exposure to high pressures of NO (5 atm, 3 d). These *N*-diazeniumdiolated aminoalkoxysilanes were evaluated as potential NO donor moieties in terms of total NO concentration ($t[\text{NO}]$), half-life of NO release ($t_{1/2}$), and amine to *N*-diazeniumdiolate conversion efficiency (%Conv) (Table 5.2). Selected example structures of secondary amine-based alkoxy silane precursors are shown in Figure 5.3 (for primary/secondary amine-based alkoxy silane structures, see Figure 1.8). Both $t[\text{NO}]$ and $t_{1/2}$ were significantly affected by the type and structure of aminoalkoxysilane precursors used. Of note, aminoalkoxysilanes with both primary and secondary amine sites usually exhibited longer $t_{1/2}$ than only secondary amine-based alkoxy silanes (i.e., 69 to 264

Table 5.2. Total NO concentration ($t[\text{NO}]$), half-life of NO release ($t_{1/2}$), and amine to *N*-diazoniumdiolate conversion efficiency (%Conv) of *N*-diazoniumdiolate-modified primary/secondary and secondary amine-based alkoxy-silanes

Aminoalkoxysilane		$t[\text{NO}]$	$t[\text{NO}]$	$t_{1/2}$ (min)	%Conv
Class	Type ^a	($\mu\text{mol}\cdot\text{mg}^{-1}$)	($\mu\text{mol}\cdot\mu\text{mol}^{-1}$)		
Primary/ secondary	AEAP3	6.61	1.47	114	74
	AHAP3	7.27	1.99	9	99
	AEMP3	0.75	0.23	264	12
	DET3	2.95	0.79	69	20
Secondary	PAP3	0.50	0.14	72	7
	MAP3	10.3	1.98	3	99
	nBAP3	8.02	1.89	7	95
	tBAP3	1.93	0.31	4	16
	cHAP3	1.67	0.44	5	22
	EAI3	6.16	1.37	10	69
	AAP3	4.70	1.05	17	53

^aAEAP3, *N*-(2-aminoethyl)-3-aminopropyltrimethoxysilane; AHAP3, *N*-(6-amino-hexyl)aminopropyltrimethoxysilane (AHAP3); AEMP3, (aminoethylaminomethyl)-phenethyltrimethoxysilane (AEMP3); DET3, *N*-[3-(trimethoxysilyl)propyl]diethylene-triamine; PAP3, *N*-phenylaminopropyltrimethoxysilane; MAP3, methylaminopropyltri-methoxysilane; nBAP3, n-butylaminopropyltrimethoxysilane; tBAP3, t-butylamino-propyltrimethoxysilane; cHAP3, cyclohexylaminopropyltrimethoxysilane; EAI3, *N*-ethylaminoisobutyltrimethoxysilane; and, AAP3, 3-(*N*-allylamino)propyltrimethoxy-silane (AAP3).

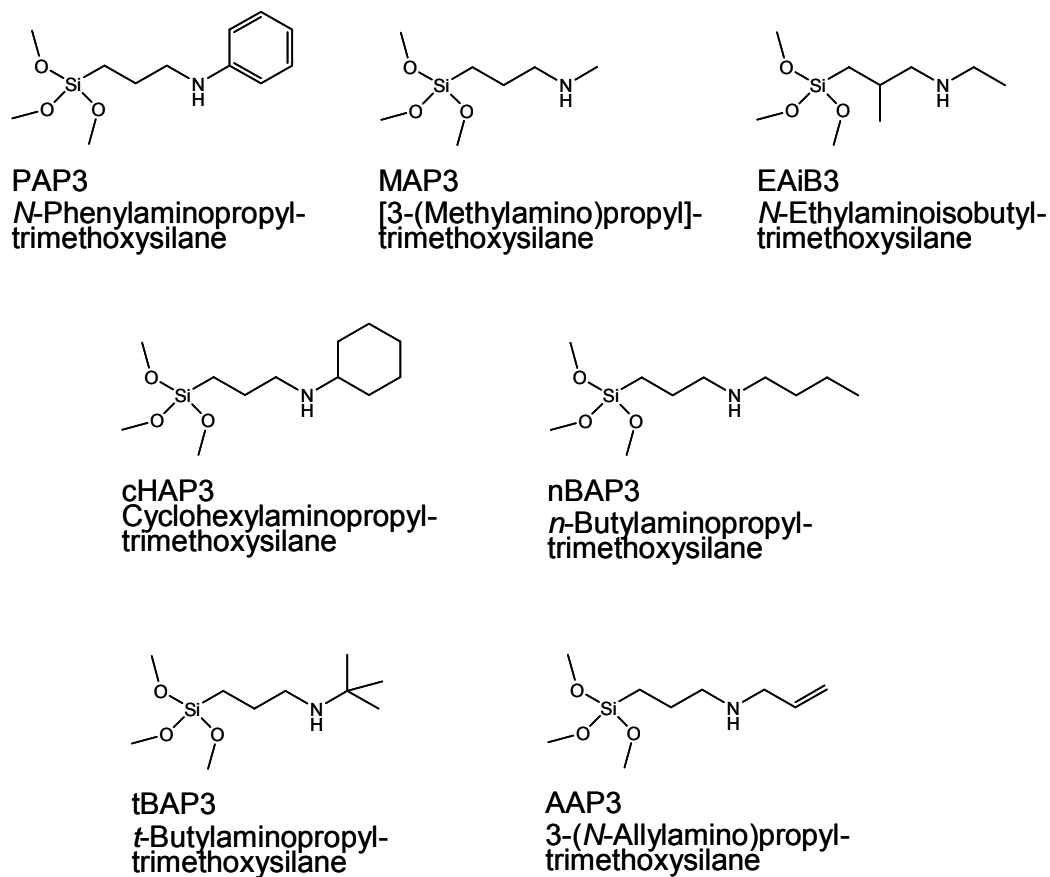


Figure 5.3. Example structures of secondary amine-based alkoxy-silanes studied.

min vs. 3 to 72 min, respectively). The NO release kinetics of primary/secondary amine-based alkoxysilanes are attributed to the stabilizing effect of *N*-diazoniumdiolates by the adjacent primary amines, forming a $N(O)N-O\cdots H-N$ structure.^{29,54} The $t_{1/2}$ of AHAP3 is exceptionally short (i.e., 9 min) because the primary amine is too far away (C6) from the *N*-diazoniumdiolate to interact favorably.

The formation of *N*-diazoniumdiolates on the secondary amine sites (%Conv) was also drastically influenced by the structure of the alkyl terminus attached to nitrogen. While *n*-butyl-terminated aminopropyltrimethoxysilane (*n*-BAP3) possessed the high yield of *N*-diazoniumdiolate formation (95%), *t*-butyl-terminated one (*t*-BAP3) exhibited a decreased conversion efficiency (16%) (Table 5.2 and Figure 5.3). The increased steric hindrance around the secondary amine by the *t*-butyl group appears to drastically influence *N*-diazoniumdiolate formation. *N*-Diazoniumdiolate-modified AEAP3, AHAP3, and MAP3 were thus selected as effective NO donors for pursuing subsequent nanoparticle synthesis due to their favorable NO release properties, (e.g., $t[NO]$, %Conv, and/or $t_{1/2}$).

5.3.2 Nitric Oxide Release Properties of Silica Nanoparticles

The NO release characteristics of *N*-diazoniumdiolate-modified silica nanoparticles prepared via the pre-charging approaches are summarized in Table 5.3. The NO release profiles of two example silica nanocomposites (45 and 75 mol% of AHAP3 and MAP3, respectively) are shown in Figure 5.4. Both the total NO released ($t[NO]$) and the maximum amount of NO released ($[NO]_m$) were increased considerably compared to NO-releasing silica prepared by the post-charging method at identical aminoalkoxysilane concentrations. For example, $t[NO]$ and $[NO]_m$ for 17 mol% AEAP3 were increased from 0.6 to 0.8 $\mu\text{mol}\cdot\text{mg}^{-1}$ and 140 to 1200 $\text{ppb}\cdot\text{mg}^{-1}$ for post- and pre-charging systems, respectively. We

Table 5.3. NO release properties of *N*-diazoniumdiolate-modified silica nanoparticles with different amine ligands and contents prepared via post- and pre-charging strategies^a

Synthetic strategy	Aminoalkoxysilane		t[NO] ($\mu\text{mol}\cdot\text{mg}^{-1}$)	$t_{1/2}$ (min)	[NO] _m (ppb·mg ⁻¹)	t_m (min)
	Type ^b	mol% ^c				
Post-charging ^d	AEAP3	17	0.6	204	140	126
	AHAP3	10	0.4	54	370	21
Pre-charging	AEAP3	17	0.8	66	1200	7
		25	1.2	90	1600	8
		35	1.5	108	1400	8
		45	1.7	132	1300	8
	AHAP3	10	0.6	18	3400	3
		25	1.6	18	9500	3
		35	2.6	24	14500	5
		45	3.8	18	21700	8
	MAP3	45	1.6	6	33000	3
		55	2.9	6	60000	3
		65	4.3	6	73000	3
		75	7.4	6	103000	3

^aValues were measured in phosphate-buffered saline (PBS) at pH 7.4 and 37 °C. ^bAEAP3, *N*-(2-aminoethyl)-3-aminopropyltrimethoxysilane; AHAP3, *N*-(6-aminoethyl)aminopropyltrimethoxysilane; and, MAP3, methylaminopropyltrimethoxysilane. ^cBalance tetraethoxysilane (TEOS). ^dData from ref. 52.

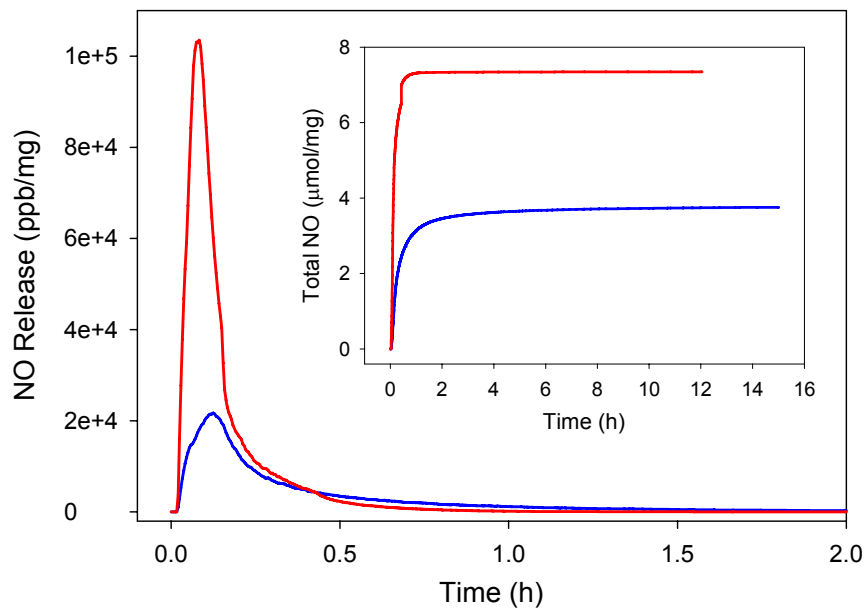


Figure 5.4. NO release profiles of 45 mol% of AHAP3 (a) and 77 mol% of MAP3 (b) silica nanoparticles. Insert: total NO concentration.

attribute the elevated quantities of NO release is attributed to a more homogeneous distribution of the diazeniumdiolate NO donors throughout the silica particle, as depicted in Figure 5.1B. More importantly, the pre-charging approach enabled us to increase the AEAP3 or AHAP3 content up to 45 mol% without aggregation, resulting in concomitant increases in $t[\text{NO}]$ and $[\text{NO}]_m$.

Methylaminopropyltrimethoxysilane (MAP3), an aminoalkoxysilane containing a methyl-terminated secondary amine, was also used to prepare NO-releasing silica nanoparticles. By removing primary amines and the potential for hydrogen-bonding interactions, we were able to synthesize silica particles with MAP3 aminoalkoxysilane concentrations up to 75 mol% with corresponding diameter ranging from 90 – 600 nm depending on the solvent⁵⁵ employed during synthesis. The advantage of MAP3 is that it contains no primary amines. This attribute with respect to cytotoxicity is discussed in greater detail below. As expected, increasing the mol% of MAP3 from 10 to 75 mol% led to a corresponding increase in total NO release (e.g., $t[\text{NO}]$ increased from 1.6 to 7.4 $\mu\text{mol}\cdot\text{mg}^{-1}$). In addition, the initial NO release of MAP3-based silica nanoparticles was characterized by a large burst (33000 – 103000 ppb $\cdot\text{mg}^{-1}$) and ~ 5 min of $t_{1/2}$.

The rapid kinetics and burst of NO from MAP3 silica represent significant strides toward developing a nanoparticle capable of releasing large amount of NO in a small volume. The pursuit of nanoparticles that release NO at different rates to study NO's effect on tumor cell toxicity represents a potential application of this work. The synthesis of NO-releasing nanoparticles thus represents a new NO delivery system that bridges the gap between small molecule *N*-diazeniumdiolates and NO-releasing dendrimers. Indeed, control over both the structure and concentration of the aminoalkoxysilane ligand and the synthetic approach used

to prepare the silica allows for the preparation of NO release scaffolds of widely varying size and NO release properties. The distinct advantages of the NO-releasing silica-based particles over dendrimers include simple one-pot synthesis and straightforward material purification and tunable size control, and low-cost.

5.3.3 *In Vitro Ovarian Cancer Cell Viability Studies*

Ovarian cancer is the leading cause of death from gynecological malignancies in the United States.⁵⁶ The high mortality rate is attributed to lack of early diagnosis and difficulties associated with treatments. Platinum-derived chemotherapy (e.g., cisplatin and carboplatin) is currently the primary ovarian cancer treatment.^{26,57,58} However, the clinical response of advanced-stage ovarian cancer to platinum-based therapy is only 40 – 60%.⁵⁷ The primary factor that limits the success of chemotherapy in the treatment of ovarian cancer is the acquired clinical resistance to chemotherapeutic agents such as cisplatin.^{57,58} Therefore, the development of novel molecular-targeted strategies for the treatment of ovarian cancer is clearly warranted.

To study the tumoricidal potential of NO donor-modified silica nanoparticles, the cytotoxicity of control and NO-releasing silica on immortalized, untransformed (T29) and cancer (A2780 and OVCAR-3) human ovarian surface epithelial (HOSE) cells was evaluated. Normal HOSE cells, the precursor cell for the majority of ovarian carcinoma cells, have only limited proliferative capacity, and are not readily available for *in vitro* testing.⁵⁹ Primary cultures of normal HOSE cells were thus immortalized by ectopic expression of the catalytic subunit of telomerase (hTERT) and the Simian virus (SV40) small and large T antigens.⁶⁰ The immortalized HOSE cells were then sensitive to tumorigenic transformation by the Ras oncogene.

The MTT cell proliferation assay was employed to determine the relative sensitivities of HOSE cells to the AHAP3-derived nanoparticles. As shown in Figure 5.5, A2780 ovarian epithelial tumor cells were treated with varying doses of control and NO-releasing AHAP3 silica (13 – 1000 $\mu\text{g}\cdot\text{mL}^{-1}$) for 48 h. The viability of the A2780 cells was reduced upon exposure to NO-releasing AHAP3 silica at low doses and the proliferation of A2780 cells was almost completely inhibited by NO-releasing AHAP3 silica at a dose of 500 $\mu\text{g}\cdot\text{mL}^{-1}$ [minimum inhibitory concentration (MIC) at <5% survival; corresponding to 0.75 mM of NO]. In addition, the IC_{50} dose (50% inhibitory concentration) of NO donor AHAP3 silica was 20 $\mu\text{g}\cdot\text{mL}^{-1}$ (30 μM NO). Notably, the inhibitory concentrations of the NO-releasing silica proved to be significantly lower than those of small molecule NO donors tested (e.g., MIC and IC_{50} for PYRRO/ N_2O_2 were 4.5 and 1.8 mM NO, respectively) (Figure 5.6).

Control silica nanoparticles also exhibited cytotoxic effects against the tumor cells (IC_{50} = 120 $\mu\text{g}\cdot\text{mL}^{-1}$), albeit less than that of their NO-releasing counterparts. Nonetheless, the undesirable cytotoxicity of control vehicles may be the result of free primary amines on the surface of the silica structures. Indeed, such amines have reported cytotoxic properties.⁶¹ To reduce the cytotoxicity of control and NO-releasing nanoparticles with primary amines, the MAP3 aminoalkoxysilane (containing only secondary amines) was employed to create more biocompatible vehicles. As expected, the cytotoxicity of MAP3 controls against the immortalized (T29) and tumor (A2780) cells was low, whereas NO-releasing MAP3 silica exhibited significant cytotoxicity against both untransformed T29 and A2780 tumor cells (Figure 5.7). OVCAR-3 ovarian adenocarcinoma cells also showed similar cytotoxic trends with increasing concentrations of NO-releasing silica nanoparticles (data not shown).

To investigate whether nanoparticle size affects cytotoxicity, two silica nanoparticles

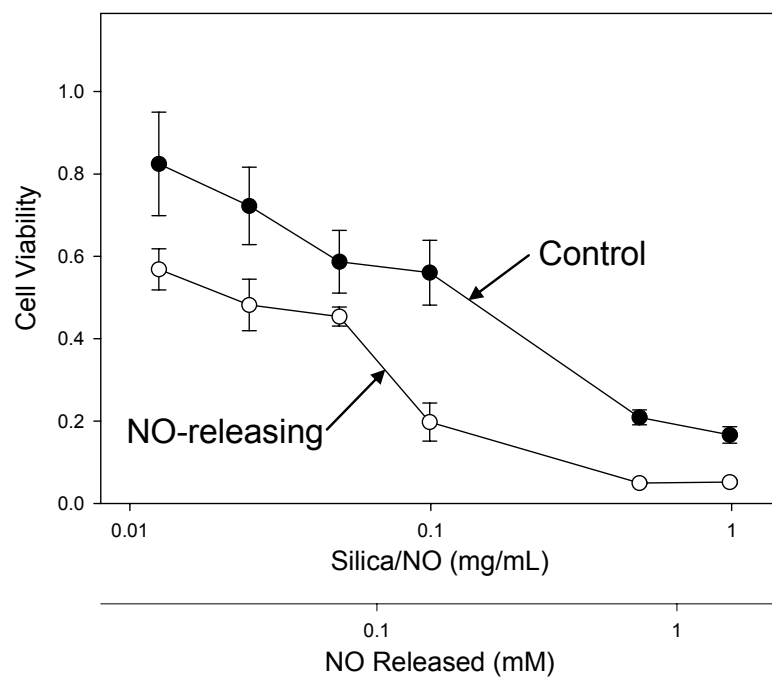
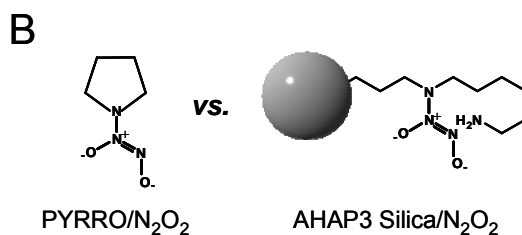
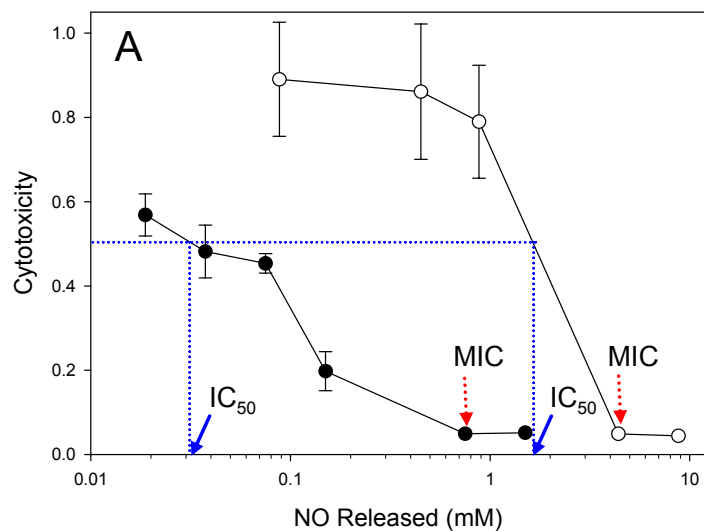


Figure 5.5. Cytotoxicity of control and NO-releasing 45 mol% AHAP3 silica on A2780 ovarian epithelial tumor cells.



C

	MIC* (mM NO)	IC ₅₀ ** (mM NO)
PYRRO/N ₂ O ₂	4.5	1.8
SNP/N ₂ O ₂ [#]	0.75	0.03

*MIC = minimum inhibitory concentration

**IC₅₀ = 50% inhibitory concentration

[#]N-Diazeniumdiolate-modified 45 mol% AHAP3 silica nanoparticles

Figure 5.6. Cytotoxicity comparison between small molecule (PYRRO/N₂O₂) and macromolecule (45 mol% AHAP3 silica/N₂O₂) NO donors against human ovarian surface epithelial cancer cells (A2780).

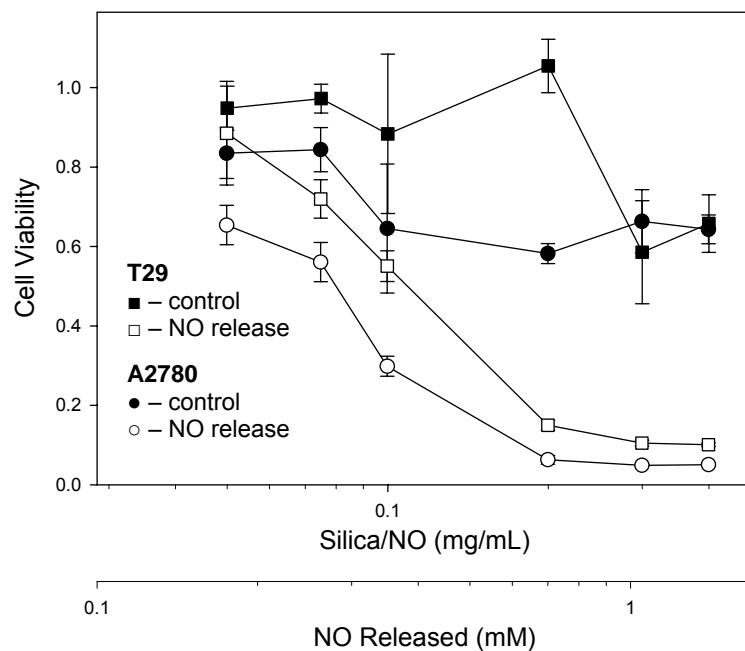


Figure 5.7. Cytotoxicity of control and NO-releasing MAP3 silica nanoparticles on ovarian epithelial normal (T29, immortalized) and tumor (A2780) cell lines.

(75 mol% MAP3, balance TEOS) of different particle sizes were synthesized (small 90 ± 10 nm s-MAP3 and large 350 ± 50 nm L-MAP3) (Figure 5.8). Indeed, silica diameter is easily tunable by varying the solvent (i.e., alcohols) system during the sol–gel process.⁵⁵ Increasing the MW of the alcohol used during synthesis led to a corresponding increase in the particle size [e.g., 100% (v/v) ethanol and 50/50% (v/v) ethanol/butanol mixture were used to prepare s-MAP3 and L-MAP3, respectively]. Cell viability was determined by incubating untransformed T29 and A2780 tumor cells with control MAP3 particles (80 nm), and NO-releasing s-MAP3 or L-MAP3 ($400 \mu\text{g}\cdot\text{mL}^{-1}$, 48 h) (Figure 5.9). Notably, the small diameter NO-releasing silica (s-MAP3) proved cytotoxic against both immortalized (T29) and cancer (A2780) cells (12 ± 1.1 and $5 \pm 0.2\%$ survival, respectively). In contrast, the larger NO-releasing silica (L-MAP3) was significantly more cytotoxic towards the tumor cells than non-tumor cells (37 ± 2.0 versus $6 \pm 1.2\%$ survival for T29 and A2780, respectively). The reduced toxicity of the larger NO delivery vehicles against T29 cells represents a major step toward the development of nanodevices capable of releasing tumoricidal concentrations of NO with little toxic effects against healthy cells.

5.3.4 Cellular Uptake and Confocal Microscopy

To study cellular uptake of the NO-releasing silica nanoparticles using confocal fluorescence microscopy, a laser scanning microscope was used. The multifunctionalized silica nanoparticles were prepared via the “one-pot” co-condensation of three silane precursors including FITC-modified APTMS, *N*-diazoniumdiolated MAP3 (75 mol%), and TEOS (Figure 5.10).

The red fluorescence of TMRM was monitored to provide a map of the intracellular location of mitochondria and an outline of A2780 nuclei (Figure 5.11). A 100- μL aliquot of

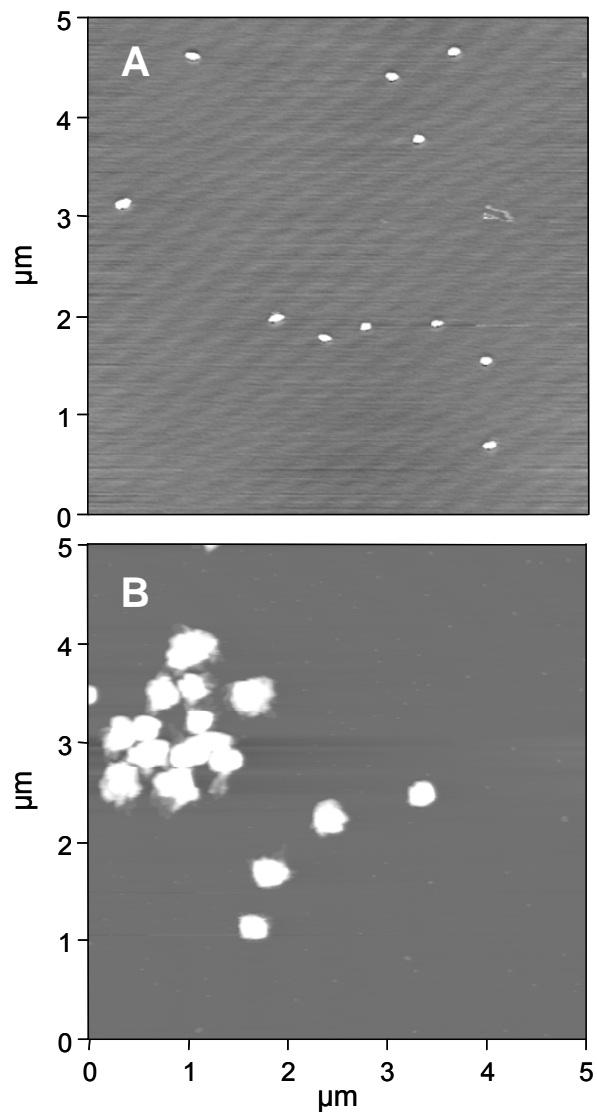


Figure 5.8. Contact mode AFM images of 75 mol% s-MAP3 (A) and L-MAP3 (B).

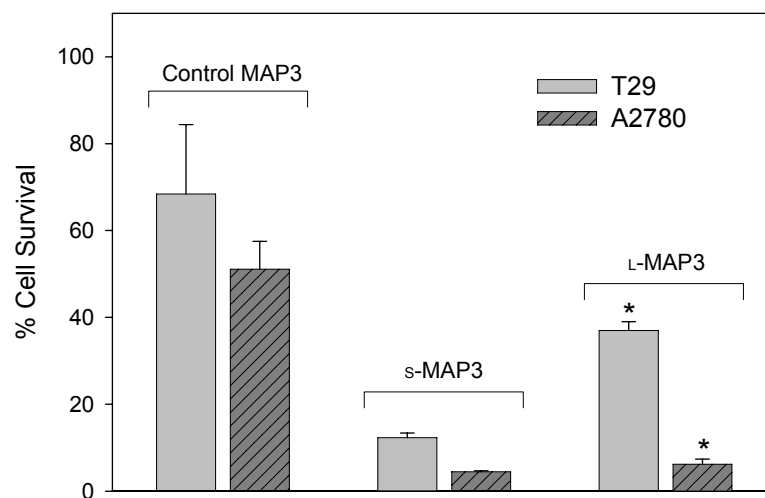


Figure 5.9. Effect of the silica particle size (75 mol% MAP3, balance TEOS) on cytotoxicity against normal T29 and tumor A2780 cell lines. * $P < 0.001$ compared with control MAP3- treated group.

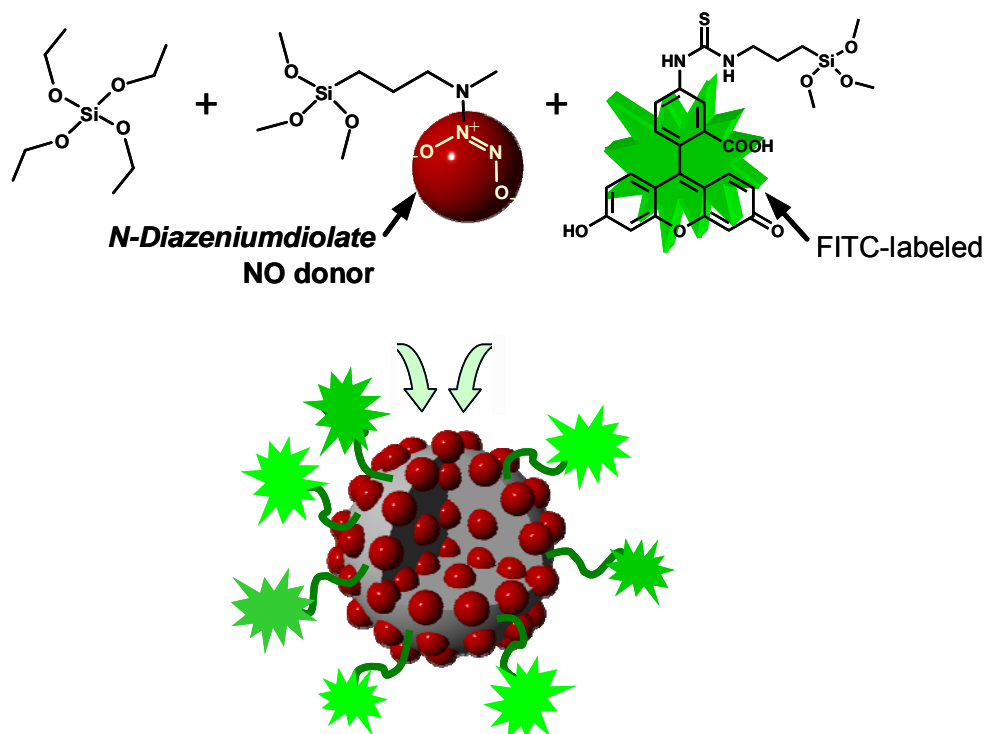


Figure 5.10. Schematic of multifunctionalized silica nanoparticles synthesized via the “one-pot” co-condensation of three silane precursors including FITC-modified APTMS, *N*-diazenium-diolated MAP3, and TEOS.

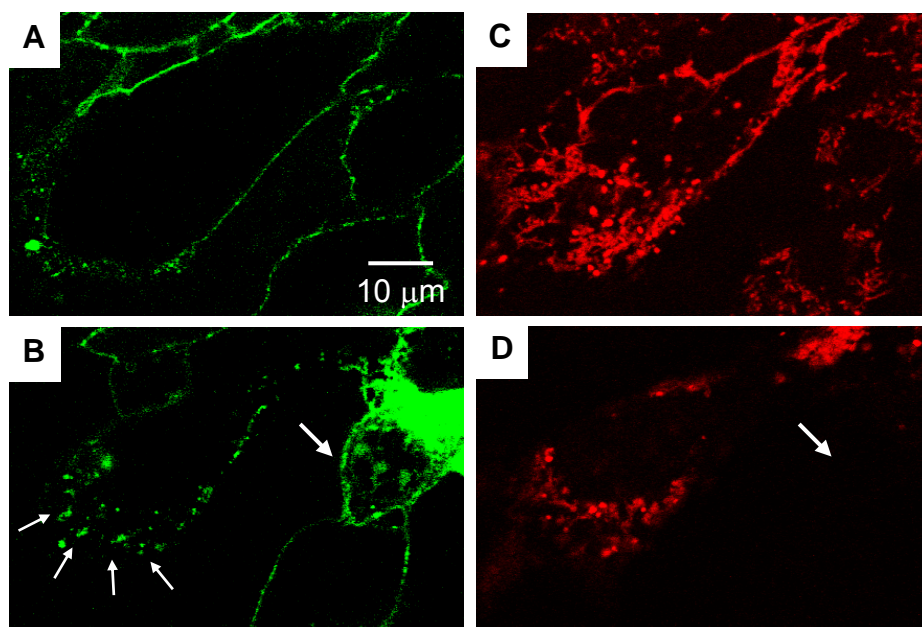


Figure 5.11. Laser scanning microscope images of A2780 ovarian cancer cells taken at 5 min (A,C) and 60 min (B,D) after incubation with (A,B) FITC-labeled MAP3 silica nanoparticles and (C,D) 100 nm tetramethylrhodamine methyl ester (TMRM) mitochondrial stain.

FITC-labeled NO-releasing MAP3 silica nanoparticles dissolved in the imaging buffer was added directly to the cells on the stage of the microscope, yielding a nanoparticle concentration of $100 \mu\text{g}\cdot\text{mL}^{-1}$. Immediately, the green fluorescence of the FITC-labeled silica nanoparticles was observed at 520 nm, resulting in a green outline of the A2780 cancer cells. Confocal images were collected at 5 min intervals to monitor the cellular uptake of the green fluorescent nanoparticles. After 1 h, substantial intracellular accumulation of nanoparticles was observed (Figure 5.11B). As well, the red fluorescence characteristic of mitochondrial viability was absent in a number of cells (Figure 5.11D) and the cells appeared to be shrinking in size, both indicative of cell death.

Currently, the mechanism of cellular uptake is not clear. Further studies will be conducted to probe whether these particles enter the cell through endocytosis or direct permeation through the plasma membrane. Confocal microscopy experiments will provide us with knowledge regarding cellular uptake, and will be used to support conclusions drawn from the tumor cell viability assays. Cellular uptake with both immortalized and cancerous cells will be studied as a function of nanoparticle size, composition, and surface modifications.

5.4 Conclusions

A silica nanoparticle-derived drug delivery system capable of controlled release of NO was developed. The NO-releasing silica scaffolds prepared via a pre-charging “one-pot” synthesis was able to store and release unprecedented quantities of NO (up to $7.4 \mu\text{mol}\cdot\text{mg}^{-1}$). Control over both the structure and concentration of the aminoalkoxysilane ligand and the synthetic approach used to prepare the silica allows for the preparation of NO release scaffolds of widely varying size ($d = 90 - 350 \text{ nm}$) and NO release kinetics ($[\text{NO}]_{\text{m}} = 1200 -$

103000 ppb·mg⁻¹ and $t_{1/2} = 6 - 132$ min). The advantages of silica-derived NO delivery systems over conventional small molecule NO donors include the ability to 1) store large quantities of NO; 2) modulate NO release kinetics; 3) tune the physical and chemical properties of the silica (e.g., the mesoporous structure, particle size, and specific surface properties); and, 4) impart multifunctionalities (e.g., immobilizing cancer cell targeting ligands and fluorescent labeling).

These nano-scale vehicles can be used as effective anticancer agents to kill tumor cells, potentially reducing tumor growth. In preliminary studies to evaluate the anti-cancer efficacy of NO-releasing silica nanocomposites, the cytotoxic activity against HOSE cancer cells was evaluated, and indicated that the viability of HOSE cancer cells is significantly reduced upon exposure to NO-releasing silica nanoparticles. More importantly, silica-derived NO delivery devices may allow for targeting via particle size (enhanced permeability/retention effect).⁶² Such cancer-specific targeting ability may be further modulated via ligand-receptor binding chemistry (e.g., folate-folate receptor interactions).⁶³ Specific toxicity against cancer over healthy cells represents a major step toward the development of nanodevices capable of releasing tumoricidal concentrations of NO with reduced side effects on healthy cells.

5.5 References

- (1) Ignarro, L. J. *Nitric oxide: Biology and pathobiology*; Academic Press: San Diego, 2000.
- (2) Moncada, S.; Higgs, A. "The L-arginine-nitric oxide pathway," *N. Engl. J. Med.* **1993**, *30*, 2002-2011.
- (3) Wink, D. A.; Vodovotz, Y.; Laval, J.; Laval, F.; Dewhirst, M. W.; Mitchell, J. B. "The multifaceted roles of nitric oxide in cancer," *Carcinogenesis* **1998**, *19*, 711-721.
- (4) Albina, J. E.; Reichner, J. S. "Role of nitric oxide in mediation of macrophage cytotoxicity and apoptosis," *Canc. Metas. Rev.* **1998**, *17*, 19-53.
- (5) Forrester, K.; Ambs, S.; Lupold, S. E.; Kapust, R. B.; Spillare, E. A.; Weinberg, W. C.; Felley-Bosco, E.; Wang, X. W.; Geller, D. A.; Tzeng, E.; Billiar, T. R.; Harris, C. C. "Nitric oxide-induced p53 accumulation and regulation of inducible nitric oxide synthase expression by wild-type p53," *Proc. Natl. Acad. Sci. U.S.A.* **1996**, *93*, 2442-2447.
- (6) Lala P. K. "Significance of nitric oxide in carcinogenesis, tumor progression and cancer therapy," *Cancer Metas. Rev.* **1998**, *17*, 1-6.
- (7) Fukumura, D.; Kashiwagi, S.; Jain, R. K. "The role of nitric oxide in tumour progression," *Nat. Rev. Cancer* **2006**, *6*, 521-534.
- (8) Sandau, K.; Pfeilschifter, J.; Brune, B. "The balance between nitric oxide and superoxide determines apoptotic and necrotic death of rat mesangial cells," *J. Immunol.* **1997**, *158*, 4938-4946.
- (9) Lo, H.-W.; Hung, M.-C. "Nuclear EGFR signalling network in cancers: linking EGFR pathway to cell cycle progression, nitric oxide pathway and patient survival," *Brit. J. Cancer* **2006**, *94*, 184-188.
- (10) Lopez-Farre, A.; Rodriguez-Feo, J. A.; Sanchez de Miguel, L.; Rico, L. "Role of nitric oxide in the control of apoptosis in the microvasculature," *Int. J. Biochem. Cell Biol.* **1998**, *30*, 1095-1106.

- (11) Hibbs, J. B.; Vavrin, Z.; Taintor, R. R. "L-arginine is required for the expression of the activated macrophage effector mechanism causing selective metabolic inhibition in target cells," *J. Immunol.* **1987**, *138*, 550-565.
- (12) Stuehr, D. J.; Nathan, C. F. "A macrophage product responsible for cytostasis and respiratory inhibition in tumor target cells," *J. Exp. Med.* **1989**, *169*, 1543-1555.
- (13) Leu, R. W.; Leu, N. R.; Shannon, B. J.; Fast, D. J. "IFN- γ differentially modulates the susceptibility of L1210 and P815 tumor targets for macrophage-mediated cytotoxicity. Role of macrophage-target interaction coupled to nitric oxide generation, but independent of tumor necrosis factor production," *J. Immunol.* **1991**, *147*, 1816-1822.
- (14) Klostergaard, J.; Leroux, M. E.; Hung, M. C. "Cellular models of macrophage tumoricidal effector mechanisms in vitro. Characterization of cytolytic responses tumor necrosis factor and nitric oxide pathways in vitro," *J. Immunol.* **1991**, *147*, 2802-2808.
- (15) Kurose, I.; Miura, S.; Fukumura, D.; Yonei, Y.; Saito, H.; Tada, S.; Suematsu, M.; Tsuchiya, M. "Nitric oxide mediates kupffer cell-induced reduction of mitochondrial energization in hepatoma cells: A comparison with oxidative burst," *Cancer Res.* **1993**, *53*, 2676-2682.
- (16) Wang, P. G.; Xian, M.; Tang, X.; Wu, X.; Wen, Z.; Cai, T.; Janczuk, A. J. "Nitric oxide donors: Chemical activities and biological applications," *Chem. Rev.* **2002**, *102*, 1091-1134.
- (17) Wang, P. G.; Cai, T. B.; Taniguchi, N. *Nitric oxide donors: For pharmaceutical and biological applications*; Wiley-VCH: Weinheim, German, 2005.
- (18) Mimeault, M.; Jouy, N.; Depreux, P.; Henichart, J.-P. "Synergistic antiproliferative and apoptotic effects induced by mixed epidermal growth factor receptor inhibitor ZD1839 and nitric oxide donor in human prostatic cancer cell lines," *Prostate* **2005**, *62*, 187-199.
- (19) Pervin, S.; Singh, R.; Chaudhuri, G. "Nitric oxide-induced cytostasis and cell cycle arrest of a human breast cancer cell line (MDA-MB-231): Potential role of cyclin D1," *Proc. Natl. Acad. Sci. USA* **2001**, *98*, 3583-3588.

- (20) Saavedra, J. E.; Srinivasan, A.; Buzard, G. S.; Davies, K. M.; Waterhouse, D. J.; Inami, K.; Wilde, T. C.; Citro, M. L.; Cuellar, M.; Deschamps, J. R.; Parrish, D.; Shami, P. J.; Findlay, V. J.; Townsend, D. M.; Tew, K. D.; Singh, S.; Jia, L.; Ji, X.; Keefer, L. K. "PABA/NO as an anticancer lead: Analogue synthesis, structure revision, solution chemistry, reactivity toward glutathione, and in vitro activity," *J. Med. Chem.* **2006**, *49*, 1157-1164.
- (21) Blachier, F.; Briand, D.; Selamnia, M.; Robert, V.; Guihot, G.; Mayeur, C. "Differential inhibitory effects of three nitric oxide donors on ornithine decarboxylase activity in human colon carcinoma cells," *Biochem. Pharmacol.* **1998**, *55*, 1235-1239.
- (22) Jia, L.; Schweizer, J.; Wang, Y.; Cerna, C.; Wong, H.; Revilla, M. "Effect of nitric oxide on cytotoxicity of taxol: Enhanced taxol transcellular permeability," *Biochem. Pharmacol.* **2003**, *66*, 2193-2199.
- (23) Babich, H.; Zuckerbraun, H. L. "In vitro cytotoxicity of glyco-S-nitrosothiols: A novel class of nitric oxide donors," *Toxicol. Vitro* **2001**, *15*, 181-190.
- (24) Hou, Y.; Wu, X.; Xie, W.; Braunschweiger, P. G.; Wang, P. G. "The synthesis and cytotoxicity of fructose-1-snap, a novel fructose conjugated S-nitroso nitric oxide donor," *Tetrahedron Lett.* **2001**, *42*, 825-829.
- (25) Kashfi, K.; Rigas, B. "Molecular targets of nitric oxide-donating aspirin in cancer," *Biochem. Soc. Trans.* **2005**, *33*, 701-704.
- (26) Bratasz, A.; Weir, N. M.; Parinandi, N. L.; Zweier, J. L.; Sridhar, R.; Ignarro, L. J.; Kuppusamy, P. "Reversal to cisplatin sensitivity in recurrent human ovarian cancer cells by NCX - 4016, a nitro derivative of aspirin," *Proc. Natl. Acad. Sci. USA* **2006**, *103*, 3914-3919.
- (27) Adami, A.; Crivellente, F.; De Prati, A. C.; Cavalieri, E.; Cuzzolin, L.; Tommasi, M.; Suzuki, H.; Benoni, G. "Biotransformation and cytotoxic properties of NO-donors on MCF7 and U251 cell lines," *Life Sci.* **1998**, *63*, 2097-2105.
- (28) Napoli, C.; Ignarro, L. J. "Nitric oxide-releasing drugs," *Annu. Rev. Pharmacol. Toxicol.* **2003**, *43*, 97-123.

- (29) Hrabie, J. A.; Keefer, L. K. "Chemistry of the nitric oxide-releasing diazeniumdiolate functional group and its oxygen-substituted derivatives," *Chem. Rev.* **2002**, *102*, 1135-1154.
- (30) Keefer, L. K. "Progress toward clinical application of the nitric oxide-releasing diazeniumdiolates," *Annu. Rev. Pharmacol. Toxicol.* **2003**, *43*, 585-607.
- (31) Rao, C. N. R.; Mueller, A.; Cheetham, A. K. *The chemistry of nanomaterials: Synthesis, properties and applications (Volumes 1 and 2)*; Wiley-VCH: Weinheim, Germany, 2004
- (32) Kumar, C. S. S. R.; Hormes, J.; Leuschner, C. *Nanofabrication towards biomedical applications: Techniques, tools, applications, and impact*; Wiley-VCH: Weinheim, German, 2005.
- (33) Reddy, L. H. "Drug delivery to tumors: Recent strategies," *J. Pharm. Pharmacol.* **2005**, *57*, 1231-1242.
- (34) Bruchez, M.; Moronne, M.; Gin, P.; Weiss, S.; Alivisatos, A. P. "Semiconductor nanocrystals as fluorescent biological labels," *Science* **1998**, *281*, 2013-2016.
- (35) Nam, J. M.; Thaxton, C. C.; Mirkin, C. A. "Nanoparticle-based bio-bar codes for the ultrasensitive detection of proteins," *Science* **2003**, *301*, 1884-1886.
- (36) Mahtab, R.; Rogers, J. P.; Murphy, C. J. "Protein-sized quantum dot luminescence can distinguish between "straight", "bent", and "kinked" oligonucleotides," *J. Am. Chem. Soc.* **1995**, *117*, 9099-9100.
- (37) Weissleder, R.; Elizondo, G.; Wittenburg, J.; Rabito, C. A.; Bengel, H. H.; Josephson, L. "Ultrasmall superparamagnetic iron oxide: Characterization of a new class of contrast agents for mr imaging," *Radiology* **1990**, *175*, 489-493.
- (38) Pulfer, S. K.; Ott, D.; Smith, D. J. "Incorporation of nitric oxide-releasing crosslinked polyethylenimine microspheres into vascular grafts," *J. Biomed. Mater. Res.* **1997**, *37*, 182-189.
- (39) Hrabie, J. A.; Saavedra, J. E.; Roller, P. P.; Southan, G. J.; Keefer, L. K. "Conversion of proteins to diazeniumdiolate-based nitric oxide donors," *Bioconjugate Chem.* **1999**,

10, 838-842.

- (40) Jeh, H. S.; Lu, S.; George, S. C. "Encapsulation of PROLI/NO in biodegradable microparticles," *J. Microencapsulation* **2004**, *21*, 3-13.
- (41) Rothrock, A. R.; Donkers, R. L.; Schoenfisch, M. H. "Synthesis of nitric oxide-releasing gold nanoparticles," *J. Am. Chem. Soc.* **2005**, *127*, 9362-9363.
- (42) Stasko, N. A.; Schoenfisch, M. H. "Dendrimers as a scaffold for nitric oxide release," *J. Am. Chem. Soc.* **2006**, *128*, 8265-8271.
- (43) Lai, C.-Y.; Trewyn, B. G.; Jęftinija, D. M.; Jęftinija, K.; Xu, S.; Jęftinija, S.; Lin, V. S.-Y. "A mesoporous silica nanosphere-based carrier system with chemically removable CdS nanoparticle caps for stimuli-responsive controlled release of neurotransmitters and drug molecules," *J. Am. Chem. Soc.* **2003**, *125*, 4451-4459.
- (44) Barbe, C.; Bartlett, J.; Linggen, K.; Finnie, K.; Qiang, L. H.; Larkin, M.; Calleja, S.; Bush, A.; Calleja, G. "Silica particles: A novel drug-delivery system," *Adv. Mater.* **2004**, *16*, 1959-1966.
- (45) Trewyn, B. G.; Whitman, C. M.; Lin, V. S.-Y. "Morphological control of room-temperature ionic liquid templated mesoporous silica nanoparticles for controlled release of antibacterial agents," *Nano Lett.* **2004**, *4*, 2139-2143.
- (46) Roy, I.; Ohulchanskyy, T. Y.; Bharali, D. J.; Pudavar, H. E.; Mistretta, R. A.; Kaur, N.; Prasad, P. N. "Optical tracking of organically modified silica nanoparticles as DNA carriers: A nonviral, nanomedicine approach for gene delivery," *Proc. Natl. Acad. Sci. USA* **2005**, *102*, 279-284.
- (47) Takahashi, H.; Li, B.; Sasaki, T.; Miyazaki, C.; Kajino, T.; Inagaki, S. "Immobilized enzymes in ordered mesoporous silica materials and improvement of their stability and catalytic activity in an organic solvent," *Microporous Mesoporous Mater.* **2001**, *44-45*, 755-762.
- (48) Brunner, T. J.; Wick, P.; Manser, P.; Spohn, P.; Grass, R. N.; Limbach, L. K.; Bruinink, A.; Stark, W. J. "In vitro cytotoxicity of oxide nanoparticles: Comparison to asbestos, silica, and the effect of particle solubility," *Environ. Sci. Technol.* **2006**, *40*,

4374-4381.

- (49) Stein, A.; Melde, B. J.; Schroden, R. C. "Hybrid inorganic-organic mesoporous silicates-nanoscopic reactors coming of age," *Adv. Mater.* **2000**, *12*, 1403-1419.
- (50) Sayari, A.; Hamoudi, S. "Periodic mesoporous silica-based organic-inorganic nanocomposite materials," *Chem. Mater.* **2001**, *13*, 3151-3168.
- (51) Zhang, H.; Annich, G. M.; Miskulin, J.; Stankiewicz, K.; Osterholzer, K.; Merz, S. I.; Bartlett, R. H.; Meyerhoff, M. E. "Nitric oxide-releasing fumed silica particles: Synthesis, characterization, and biomedical application," *J. Am. Chem. Soc.* **2003**, *125*, 5015-5024.
- (52) Hicks, J. C.; Dabestani, R.; Buchanan, A. C., III; Jones, C. W. "Spacing and Site Isolation of Amine Groups in 3-Aminopropyl-Grafted Silica Materials: The Role of Protecting Groups," *Chem. Mater.* **2006**, *18*, 5022-5032.
- (53) McKittrick, M. W.; Jones, C. W. "Toward single-site functional materials-preparation of amine-functionalized surfaces exhibiting site-isolated behavior," *Chem. Mater.* **2003**, *15*, 1132-1139.
- (54) Wang, Y.-N.; Bohle, D. S.; Bonifant, C. L.; Chmurny, G. N.; Collins, J. R.; Davies, K. M.; Deschamps, J.; Flippen-Anderson, J. L.; Keefer, L. K.; Klose, J. R.; Saavedra, J. E.; Waterhouse, D. J.; Ivanic, J. "Chemistry of the diazeniumdiolates: $Z \rightleftharpoons E$ isomerism," *J. Am. Chem. Soc.* **2005**, *127*, 5388-5395.
- (55) Harris, M. T.; Brunson, R. R.; Byers, C. H. "The base-catalyzed hydrolysis and condensation reactions of dilute and concentrated TEOS solutions," *J. Non-Cryst. Solids* **1990**, *121*, 397-403.
- (56) Greenlee, R. T.; Hill-Harmon, M. B.; Murray, T.; Thun, M. "Cancer statistics, 2001," *CA Cancer J. Clin.* **2001**, *51*, 15-36.
- (57) Harries, M.; Gore, M. "Part I: Chemotherapy for epithelial ovarian cancer-treatment at first diagnosis," *Lancet Oncol.* **2002**, *3*, 529-536.
- (58) Harries, M.; Gore, M. "Part II: Chemotherapy for epithelial ovarian cancer-treatment at first diagnosis," *Lancet Oncol.* **2002**, *3*, 537-545.

- (59) Hahn, W. C.; Weinberg, R. A. "Rules for making human tumor cells," *N. Engl. J. Med.* **2002**, *347*, 1593-1603.
- (60) Liu, J.; Yang, G.; Thompson-Lanza, J.; Glassman, A.; Hayes, K.; Patterson, A.; Marquez, R.; Auersperg, N.; Yu, Y.; Hahn, W.; Mills, G.; Bast, R., Jr. "A genetically defined model for human ovarian cancer," *Cancer Res.* **2004**, *64*, 1655-1663.
- (61) Hong, S.; Bielinska, A. U.; Mecke, A.; Keszler, B.; Beals, J. L.; Shi, X.; Balogh, L.; Orr, B. G.; Baker, J. R., Jr.; Banaszak-Holl, M. M. "Interaction of poly(amidoamine) dendrimers with supported lipid bilayers and cells: Hole formation and the relation to transport," *Bioconjugate Chem.* **2004**, *15*, 774-782.
- (62) Maeda, H.; Wu, J.; Sawa, T.; Matsumura, Y.; Hori, K. "Tumor vascular permeability and the EPR effect in macromolecular therapeutics. A review," *J. Control. Release* **2000**, *65*, 271-284.
- (63) Stella, B.; Arpicco, S.; Peracchia, M. T.; Desmaele, D.; Hoebeker, J.; Renoir, M.; D'Angelo, J.; Cattel, L.; Couvreur, P. "Design of folic acid-conjugated nanoparticles for drug targeting," *J. Pharm. Sci.* **2000**, *89*, 1452-1464.

Chapter 6:

Summary and Future Research Directions

6.1 Summary

The continuous, real-time monitoring of clinically important analytes (e.g., PO_2 , PCO_2 , pH, K^+ , Na^+ , glucose, and lactate) is of great importance to human health care. Despite considerable efforts spanning several decades, the clinical utility of *in vivo* sensors remains limited due to inadequate biocompatibility. The discovery of nitric oxide (NO) as an effective inhibitor of platelet and bacterial adhesion has opened a new direction of research related to designing the next generation of *in vivo* sensors. While advances in the synthesis of NO-releasing materials have led to significant progress in the development of intravascular (i.e., blood-based) chemical sensors,¹⁻³ the application of these materials to enzyme-based biosensors has yet to be explored. In my dissertation research, I have focused on developing a subcutaneous glucose sensor by coupling sol-gel derived NO release with the chemistry of enzymatic biosensing.

As described in Chapter 2, a *hybrid* xerogel/polyurethane glucose biosensor that releases NO was developed and characterized. The biosensor consisted of a platinum electrode coated with four polymeric membranes including: (1) xerogel with immobilized glucose oxidase (GOx); (2) polyurethane to protect the enzyme; (3) NO donor-modified xerogel particle-doped polyurethane; and (4) polyurethane. This configuration was developed in response to the drastic reduction in sensitivity observed for NO donor-modified xerogel

film-based glucose sensors. For the *hybrid* xerogel/polyurethane biosensor, xerogel particles ($d = 10 - 200 \mu\text{m}$) were first modified with the NO donor and then incorporated into a polyurethane layer that was coated onto the pre-immobilized GOx electrode. In this manner, the GOx layer was not exposed to the harsh conditions necessary to impart NO release ability to the biosensor. As such, only a minimal decrease in sensitivity due to NO release was observed (-5.7×10^{-2} vs. $-4.8 \times 10^{-2} \mu\text{A}\cdot\text{mM}^{-1}$ for control and NO-releasing sensors, respectively). The NO release properties were readily tunable by varying the amount of *N*-diazoniumdiolate-modified xerogel particles in the polyurethane. *In vitro* bacterial adhesion assays confirmed that NO-releasing *hybrid* xerogel/polyurethane films were effectively resistant to cell adhesion at NO fluxes $\geq 5 \text{ pmol}\cdot\text{cm}^{-2}\cdot\text{s}^{-1}$ for 20 h. Although the NO-releasing xerogels represent promising coatings for reducing platelet and bacterial adhesion *in vitro*, their *in vivo* applications still have limitations. Specifically, the NO release longevity of such coatings is limited by both the relatively small reservoir of NO donors that may be loaded into a thin film and the restricted control in NO release kinetics. Improving the duration of NO release is likely to impact the development of more biocompatible *in vivo* NO-releasing sensors, particularly with respect to reducing platelet and bacterial aggregation at extended periods. Therefore, methods to lengthen the NO release duration are discussed in Future Research Directions.

An amperometric sol-gel derived NO microsensor was described in Chapter 3. Several silicon-based xerogel membranes (the combinations of alkyl- and aminoalkoxy-silanes) were evaluated to identify the optimum composition for maximizing NO permeability while providing sufficient selectivity for NO in the presence of common interfering species. Xerogel permeability and selectivity were further manipulated as a function of

reaction/processing conditions (i.e., drying/aging time and temperature, and exposure of the cured film to high pressures of NO or Ar). In addition, the effects of incorporating Nafion into the xerogel matrix on sensor performance and the stability of the ensuing xerogel/Nafion *hybrid* film were evaluated. The optimal permselective membrane was achieved by catalyzing polycondensation of the xerogel composed of 20 v/v% (aminoethylamino-methyl)phenethyltrimethoxysilane (AEMP3)/methyltrimethoxysilane (MTMOS) and Nafion (17 v/v%) with exposure to NO (5 atm, 10 min). The resulting NO microsensor (prepared using 127 and 250 μm o.d. of platinized Pt working and Ag/AgCl reference electrodes, respectively) exhibited comparable sensor performance to previously reported NO sensors with respect to: sensitivity of $0.17 \pm 0.02 \text{ pA}\cdot\text{nM}^{-1}$ (from 25 to 800 nM, $r = 0.9991$), linearity ($r = 0.9991$, 25 – 800 nM NO range), detection limit of 25 nM (S/N = 3), response time of 9 s ($t_{95\%}$, a NO concentration change from 400 to 500 nM), selectivity ($\log K_{\text{NO},j}^{\text{amp}}$) of -5.8, <-6, <-6, and <-6 for $j =$ nitrite, ascorbic acid, uric acid, and acetaminophen, and lifetime of 8 d (82% of initial sensitivity without serious deterioration in selectivity). In contrast to other electrochemical NO sensor designs, however, the fabrication of xerogel-based NO microsensors is both simple and reproducible. Such sensors may prove useful employed for *in vivo* monitoring of NO and *in situ*, real-time measurements at or near the surface of materials that controllably release NO to elucidate the relationship between local NO concentrations and surface fouling. Such studies might aid in the design of more effective biomaterials.

As outlined in Chapter 4, the synthesis and characterization of a new NO-releasing scaffold prepared from amine-functionalized silica nanoparticles were reported. Inorganic-organic *hybrid* silica was prepared via co-condensation of tetraethoxy- or tetramethoxysilane

(TEOS or TMOS) and aminoalkoxysilane [e.g., *N*-(2-aminoethyl)-3-aminopropyltrimethoxysilane (AEAP3), *N*-(6-aminoethyl)aminopropyltrimethoxysilane (AHAP3), and *N*-[3-(trimethoxysilyl)propyl]diethylenetriamine (DET3)] with appropriate amounts of ethanol (or methanol), water, and ammonia. The amine functional groups in the silica were converted to *N*-diazoniumdiolate NO donors via exposure to high pressures of NO (5 atm) under basic conditions. Control over both the structure and concentration of the silane precursors (i.e., tetraalkoxy- and aminoalkoxysilanes) and specific synthetic conditions allowed for the preparation of NO donor silica particles of varying size ($d = 20 - 500$ nm), NO payloads (50 – 1780 nmol·mg⁻¹), maximum amounts of NO released (10 – 5500 ppb·mg⁻¹), half-lives (0.1 – 12 h), and NO release durations (up to 30 h). The advantages of silica-derived NO storage/delivery systems over previously reported macromolecular NO donors include the ability to 1) store large quantities of NO; 2) modulate NO release kinetics; and, 3) readily tune particle size based on the composition of the particle. In addition, a one-pot strategy for preparing the NO donor-modified silica enables straightforward, high-throughput synthesis and purification. The NO-releasing silica nanoparticles may prove useful for developing sensor biomaterials with extended NO release durations.

The development of a NO-releasing silica nanoparticle-derived drug delivery system with cytotoxic efficacy against human ovarian surface epithelial (HOSE) immortalized (T29) and cancer (A2780 and OVCAR-3) cell lines was described in Chapter 5. These nano-scaffolds were demonstrated as effective anticancer agents by preferentially killing tumor cells. My studies indicated that the viability of HOSE cancer cells (A2780) was significantly reduced upon exposure to NO-releasing 45 mol% AHAP3 silica nanoparticles (MIC = 750 μM NO and IC₅₀ = 30 μM NO). These values were significantly lower than those of small

molecule NO donors (e.g., MIC and IC₅₀ for PYRRO/N₂O₂ were 4.5 and 1.8 mM NO, respectively), indicating that the nanoparticle-based NO delivery system is more effective against ovarian cancer cells. To evaluate the effect of particle size on cytotoxicity, silica nanoparticles (75 mol% MAP3, balance TEOS) of different sizes were synthesized (small 90 ± 10 nm and large 350 ± 50 nm). While the small diameter NO-releasing silica (s-MAP3) proved cytotoxic against both T29 and A2780 cells (12 ± 1.1 and 5 ± 0.2% survival, respectively), the larger NO-releasing silica (L-MAP3) exhibited greater cytotoxicity towards the tumor cells than non-tumor cells (37 ± 2.0 versus 6 ± 1.2% survival for T29 and A2780, respectively). Such size-dependent cytotoxicity of silica NO donors was attributed to the enhanced permeability and retention (EPR) effect, also known as a “passive” targeting. A couple of “active” targeting strategies for further modification of silica nanoparticles are discussed below.

6.2 Future Research Directions

The ability to tailor nanoparticle surface chemistry may allow for the doping of large stores of NO into polymer films without undesirable leaching of the nanoparticles and/or NO donor byproducts that have plagued previously reported systems.⁴ Furthermore, the hydrophobic nature of silica particles may prolong NO release duration because water triggers *N*-diazeniumdiolate decomposition.⁵ Hydrophobic silica nanoparticles may be synthesized using various ratios of aminoalkoxysilane (e.g., AHAP3 and MAP3), tetraalkoxysilane (e.g., TEOS), and hydrophobic or alkylalkoxysilanes. The addition of alkylalkoxysilanes of different alkyl lengths (e.g., methyl-, ethyl-, hexyl- or octyltrimethoxysilane) and/or perfluorinated silanes (e.g., nonafluorohexyltrimethoxysilane, tridecafluoro-1,1,2,2-tetrahydrooctyl)trimethoxysilane, and [heptadecafluoro-1,1,2,2-tetrahydrodecyl]trimethoxy-

silane) may also prove useful for preparing more hydrophobic nanoparticles.

Alternatively, the nanoparticles may be coated with polymers (i.e., shells) to prolong NO release. Core/shell composites have been previously synthesized by encapsulating silica with shells consisting of polymers that are degradable, swell, and/or hydrophobic.⁶ The properties of the shell may prove useful for controlling NO release. For example, the degradation rate of poly(lactic acid-co-glycolic acid) (PLGA), a fully biodegradable aliphatic polyester,⁷ may be tuned by altering molecular weight and the ratio of copolymer composition, leading to a range of polymer degradation kinetics and associated NO release rates. As depicted in Figure 6.1, the shell decomposition would be an irreversible process that exposes NO donors to a protic environment (water) for subsequent *N*-diazoniumdiolate decomposition (i.e., NO release). Similar to the degradable polymer core/shell system, hydrophobic xerogel polymers may slow the rate of water diffusion into the nanoparticle.

The future for developing NO-releasing silica-derived anti-cancer agents includes synthesizing biocompatible nanoparticles capable of delivering NO to a specific site of interest. To deliver therapeutic concentrations of NO to tumor tissue, for example, the use of active targeting strategies including folate-folate receptor (FR) interactions should be investigated (Figure 6.2). Folate receptors are frequently overexpressed in many cancer types, with the highest frequency being ovarian cancers (>90%).⁸ Normal ovarian epithelial cells display lower levels of FR expression making the FR a valuable therapeutic target for the delivery of NO-releasing nanoparticles.⁹ The FR density also appears to increase with advanced stages of cancer tissue growth.¹⁰ A major advantage of folate-mediated drug conjugates is their incredibly low toxicity towards healthy tissue. The minimal normal cell expression of the FR coupled with the high binding affinity of folate to folate receptor should

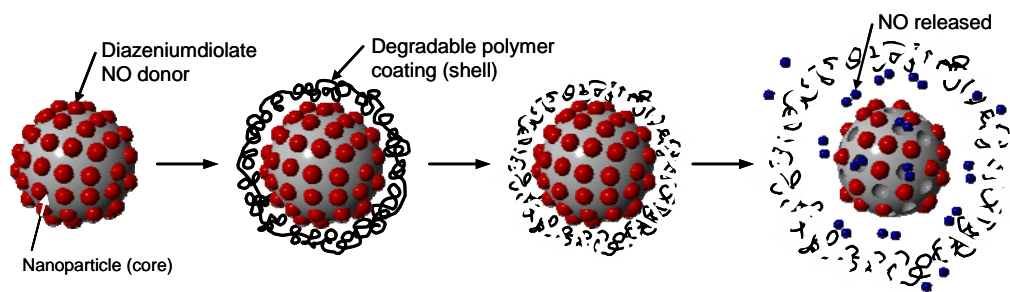


Figure 6.1. Illustration representing formation of the NO donor silica core/ biodegradable polymer shell structure and its deformation/ degradation.

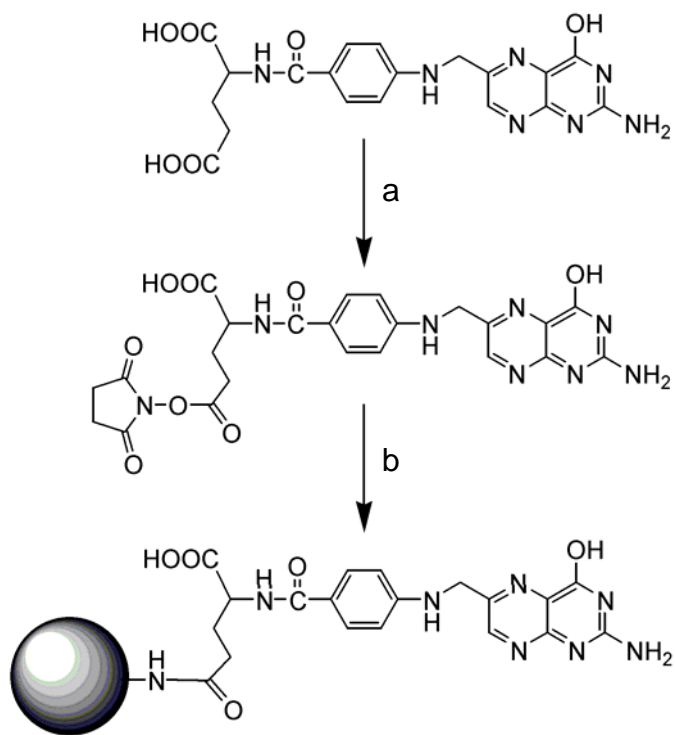


Figure 6.2. Folic acid activation and coupling to nanoparticle exterior: a) *N*-hydroxysuccinimide (NHS), dicyclohexylcarbodiimide (DCC), and dimethyl sulfoxide (DMSO); and b) primary amine terminated nanoparticle and DMSO.

allow the use of folate-modified nanoparticles to exhibit elevated selectivity for diseased tissue.¹¹

Alternative chemistries for “active” targeting may include the use of magnetic core nanoparticles. Indeed, the use of magnetic nanoparticles for targeted delivery has been widely studied.^{12,13} The attractive characteristics of magnetic therapy over traditional drug delivery methods include: 1) minimally invasiveness and suitability for *in vivo* applications since magnetic fields are not screened by biological fluids and do not interfere with most physiological processes; and, 2) the delivery of high concentrations of drug to targeted areas without undesirable side effects on neighboring normal organs and tissues.^{14,15} Since the first reports on clinical experiments for the treatment of solid tumors in human patients with magnetic targeting of drugs in the mid 1990s, this strategy has been one of the most active research topics in drug delivery.^{14,15}

The efficacy of magnetic therapy *in vivo* depends on the applied field strength as well as the size, stability, biocompatibility, and specific magnetic properties of the particle.¹² Many of these critical requirements may be achieved by varying the composition of the particle core (e.g., FePt, γ -Fe₂O₃, Fe₃O₄, and MnFe₂O₄), specific reaction/processing conditions (e.g., solvent systems, temperatures, reaction times, and types of catalysts and stabilizers), and/or the use of an appropriate shell structure.¹⁶ The shell layer may be a bi-functional coating to both reduce cytotoxicity and the formation of bioaggregates, and impart NO storage/delivery compartments. To evaluate the feasibility of developing a magnetic NO delivery system, a novel core/shell composite could be synthesized by coating iron oxide (Fe₃O₄; magnetite) magnetic particles with an amine-modified silica shell structure. The synthetic route for preparing such nanoparticles is shown in Figure 6.3.

6.3 Conclusions

Sol–gel chemistry represents a novel approach for synthesizing NO-releasing materials due to its tremendous flexibility in tuning NO release properties. In addition, control over reaction/processing conditions allows for the selection of physicochemical properties (e.g., density, permeability, and mesoporosity) that may also impact NO release. In my dissertation research, NO-releasing xerogel particle/polyurethane *hybrid* glucose biosensors were developed and characterized with respect to electrochemical performance and *in vitro* bacterial adhesion characteristics. Furthermore, xerogel membranes were synthesized via combination of various alkyl- and aminoalkoxysilanes as membrane for amperometric NO sensors. Finally, NO-releasing silica nanoparticles were synthesized using similar sol–gel processing methods. Both the synthetic approach used to prepare the *N*-diazoniumdiolate-modified silica and the cytotoxic efficacy of such particles against human ovarian surface epithelial cancer cell lines were evaluated.

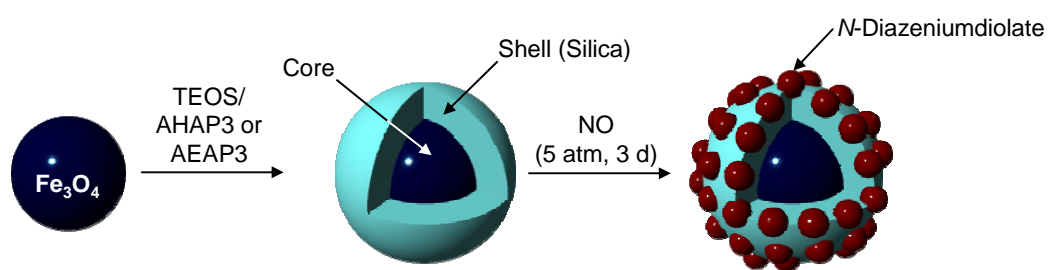


Figure 6.3. Synthesis of *N*-diazeniumdiolate-modified magnetic silica (core/shell) nanospheres.

6.4 References

- (1) Mowery, K. A.; Schoenfisch, M. H.; Baliga, N.; Wahr, J. A.; Meyerhoff, M. E. "More biocompatible electrochemical sensors using nitric oxide release polymers," *Electroanalysis* **1999**, *11*, 681-686.
- (2) Schoenfisch, M. H.; Zhang, H.; Frost, M. C.; Meyerhoff, M. E. "Nitric oxide-releasing fluorescence-based oxygen sensing polymeric films," *Anal. Chem.* **2002**, *74*, 5937-5941.
- (3) Frost, M. C.; Meyerhoff, M. E. "Implantable chemical sensors for real-time clinical monitoring: Progress and challenges," *Curr. Opin. Chem. Biol.* **2002**, *6*, 633-641.
- (4) Frost, M. C.; Reynolds, M. M.; Meyerhoff, M. E. "Polymers incorporating nitric oxide releasing/generating substances for improved biocompatibility of blood-contacting medical devices," *Biomaterials* **2005**, *26*, 1685-1693.
- (5) Hrabie, J. A.; Keefer, L. K. "Chemistry of the nitric oxide-releasing diazeniumdiolate functional group and its oxygen-substituted derivatives," *Chem. Rev.* **2002**, *102*, 1135-1154.
- (6) Jeffery, H.; Davis, S. S.; O'Hagan, D. T. "The Preparation and characterisation of poly(lactide-co-glycolide) microparticles. I: Oil-in-water emulsion solvent evaporation," *Int. J. Pharm.* **1991**, *77*, 169-175.
- (7) Raiche, A. T.; Puleo, D. A. "Modulated release of bioactive protein from multilayered blended PLGA coatings," *Int. J. Pharm.* **2006**, *311*, 40-49.
- (8) Corona, G; Giannini, F.; Fabris, M.; Toffoli, G.; Boiocchi, M. "Role of folate receptor and reduced folate carrier in the transport of 5-methyltetrahydrofolic acid in human ovarian carcinoma cells," *Int. J. Cancer* **1998**, *75*, 125-133.
- (9) Parker, N.; Turk, M. J.; Westrick, E.; Lewis, J. D.; Low, P. S.; Leamon, C. P. "Folate receptor expression in carcinomas and normal tissues determined by a quantitative radio-ligand binding assay," *Anal. Biochem.* **2005**, *338*, 284-293.
- (10) Lu, Y.; Low, P. S. "Folate-mediated delivery of macromolecular anticancer therapeutic agents," *Adv. Drug Del. Rev.* **2002**, *54*, 675-693.

- (11) Low, P. S. "Folate receptor-targeted drugs for cancer and inflammatory diseases," *Adv. Drug Del. Rev.* **2004**, *56*, 1055-1058.
- (12) Gupta, A. K.; Gupta, M. "Synthesis and surface engineering of iron oxide nanoparticles for biomedical applications," *Biomaterials* **2005**, *26*, 3995-4021.
- (13) Schillinger, U.; Brill, T.; Rudolph, C.; Huth, S.; Gersting, S.; Krotz, F.; Hirschberger, J.; Bergemann, C.; Plank, C. "Advanced in magnetofection - magnetically guided nucleic acid delivery," *J. Magn. Magn. Mater.* **2005**, *293*, 501-508.
- (14) Lubbe, A. S.; Bergemann, C.; Riess, H.; Schriever, F.; Reichardt, P.; Possinger, K.; Hohenberger, P.; Haas, N.; Sohr, R.; Sander, B.; Lemke, A.-J.; Ohlendorf, D.; Huhnt, W.; Huhn, D. "Clinical experiments with magnetic drug targeting: A phase i study with 4'-epidoxorubicin in 14 patients with advanced solid tumors," *Cancer Res.* **1996**, *56*, 4686-4693.
- (15) Lubbe, A. S.; Bergemann, C.; Huhnt, W.; Fricke, T.; Riess, H.; Brock, J. W.; Huhn, D. "Preclinical experiments with magnetic drug targeting: Tolerance and efficacy," *Cancer Res.* **1996**, *56*, 4694-4701.
- (16) Gould, P. "Nanoparticles probe biosystems," *Mater. Today* **2004**, 36-43.